COMMONWEALTH OF AUSTRALIA
DEPARTMENT OF SUPPLY

AUSTRALIAN NATIONAL ANTARCTIC RESEARCH EXPEDITIONS

ANARE SCIENTIFIC REPORTS

SERIES A (IV) GLACIOLOGY

PUBLICATION No. 108

THE DYNAMICS OF ICE MASSES

by

W. F. BUDD

ISSUED BY THE ANTARCTIC DIVISION
DEPARTMENT OF SUPPLY, MELBOURNE
1969

Registered at the G.P.O. Melbourne
for transmission by post as a book.

Printed in Australia by
Brown Prior Anderson Pty Ltd 5 Evans Street Burwood Victoria

LIST OF CONTENTS

LIST OF FIGURES

LIST OF TABLES

FOREWORD

The study of the dynamics of the large ice caps, Greenland and Antarctica, is still in its infancy. The inland regions are so far from fixed measuring points, and the movement rates are so small, that it is very difficult to determine their motion. Yet, the quantities of ice are so large, and the history held in the annual layers within the ice go back so many thousands of years, that the study of the dynamics of the large ice masses is of great interest to many research workers in fields such as glaciology, hydrology, climatology, geography and geophysics. The present report develops the theory of ice masses in general, largely from the investigation of two major ice masses in the Antarctic.

As a glaciologist with the Australian National Antarctic Research Expeditions the author spent one year at Wilkes, on the edge of the East Antarctic ice cap, and one year at Mawson, working mainly on the Amery Ice Shelf. Since then the author has collaborated with Dr. U. Radok of the Meteorology Department, Melbourne University, in supervising the glaciological research programme of the Antarctic Division of the Commonwealth Department of Supply.*

The major project in the Wilkes region has been the detailed study of the Wilkes local ice cap—a medium-scale ice cap, some 200 km in diameter, which serves as a convenient model of ice caps generally.

The Amery Ice Shelf, some 400 km from Mawson, is 300 km long and 200 km wide and serves as a model to study the dynamics of a typical ice shelf.

In conducting the investigations into the dynamics and change of these two ice masses it has been possible to examine the existing theories of ice motion, and to re-assess and extend them to enable general laws to be derived which can be used to calculate the dynamics of other ice masses.

This work, some of which already has been published in part, brings together the theory of the dynamics of ice masses generally and tests this briefly by application primarily to the results of the measurements made on the Wilkes ice cap and the Amery Ice Shelf, although other ice masses, including temperate glaciers, are referred to for completeness.

One of the chief difficulties encountered in this project has been the high dependence of the flow law on ice type and temperature. The temperature has proved such an important parameter that the largest chapter of the present work has been devoted to the study of temperature profiles in ice masses.

The major results of the theory are confirmed by the present measurements so far. Further predictions are made about the velocity and strain rates in ice masses but these predictions are highly dependent on the temperature distribution

* Responsibility for the Antarctic Division was transferred to the Department of Supply from the Department of External Affairs in May 1968.

in the ice, and hence complete confirmation will not be achieved until the temperature distributions are also known.

Measurements are continuing on the Wilkes ice cap and the Amery Ice Shelf with the aim of determining both the velocity distribution and the temperature in sufficient detail to establish the flow law of ice in natural ice masses and allow the theory to be developed to sufficient precision to calculate the temperature and velocities in other ice masses.

Finally, the study of the dynamics makes it possible to analyse the state of balance, rate of change, and recent history of ice masses. The measurements on the Wilkes ice cap and the Amery Ice Shelf already indicate what is now happening to the ice in these regions of Antarctica.

THE DYNAMICS OF ICE MASSES

By

W. F. BUDD

Antarctic Division, Department of Supply, Melbourne
(Manuscript received January 1969)

ABSTRACT

The study of the dynamics of ice masses involves establishing the equations of motion in terms of stresses, introducing the stress strain rate relation, or flow law, for ice and solving the equations of motion to obtain velocity distributions for the particular ice masses: glaciers, ice shelves, and ice caps.

The flow law of ice is complex. For lower stresses the stress strain rate relation is approximately linear but for high stresses it approaches a high power law. The strain rate increases rapidly with temperature and for polycrystalline ice also depends on the crystal sizes and orientation fabrics, the ice density and impurity content. To supplement laboratory measurements it is necessary to determine large scale flow law parameters from existing ice masses.

For the special symmetry of typical ice masses the longitudinal strain rates only slightly affect the cross-section profiles of velocity and hence these and the longitudinal profile can be treated somewhat independently.

In cold ice masses the most important parameter governing the stress-strain rate relation is the temperature. In regions of high ice-movement rates the heat produced by internal deformation of the ice becomes more important than the geothermal flux in determining the temperature profile. High accumulation rates at the surface of the ice cap tend to make the temperature depth profile more isothermal. Negative temperature—depth gradients at the surface are caused by surface warming due to either climatic change or the normal outward downward movement of the ice. Even long-term climatic changes fail to penetrate the thick ice caps with the present low accumulation rates.

Along the line of flow of an ice mass on the large scale the longitudinal velocity depends on the ice thickness, the mean surface slope and the flow parameters of the ice, which incorporates the temperature profile but with greatest weight on the conditions at the base. On the smaller scale the average longitudinal strain rate gradient is proportional to local deviations in surface slope from the mean slope. By incorporating the divergence or convergence of the flow lines these results may be extended to three dimensions.

For steady state flow of ice over undulating bedrock similar undulations occur on the ice mass surface, but with a reduced amplitude and a phase shift. The damping of the waves depends on the ice thickness, its velocity, the ice flow

parameters and the wavelength of the undulations. Since the minimum damping occurs for wavelengths of about three times the ice thickness, waves of this length tend to predominate on ice mass surfaces.

Actual measurements of longitudinal strain rates and velocities on ice shelves, ice caps and glaciers, together with the ice mass dimensions, allow the flow parameters of the ice to be calculated. Independent calculations can be made from the amplitudes of the surface and bedrock undulations.

Finally, from the profiles of the bedrock elevation, accumulation rate and the flow parameters of the ice, steady-state shapes of the ice masses may be calculated. From the existing shapes and the measured velocity and accumulation rates it is possible to calculate the state of balance, present rate of change, the particle paths and the recent past history of the ice mass. These calculations are carried out for the Wilkes ice cap and the Amery Ice Shelf from measurements made by the Australian National Antarctic Research Expeditions.

ANTARCTICA

POLAR STEREOGRAPHIC PROJECTION

SCALE IN LATITUDE 71° 1:20,000,000

STATUTE MILES

100 0 100 200 300 400 500

KILOMETRES

100 0 100 200 300 400 500 600 700 800

ANTARCTIC PENINSULA STATIONS

		Latitude	Longitude
TAIN			
e B	DECEPTION ISLAND	62°59'S	60°34'W
e E	STONINGTON ISLAND	68°11'S	67°00'W
e F	ARGENTINE ISLANDS	65°15'S	64°16'W
e T	ADELAIDE	67°46'S	68°55'W
GENTINA			
CEPCIÓN"		62°59'S	60°43'W
PERANZA"		63°24'S	56°59'W
NIENTE MATIENZO"		64°58'S	60°03'W
ILE			
e A	"ARTURO PRAT"	62°30'S	59°41'W
e B	"GENERAL BERNADO O'HIGGINS"	63°19'S	57°54'W
e C	"GABRIEL GONZALEZ VIDELA"	64°49'S	62°52'W
e D	"PEDRO AGUIRRE CERDA"	62°56'S	60°36'W
ITED STATES OF AMERICA			
LMER		64°46'S	64°05'W

LEGEND

coastline (definite)

(approximate)

ontour (approximate)

(conjectural)

Exposed rock

Ice shelf and front

Glacier

Balleny Islands

Heard I

Peter I Øy

AUSTRALIA

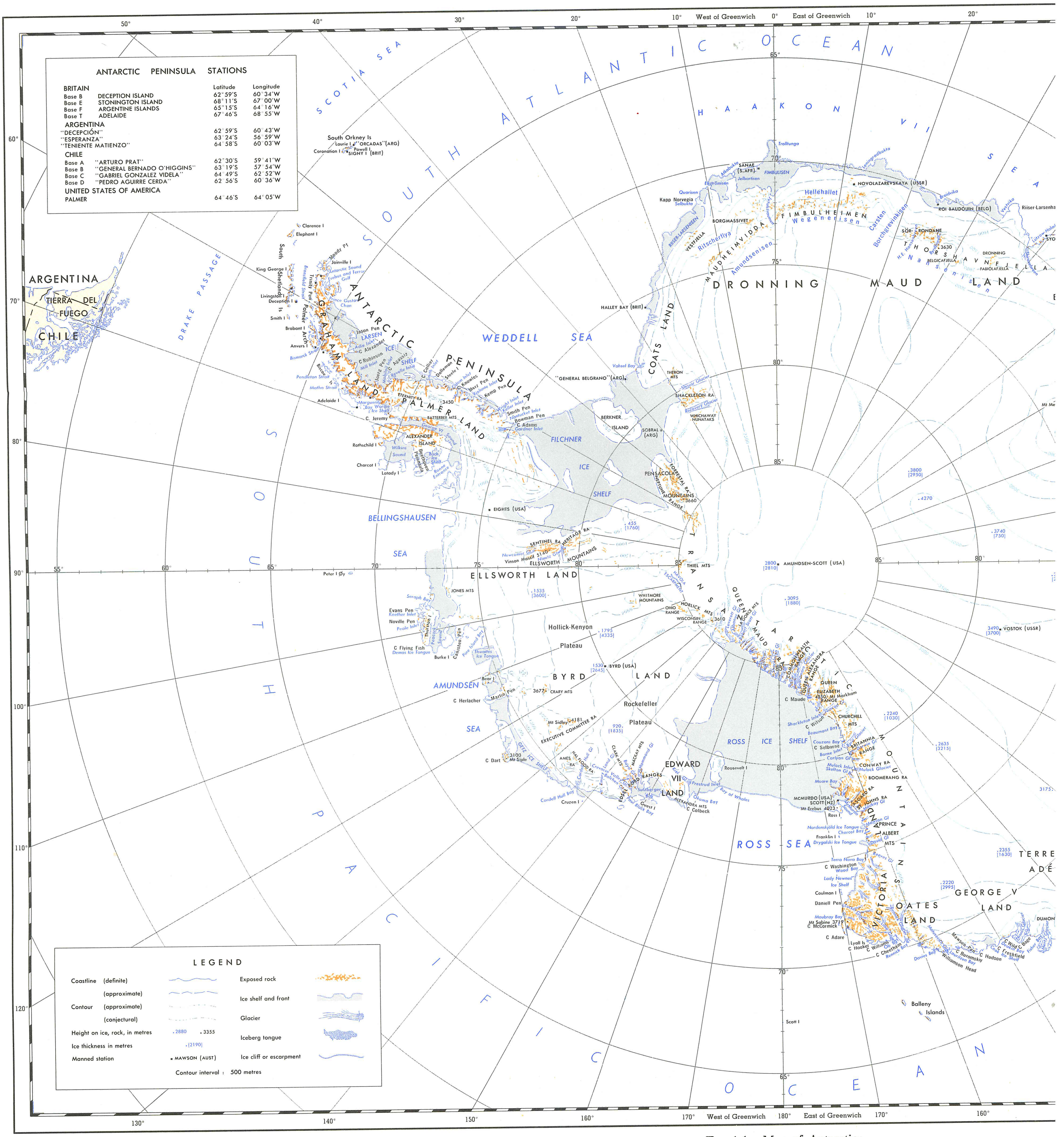

FIG. 1.1. Map of Antarctica

"ESPERANZA"		63° 24'S	56° 59'W
"TENIENTE MATIENZO"		64° 58'S	60° 03'W
CHILE			
Base A	"ARTURO PRAT"	62° 30'S	59° 41'W
Base B	"GENERAL BERNADO O'HIGGINS"	63° 19'S	57° 54'W
Base C	"GABRIEL GONZALEZ VIDELA"	64° 49'S	62° 52'W
Base D	"PEDRO AGUIRRE CERDA"	62° 56'S	60° 36'W
UNITED STATES OF AMERICA			
PALMER		64° 46'S	64° 05'W

KILOMETRES 100 0 100 200 300 400 500 600 700 800

LEGEND

Coastline	(definite)	Exposed rock	
	(approximate)	Ice shelf and front	
Contour	(approximate)	Glacier	
	(conjectural)	Iceberg tongue	
Height on ice, rock, in metres	.2880 .3355	Ice cliff or escarpment	
Ice thickness in metres	.[2190]		
Manned station	• MAWSON (AUST)		

Contour interval : 500 metres

Produced by the Division of National Mapping, Department of National Development, Canberra, Australia.

This map has been compiled from the latest information received from the Antarctic Treaty nations.

FIRST EDITION 1965 NMP/63/088

FIG. 1.1. Map of Antarctica

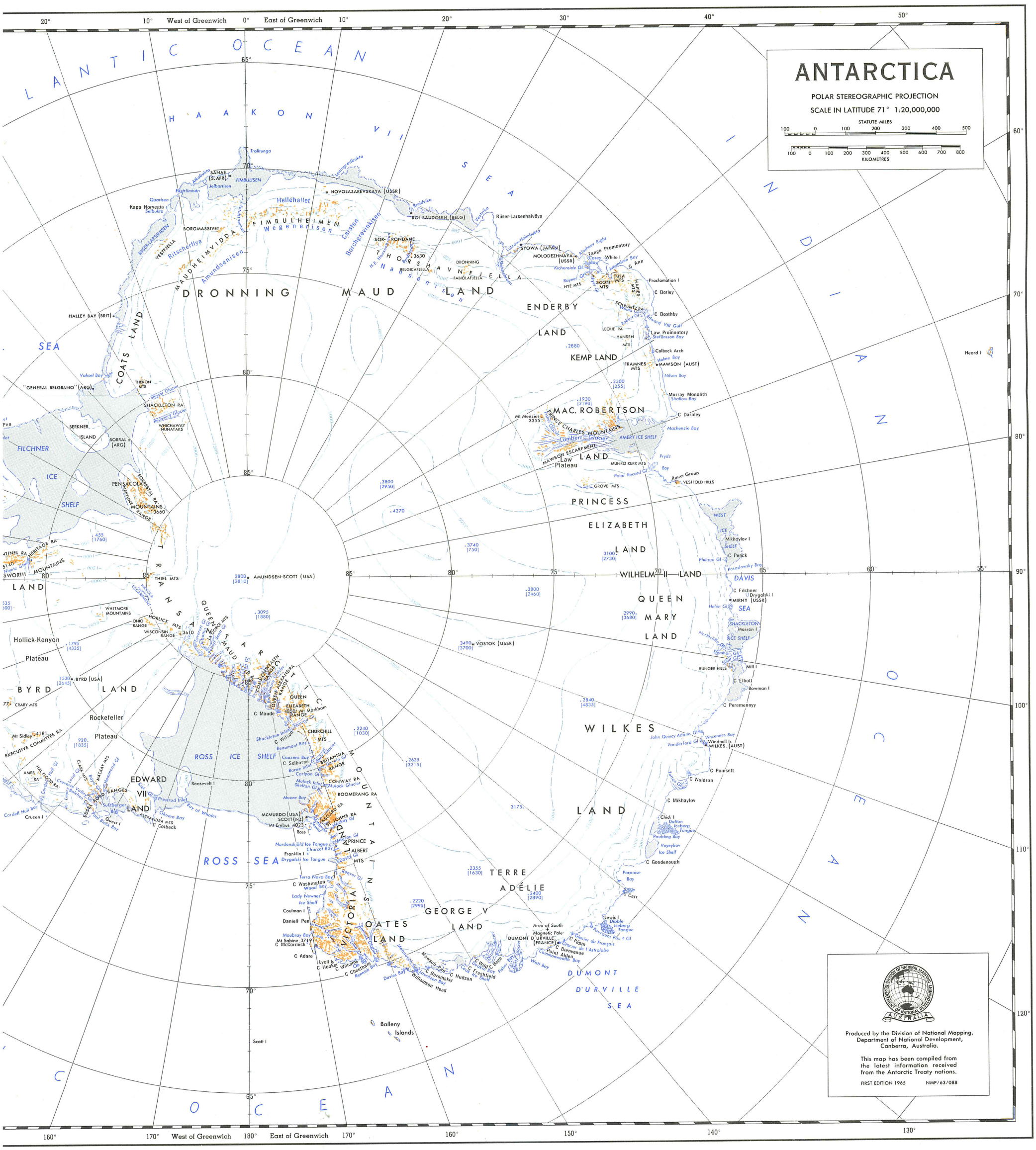

FIG. 1.1. Map of Antarctica

1. INTRODUCTION

1.1. OUTLINE OF PROBLEM

The major problem in the study of the dynamics of large natural ice masses is to find the laws governing their motion and to show how these laws may be used to calculate the present movement and the past and future histories of an ice mass with the minimum of measurements. The three major classes of naturally occurring ice masses are discussed below in Section 1.2.

The basic problem may be subdivided into three sections.

1.1.1. *The equations of motion*

Denote the position vector of a point in the ice medium, of density ρ, by x_i $(i = 1 \ldots 3)$ with respect to orthogonal axes, generally taken with

x_1 horizontal in the direction of motion

x_2 upwards vertically

x_3 across the line of motion.

Let the stress at x_i be denoted by σ_{ij}.

The external force on unit volume of the medium may generally be taken simply as the gravitational force ρg_i.

Now, for naturally occurring ice masses deforming slowly under their own weight, accelerations are much smaller than the other forces, and hence may be neglected.

We have then the equations of motion (summing on dummy suffixes)

$$\frac{\partial \sigma_{ij}}{\partial x_j} = \rho g_i \tag{1}$$

Now, generally, because the ice medium is deforming we do not know all the boundary conditions for the stress. However, the boundary velocities can usually be measured. Thus we require the relation between stress and strain rate in order to obtain the equations of motion in terms of velocities and velocity gradients (strain rates).

1.1.2. *The relation between stress and strain rate*

For most practical purposes the ice may be considered as incompressible. Therefore, the only deformation we are concerned with is pure shear with no change in volume, i.e., if $\dot{\varepsilon}_{ij}$ is the strain rate tensor at x_i

$$\left[\dot{\varepsilon}_{ij} = \frac{1}{2}\left(\frac{\partial u_i}{\partial x_j} + \frac{\partial u_j}{\partial x_i}\right) \text{where } u_i \text{ is the velocity at } x_i\right],$$

then

$$\dot{\varepsilon}_{ii} \equiv \dot{\varepsilon}_{11} + \dot{\varepsilon}_{22} + \dot{\varepsilon}_{33} = 0 \tag{2}$$

The details of the flow law relation between stress and strain rate for ice will be discussed in Section 2. For the moment it will suffice to say that we can express σ_{ij} as a function of the $\dot{\varepsilon}_{ij}$ by means of the stress deviator tensor $\sigma_i'_j$ defined by

$$\sigma'_{ij} = \sigma_{ij} - \tfrac{1}{3}\sigma_{ii}\delta_{ij} \tag{3}$$

$$\delta_{ij} = 1, \; i = j$$

$$= 0, \; i \neq j$$

and the flow law $\sigma'_{ij} = \eta \dot{\varepsilon}_{ij}$ (4)

where η is a scalar function of the stress invariants and the properties of the ice such as the temperature.

To solve the equations (1) and (4) for the strain rates we require the strain rates at the boundary. Then to solve for velocities we require the velocity at the boundary.

These two points indicate that, given an ice mass of a particular shape and size (i.e., a full specification of elevation profile, bedrock profile and plan) then the velocity solution is not unique but depends on the boundary velocity and strain rate which may be expected in general to vary with time. The very special case of steady state, where the boundary dimensions and velocities are kept constant by a particular pattern of accumulation, ablation, calving, etc., will be treated separately.

1.1.3. *Solution of the equations of motion in practice for different boundary conditions*

In studying the dynamics of natural ice masses it is generally required to know the shape and size of the ice mass. This requires

(i) mapping the boundaries (horizontal) (e.g., by aerial photography and land trignometric surveying);
(ii) determining the elevation contours (by barometric or optical levelling or photogrammetry by aircraft flights or ground traverses);
(iii) determining the bedrock contours (by seismic surveys supplemented by gravity measurements or by use of radio echo sounders).

This would be sufficient to determine the stress in the ice if it were motionless, but as it is deforming we require the velocity and the strain rates at the boundary. These are generally determined at several points by land or aerial survey techniques.

Then, starting from these boundary conditions it should be possible from the equations of motion and the flow law to determine by numerical integration the strain rates and velocities throughout the ice mass. The numerical approach, however, is only appropriate to specific examples. To obtain insight into the general principles of ice mass dynamics an attempt will be made in this work to examine analytical solutions for the velocity for certain general types of ice masses to be considered below.

The necessity for the velocity and strain rate boundary conditions to be known, and its consequences, deserves special emphasis. Several studies have been

made of the variation in the velocity, shape and size of ice masses, in time, for a varying accumulation rate. But even if the accumulation rate remains constant we can in general expect the shape, size and velocity distribution to vary with time, perhaps oscillating about an "equilibrium" or "steady-state" profile, which may be occupied only momentarily.

1.2 MAJOR TYPES OF ICE MASSES

For studies of dynamics the major types of natural ice masses have been divided into three main groups primarily because of their basically different boundary conditions. The three groups are glaciers, ice shelves, and ice caps, and are generally quite distinct with their own salient features. The map of Antarctica (Fig. 1.1) shows the three forms of ice mass. The boundaries where one form of ice mass merges into another are usually sharp, hence each of the three basic types will be considered separately.

1.2.1. *Glaciers*

Typically, for many purposes, glaciers may be considered as one-dimensional and we are here primarily concerned with the variation of velocity along the length in the line of motion.

A typical glacier plan, profile and cross-section are shown in Fig. 1.2. The shape and size of the cross-section are important but vary mainly due to the change in vertical thickness along the glacier. The transverse extension and compression are generally not as important as the other strain rates.

For temperate glaciers the temperature through the ice mass is normally close to freezing and so the temperature distribution does not produce a wide range of ice flow law parameters. Near the bedrock boundary, however, where the shear is highest, the frictional energy released may cause higher temperatures or even melting, giving a positive feedback to cause even higher flow rates.

The velocity of the glacier is generally highest at the surface at the position furthest from the rock. The velocity at the sides is often zero but some sliding may occur as in the case of the base, especially if the temperature is close to pressure melting.

The problem of sliding is difficult, particularly if the ice rock interface is not sharp but, instead, associated with a gradual transition from ice, ice rock mixture, moraine, to solid rock. In this case it may be impossible to distinguish between "sliding" and high differential shear in the most basal layers. To clarify this point it would be necessary to obtain drill cores across the ice rock boundary, together with the flow rates at different depths through these layers.

Generally then, the boundary conditions required for glaciers are: longitudinal elevation profile, bedrock profile, surface plan map, typical cross-section profiles, and sufficient boundary values of velocity and strain rate, e.g., at the terminus.

1.2.2. *Ice shelves*

In the map of Fig. 1.1 the major Antarctic ice shelves can be seen. A typical longitudinal profile is shown in Fig. 1.3 for the Amery Ice Shelf. Generally, ice

shelves are characterized by being free-floating with no shear at their base but held at their sides, and projecting into the sea at their front. They are comparatively flat with a slight slope downwards towards the front. The velocity and strain rate can be expected to be comparatively constant from the upper surface to the lower surface. But high velocity gradients exist *across* the ice shelf and also longitudinally inwards near the front.

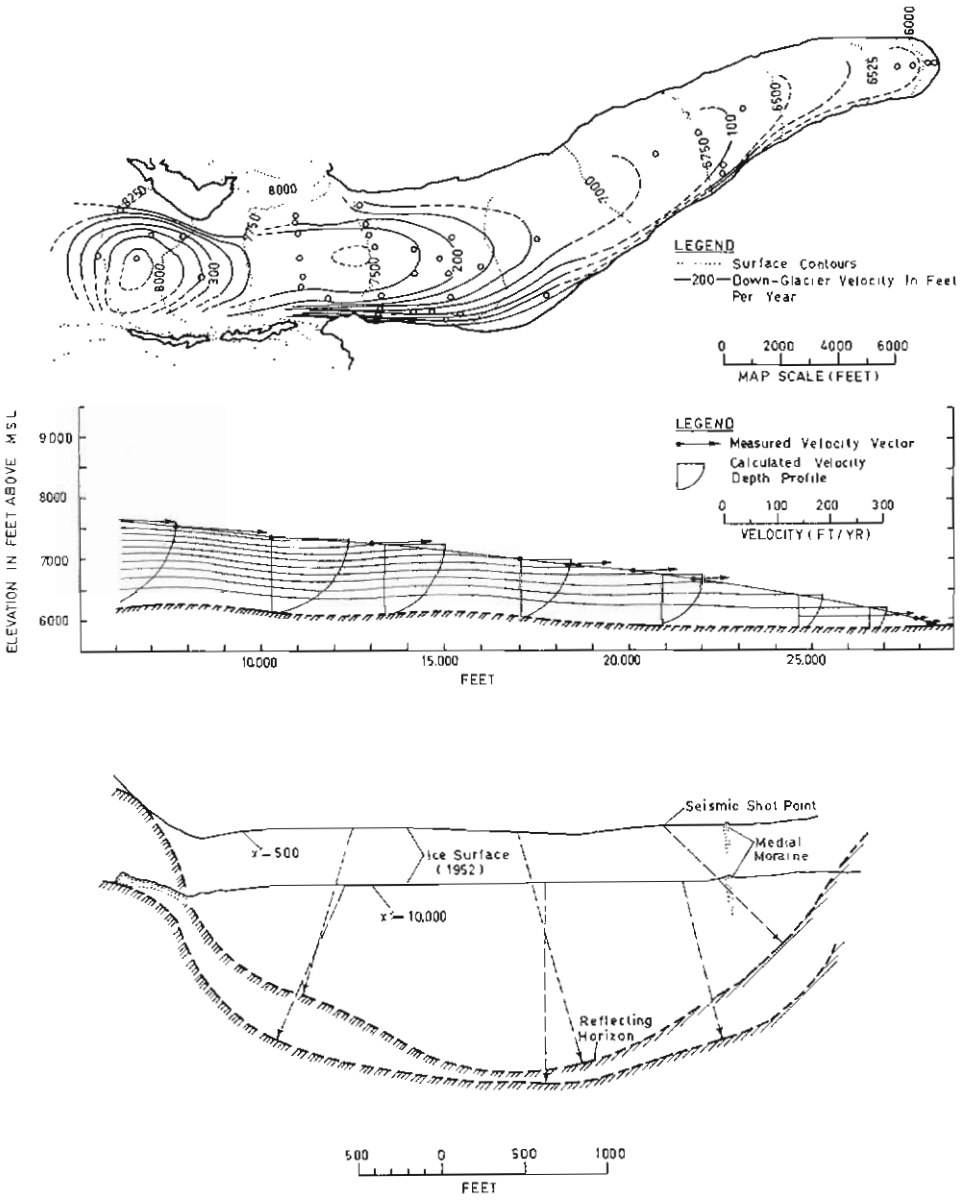

FIG. 1.2. Typical glacier plan, profile, and cross-section for Saskatchewan Glacier, after Meier (1960).

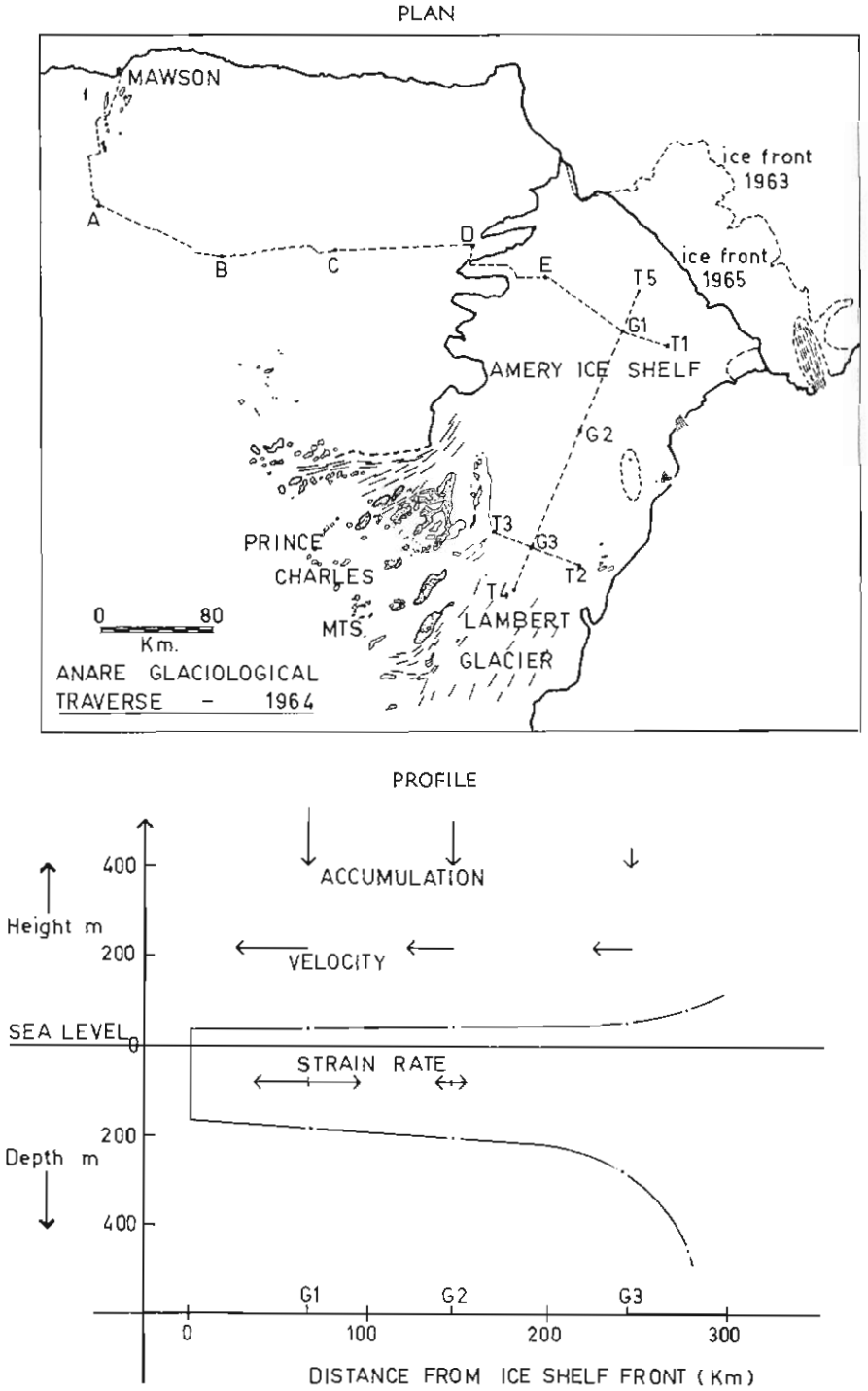

FIG. 1.3. Typical ice shelf plan and profile for the Amery Ice Shelf from Budd (1966).

The temperature at the base of the ice shelf will be close to sea water freezing temperature. The temperature at the surface typically decreases going inland from the front, but only slightly so, owing to the flat surface. The average temperature through the ice shelf depends not only on the surface and base temperatures but also on the accumulation, melt and flow rates. But in general the average temperature does not vary greatly along the ice shelf and consequently the variation in temperature only has a small effect on the flow rate along a flow line.

The boundary conditions required for ice shelves are the plan map of the boundary, the elevation and ice thickness profile and the velocity and strain rate at one position such as the front.

1.2.3. *Ice caps*

Since the ice caps of Antarctica and Greenland contain most of the world's ice (and freshwater) the study of their dynamics is a major prerequisite for the understanding of the world hydrological balance. Other small ice caps, such as the Wilkes dome, Anverse Island, Penny Ice Cap, Baffin Island, Roosevelt Island and Drygalski Island are much easier to study, and by obtaining a complete knowledge of such small ice caps it may be much easier to deduce the laws valid for the great ice caps.

The ice caps are generally three-dimensional domes of ice spreading outwards to their boundaries with appreciable lateral strain rates. Because of the irregularities of the bedrock the outward flowlines may be quite curved, and then the transverse velocities and strain rates also have to be considered.

The prime factor of interest is the velocity profile along a flow line from the summit to the edge, and how this profile depends on the surafce slope and ice thickness. The plan and profile of a typical small ice cap is shown in Fig. 1.4. The temperature of the ice at the surface decreases with elevation. The temperature at the base of the major ice caps is still largely unknown but in some cases it may approach the pressure melting point. The temperature has two important consequences for the ice motion.

(i) The average temperature in a vertical section through the ice cap decreases going inland from the coast—hence causing lower strain rates for a given stress;

(ii) the temperature normally increases as the base of the ice is approached, giving rise to even greater shear rates in the basal layers, and higher temperature gradients, due to the positive feedback of the frictional heating, than would be present with no motion.

The boundary conditions required for ice caps are the elevation and bedrock contours over the ice cap (in broad detail) and the velocity and strain rates at the boundary. For a fully adequate treatment the temperature profiles through the ice cap at several positions along a flow line are also necessary.

1.3. HORIZONTAL VELOCITY

From the equations of motion it is desired to obtain the complete velocity distribution throughout the ice mass. Taking account of tbe symmetry of the natural ice masses it is appropriate to consider three different velocity profiles:

(i) the "vertical" velocity profile from surface to base;
(ii) the "transverse" velocity profile across the lines of flow;
(iii) the "longitudinal" velocity profile along the lines of flow.

1.3.1. *The vertical profile of velocity*

The calculation of the vertical velocity profile has been carried out by Nye (1957, 1959, 1965), with modifications due to varying temperatures by Lliboutry (1963), and Shoumskiy (1963).

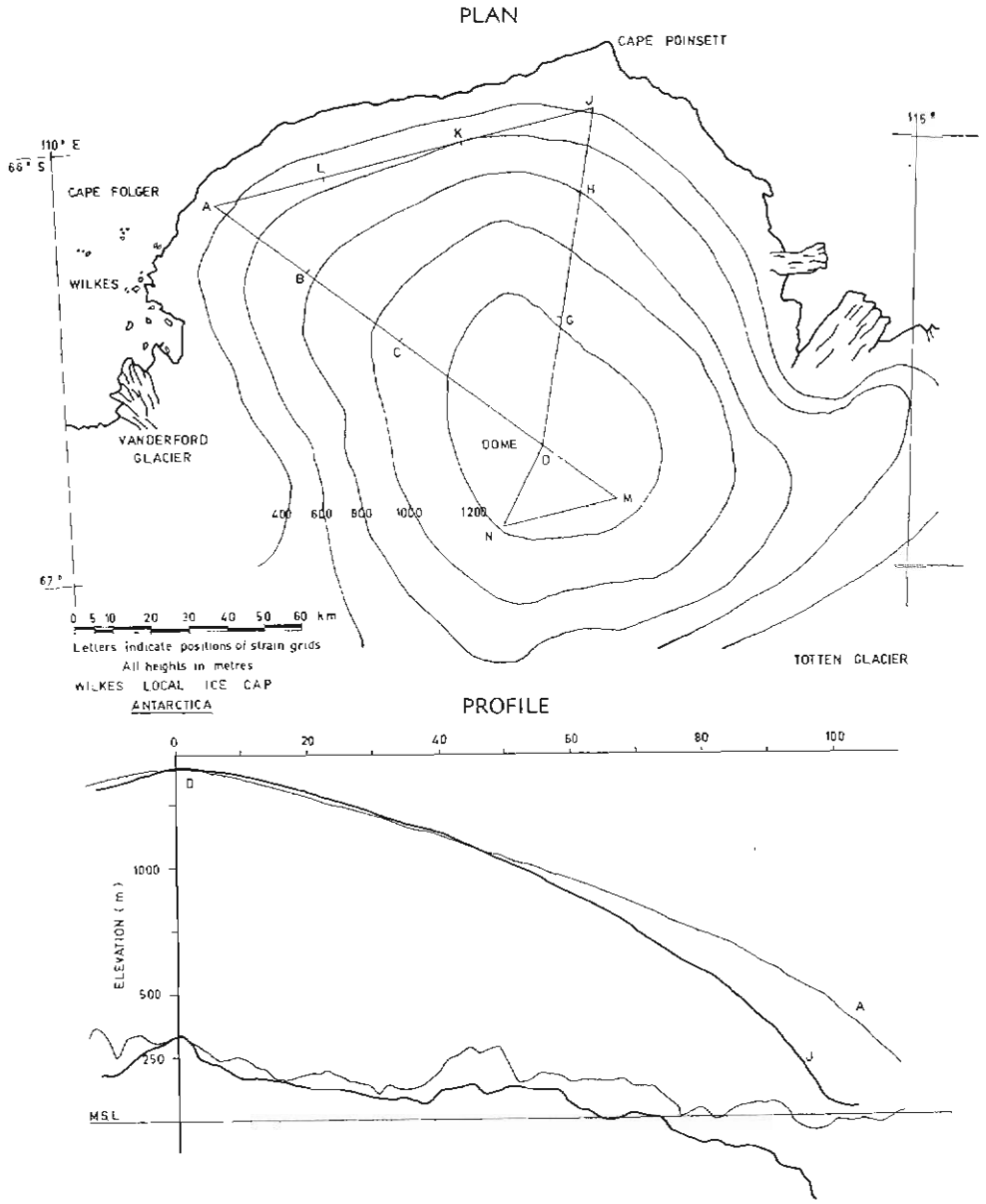

FIG. 1.4. Typical ice cap plan and profiles for the Wilkes Ice Cap from McLaren (1968).

These results have already been successfully used to determine the ice flow law parameters from measurements of the vertical velocity profile in glaciers using boreholes and inclinometers. The results so far (Mathews 1959, Gerrard, Perutz and Roch 1952, Meier 1960, Paterson 1963) are very encouraging for the application of the theory.

1.3.2. *The transverse velocity profile*

The transverse velocity profile has also been calculated for special cases of cross-section shape by Nye (analytically 1952, numerically 1965). Many cross-sectional shapes of glaciers and their associated horizontal velocity profiles have been measured and then have been used to determine the natural ice flow parameters with reasonable success.

1.3.3. *The longitudinal profiles of velocity* and strain rate are still comparatively little known and their theory has not yet advanced to the stage of verifiable predictions in terms of the boundary conditions. Much of the present work will be concerned with this problem and the theoretical interpretation of some of the few longitudinal profiles of velocity elevation and ice thickness at present available for glaciers, ice shelves and ice caps.

1.4. VERTICAL VELOCITY

Once the longitudinal profile of the average horizontal velocity has been obtained the vertical motion of the surface can be calculated from the ice thickness, velocity, strain rate, and slopes of the surface and bedrock.

It is necessary here to distinguish between the vertical velocity of the ice at the surface and the vertical velocity of the surface itself. The former gives the flow paths within the ice mass while the latter gives the rate of change of the ice mass thickness and elevation. Both these velocities are important for understanding the state of balance of the ice mass and its history of change.

1.5. MASS BALANCE, STATIONARY STATE AND BALANCED STATE

Once the vertical velocities have been calculated, the question arises whether the surface is rising, falling with time, or is remaining stationary. To answer this, the vertical velocities must be compared with the accumulation (or ablation) pattern. Only in regions where the accumulation rate matches the vertical velocity of the surface will the surface profile be stationary at that moment. But since the velocity profile may be changing with time, so may the state of balance.

For a given size and shape of an ice mass, and a given accumulation pattern, there exists an ideal velocity distribution which maintains this shape, and size, with the net loss from flow equalling the total accumulation gain everywhere. By comparing the actual measured velocity distribution with that calculated for balance a further check can be made on how the shape and size of the ice mass is changing with time.

1.6. CHANGE OF FORM AND HISTORY OF AN ICE MASS

The rate of change of the ice mass shape with time may be obtained for a given moment from the velocity distribution and the accumulation pattern. This

rate of change may then be extrapolated forward or backwards in time to obtain the future or past historics of the ice cap. But as the form changes, so will the velocity distribution and therefore also the rate of change. Hence, in calculating the history of change, in the ice cap, size and velocity changes must be considered together.

This applies even with the climate (and accumulation pattern) constant. Further variation in the history may be studied by considering patterns of accumulation which change with time.

* * * *

These are the main topics of discussion in this work. A short synopsis of their treatment in the remaining sections is now presented.

1.7. SYNOPSIS

In the introduction it is shown that the basic problem of ice dynamics may be divided into three sections: (i) establishing the equations of motion; (ii) introducing the stress—strain rate relation for ice; and (iii) solving the equations of motion for the three special types of ice masses: glaciers, ice shelves, ice caps.

In Section 2 the *flow law of ice* is examined. The dependence is considered of the stress—strain rate relation on various parameters such as the stress magnitude and configuration, the ice temperature, the density or porosity, the crystal size, and the crystal orientation. Variations in the ice type cause variations in the stress—strain relation of such a magnitude that the resultant range of velocities calculated in ice masses from various experimental flow laws is too large to be used for balance calculations. This suggests that, at this stage, it is more profitable to determine the flow parameters from measured velocity distributions in ice masses. In cold ice masses the most important parameter governing the stress—strain rate relation is the ice temperature.

Section 3 sets out the *basic equations of motion* generally, incorporating the flow law, and shows how symmetry considerations and the boundary conditions of the three special types of ice mass allow certain simplifications to be made. The profile of velocity in the plane perpendicular to the direction of flow is then examined (*vertical and transverse profiles*) for the case of zero longitudinal strain rate and constant temperature.

Section 4 deals with the *temperature* distribution in ice masses and its influence on the velocity profile. Because the motion generates heat from internal viscous friction the velocity distribution also effects the temperature, so that this positive feedback is taken into consideration. Steady-state temperature distributions are calculated incorporating accumulation at the surface, vertical motion, horizontal motion, temperature change at the surface, and the growing or subsiding of ice caps. Finally, special cases of non-steady-state temperatures are considered to assess the approach to steady state in existing ice masses.

In Section 5 the results of the earlier sections on cross-section profiles and temperature distributions are used in developing equations for the *longitudinal velocity* and strain rates along a flow line in terms of the boundary dimensions of the ice mass and the ice flow law parameters. Two-dimensional flow is first con-

sidered, next this is generalized to parallel three-dimensional flow, and then a method to account for diverging flow and transverse strain is developed. Finally, an analysis of steady-state flow over undulations is carried out.

Section 6 *applies* the theoretical considerations developed in Section 5 to the three major type of ice masses—ice shelves, glaciers and ice caps. Equations for longitudinal velocity and strain rates are obtained and used to determine empirical estimates of the ice flow law parameters from measurements made on typical examples of these ice masses.

Once the velocity distributions and the ice mass boundary dimensions are known, the *state of balance* and *rate of change* of the ice mass can be calculated, given the pattern of supply, i.e., accumulation rate. Steady-state profiles are examined and their dependence on the flow parameters, accumulation pattern, and bedrock shape are analysed. Equations for particle paths are discussed and trajectories calculated for typical examples of ice masses. Finally, non-steady-state changes in ice cap shape are considered and short term calculations illustrated.

The final section presents a summary and conclusions, setting out the major results of the report and indicating their use, limitations and possible lines of extension.

2. THE FLOW LAW OF ICE

Many measurements of the deformation rates of ice have been made by various workers under different conditions and using a large variety of types of ice. In this section an attempt is made to review these results in order to establish a general empirical flow law and to determine how it depends on such parameters as stress, temperature, and the properties of the ice sample. For ice masses which are naturally deforming we are not concerned with rapid changes of loading, and hence we here deal only with steady-state creep.

For stress ranges occurring in natural ice masses (less than 400 bars), the ice may be regarded as incompressible. Dorsey (1940) quotes values of compressibility less than $40 \times 10^{-6}\text{bar}^{-1}$ between 0 and 300 bars. The most important effect of the hydrostatic pressure on the ice is the lowering of the melting point which falls approximately linearly with hydrostatic pressure to $-5°\text{C}$ at 590 bars (Dorsey 1940). Rigsby (1958) showed that the effect of the hydrostatic pressure up to 350 bars had negligible effect on the shear strain rate of the ice, provided the temperature difference from the melting point was kept constant. Hence, we need only consider deformations of the "pure shear" type (no change in volume) and neglect the effect of hydrostatic pressure, keeping in mind that the temperature must be referred to the melting point.

2.1. STRESS AND STRAIN RATE TENSORS

We denote the stress and strain rate tensors σ_{ij}, $\dot{\varepsilon}_{ij}$ by

$$\sigma_{ij} = \begin{pmatrix} \sigma_x & \tau_{xy} & \tau_{xz} \\ \tau_{xy} & \sigma_y & \tau_{yz} \\ \tau_{xz} & \tau_{yz} & \sigma_z \end{pmatrix} \qquad \dot{\varepsilon}_{ij} = \begin{pmatrix} \dot{\varepsilon}_x & \dot{\gamma}_{xy} & \dot{\gamma}_{xz} \\ \dot{\gamma}_{xy} & \dot{\varepsilon}_y & \dot{\gamma}_{yz} \\ \dot{\gamma}_{xz} & \dot{\gamma}_{yz} & \dot{\varepsilon}_z \end{pmatrix}$$

The principal stress and strain rates will be taken as

$$\sigma_{ij} = (\sigma_1, \sigma_2, \sigma_3) \qquad \dot{\varepsilon}_{ij} = (\dot{\varepsilon}_1, \dot{\varepsilon}_2, \dot{\varepsilon}_3).$$

The condition of incompressibility may then be written

$$\dot{\varepsilon}_{ii} = \dot{\varepsilon}_1 + \dot{\varepsilon}_2 + \dot{\varepsilon}_3 = \dot{\varepsilon}_x + \dot{\varepsilon}_y + \dot{\varepsilon}_z = 0 \tag{1}$$

The hydrostatic pressure p is given by

$$p = \frac{\sigma_1 + \sigma_2 + \sigma_3}{3} = \frac{1}{3}\sigma_{ii} \tag{2}$$

For deformations of the pure shear type ($\dot{\varepsilon}_{ii} = 0$) we are interested in the stress deviator tensor σ'_{ij}, which is independent of the hydrostatic pressure and defined by

$$\begin{aligned} \sigma'_{ij} &= \sigma_{ij} - \tfrac{1}{3}\sigma_{ii}\,\delta_{ij} \\ \delta_{ij} &= 1, \; i = j \\ &= 0, \; i \neq j \end{aligned} \tag{3}$$

Glen (1958) discusses generalized forms of the flow law involving both the second and third invariants of the stress deviator and strain rate tensors. At this stage, however, it appears that the experimental evidence can be explained satisfactorily by a simpler flow law involving only the second invariants, which we denote by:

$$I_2 = \sigma'_{ij}\sigma'_{ij} \quad \text{and} \quad E_2 = \dot{\varepsilon}_{ij}\dot{\varepsilon}_{ij} = \dot{\varepsilon}'_{ij}\dot{\varepsilon}'_{ij} \tag{4}$$

Nye (1953) postulated a flow law of the type

$$\dot{\varepsilon}_{ij} = \lambda\sigma'_{ij} \tag{5}$$

where λ is a function of the invariants I_2 and E_2.

Nye defined "effective shear stress" τ_e, and "effective shear strains" $\dot{\varepsilon}_e$, in terms of the second invariants as (cf., e.g., Jaeger 1964),

$$\tau_e^2 = \tfrac{1}{2}\sigma'_{ij}\sigma'_{ij} = \tfrac{1}{2}(\sigma_1'^2 + \sigma_2'^2 + \sigma_3'^2) = \tfrac{1}{6}[(\sigma_2 - \sigma_3)^2 + (\sigma_3 - \sigma_1)^2 + (\sigma_1 - \sigma_2)^2] \tag{6}$$

and

$$\dot{\varepsilon}_e^2 = \tfrac{1}{2}\dot{\varepsilon}_{ij}\dot{\varepsilon}_{ij}.$$

The second invariants may also be interpreted in terms of the shear stress across the octahedral shear plane, whose normal has direction cosines $l = m = n = \dfrac{1}{\sqrt{3}}$, with respect to the principal axes. The normal stress on this plane is equal to the hydrostatic pressure. The octahedral shear stress and strain rates have the values

$$\begin{aligned} \tau_0 &= \frac{1}{\sqrt{3}}(\sigma'_{ij}\sigma'_{ij})^{\frac{1}{2}} = \tfrac{1}{3}[(\sigma_2 - \sigma_3)^2 + (\sigma_3 - \sigma_1)^2 + (\sigma_1 - \sigma_2)^2]^{\frac{1}{2}} \\ \dot{\varepsilon}_0 &= \frac{1}{\sqrt{3}}(\dot{\varepsilon}'_{ij}\dot{\varepsilon}'_{ij})^{\frac{1}{2}} = \tfrac{1}{3}[(\dot{\varepsilon}_2 - \dot{\varepsilon}_3)^2 + (\dot{\varepsilon}_3 - \dot{\varepsilon}_1)^2 + (\dot{\varepsilon}_1 - \dot{\varepsilon}_2)^2]^{\frac{1}{2}} \end{aligned} \tag{7}$$

We note that

$$\tau_e = \sqrt{3/2}\,\tau_0 \qquad \text{and} \qquad \dot{\varepsilon}_e = \sqrt{3/2}\,\dot{\varepsilon}_0.$$

The maximum shear stress and strain rates are given by

$$\tau_m = \frac{\sigma_1 - \sigma_3}{2} \qquad \text{and} \qquad \dot{\varepsilon}_m = \frac{\dot{\varepsilon}_1 - \dot{\varepsilon}_3}{2} \tag{8}$$

where $\sigma_1, \sigma_3, \dot{\varepsilon}_1, \dot{\varepsilon}_3$ are the maximum and minimum principal stresses and strain rates.

We now determine these generalized shear stresses in several common stress situations.

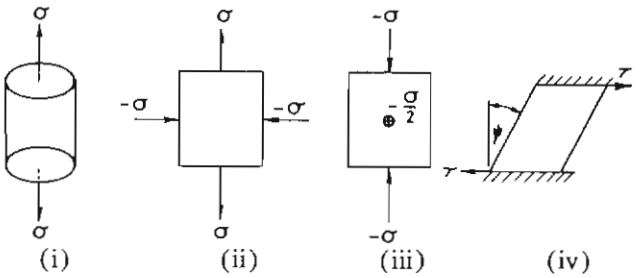

(i) Extension in one dimension with contraction in the other two.
(ii) Pure shear (two dimensions).
(iii) Pure shear plns hydrostatic pressure (two dimensions).
(iv) Simple shear.

(i) In *simple extension* we have principal stresses $(\sigma, 0, 0)$, the hydrostatic pressure is $p = \sigma/3$, and $\sigma'_{ij} = (2/3\sigma, -\sigma/3, -\sigma/3)$, hence

$$\tau_0 = \frac{\sqrt{2}}{3}\sigma, \qquad \tau_e = \frac{1}{\sqrt{3}}\sigma, \qquad \tau_m = \tfrac{1}{2}\sigma$$

$$\simeq .471\sigma \qquad \simeq .578\sigma \qquad = .5\sigma.$$

The principal strain rates are $(\dot{\varepsilon}, -\dot{\varepsilon}/2, -\dot{\varepsilon}/2)$, hence

$$\dot{\varepsilon}_0 = \frac{1}{\sqrt{2}}\dot{\varepsilon}, \qquad \dot{\varepsilon}_e = \frac{\sqrt{3}}{2}\dot{\varepsilon}, \qquad \varepsilon_m = \tfrac{3}{4}\dot{\varepsilon}$$

$$\simeq .707\dot{\varepsilon} \qquad \simeq .865\dot{\varepsilon} \qquad = .75\dot{\varepsilon}.$$

We note here that the "effective shear stress" is larger than the maximum shear stress and hence cannot correspond to an actual shear stress in the body.

(ii) For *pure shear* in *two dimensions* with zero hydrostatie pressure, the principal stresses are $(\sigma, 0, -\sigma)$, also $p = 0$ and $\sigma'_{ij} = (\sigma, 0, -\sigma)$.

$$\therefore \quad \tau_0 = \sqrt{2/3}\,\sigma, \qquad \tau_e = \sigma, \qquad \tau_m = \sigma.$$

The prineipal strain rates are $(\dot{\varepsilon}, 0, -\dot{\varepsilon})$.

$$\therefore \quad \dot{\varepsilon} = \sqrt{2/3}\,\dot{\varepsilon}, \qquad \dot{\varepsilon}_e = \dot{\varepsilon}, \qquad \dot{\varepsilon}_m = \dot{\varepsilon}.$$

(iii) The deformation consisting of a *simple compression* with movement confined to *two dimensions* is equivalent to a pure shear $(\sigma/2, 0, -\sigma/2)$, of the type (ii) plus a hydrostatic pressure $-\sigma/2$.
The principal stresses are $(\sigma, \sigma/2, 0)$, $p = \sigma/2$, $\sigma'_{ij} = (\sigma/2, 0, -\sigma/2)$.
Hence

$$\tau_0 = \sqrt{2/3}\,\sigma/2, \qquad \tau_e = \sigma/2, \qquad \tau_m = \sigma/2.$$

The principal strain rates are $(\dot{\varepsilon}, 0, -\dot{\varepsilon})$.
Hence

$$\dot{\varepsilon} = \sqrt{2/3}\,\dot{\varepsilon}, \qquad \dot{\varepsilon}_e = \dot{\varepsilon}, \qquad \dot{\varepsilon}_m = \dot{\varepsilon}.$$

(iv) The *"simple shear"* type deformation corresponds to the typical gradient of horizontal velocity V with depth z in an ice mass fixed at the base.
i.e.,

$$\dot{\psi} = \frac{dV}{dz}$$

The principal stresses are the same as for pure shear, viz., $(\tau, 0, -\tau)$, $p = 0$.

Hence

$$\tau_0 = \sqrt{2/3}\,\tau, \qquad \tau_e = \tau, \qquad \tau_m = \tau.$$

The principal strain rates are $(\dot{\psi}/2,\ 0,\ -\dot{\psi}/2)$.

Hence,

$$\dot{\varepsilon} = \sqrt{2/3}\,\frac{1}{2}\frac{dV}{dz}, \qquad \dot{\varepsilon}_e = \frac{1}{2}\frac{dV}{dz}, \qquad \dot{\varepsilon}_m = \frac{1}{2}\frac{dV}{dz}.$$

Since the "effective shear stress" equals the shear stress in simple shear and is a constant factor times the octahedral shear stress in a more complex stress situation, the term "shear stress", τ, unspecified, will be taken generally in what follows to imply the effective shear stress. We adopt a similar convention for the shear strain rate $\dot{\varepsilon}$.

From equations (5) and (6) Nye (1953) obtained the relation between shear stress and strain rate as

$$\dot{\varepsilon} = \lambda\tau \tag{9}$$

For a given ice type I and temperature T it may be expected that λ is a function only of the shear stress τ.
i.e.,

$$\lambda = \lambda_{IT}(\tau) \tag{10}$$

To determine the flow law of ice, then, it is necessary to establish the function λ, i.e., the ratio of the shear strain rate to the shear stress, and show how this function depends on stress, temperature and the type of ice, defined by certain properties such as crystal sizes, and orientations, density and type of porosity.

Since we are concerned here with the application of the knowledge of the flow law to the study of the dynamics of large ice masses, we concentrate mainly on the stress, temperatures and types of ice found in large ice masses.

2.2. SHEAR STRESSES IN NATURAL ICE MASSES

As a first approximation, we consider the expression of Nye (1952) for the shear stress τ_b at the base of an ice mass of surface slope α, ice thickness h, and density ρ.

$$\tau_b = \rho g h \alpha \tag{11}$$

Since the surface slope α is zero for positions on dome summits or ice divides there is essentially no lower limit for τ_b.

However, it is found that for the various ice masses τ_b has a fairly narrow range. Fig. 2.1 shows a profile through the Antarctic ice cap from Wilkes to Vostok from Walker (1966). Here τ_b generally increases from 0·3 to 1·5 bars as the coast is approached.

For a cross-section of Greenland, Haefeli (1961) shows τ_b to increase from 0 at the summit to 0·98 bars at 150 km from the coast.

Other examples include:

Wilkes local ice cap (McLaren 1968)	0·2 bars near the summit to 1·2 bars near the coast.

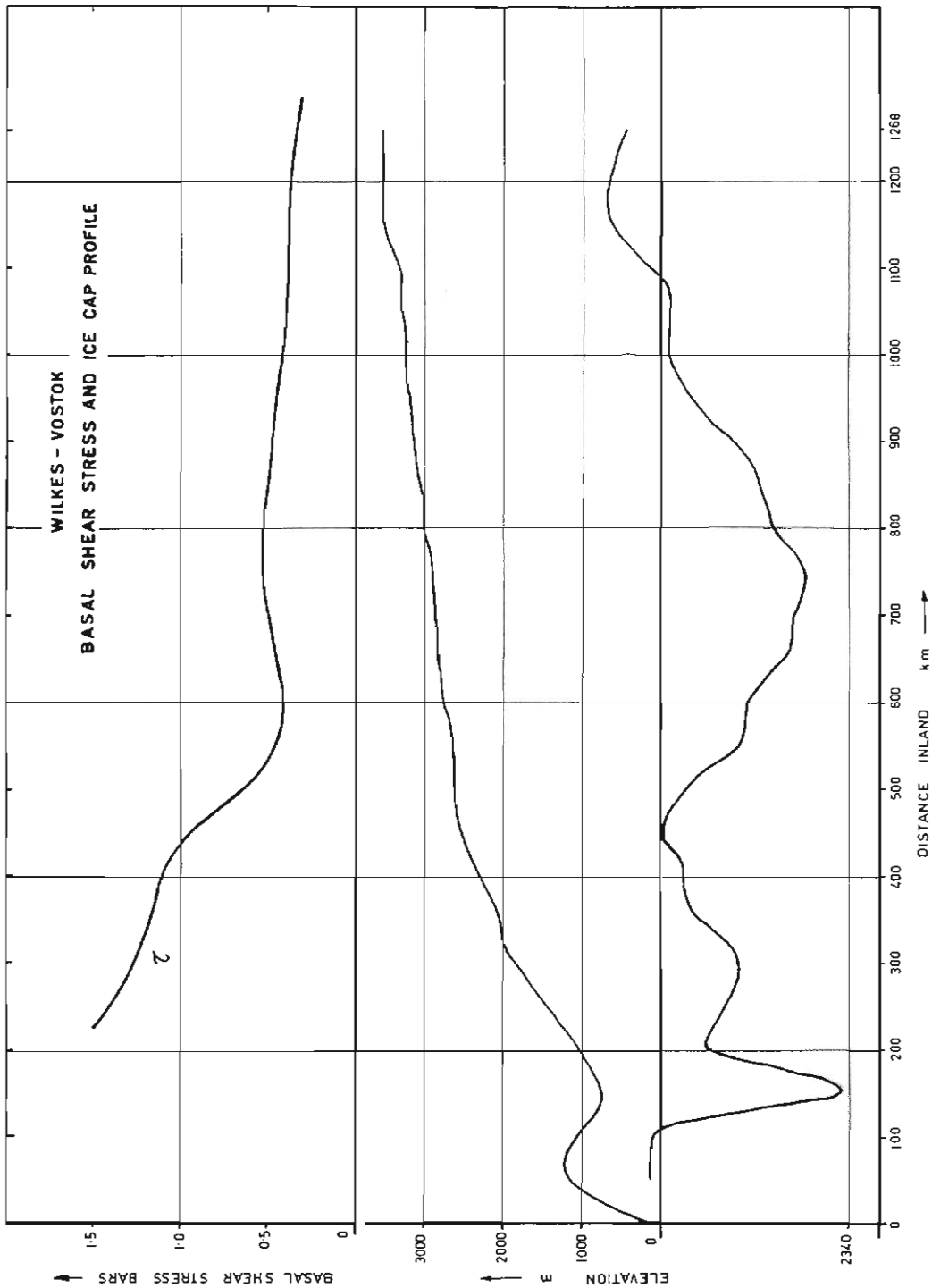

FIG. 2.1. Basal shear stress for an ice cap shown with elevation and bedrock profile for Antarctica, Wilkes—Vostok profile, from Walker (1966).

Roosevelt Island (Clapp 1965)	0·2 bars near the summit to 1·0 bars near the edge.
Athabasca Glacier (Paterson unpublished)	Calculated shear stresses at the base vary between 0·5 and 1·1 bars.
Satskatchewan Glacier (Meier 1960)	Basal stresses along the tongue vary between 0·6 and 1·2 bars.
Barnes ice cap, Baffin Island (Orvig 1953)	The basal stress varies largely between 0·1 and 1·0 bars with an average about 0·5 bars.

Since in ice caps or glaciers the shear stress may be expected to have its greatest values at the base, the shear stresses encountered elsewhere in the ice will normally be less than the values listed above.

Other shear stresses in ice masses may be estimated from measurements of strain rates at the surface. Some typical values are listed in Table 2.1 below.

TABLE 2.1

MEASURED LONGITUDINAL STRAIN RATES

Ice Mass	Longitudinat strain rate 10^{-4} yr^{-1}	Temperature —°C	Estimated shear stress bars	Reference
Wilkes ice cap	1–30	24–12	0 01–0·40	McLaren 1968
Amery Ice Shelf	5–60	23–20	0·02–0·70	Budd 1966
Roosevelt Island	2–8	24	0·02–0·30	Clapp 1965
Saskatchewan Glacier	300	0	0·40	Meier 1960
Athabasca Glacier	200	0	0·20	Paterson (unpublished)

Although higher strain rates and stresses may exist in glaciers, especially near crevassed zones and ice falls, the shear stress seldom reaches 2 bars. Hence, the stresses we are chiefly concerned with in natural ice masses range from 0·1 to 1·5 bars, with strain rates from 10^{-11} to 10^{-8} sec^{-1}. Laboratory and field measurements of stress and strain rates of ice in this region and beyond it, from 0·01 to 10 bars, will now be reviewed.

2.3. LABORATORY MEASUREMENTS OF THE FLOW LAW OF ICE

The results of various laboratory measurements of the deformation of ice by Glen (1954, 1955), Steinemann (1958), Butkovitch and Landauer (1960), Mellor and Smith (1966), Voitkovski (1963), are illustrated in Figs. 2.2 and 2.3. Some results of field measurements on natural ice masses by Butkovitch and Landauer (1958), Gow (1963), Gerrard et al. (1953) are included. All values have been converted to the same units, viz., octahedral shear stress, and strain, rates in bars and sec^{-1} respectively.

Table 2.2 lists the types of ice used in the flow measurements. We will examine the dependence of the stress—strain rate relation separately on the parameters stress, temperature, and the ice type which includes density, crystal size, and crystal orientation.

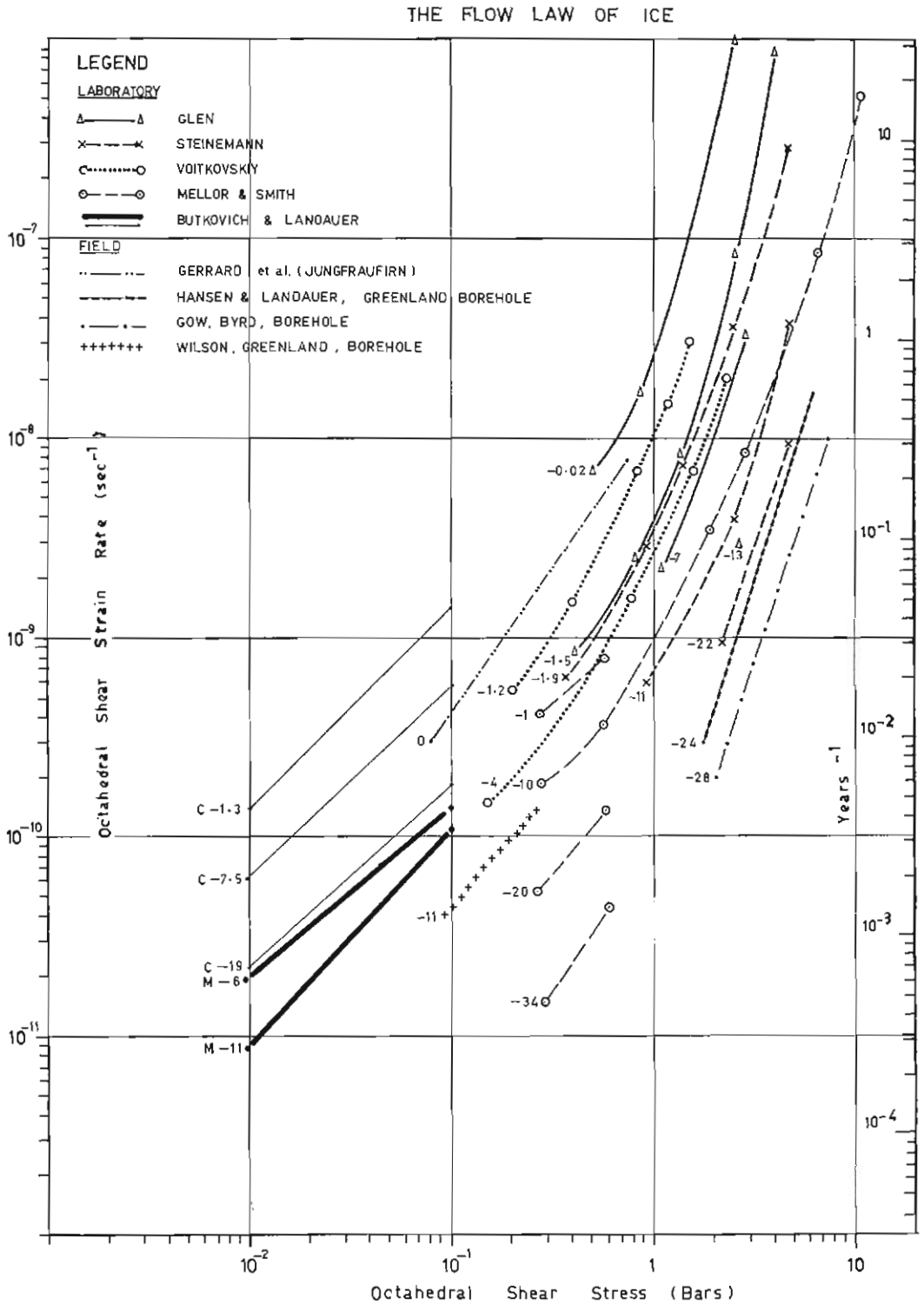

FIG. 2.2. Ice strain rates versus stress from laboratory and field measurements. The values of Mellor and Smith have been extrapolated to density 0.917 g cm^{-3}. The temperatures are indicated in degrees centigrade.

2.3.1. STRESS DEPENDENCE OF FLOW LAW

The results of Glen (1955), Steinemann (1958) and also Mellor (1959) are largely in the high stress range 1 to 10 bars shear stress and these conform closely to a power law of the form

$$\dot{\gamma} = \left(\frac{\tau}{B}\right)^n \tag{12}$$

where $n = 3$ to 4,

Even in these stress ranges a slight upward curvature in the graphs suggests that n may increase with stress. Voitkovski (1960) considered that Glen's measurements, however, were not appropriate to the study of steady-state creep

TABLE 2.2

TYPES OF ICE USED IN DEFORMATION EXPERIMENTS

Author	Density g cm^{-3}	Crystal size approx. diameter	Orientation	Comments
Glen (1954)	(≈0.917)	(0·2 cm)	≈random	Artificial ice made in mould. slightly cloudy but density indistinguishable from pure ice.
Steinemann (1958)	(≈0·917)	≈0·85 mm	≈random	Small-grained polycrystalline artificial ice.
Voitkovski (1960)	≈0·917	Much smaller than sample size	(≈random)	Artificial ice beams and cylinders.
Butkovitch and Landauer (1960)	0·917	3 cm	Elongated axes parallel to load direction	C2 ice: Commercial artificial ice 1-2cm × 4-5 cm, bubble-free and with one axis elongated,
	0·905	0·3 cm	≈random	MP1 ice: Small-grained glacier ramp ice (Greenland) with small irregular air bubbles.
Mellor & Smith (1966)	0·83	0·8 mm	random	Artificial ice made from water-soaked snow cylinders. Air bubbles (0·5 mm diameter) uniformly distributed.

because they were for stresses largely above the limit of the range required for prolonged steady-state creep. As a consequence, the secondary creep stage in most of Glen's measurements was simply a stage between the primary and tertiary creep stages. Voitkovski (1960) found that the magnitude of the stress which exceeded the limit for prolonged steady-state creep varied with temperature. It ranged from 1·6 to 3 bars between −1·2 and −4°C. Below this limit-stress the steady-state creep continued at a constant rate for long periods, e.g., at 1 bar, at −1°C, a constant creep rate was measured for over 5,000 hours (i.e., ≃ 7 months). It is this long-term type of steady-state deformation which is relevant to the movement of ice masses (except perhaps in the case of "glacier surges").

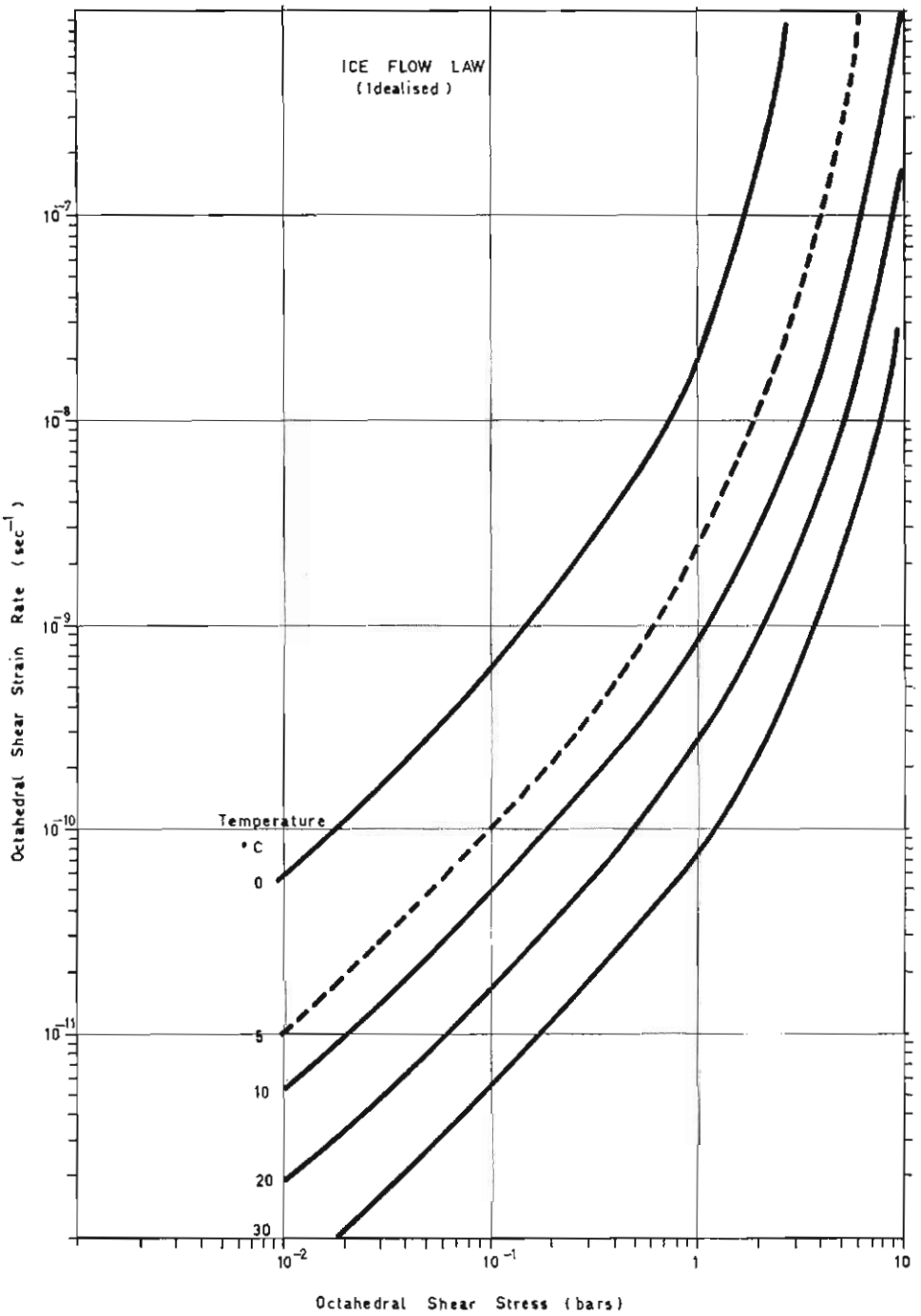

FIG. 2.3. Idealised curves for the flow law of ice are shown compiled and interpolated from Fig. 2.2. The resultant accuracy is about 50% for strain rates.

The measurements below 1 bar by Butkovitch and Landauer (1960), Mellor and Smith (1966) and the more difficult to interpret field data of Meier (1960) suggest that the decrease of n, the power law index, as the stress decreases, continues so that for low stress (up to 0 5 bars) the stress-strain rate is essentially linear.

This means that the simple power form of the flow law is only appropriate for a small range of stress over which n can be considered constant. In order to cover the range of stresses from 0·1 to 2 bars it is necessary to use a flow law which allows for the varying slope of the curves in Fig. 2.2. Meier (1958, 1960) suggested a flow law of the type

$$\dot{\gamma} = a\tau + b\tau^n \tag{13}$$

where a and b are constant for a given temperature and ice type and n is constant about 4·5. He found this satisfactory for interpreting the ice flow data of the Saskatchewan Glacier.

This form of flow law was also examined by Butkovitch and Landauer (1960) together with a flow law of the type

$$\dot{\gamma} = a \sinh\left(\frac{\tau}{\tau_0}\right) \tag{14}$$

It was found that the form (13) was most suitable in covering both their low and high stress tests with the constants given by

$$\dot{\gamma} = .41 \times 10^{14}\tau + .90 \times 10^{-26}\tau^3,$$

where $\dot{\gamma}$ is in sec^{-1} and τ is in dynes cm^{-2}, at $-5°\text{C}$.

Mellor and Smith (1966) confirmed the flow law of the type (13) and obtained values of the constants as follows:

$$\dot{\varepsilon}_z = 1{\cdot}8 \times 10^{-9}\sigma_z + 1{\cdot}5 \times 10^{-10}\sigma_z^{3{\cdot}5} \text{ at } -4°\text{C}$$

and

$$\dot{\varepsilon}_z = 1{\cdot}5 \times 10^{-9}\sigma_z + {\cdot}8 \times 10^{-10}\sigma_z^{3{\cdot}5} \text{ at } -10°\text{C},$$

where $\dot{\varepsilon}_z$ and σ_z are the strain rate and stress of uniaxial longitudinal compression, in units of sec^{-1} and bars respectively.

It should be noted that the density of their samples was 0·83 g cm^{-3} and the effect of this will be discussed in 2.3.1. However, they supply data which allow their measurements to be extrapolated to pure ice density. This then brings their results to closer agreement with the others of Fig. 2.2 made on high density ice.

Thus we conclude that in the range 0.01 to 2 bars the stress dependence indicated by equation (13) for the ice flow law is satisfactory.

For still higher shear stresses the results of Gow (1963) suggest that the value of n tends to increase even further, to values of 5 and 6 as the stress increases from 10 bars to 30 bars. However, it is important here to note the difference between measurements made on naturally deforming ice and measurements made on disturbed ice, such as in bores holes or tunnels. In the latter cases the crystal orientation (cf. Section 2.5.3. below) are not initially appropriate for the new deformation of closure. As deformation proceeds it may be expected that the crystal fabrics

change to become compatible with and enhance the deformation. This may account for the accelerating closure rates observed by Gow. On the other hand, the high shear stresses occurring in the borehole may simply be beyond the limit for prolonged steady-state creep.

A close look at the available measurements of stress and strain rates in ice, as illustrated in Fig. 2.2, reveals that the range in which we are most interested for the dynamics of large ice masses (0·1 to 1 bar) is also the one in which there is the largest gap in the laboratory measurements. This suggests that an extensive laboratory study is warranted to fill this gap. In this regard it is also important that the stress-strain rate tests be carried on over a long period to ensure that the prolonged steady-state creep as observed in natural ice masses occurs in the laboratory samples. To obtain results applicable to the major ice caps the temperature range of the measurements will have to be extended to —60°C.

2.4. THE EFFECT OF TEMPERATURE ON THE FLOW LAW OF ICE

Fig. 2.4 shows the results of strain rate versus temperature for different stresses compiled from the laboratory measurements of Mellor and Smith (1966), Butkovitch and Landauer (1960), Steinemann (1958) and Voitkovski (1960).

To represent the dependence of strain rate on temperature, some previous workers have used a relation of the form

$$\dot{\gamma} = A(\tau)e^{-Q/RT} \tag{15}$$

where A (τ) is the stress dependent function for constant temperature;
Q is the "activation energy" (cal/mole);
R is the gas constant ($\sim$1·90 cal/mole/°K);
T is the absolute temperature.

For the low stresses (0·5 to 1 bar) Mellor and Smith found $Q \simeq$ 10 — 12 k cal/mole, Butkovitch and Landauer (1960) $Q \simeq$ 14 k cal/mole.

The results of Steinemann (1958) and Glen (1955) suggest that, for higher stresses and strain rates, Q may be higher. Mellor and Smith (1966) pointed out that the Arrhenius function $\exp(-Q/RT)$ is not relevant for the range of temperatures encountered in natural ice masses. The observations can be more simply represented by an empirical law of the form

$$\dot{\gamma} = A(\tau)e^{K\theta} \tag{16}$$

where K is constant
and θ is the temperature in °C.

From Mellor and Smith's (1966) data ($\tau \simeq$ 0·5 to 1 bar) we find $K \simeq 1/11$. From Butkovitch and Landauer's (1960) data $K \simeq 1/9$. From Steinemann's (1958) data at high stresses $\simeq$ 2 bars, we find $K \simeq 1/6$. Voitkovski (1960) states that equation (15) was not suitable for representing the dependence of the flow law on temperature because it did not match his experimental data's high increase in strain rate as freezing point is approached. He found the following relation more appropriate,

$$\dot{\gamma} = \frac{K}{1-\theta}\tau^n \tag{17}$$

where γ, τ are the shear-strain rate, and stress, θ is the temperature in °C and n is a constant $\simeq 1{\cdot}6$ to $2{\cdot}2$ in the stress range $0{\cdot}1$ to 3 bars, and $K = (1{\cdot}6$ to $4) \times 10^5$ °C/Kg/hr. Voitkovsky's results to −40°C also may be approximated by the expression (16)

$$\dot{\gamma} = A(\tau)e^{K\theta}.$$

In this case $K \simeq 1/10$. This relation fits well at low temperatures but, as zero is approached, the measured deformation rate becomes greater.

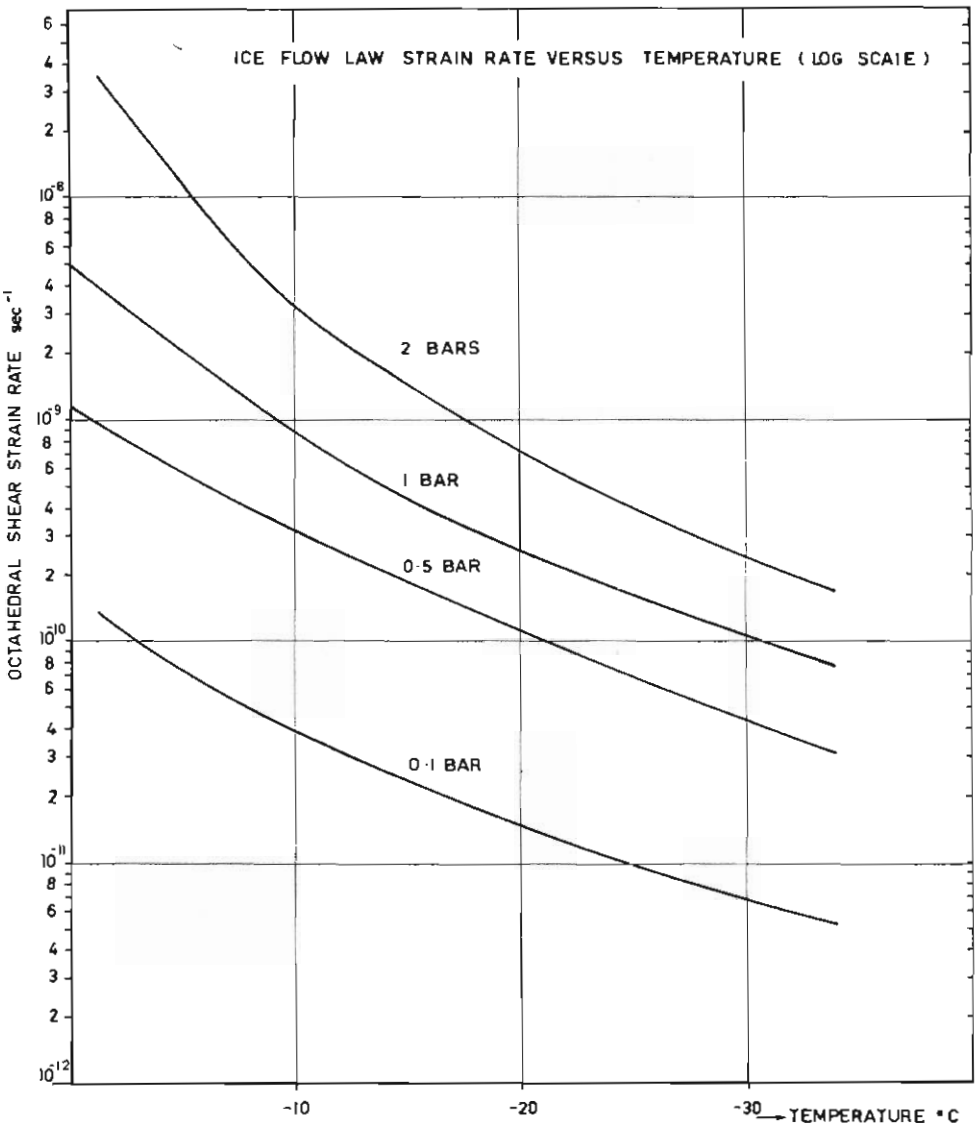

FIG. 2.4. Shear strain rate versus temperature for different stresses compiled and extrapolated from Fig. 2.2.

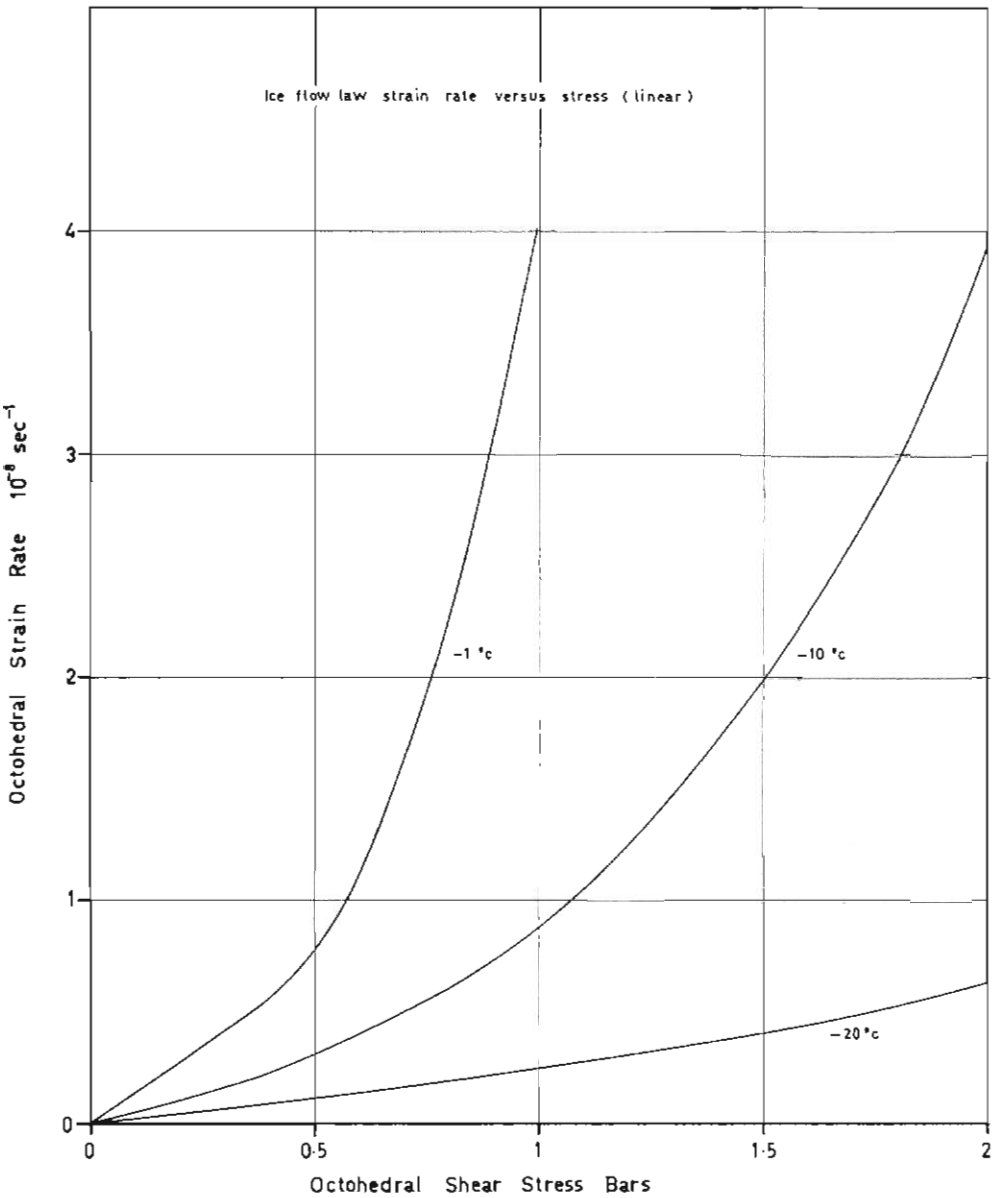

FIG. 2.5. Shear strain versus shear stress for different temperatures on linear co-ordinates shows the rapid increase of strain rate at high stresses. Compiled from Fig. 2.2.

Pending more precise data, then, we may adopt any of the temperature functions (15), (16) or (17) to represent the temperature dependence of the flow law and, with appropriately chosen values of the constants in a given temperature range, we may expect reasonable agreement provided extrapolation is not taken too far out of the range.

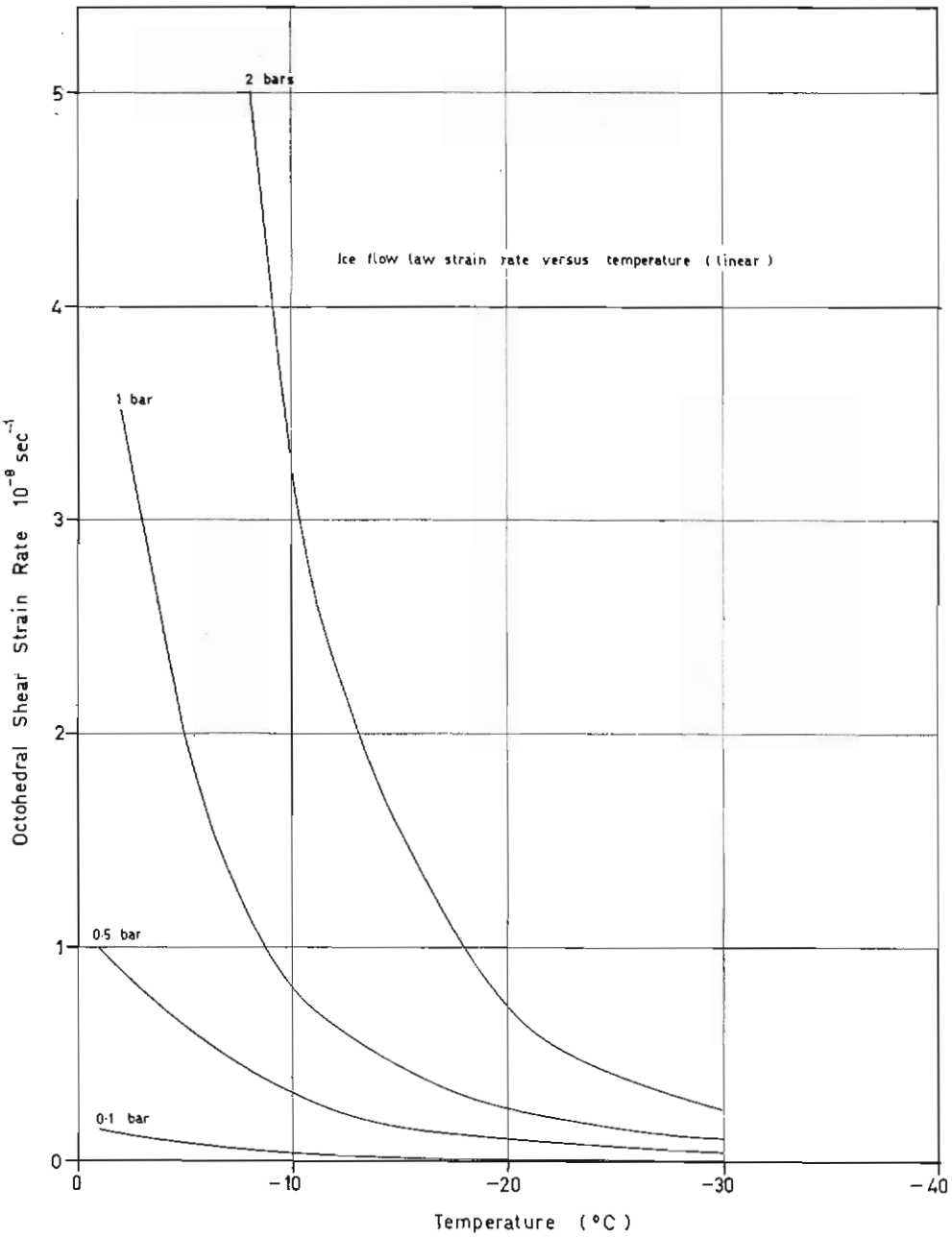

FIG. 2.6. Shear strain rate versus temperature, for different stresses on linear co-ordinates, shows the increase of strain rate at high temperatures and high stresses. Compiled from Fig. 2.2.

To illustrate the rapid change of the strain rate of ice with temperature and stress we refer to the plots in linear co-ordinates of strain rate versus stress (Fig. 2.5) and strain rate versus temperature (Fig. 2.6).

Figures 2.5 and 2.6 show that the strain rate becomes very large as the shear stress increases over 0·5 bars and as the temperature approaches zero. From this it is hardly surprising to find that in naturally deforming ice the shear stress is generally not much greater than 1 bar, unless the temperature is very low.

2.5. OTHER PARAMETERS INVOLVED IN THE FLOW LAW OF ICE

2.5.1. *Ice density*

The results of Mellor and Smith (1966) show (Fig. 2.7) that the strain rate tends to decrease with increasing density. This is further confirmed by comparison of Mellor's results for ice of density 0·83 (1966) and 0·87 (1959) with those of workers using ice of higher density [Steinemann (1958) and Glen (1955)].

Extrapolation of Mellor and Smith's (1966) density—strain rates dependence (Fig. 2.7) to the density of pure iee allows his curves of strain rates vs. stress to be converted to curves for ice of density 0·917. The agreement with other workers then becomes very good, as shown in Fig. 2.2.

The range of change of about an order of magnitude decrease in strain rate with a 0·15g cm^{-3} increase in density is about double the rate found by Nakaya (1958) from the viscous damping of 200-400 cycle frequency vibrations in the ice. However, the relation between viscosity values determined by these different methods is still not well known.

Now, since we find that in naturally deforming ice (glaciers and ice caps below the surface firn) the density is generally high and relatively constant, we need expect variations in the density to have only a slight effect on the ice strain rate. In most ice caps and glaciers the low-density surface firn layer is usually only a small fraction of the total thickness, and hence may be neglected.

Bender and Gow (1961) show the increase in density with depth for the Antarctic ice cap at Byrd to the depth of 250 m. The 0 90 g cm^{-3} density is reached by 120 m. depth. Langway (1962) shows the density—depth rate profile from the 411 m hole at site 2 Greenland. The 0.90 density is reached by the depth of 110 m. The thickness at Byrd is ~2, 300 m. and site 2 is ~1,800 m.

Gow (1963) shows how the density increases with depth for several Antarctic ice shelves. For ice shelves the average density from surface to base is often well below that of ice; e.g., for the Ross Ice Shelf, Gow (1963) found the average density through the ice shelf at Little America to be 0.853 g cm^{-3}. Hence, in these cases, the density of the ice must be considered in relation to the flow parameters.

2.5.2. *Ice crystal size effect on the flow law*

Butkovitch and Landauer (1958, 1960) found that, in general for randomly orientated polycrystalline samples of ice, the large crystal samples tended to deform more rapidly than the small crystal samples. The study at low stresses

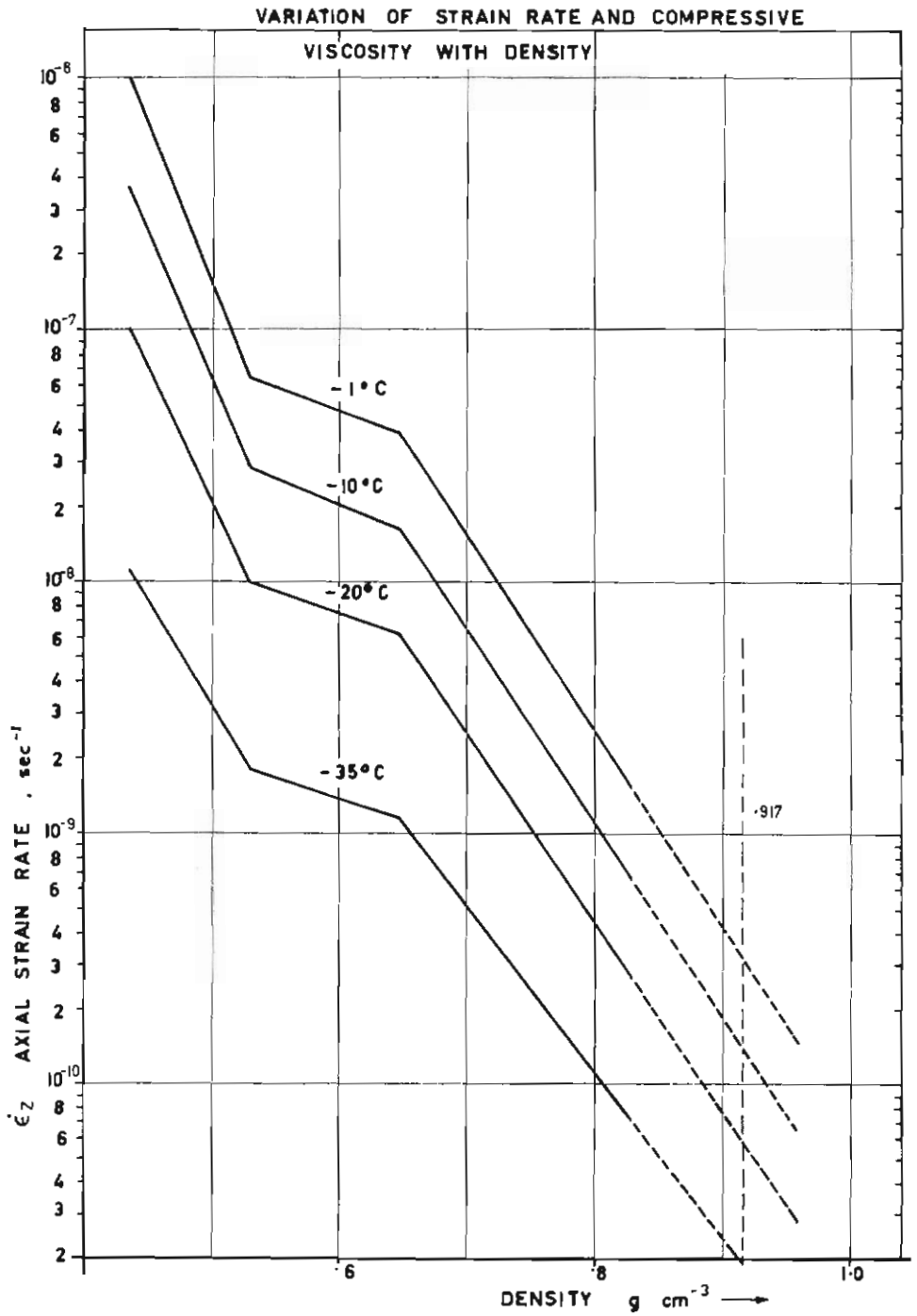

FIG. 2.7. Strain rate versus density for snow and ice samples from Mellor and Smith (1966) and extrapolated to the density of pure ice.

(1960) showed that the deformation rate of the "C1" and "C2" ice with large crystals, ≃ 1 to 2 cm diameter and 4 to 5 cm long, was about 4 to 5 times as great as that for "MP1" ice with small grains, ≃ 3 mm in diameter. A detailed general study of the variation of creep rate with crystal size has not yet been carried out. This will not be a great problem in the study of the dynamics of ice masses if the crystal sizes in the deforming ice tend to have similar sizes. An indication that this may be the case for the polar ice masses is provided by Langway (1962) and Gow [1963(a) and (b)]. These authors show the increase in average crystal size with depth to 300 m in Greenland and 150 m in the Ross Ice Shelf, and 300 m in the Antarctic ice cap at Byrd. For the Ross Ice Shelf the crystal area reached ≃ 40 mm by 150 m and increased even more below this. Some crystals ≃ 10 cm were observed at about 240 m depth. For the Greenland and Antarctic ice caps the size reached ≃ 20 mm by 300 m depth.

In temperate glaciers the variation in crystal size is very great but the development of strong foliations of crystals of different sizes and bubble concentrations in zones of high shear appears to be universal.

Rigsby (1958, 1960) shows that high shear on samples of randomly orientated large crystals can produce zones of small crystals in deformation planes. Shoumsky (1958) showed that the change in crystal size with deformation was closely linked with the orientation of the crystals. Those crystals not orientated appropriately for the deformation (cf. 2.5.3 below) tended to break into small crystals. Over a prolonged period ≃ 20 days crystals with a new orientation, favourable for the deformation, grew. Rigsby (1960) also showed how crystals could be broken into small crystals and new crystals grow with a favourable orientation.

Voitkovski (1960) states that for low stresses (i.e., below the limit for prolonged steady-state creep) the favourably orientated crystals tend to grow at the expense of the others, so that after a long period the sample consists of larger crystals, rather than the smaller crystals produced by the high shear rates mentioned by Rigsby.

Kizaki (1969) found a high correlation between crystal growth and the development of a strong fabric in moving ice on the surface of the ice cap near Mawson, Antarctica. The typical size of the crystals observed by Kizaki were ≃ 10 cm long ≃ 1 to 2 cm across.

So far, data are still not available on the crystal structure deep into the shear zone at the base of large ice masses (although this may be soon forthcoming [Ueda and Hansen (1967)]. Pending more data, then, the effect of crystal size on the flow of ice in large ice masses remains unknown. However, since we find that the crystals tend to adopt specific structures under certain conditions, and that these conditions change only slowly with time and space in the ice masses, then we need not regard the variation in crystal size as a serious obstacle to the study of the dynamics of the ice masses, but it must be considered when comparing flow parameters from laboratory and field measurements.

2.5.3. *Ice crystal orientation and flow rate*

We first consider laboratory measurements of creep rates for different orientations. Shoumsky (1958), Rigsby (1958, 1960), Butkovitch and Landauer (1958)

and Vialov (1958) have all shown that the rate of deformation of ice crystals with their basal planes parallel to the shear planes (easy glide) is several hundred times higher than for crystals with basal planes perpendicular to the shear plane (hard glide). Rigsby (1960) showed that single crystals tended to bend rather than deform, other than by shear on the basal plane. Vialov (1958) showed that randomly oriented polycrystalline ice deformed at a rate between the two extremes for single crystals, but closer to the lower rate. Butkovich and Landauer (1958) found that various samples of polycrystalline ice tended to deform on the average slightly more rapidly than single crystals in hard glide—but about 2 orders of magnitude lower than single crystals in easy glide.

Secondly, we consider crystal orientation fabrics observed in naturally deforming ice masses. Although many detailed studies of ice crystal orientation fabrics have been made in natural ice masses, e.g., Rigsby (1955, 1960), Kamb [1959(b)], Allen et al. (1960), Reid (1964), Kizaki (1962), very few studies have included sufficient information on the deformation pattern of the ice to associate the fabric pattern with the deformation. Meier's (1960) study of the Saskatchewan Glacier showed cases in which distinct 2-pole fabrics appear to vary with the form of the deformation in different parts of the glacier. Kizaki (1969) showed that the fabric on the surface of the ice cap near Mawson varied gradually from place to place in a similar way to the deformation pattern as determined by measurements of the strain rate tensor on the ice surface. The fabrics of samples taken from the surface, however, may not be true guides to the patterns within the ice, because of other factors which may influence the orientation, such as the penetration of radiation and temperature gradients in the surface layers. To avoid these disturbances, samples need to be taken from a depth of 10 m below the surface,

Several theories have been put forward to explain the fabric patterns of ice in terms of the stress situation: MacDonald (1959), Brace (1959), Kamb [1959(a), 1959(b)]. Brace considers the thermodynamic equilibrium state for ice under certain stress and elastic strain situations. His predictions form a good basis for experimental field-testing to associate the stress and fabric patterns. However, we are concerned with deforming ice masses with steady-state creep, not elastic strain, and this condition of continuous deformation and rotation must be also considered in the development of a stable fabric. Kamb offers an alternative theory including consideration of recrystallization and reorientation, with a consequent different prediction for the resulting ice fabric.

Gow (1963) showed strong fabrics to exist in the denser ice of large crystal sizes below the firn of the Ross Ice Shelf. A similar increase in fabric strength and crystal size was observed in the ice cap at Byrd. The measurements, then, suggest that in prolonged steady deformation the ice crystals tend to adopt a pattern appropriate to the deformation. Although the relation between the deformation pattern and the fabric pattern is still not well understood, we may suppose that, provided the stress situation changes sufficiently slowly in an ice mass, then so does the crystal fabric. In this case the lack of knowledge of the details of the fabric patterns throughout the ice mass will not be a serious obstacle to determining the ice mass dynamics. However, the flow rate as determined in the laboratory cannot

be expected to correspond exactly with that operating in the ice mass, unless the crystal sizes and orientations are matched as well as the state of stress. To do this, samples of ice could be taken from an ice mass where strain rate measurements have been carried out and the same state of stress placed on the sample in the laboratory.

Also, the flow law as determined from measurements of disturbances in natural ice masses, such as closure rates of boreholes and tunnels, may not be typical of the natural deformations that occur in the ice mass, because the crystal orientations are not appropriate.

The accelerating deformation rate observed by Gow in the Byrd borehole may be an example of this, with the deformation rate increasing as the crystals tend to adopt a preferred orientation appropriate to the deformation.

2.6. ICE DEFORMATION RATES FROM MEASUREMENTS ON NATURALLY DEFORMING ICE

The relation between the stress and the strain rates in naturally deforming ice have been studied by many observers from vertical and horizontal velocity gradients and closure rates of boreholes and tunnels in various ice masses. Since 1948, vertical boreholes have been drilled through several temperate glaciers and the vertical gradient of the horizontal velocity determined from the surface to near the bedrock: Gerard et al. (1953), Meier (1960), Mathews (1959), Paterson and Savage (1963), Sharp (1960). Some of these profiles are shown in Fig. 2.8.

The stress or pressure gradients acting on the cross-sections of the glaciers, causing the velocity gradient with depth, have been inferred from the shape and size of the ice mass. The details of these studies are discussed in more detail in Section 3. They lead to an estimate for the octahedral shear stress and shear strain rates and permit the relation between them to be compared with those of the laboratory measurements, as is shown in Fig. 2.2. So far, most values are for temperate glaciers only, except for that of Wilson (1959) for the Tuto ice ramp in Greenland. Paterson (1963) points out the difficulty in interpreting these results by a simple laminar flow theory, due to the presence of longitudinal strains, However, since the longitudinal stresses and the variation in longitudinal strain rate with depth are still not well known, we consider the lamimar flow analysis as a first approximation. We may expect closest agreement with laboratory results where the longitudinal strain rates are small. In Fig. 2.2 the various field measurements show quite good agreement with the various laboratory measurements, especially when the large variability among the laboratory measurements is considered.

Similar results obtained by measurements of velocity gradient across a glacier by Meier (1960) and Paterson and Savage (1963) show further confirmation of the general trend, but in this context low stresses were involved and the errors are proportionately large and produce a lot of scatter.

As was noted earlier, the results from the disturbed ice around tunnels and boreholes may not be directly comparable with the natural deformations because of the different crystal orientations and the high shears encountered. However,

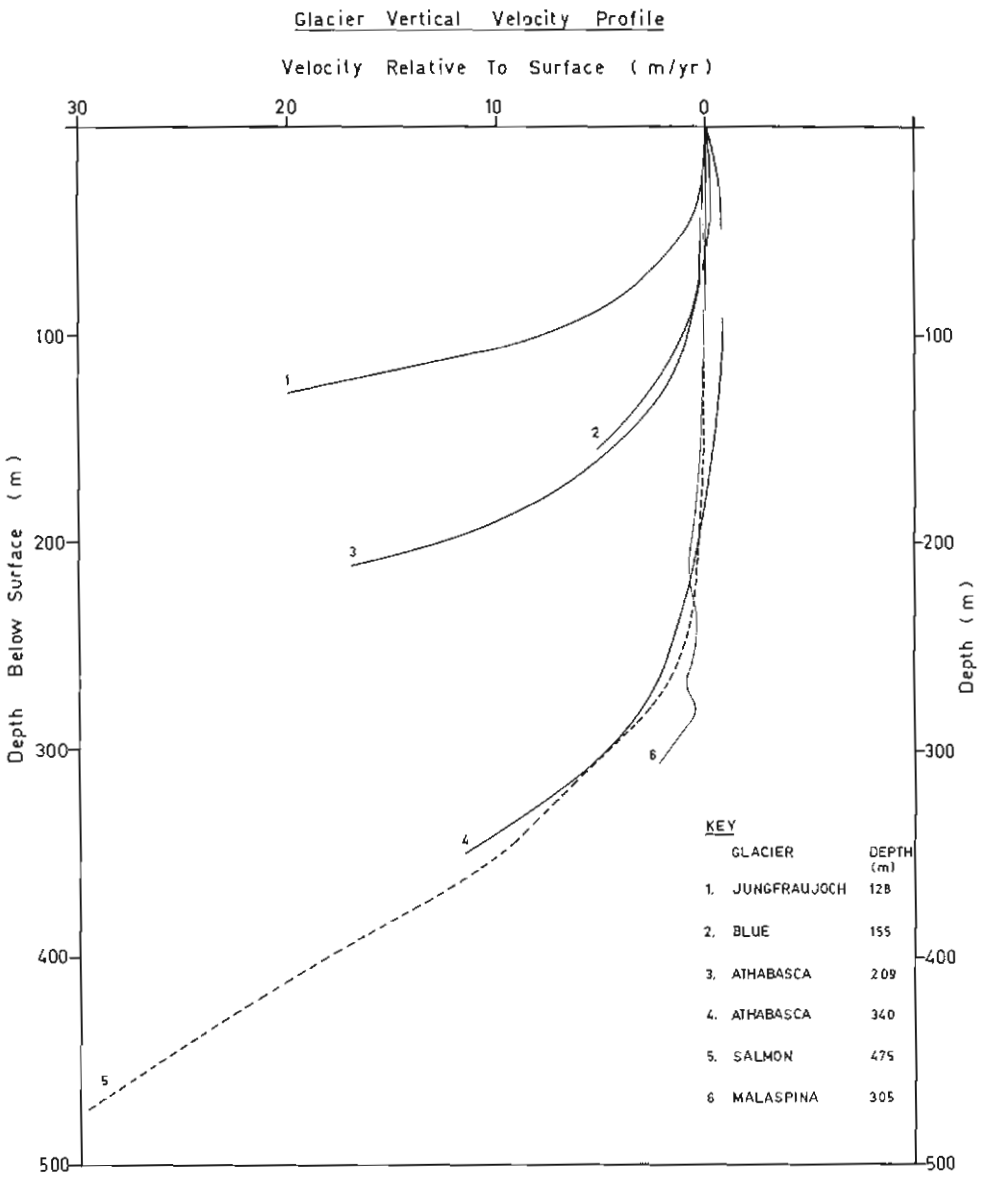

FIG. 2.8. The velocity—depth profile relative to the surface velocity plotted on the same scale for various glaciers.

Fig. 2.2 shows that the results of borehole closure rates measured at Byrd [Gow (1963)] and Camp Century [Hansen and Landauer (1958)] agree essentially with the results of the laboratory measurements and provide a valuable guide to the deformation rates at the lower temperatures found in the cold ice caps. It should be noted here that the closure rate relationship of Nye (1953),

$$\dot{\gamma} = \left(\frac{p}{nB}\right)^n,$$

where $\dot{\gamma}$ is the shear strain rate,

$\tau = p/n$ is the stress for an overburden pressure p,
and B and n are the flow law parameters,

requires a constant value of n to determine the shear stress, and so is only appropriate over the range for which n is constant.

More significant data on the flow law of ice in natural ice masses are obtained from the complete measurement of the dynamics of small ice caps. In particular, besides using the vertical and transverse velocity gradients for determining the flow parameters of the ice, we can also use the longitudinal velocity gradients. This work is more complicated and is developed in detail in Sections 5 and 6.

3. BASIC EQUATIONS OF MOTION AND CROSS-SECTION VELOCITY PROFILES

3.1. GENERAL EQUATIONS OF MOTION IN THREE DIMENSIONS

To establish the equations of motion of an ice mass we take orthogonal axes as follows: x parallel to the bedrock (which has slope β, say) and in the plane of motion, z upwards, perpendicular to the bedrock and y across the line of motion.

Let σ_{ij} $(i, j = x, y, z)$ be the stress tensor at point (x, y, z),

$$\sigma_{ij} = \begin{pmatrix} \sigma_x & \sigma_{xy} & \sigma_{xz} \\ \sigma_{xy} & \sigma_y & \sigma_{yz} \\ \sigma_{xz} & \sigma_{yz} & \sigma_z \end{pmatrix} \quad \text{or} \quad \begin{pmatrix} \sigma_{11} & \sigma_{12} & \sigma_{13} \\ \sigma_{21} & \sigma_{22} & \sigma_{23} \\ \sigma_{31} & \sigma_{32} & \sigma_{33} \end{pmatrix} \quad \text{or} \quad \begin{pmatrix} \sigma_x & \tau_{xy} & \tau_{xz} \\ \tau_{yx} & \sigma_y & \tau_{yz} \\ \tau_{zx} & \tau_{zy} & \sigma_z \end{pmatrix}$$

the ice density ρ, and the gravitational acceleration g. Then we have for equilibrium or "quasi-static creep" (acceleration forces neglected)

$$\begin{aligned} \frac{\partial \sigma_x}{\partial x} + \frac{\partial \sigma_{xy}}{\partial y} + \frac{\partial \sigma_{xz}}{\partial z} &= \rho g \sin \beta, \\ \frac{\partial \sigma_y}{\partial y} + \frac{\partial \sigma_{xy}}{\partial x} + \frac{\partial \sigma_{yz}}{\partial z} &= 0 \\ \frac{\partial \sigma_z}{\partial z} + \frac{\partial \sigma_{zx}}{\partial x} + \frac{\partial \sigma_{zy}}{\partial y} &= -\rho g \cos \beta. \end{aligned} \tag{1}$$

In general, the average bedrock slope (β) over the intervals concerned is sufficiently small for the following approximations to hold:

$$\sin \beta \simeq \tan \beta \simeq \beta \qquad \cos \beta \simeq 1 .$$

For the particular case in which the base is flat and horizontal, $\beta = 0$ and the equations reduce to the form discussed by Weertman (1957a). This form may be suitable for studying the dynamics of free-floating tabular ice bergs, but for ice shelves and other bounded ice masses both the basal slope and the thickness gradient towards the free boundary are very important in regard to the longitudinal velocity and strain profiles.

Two special cases of the general three-dimensional equations are of particular importance.

(i) Two-dimensional longitudinal profile equations.

Consider the case in which the strain rates $\dot{\varepsilon}_y$, $\dot{\varepsilon}_{xy}$, $\dot{\varepsilon}_{yz}$ are all zero. This is found along the centre line at the surface of a glacier of constant width where the longitudinal velocity gradient is negligible. For the central flow plane

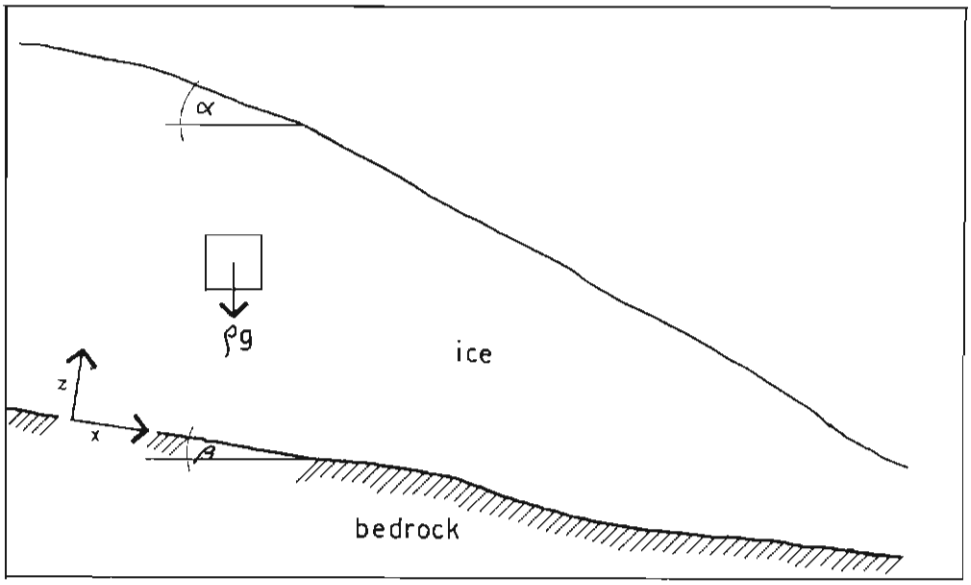

FIG. 3.1.

$$\frac{\partial \sigma_y}{\partial y} = \sigma_{xy} = \sigma_{yz} = 0,$$

due to symmetry, and we are left with the two-dimensional equations

$$\begin{aligned} \frac{\partial \sigma_x}{\partial x} + \frac{\partial \sigma_{xz}}{\partial z} &= \rho g \beta \\ \frac{\partial \sigma_z}{\partial z} + \frac{\partial \sigma_{xz}}{\partial x} &= -\rho g. \end{aligned} \tag{2}$$

We will find (Section 3.3) that, due to the symmetry of the flow of natural ice masses, a modified form of these equations allows the longitudinal and vertical velocity profiles to be calculated. Consideration of the shape of the cross-section makes it possible to extend this treatment to three dimensions (cf. Section 5.2).

(ii) Cross-sectional profiles.

If the longitudinal velocity gradient is small (the usual case for smoothly flowing ice masses away from disturbed regions such as ice falls) and if there is no lateral expansion (as for flow in a channel of constant cross-section) then the general equations (1) reduce to

$$\begin{aligned} \frac{\partial \sigma_x}{\partial x} + \frac{\partial \sigma_{xy}}{\partial y} + \frac{\partial \sigma_{xz}}{\partial z} &= \rho g \beta \qquad \text{(i)} \\ \frac{\partial \sigma_z}{\partial z} + \frac{\partial \sigma_{xz}}{\partial x} &= -\rho g \qquad \text{(ii)} \end{aligned} \tag{3}$$

over a cross-section.

These two-dimensional cross-section equations are generally sufficient for the calculation of the cross-sectional velocity and stress distributions.

Now, since there is no longitudinal or transverse extension,

$$\sigma_x = \sigma_z$$

and hence from 3(ii) integrating from bed to surface, $z = Z$,

$$\frac{\partial \sigma_x}{\partial x} = \frac{\partial\left(\int_0^Z \frac{\partial \sigma_z}{\partial z}\, dz\right)}{\partial x}$$

$$= -\rho g \frac{\partial Z}{\partial x} - \frac{\partial^2 \int_0^Z \sigma_{xz}\, dz}{\partial x^2}.$$

Since the surface and base slopes are constant, the second term on the right, which may be taken as $\frac{\partial^2 \rho g \alpha Z}{\partial x^2}$, is zero. Hence

$$\frac{\partial \sigma_x}{\partial x} = -\rho g \frac{\partial Z}{\partial x} \tag{4}$$

Hence from (3) and (4) the equations of motion relevant to cross-section profiles reduce to

$$\frac{\partial \sigma_{xy}}{\partial y} + \frac{\partial \sigma_{xz}}{\partial z} = \rho g\left(\frac{\partial Z}{\partial x} + \beta\right)$$

$$= \rho g \alpha \tag{5}$$

where α is the surface slope, assumed constant across the section. The solution of this equation has been examined for various cross-section shapes by Nye (1965) and will be discussed in Section 3.4.

In general, the equations of motion have to be integrated to their boundaries. Typical ice mass boundaries are shown in Fig. 3.2, for the three major types of ice masses discussed here.

Since the ice mass is deforming, the boundary stresses may not be well known, but boundary velocities are generally obtainable. Hence, we convert the equations of motion in terms of stresses to equations in terms of velocities and strain rates, by means of the flow law relation.

3.2. FLOW LAWS

The results of the studies of the ice flow law in Section 2 show that the strain rate $\dot{\varepsilon}_{ij}$ may be related to the stress deviator $\sigma'_{ij} = \sigma_{ij} - \frac{1}{3}\delta_{ij}\sigma_{ii}$ by the relation

$$\dot{\varepsilon}_{ij} = \lambda \sigma'_{ij} \tag{6}$$

where λ is not a constant, but rather a function of the shear stress, the temperature, crystal type, etc. In some contexts, over limited ranges of the variables on which λ depends, we may adopt simple forms for the flow law, such as:

$$\lambda_1 = A^{-n}\tau^{n-1} \tag{7}$$

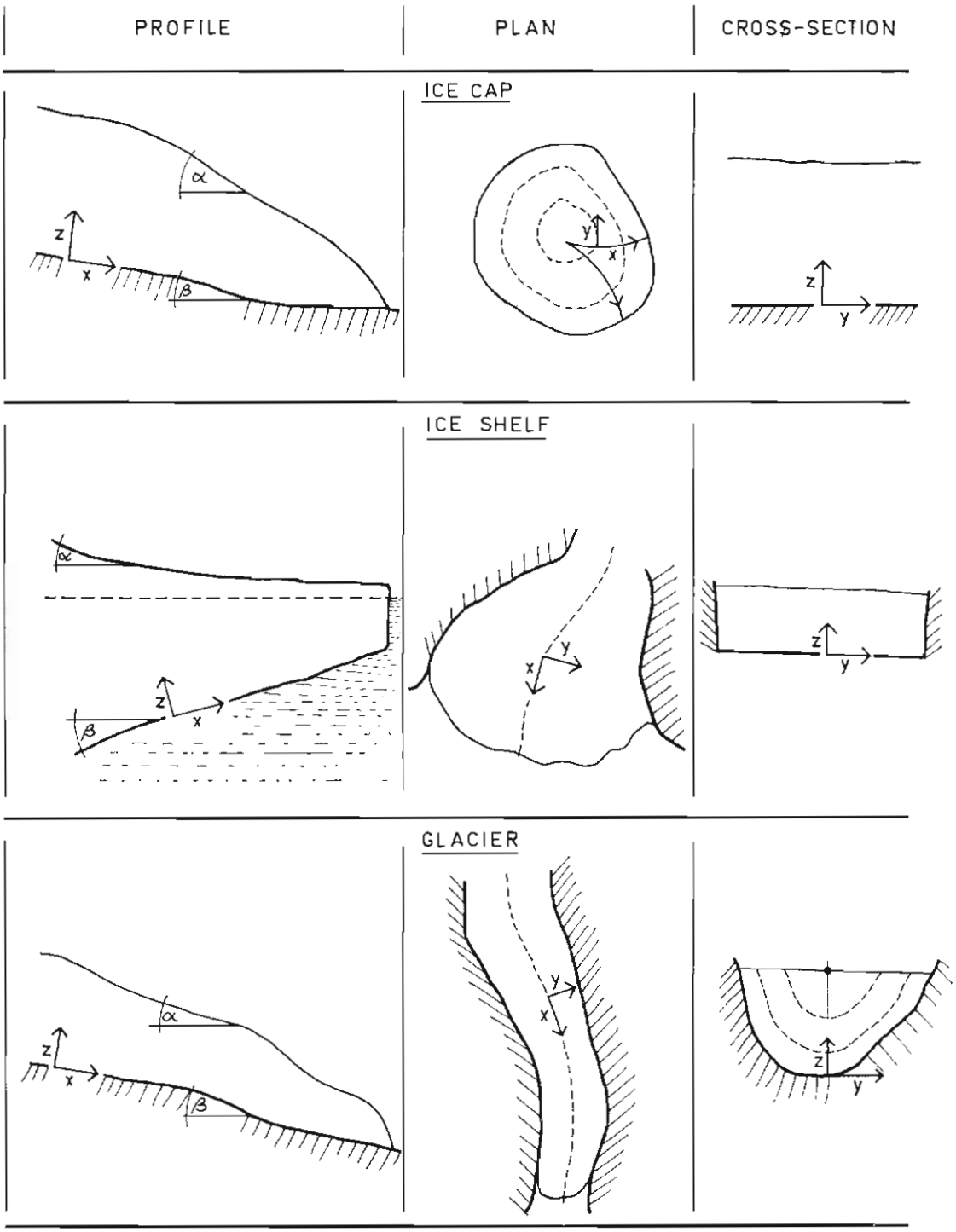

FIG. 3.2. Typical boundaries for the three major types of ice masses.

(n dependent on stress, A dependent on temperature)

$$\lambda_2 = k_2 + k_1 \tau^{n-1} \tag{8}$$

(k_1, k_2 dependent on temperature)

$$\lambda_3 = \frac{1}{\tau} A_2 \sinh \frac{\tau}{\tau_0} \tag{9}$$

$$\text{where} \quad \tau = \tfrac{1}{2}\sigma'_{ij}\sigma'_{ij} \tag{10}$$

is the "effective shear stress" (cf. Section 2.1).

The special case of perfect plasticity can be deduced from the general power law relation, by noting the result of letting the index n approach infinity. For the case of constant Newtonian viscosity, the index n is equal to one.

Since the $\dot{\varepsilon}_{ij}$ are related to the velocity gradients $\dfrac{\partial u_i}{\partial x_j}$ by

$$\dot{\varepsilon}_{ij} = \frac{1}{2}\left(\frac{\partial u_i}{\partial x_j} + \frac{\partial u_i}{\partial x_i}\right) \tag{11}$$

we see that the general equations of motion in terms of stress may be transformed by means of the flow law into equations in terms of velocities. This procedure would also require the stress boundary conditions to be also transformed to velocity or strain rate boundary conditions.

The general problem of solving the equations of motion for the velocities in terms of the boundary values (velocity and velocity gradient) is very complex. However, to solve the system for the three major types of ice mass, several simplifications may be made, due to the special properties of the boundary conditions of the ice masses, such as symmetry, zero velocity regions, free surfaces, etc.

3.3. SYMMETRY CONSIDERATIONS AND SEPARATION OF LONGITUDINAL FROM TRANSVERSE MOTION

One of the main outstanding problems in the dynamics of ice masses is to determine the longitudinal variation (along a flow line) of the average velocity. As was pointed out in Section 1, this may be used to determine the change in the velocity distribution with time, the history of the glacier, the mass flux variation, etc. The forms of the other velocity profiles (transverse, vertical) do not vary so greatly and hence, for many purposes, may be regarded as constant or treated simply as slowly varying parameters along the line of flow. The cross-section averaged longitudinal velocity is not as easy to measure directly as the surface velocity. But since the shapes of the profiles of the transverse velocities only vary slowly along the flow line, it is often possible to relate the average velocity $\bar{u}$ to the maximum veloeity at the surface u_e by writing

$$u = su_e \tag{12}$$

where s is dependent on the shape of the transverse velocity profiles and determined largely by the boundary eonditions.

We now examine the boundary conditions of the three major types of ice masses.

3.3.1. *Glaciers*

Glaciers generally have small horizontal divergence and small or zero velocity at the side boundaries. At the "centre" of a symmetric cross-sectional glacier we observe that the transverse shear is zero. This shear increases away from the centre to reach a maximum near the boundary, where the longitudinal velocity and velocity gradients are both zero if there is no direct sliding. When sliding occurs at the base or edges then this becomes an extra boundary value that is required.

3.3.2. *Ice shelves*

For ice shelves we may assume zero velocity at the edges and constant velocity from top to bottom. Again the greatest velocity of a cross-section is at the centre. The magnitude of the transverse velocity u_y depends largely on the angle of divergence of the boundaries. Again, along the centre line the transverse shear strain rates (and hence stress deviator gradients) are zero because of the symmetry.

3.3.3. *Ice caps*

For an ideal circular ice cap on a flat base, the flow lines are straight lines radiating from the centre. The horizontal divergence is small and depends only on the forward velocity and the distance from the centre. In practice, bedrock irregularities cause divergence and convergence of the flow lines (cf. Fig. 3.2); but provided these convergence or divergence rates are known it will be shown that the effect of transverse strains can be taken into consideration by incorporating them as slowly changing parameters along the flow line (cf. Section 5.5). Again, the vertical longitudinal shear strain rates $\dot{\varepsilon}_{xz}$ and the transverse longitudinal shear strain rates $\dot{\varepsilon}_{xy}$ can generally be considered zero at the surface, and ideally the shape of the profile does not change greatly laterally, i.e., at right angles to the flow direction.

3.3.4. *General results from symmetry*

In general at the boundaries of ice masses where there is no sliding, since the velocity is zero, the longitudinal velocity gradient is also zero. Similarly, at the position of maximum velocity (i.e. the centre at the surface) we may also expect the longitudinal velocity gradient to be greatest.

On the other hand, the transverse gradients are greatest at the boundary where the longitudinal gradient is smallest. This suggests that we may well study separately the transverse stresses and the resulting velocity gradients on the one hand, and the longitudinal stresses, and the velocity gradients caused by them, on the other.

Hence the next Section considers the transverse velocity gradients of a cross-section, first for laminar flow and zero longitudinal strain, and then for a constant longitudinal strain rate. Having done this, we are then in a position to study the variation in longitudinal velocity due to longitudinal stress changes, with the transverse parameters remaining constant or at least only varying slowly along the flow line.

3.4. TRANSVERSE VELOCITY FOR LAMINAR FLOW

The transverse velocity profile for glaciers has been considered in detail by Nye (two-dimensional plastic flow 1952; two-dimensional power law flow 1957;

three-dimensional rectangular, elliptical, parabolic cross-sections 1965). Thus, only an outline of his basic results will be given here. Consider axes at the centre of the surface of a glacier: x in the line of motion, z downwards, and y across the glacier.

For zero longitudinal velocity gradient $\frac{\partial u_x}{\partial x} = 0$. For constant cross section shape $u_y = u_z = 0$. Hence the only non-zero velocity gradients are $\frac{\partial u_x}{\partial y}, \frac{\partial u_x}{\partial z}$. From symmetry, $\sigma_{yz} = 0$ and, as we have seen in Section 3.1, the general equations (1) reduce to (5)

$$\frac{\partial \tau_{xy}}{\partial y} + \frac{\partial \tau_{xz}}{\partial z} = \rho g \alpha \tag{13}$$

Adopting a flow law of the form

$$\dot{\varepsilon}_{ij} = \tfrac{1}{2} A \tau^{n-1} \sigma'_{ij},$$

where

$$\tau = (\tau_{xy}^2 + \tau_{xz}^2)^{\frac{1}{2}} \tag{14}$$

the transverse and vertical velocity gradients may be written as

$$\frac{\partial u}{\partial y} = A \tau^{n-1} \tau_{xy}; \qquad \frac{\partial u}{\partial z} = A \tau^{n-1} \tau_{xz} \tag{15}$$

3.4.1. *Special cross-sections*

(i) Firstly, for laminar flow between two parallel vertical plates (infinitely deep) we have no vertical velocity gradient, i.e.,

$$\frac{\partial u}{\partial z} = 0, \qquad \text{and therefore} \qquad \tau_{xz} = 0.$$

Hence

$$\frac{d\tau_{xy}}{dy} = \rho g \alpha \qquad \frac{du}{dy} = A \tau^{n-1} \tau_{xy}$$

from which we obtain

$$u_c - u_y = A \frac{(\rho g \alpha)^n}{n+1} |y|^{n+1} \tag{16}$$

where u_c is the velocity at the centre, and u_y is the velocity at distance y from the centre.

(ii) Similarly, for laminar flow (infinitely wide) over a flat base

$$u_c - u_z = A \frac{(\rho g \alpha)^n}{n+1} z^{n+1} \tag{17}$$

(iii) For flow in a semi-circular channel we may adopt cylindrical polar co-ordinates from the origin at the centre of the surface as follows:

$$r^2 = y^2 + z^2 \qquad z = r \cos \theta \qquad y = r \sin \theta$$

and obtain for the basic equations:

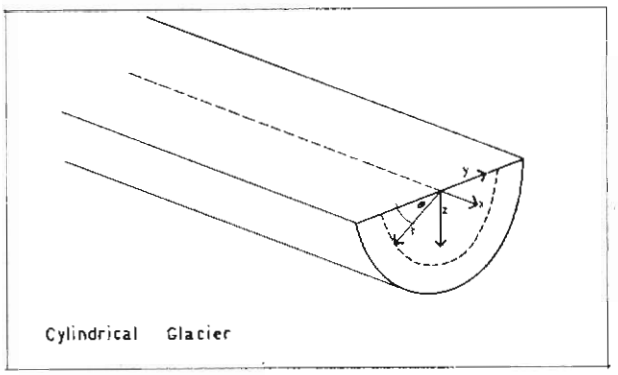

FIG. 3.3

$$\frac{\partial u}{\partial r} = A\tau^{n-1}\tau_r, \qquad \frac{\partial u}{\partial \theta} = A\tau_\theta^{n-1}$$

$$\frac{1}{r}\frac{\partial(r\tau_r)}{\partial r} + \frac{1}{r}\frac{\partial \tau_{r\theta}}{\partial \theta} = \rho g\alpha \tag{18}$$

With the flow independent of θ we obtain

$$\tau_r = \frac{\rho g\alpha}{2} r$$

and hence

$$u_c - u_r = \frac{A}{n+1}\left(\frac{\rho g\alpha}{2}\right)^n r^{n+1} \tag{19}$$

Nye (1965) also gives the following solution (due to Chester, unpublished), obtained by perturbation methods for a cross-section shape slightly different from a semi-circle.

$$u = \frac{aA}{n+1}\left(\frac{k}{2}\right)^n\left[1 - \left(\frac{r}{a}\right)^{n+1} + \tfrac{1}{2}\epsilon(n+1)\left\{1 - \left(\frac{r}{a}\right)^c \cos 2\theta\right\}\right] \tag{20}$$

where $k = \rho g \sin\alpha$ and ϵ is the increase in horizontal radius greater than circular and

$$c = \tfrac{1}{2}(n-1) + \tfrac{1}{2}(n^2 + 14n - 1)^{\frac{1}{2}} \tag{21}$$

3.4.2. *Numerical solutions for cross-section profiles*

By solving equations (13), (14), (15) above (with $n = 3$) numerically, velocity and stress solutions were obtained by Nye (1965) for different cross-sections, such as parabola, ellipses and rectangles. These are shown in Fig. 3.4a. From the resultant solutions for shear stress and velocity, the values of the shape factor f in the approximate formula

$$\bar{\tau}_{xy} = -\bar{f}\rho g z \sin\alpha \tag{22}$$

are listed in Table I. Nye found, however, that τ_{xy} deviated from the linear relation with y, as the boundary was approached, the degree of deviation depending on

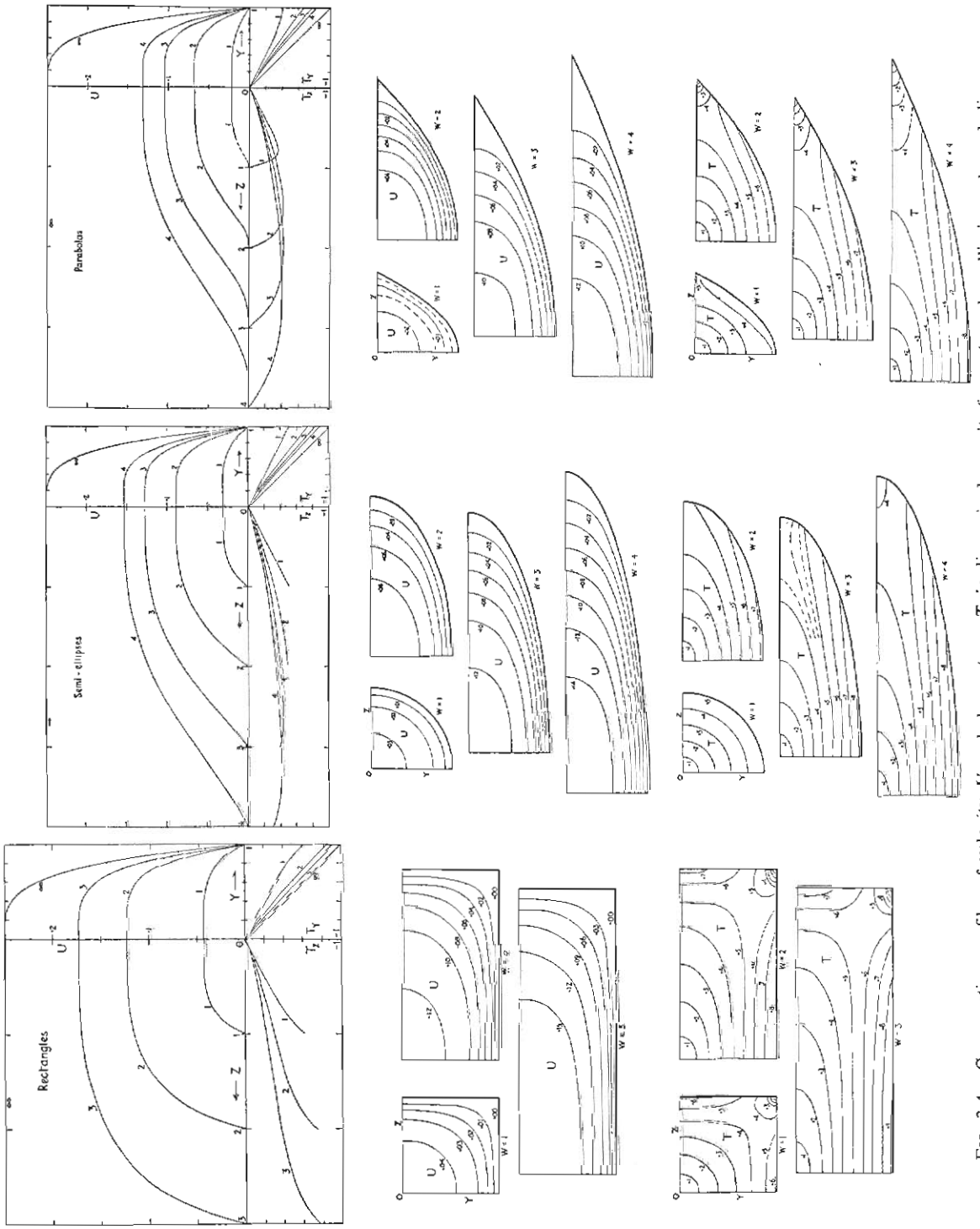

FIG. 3.4a. Cross-section profiles of velocity U and shear stress T, in dimensionless units for rectangular, elliptic, and parabolic channels, and ice with a cubic power law for flow, after Nye (1965).

the shape. Approximate shape factors for the central vertical velocity profile have been estimated in the past: cf. Nye (1952), Meier (1960), Paterson (1963c), Budd (1966), by the relationship

$$f \simeq \frac{S}{pZ},$$

where S is the glacier cross-section area,
p is the glacier cross-section parameter,
and Z is the depth in the centre.

In Table I are also listed the values of S/pZ for the rectangle, ellipse and the parabola. We note that, for very wide channels, S/pZ approaches 1 only for the rectangle, whereas Nye's calculated values of f tend quite rapidly to 1. There appears to be close agreement in the range $W \simeq 1$ but, for high values of W, $f > S/pZ$ and, for low values of W, $f < S/pZ$.

It must be remembered, however, that Nye's curves of Fig. 3.4a have been calculated, using a flow law of the form

$$\dot{\varepsilon}_{ij} = \tfrac{1}{2}A\tau^{n-1}\sigma'_{ij} \qquad \text{with } n = 3.$$

If a flow law of the form

$$\dot{\varepsilon}_{ij} = (A_1 + A_2\tau^2)\sigma'_{ij}$$

is used, the effect of the linear term (A_1) will be quite important at low stresses (less than 1 bar) which are found in glacier profiles.

As a consequence, it may be expected that in practice the shape factor will depend on not only the cross-section shape but also the form of the flow law.

TABLE 3.1

[VALUES OF f FROM NYE (1965)]

Shape factor f in $\tau_{xy} = -f\rho gz\alpha$.

W = half-width/depth.

W	Rectangle		Ellipse		Parabola	
	f	S/pZ	f	S/pZ	f	S/pZ
½	0·31	0·33	0·28	0·33	—	0·29
1	0·56	0·50	0·50	0·50	0·45	0·45
2	0·79	0·67	0·71	0·65	0·65	0·58
3	0·88	0·75	0·80	0·70	0·75	0·62
4	—	0·80	0·85	0·73	0·81	0·64
∞	1·0	1·0	1·0	0·785	1·0	0·67

The value of f listed is chosen such that the true velocity at the surface is obtained by integrating the approximate shear stress $\tau_{xy} = f\rho gaz$ up the z axis.

Once the shape factors have been determined, it may be possible to determine appropriate values of the flow parameters from the shape of the cross-section velocity profiles. To do this it is valuable to have the profiles in relative co-ordinates—as shown in Fig. 3.4b. Here it may be seen that the varying cross-section shapes cause quite different shapes of the transverse profiles, but the shape of the vertical profile is not greatly affected by increasing the width beyond $W = 1$. For

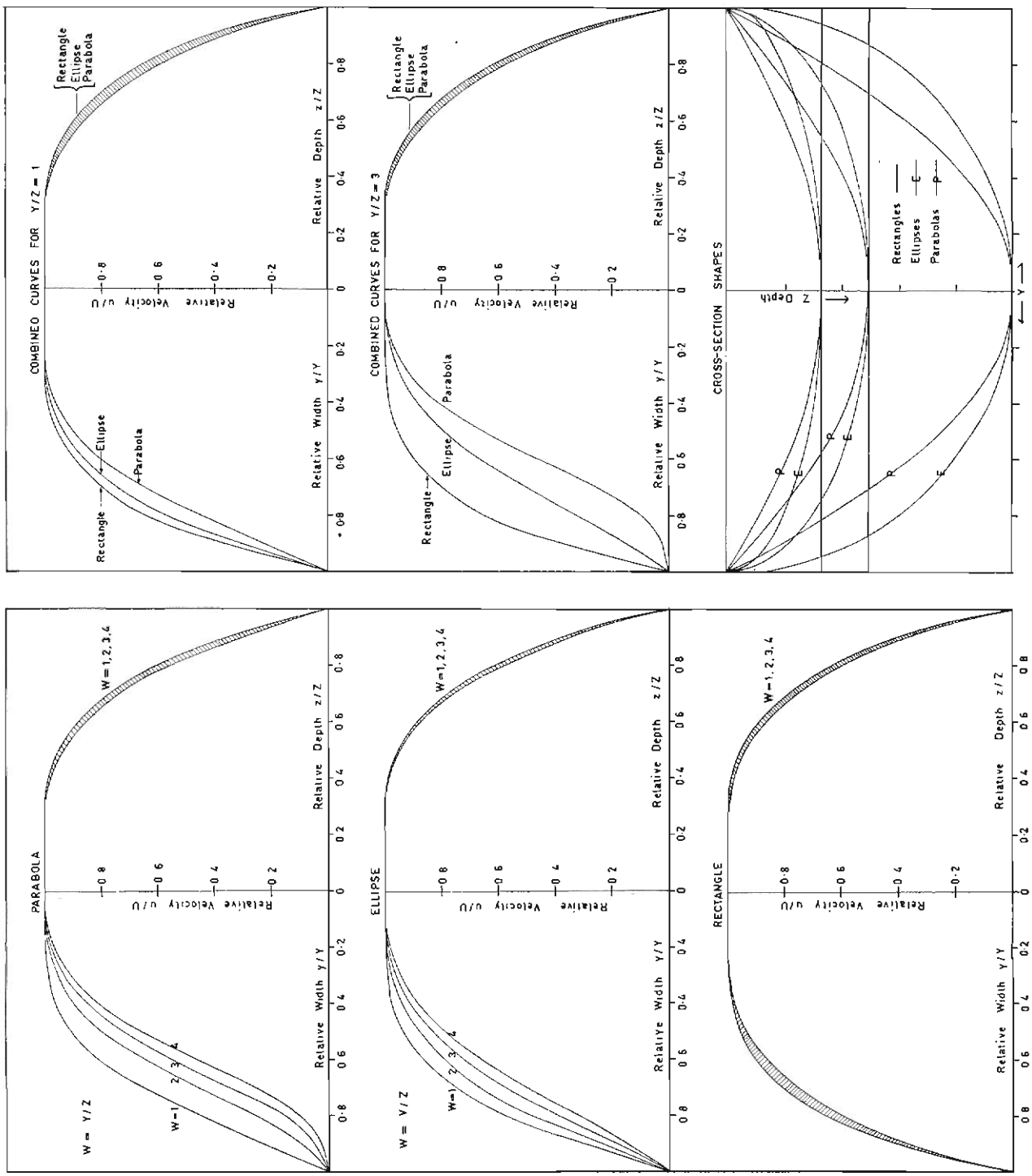

FIG. 3.4b. Relative velocity profiles for the cross-sections of Fig. 3.4a from Nye (1965) showing that, for wide cross-sections,

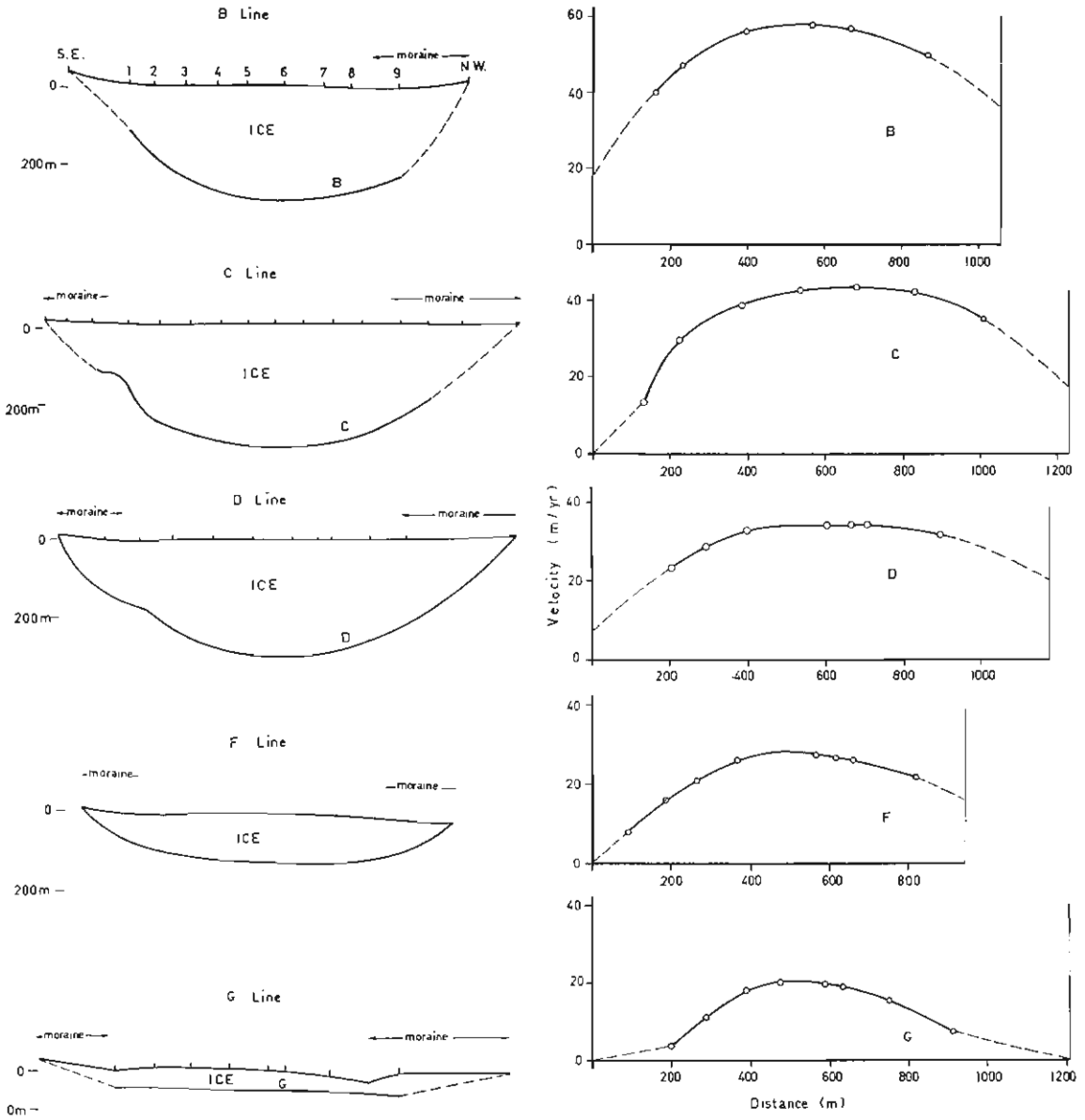

FIG. 3.5. Measured cross-section profiles of ice thickness and velocity at various distances along the Athabasca Glacier (cf. Fig. 6.1) after Paterson (unpublished).

different values of n in the power flow law different shapes would be obtained. Hence, for wide glaciers of these types of shape, the shape of the vertical velocity profile is not greatly affected by the shape of the cross-section and would therefore provide a satisfactory means of determining the parameter n. For glaciers of the rectangular cross-section shape, or with steep sides, the shape of the transverse

velocity profile is not greatly affected by the shape and so the transverse profile may also be profitably used to estimate the flow parameter n.

Palmer (1967) gives a numerical method for calculating upper and lower bounds of the transverse velocity profile at the surface of a glacier, and also the mean velocity of flow.

As mentioned earlier, many glacier cross-section shapes have been measured and the transverse velocity profile determined. A very detailed set of results was obtained for the Athabasca Glacier by Paterson (unpublished) whose series of cross-sections and velocity profiles is partly reproduced in Fig. 3.5.

These results show that the glacier bedrock cross-section is comparatively smooth and changes only slowly along the glacier. They confirm Nye's (1965b, Table IV) conclusion that the mean surface velocity and mean cross-section velocity are not highly sensitive to small variations in the cross-section shape, or the value of the flow law parameter, or the amount of bed slip.

For determining the velocity distribution across real glaciers, given the cross-section, an interpolation or extrapolation of Nye's numerical solutions may be used.

3.5. EFFECT OF LONGITUDINAL STRAIN RATE ON CROSS-SECTION FLOW

3.5.1. *Plastic flow*

By considering the flow of ice down a slope as analogous to the plastic flow of a medium between two parallel plates, moving apart or together at a constant rate, Nye (1952) derived a velocity solution for two-dimensional ice flow when a constant longitudinal velocity gradient from surface to base (strain rate) is present.

The velocity solution for ice of thickness h is

$$u = \mathrm{C} \pm \frac{Vx}{h} + 2V\sqrt{1 - (y/h)^2} \tag{23}$$

$$v = \mp V\left(1 - \frac{y}{h}\right) \tag{24}$$

where u is the horizontal velocity at distance x along the surface and distance y below the surface, v the corresponding vertical velocity, and C, V are the initial horizontal and vertical velocities respectively.

In this case the vertical profile of the horizontal velocity is an ellipse which remains constant along the flow line. The change in velocity along the glacier is accounted for by a change in the sliding velocity $\frac{Vx}{h}$ at the base (cf. Fig. 3.8, $n = \infty$).

This solution was used by Nye to study the velocity profile along a glacier for steady-state conditions, i.e., with constant thickness and with the change due to flow being exactly balanced by the gain in accumulation or loss by ablation. In this approach the flow is necessarily determined by the accumulation ablation

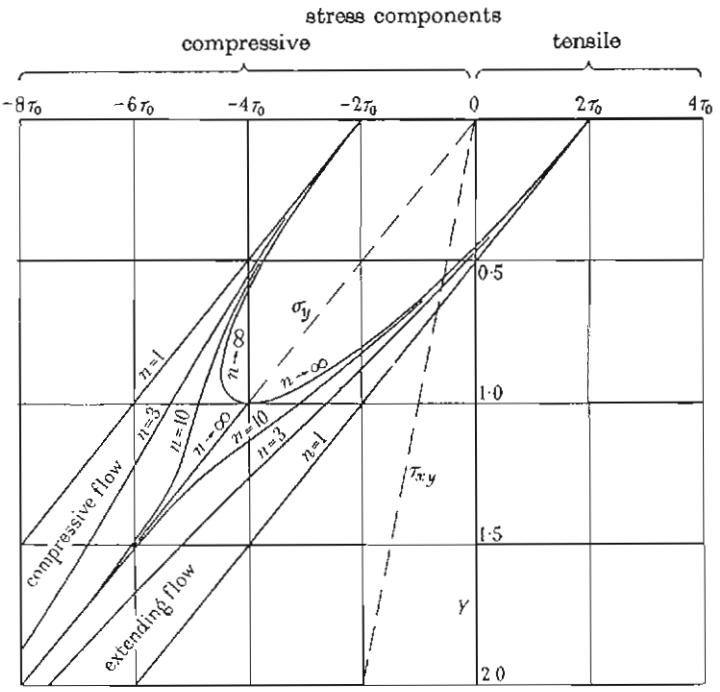

FIG. 3.6. Effective shear stress T as a function of the depth Y, both quantities being expressed non-dimensionally; for uniform density and a power law of flow, c is taken to equal 1.

(Figures 3.6, 3.7, 3.8 are from Nye (1957) to show the effect of a constant longitudinal strain rate through the ice on the vertical profiles of velocity, horizontal and vertical stress and the shear stress.)

pattern. A more general treatment is to consider the state of balance to be an independent parameter and find the velocity solution which is determined by the dimensions of the ice mass, together with the iceflow law and the boundary velocities. The velocity distributions thus found can be compared with the accumulation pattern to determine the state of balance and the rate of change of the ice cap dimensions. This approach is followed in Sections 5, 6 and 7.

3.5.2. *Power flow law*

Adopting a more general flow law of the type $\dot{\varepsilon} = \left(\frac{\sigma'}{B}\right)^n$, Nye (1967) obtained a stress and velocity distribution for the model (ii) of Section 3.5.1.

In this case the equations proved not so tractable and no simple analytical velocity solution was obtained. However, it proved possible to express the stress and velocity solutions in terms of the parameter "effective shear stress" τ given by

$$4\tau^2 = (\sigma_x - \sigma_y)^2 + 4\tau_{xy}^2 \tag{25}$$

The stress solutions, depicted in Fig. 3.6 from Nye (1957) are given by

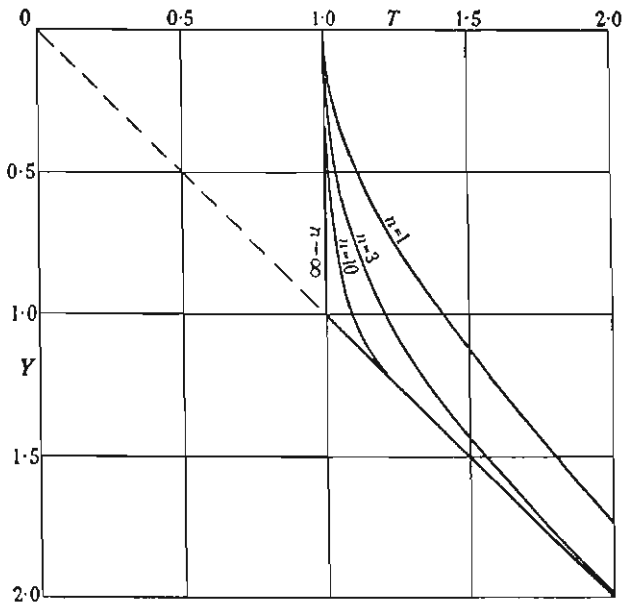

FIG. 3.7. Stress components as functions of depth Y, measured in dimensionless units, for uniform density and a power law of flow. The distribution of σ_x is given by the double family of full curves; each value of n gives one curve for extending flow and one for compressive flow. The distributions of σ_y and τ_{xy} are shown by the broken lines and are the same for all n. All curves are drawn for a slope of $a = 14° 2'$ (cot $a = 4$) and the units are such that $c = 1$.

$$\sigma_x = -\rho g_y y \pm 2\sqrt{\tau^2 - (\rho g_x y)^2}$$

$$\begin{aligned} \sigma_y &= -\rho g_y y \\ \tau_{xy} &= -\rho g_x y \end{aligned} \tag{26}$$

These profiles of Fig. 3.6 show the difference between the cases of no longitudinal strain, and the compresive and tensile flow, for different values of n. Fig. 3.7 shows the variation of τ with depth in non-dimensional units.

The velocity solutions are

$$u \pm rx - 2rg_x \int_0^y \frac{\rho y\, dy}{\sqrt{\tau^2 - (\rho g_x y)^2}} + u_0 \tag{27}$$

and

$$v = \mp r(y - h) \tag{28}$$

where r is the constant longitudinal strain rate.

Taking dimensionless units

$$T = \frac{\tau}{\tau_0} \qquad X = \frac{x}{l_0} \qquad Y = \frac{y}{l_0} \qquad U = \frac{u}{v_0} \qquad V = \frac{v}{v_0},$$

the expression for the horizontal velocity U is

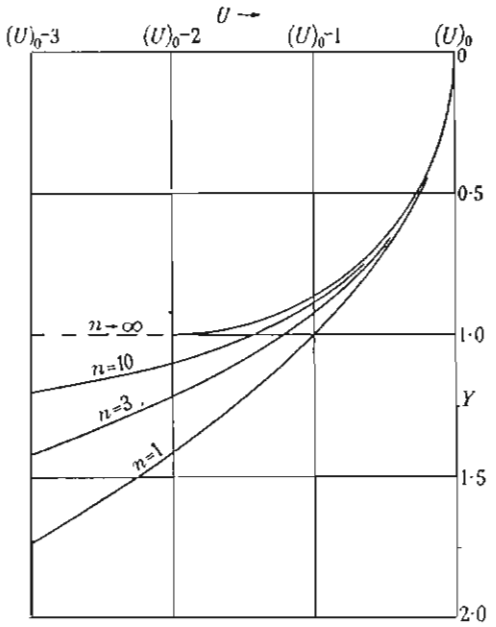

FIG. 3.8a. Longitudinal velocity U as a function of depth Y, both quantities being expressed non-dimensionally, for uniform density and a power law of flow. The curves are drawn for $X = 0$; $(U)_0$ is the surface velocity at $X = 0$. c is taken equal to 1.

$$U = U_0 \pm rX - \frac{2}{n+1}(T^{n+1} - r^2(n+1)T^{1-n} + nr^{1+1/n}) \tag{29}$$

and this is illustrated in Fig. 3.8, which shows the velocity distribution for different values of n.

From these results Nye deduced several important consequences:

(1) Longitudinal strain rate zero. From equations (27) and (28) above we find, by putting $r = 0$, that the velocity U reduces to

$$U = \frac{2}{n+1} Y^{n+1} + U_0 \tag{30}$$

and also

$$V = 0.$$

This result is the same as deduced previously [equation (17)] for laminar flow (i.e., with no longitudinal extension or compression, and consequently the flow lines remain parallel).

Hence, we may expect that the laminar flow solutions will apply closely for small or negligible longitudinal strain rates.

(2) Newtonian viscosity ($n = 1$).

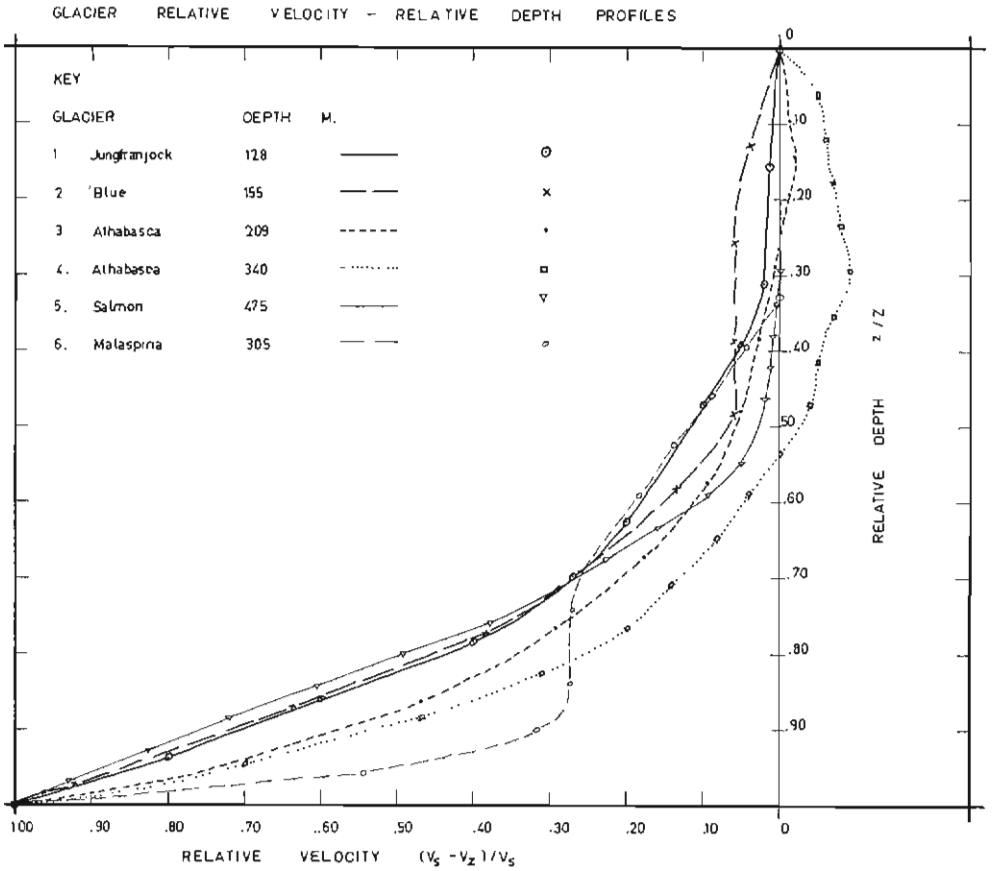

FIG. 3.8b. Glacier relative velocity—relative depth profiles (from Fig. 2.8a).

In this case the velocity profiles are:

$$U = \pm rx - \frac{\rho g_x y^2}{A} + U, \qquad V = \mp r(y - h) \tag{31}$$

i.e., identical to the case for laminar flow. Hence, for values of n approaching 1, the longitudinal strain rate r does not affect the vertical profile of velocity.

(3) Perfect plasticity ($n \to \infty$) (yield stress $A = \tau$). In this case

$$U = \pm X + 2(\sqrt{1 - Y^2} - 1) + U_0, \qquad V = \mp (Y - Y_{\text{bed}}) \tag{32}$$

which is the elliptical velocity profile identical to equation (23) as was derived previously for perfect plasticity.

Finally, consider a cross-section of a glacier and denote V_s and $\dot{\varepsilon}_s = \frac{\partial V_s}{\partial x}$ as the longitudinal velocity and strain rate at the centre of the surface. If we assume that the longitudinal strain rate varies in a similar way to the velocity going away

from the centre of the surface, then at distance r, where the velocity and strain rate are V_r and $\dot{\varepsilon}_r$, we have

$$\frac{\dot{\varepsilon}_r}{\dot{\varepsilon}_s} = \frac{V_r}{V_s} \tag{33}$$

Furthermore, if we have a flow law of the form $\dot{\varepsilon} = \alpha_1 \tau + \alpha_2 \tau^n$ (cf. Section 2) the flow is approximately Newtonian at low stresses. If the longitudinal strain rate is small compared with the transverse strain rate at the boundary, then from (33) the longitudinal strain rate is greatest in the upper layers at the centre where the transverse shear is lowest. Hence, these layers are closest to Newtonian flow (low strain rates). In the basal layer, where the transverse shear is large, the longitudinal strain rate is small. Hence, we may expect the presence of a longitudinal strain rate in these circumstances to have a very little overall effect on the transverse velocity profiles, and equally little effect on the average velocity over a cross-section perpendicular to the direction of flow. For large longitudinal strain rates, however, the problem of its precise effect on the cross-section velocity profile is still unsolved (cf. the Jungfrau borehole experiment, Nye 1953).

For cold ice masses the condition, that the longitudinal strain rate is constant throughout the thickness, in general, may not apply since the velocity at the bedrock may be zero everywhere. In this context it may be more realistic to take the longitudinal strain rate as proportional to the longitudinal velocity, as in (33) above. A velocity profile with this condition has not yet been calculated, but for *small* longitudinal strain rates, as typically observed in cold ice caps, we may expect that the effect on the vertical profile of the longitudinal velocity is still negligible.

Throughout this section the variation of the flow law with temperature has been neglected. Although this may be appropriate for temperate glaciers, for cold ice masses it will be shown that the variation in temperature is of major importance to the velocity profiles. Hence, in Section 4 we next examine the variation of temperature throughout cold ice masses and the effect of this on the velocity profiles.

4. TEMPERATURE PROFILES IN ICE MASSES

4.1. MEASURED TEMPERATURE PROFILES

For temperate ice the variation of temperature with depth is small. Thus, in this section we shall be concerned mainly with cold ice masses. Firstly, the *measured* temperatures in cold ice masses will be reviewed,

Temperature distributions with depth in cold ice masses have been measured in detail in only a few places, largely due to a lack of efficient drilling techniques for ice. This difficulty now seems to have been largely surmounted with the development of the electromechanical drill by USA CRREL (Hansen 1966), and the meltsonde probe (Philberth 1966), so that a great deal of temperature data may be expected to become available in the near future.

The table below lists the main measured temperature distributions available at the time of writing. Some of these profiles are illustrated in Fig. 4.1 (a) and (b).

These profiles, although very few in number, still show a great deal of variety in shape. All the land-based profiles show a typical positive gradient at the base. This is caused partly by the geothermal heat flux, corresponding to a temperature gradient of about 2°C/100 m. Where the ice has a significant horizontal velocity, this positive gradient near the base may be increased by friction due to movement. The profile through the Ross Ice Shelf shows an even grater basal gradient, suggesting high heat flux from the ocean. The temperature gradients at the surface show much more variation from high negative to high positive values. High accumulation rates tend to make the temperature profile near the surface more isothermal.

TABLE 4.1

TEMPERATURE DISTRIBUTIONS MEASURED IN COLD ICE MASSES.

Place	Ice thickness (m)	Depth measured (m)	Authority
Byrd	2164	305	Gow 1963
		2164	Gow *et al.* 1968
Ross Ice Shelf	250	250	Crary 1961
Greenland Site II	2000	411	Hansen & Landauer 1958
Camp Century	1387	1387	Hansen 1967
Maudheim	200	100	Schytt 1954
Filchner	230	57	Wexler 1960
Mirny-Vostok	540	350	Bogoslovski 1958
	2-3,000	40-70	
Wilkes-Vostok	2-4,500	60	Battye (unpubl.)
Mawson	1-3,000	30	Mellor 1960
Amery	350	310	Nickols (pers. comm.)

In many profiles (Filchner Ice Shelf, Byrd, Camp Century, 5 km inland Mirny) a most interesting feature is the negative temperature gradient at the surface.

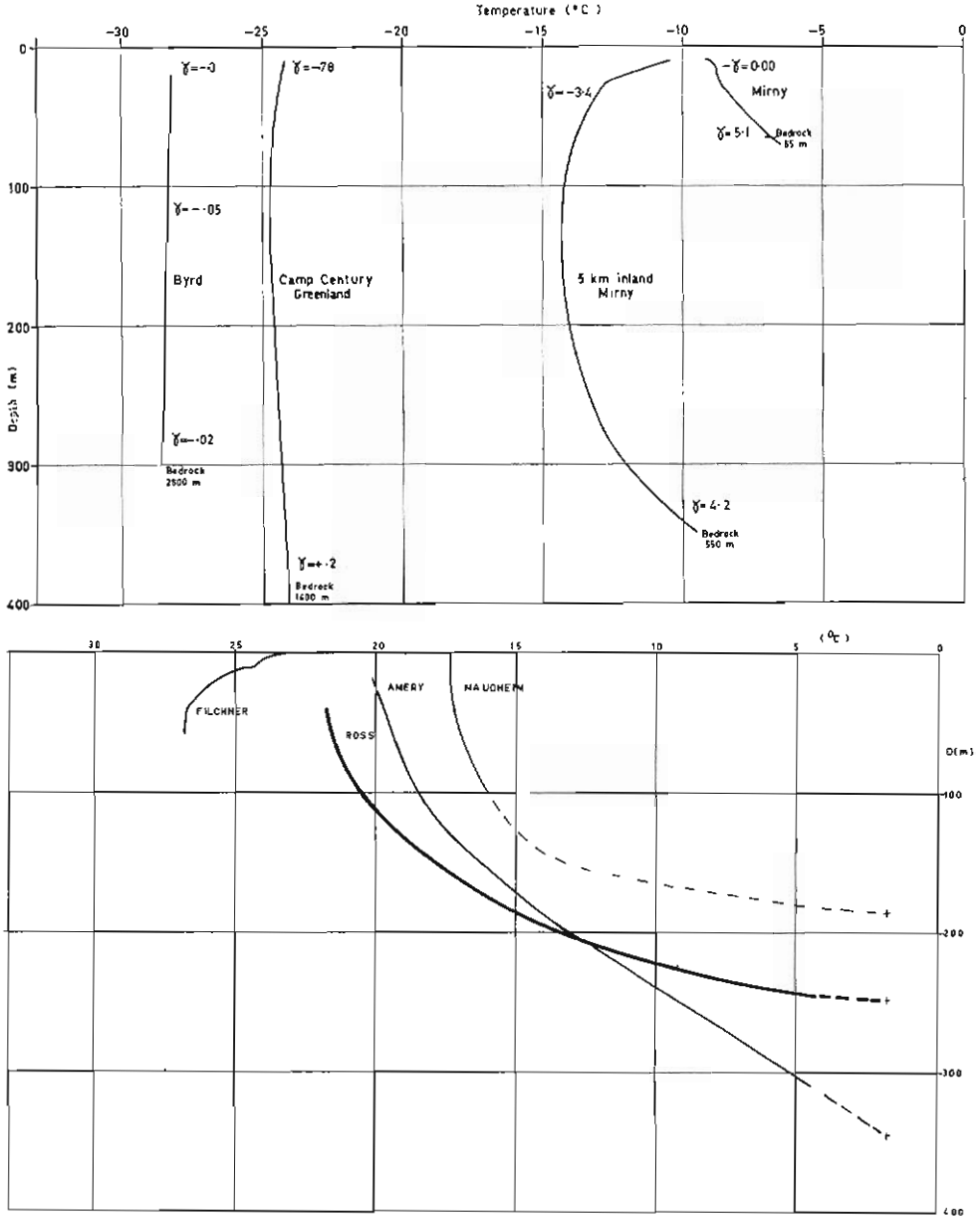

FIG. 4.1a. Measured temperature profiles in ice caps and ice shelves showing the temperature gradients γ in the upper layers (Ref. Table 4.1) in °C/100 m.

Robin (1955) showed that such a gradient could be caused by the warming of the surface of the ice as the ice flowed outwards and downwards.

We now review the theoretical studies which have been made to calculate temperature profiles through ice masses and then consider further modifications which can give more accurate predictions of temperature profiles in moving ice masses.

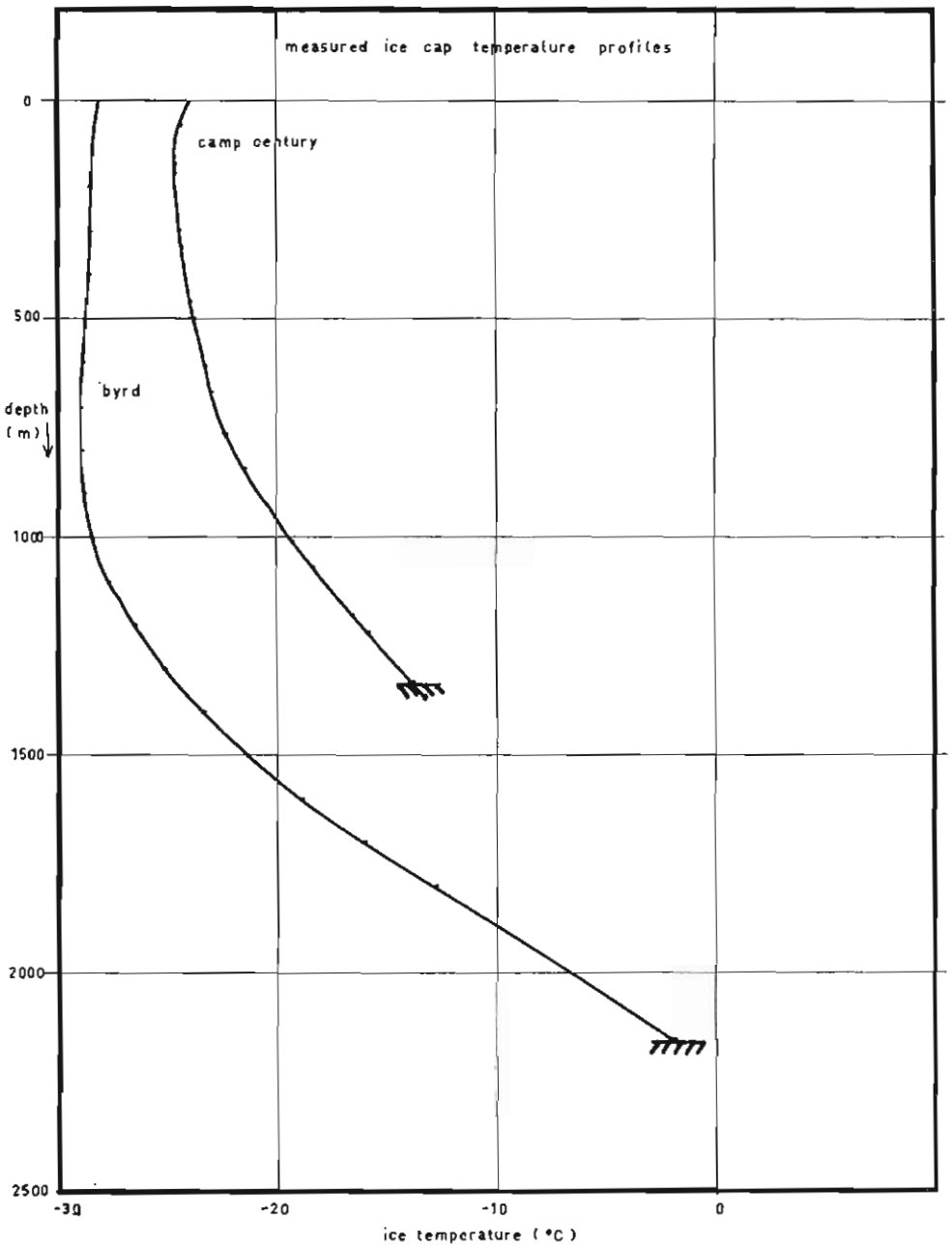

FIG. 4.1.b. Measured ice cap temperature profiles: deep profiles (from Gow *et al.* (1968) and Hansen (pers. comm.)).

4.2. CALCULATED TEMPERATURE PROFILES

If the ice mass were completely stationary with no accumulation and no movement, the temperature profile would simply be a straight line determined by the mean air tempearture at the surface and the gradient corresponding to the geothermal heat flux at the base; or by the basal temperature, in the case of the basal temperature reaching the pressure melting point. Processes such as the accumulation at the surface, basal melting, vertical movement and strain, horizontal motion, and also long-term climatic change, all affect the temperature profile, and are reflected in the typical convex down curvature of the measured profiles, and in some cases in negative temperature gradients at the surface.

Calculations will be given in this section incorporating as many of the above parameters which are known, or could be estimated, into the governing equations to account for the temperature profiles observed in the ice.

In what follows, reference is made to the results of the following previous workers: Robin (1955), Bogoslovski (1958), Wexler (1959, 1960, 1961), Radok (1959), Jenssen and Radok (1961), Chi Tien (1960), Crary (1961), Shoumsky and Zotikov (1963), Zotikov (1963) and Budd (1966).

Robin's (1955) steady-state temperature results for the temperature θ at height z above the ice base,

$$\frac{d\theta}{dz} = \left(\frac{d\theta}{dz}\right)_b e^{-(A/2H\kappa)z^2} \tag{1}$$

and

$$\theta = \theta_H - \left(\frac{d\theta}{dz}\right)_b \sqrt{\frac{2H\kappa}{A}} \left(\operatorname{erf} \sqrt{\frac{A}{2H\kappa}}\, H - \operatorname{erf} \sqrt{\frac{A}{2H\kappa}}\, z\right) \tag{2}$$

where H is the ice thickness,

A is the surface accumulation rate,
$(d\theta/dz)_b$ is the basal temperature gradient,
κ is the ice thermal diffusivity,

are relatively simple to apply. They incorporate the accumulation rate at the surface and a balancing vertical sinking, but do not allow for horizontal motion and warming or non-steady-state change in thickness. Robin also found a very simple and useful result for the negative surface temperature—depth gradient, due to horizontal movement downhill to warmer temperatures in absence of conduction, viz.,

$$\frac{d\theta}{dz} = -\frac{V\alpha\lambda}{A} \tag{3}$$

where V is the downslope velocity,

α is the surface slope,
λ is the rate of change of air temperature in the vertical.

The numerical results of Jenssen and Radok (1961) (1963) incorporate both the effects of conduction and downslope movement. To apply their results to a real situation, the values of accumulation, velocity, and ice thickness can be extra-

polated from their graphs. The horizontal velocities which they used were calculated from an equation of continuity which implied a steady-state ice cap. It will be shown here that a simple extension allows this approach to be applicable to rising or sinking ice caps as well.

The effect of climatic change has been examined by Wexler (1959) and Jenssen and Radok (1961), but it will be shown that the available temperature profiles may to a large degree be accounted for by the effects of movement and accumulation. Hence, these effects must first be studied in detail, then leaving only the remaining discrepancies to be examined in reference to climatic change.

Since the flow law of ice is highly temperature-dependent, we require these temperature distributions throughout an ice mass in order to calculate the velocity

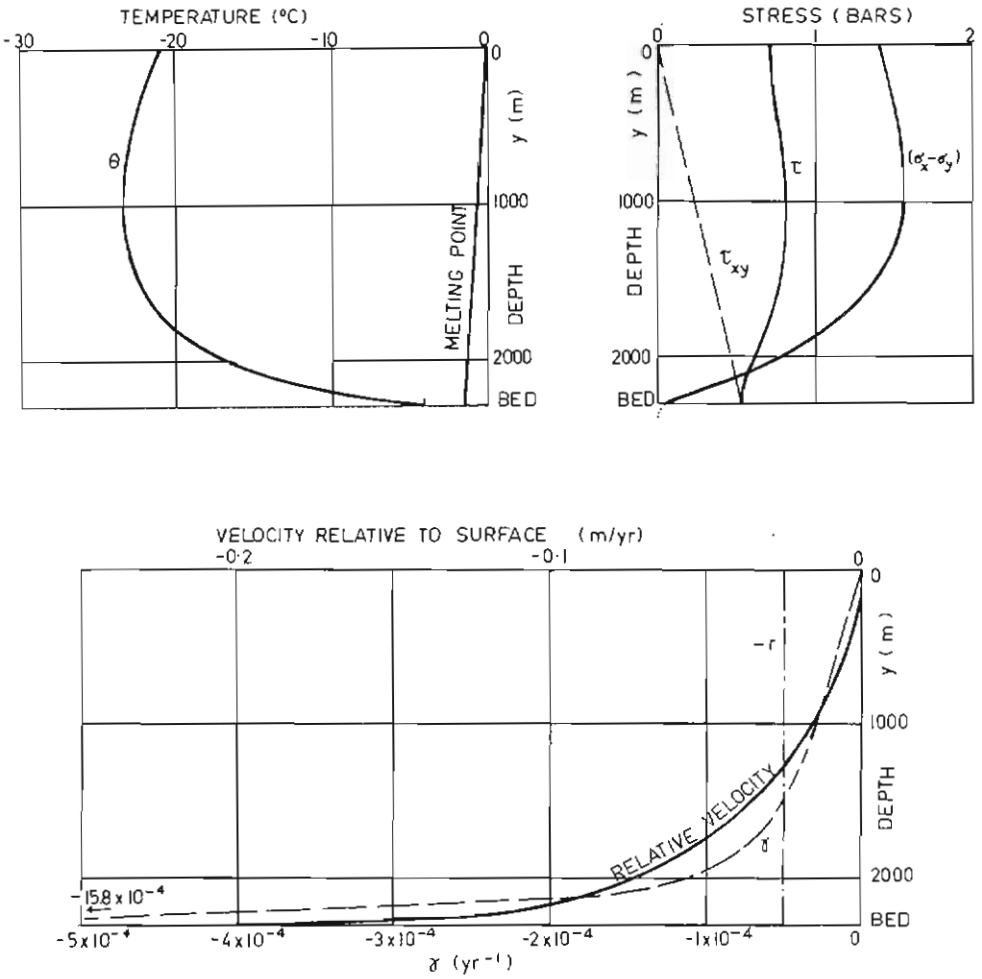

FIG. 4.2. Calculated depth profiles of temperature θ, longitudinal, vertical, shear and "effective" shear stresses (σ_x, σ_y, τ_{xy},τ), relative velocity, shear strain rate γ, and longitudinal strain rate r for a position on the Greenland ice cap, by Nye (1959). It is concluded that $\tau \simeq (\sigma_z - \sigma_y)/2$ throughout the thickness.

distribution. We shall now examine the effect of the temperature profile from the surface to base on the corresponding velocity profile. Following that, it will be shown that the velocity of the ice also affects the temperature profile through internal viscous friction, so this is also considered for various flow laws. Next, the effect of accumulation at the surface, horizontal velocity and surface warming, rising and sinking of the ice mass, the approach of the temperature profiles to steady-state, and the effect of climatic temperature variations at the surface are all examined in order to be able to calculate the temperature profiles along a flow line of an ice mass. In the later sections these temperature distributions will be used in the study of the variation of velocity and strain rate along a flow line.

4.3. EFFECT OF TEMPERATURE PROFILE ON VELOCITY PROFILE

Nye (1959) showed how a typical temperature distribution estimated for Greenland affected the vertical profiles of strain rate and velocity calculated from Glen's (1955) flow law, cf. Fig. 4.2. The results of Section 2 suggest that Glen's simple power law extrapolated to low stress gives strain rates much too low, but nevertheless the high concentration of shear in the basal layers is immediately apparent, due to both the high shear stress and higher temperatures near the base.

To illustrate the direct effect of the shape of the temperature distribution on the velocity profile, Fig. 4.3 shows relative velocity distributions calculated for three different temperature profiles from a flow law of the form (cf. Section 4)

$$\dot{\gamma} = \left(\frac{\tau}{B}\right)^n e^{v\theta}$$

and with equal velocities at the surface and zero velocity at the base.

These results illustrate clearly that, for temperature—depth profiles with the warmest ice at the base (the usual case in cold ice caps), the velocity gradient is largely concentrated in the lowest layers. It is then not of much importance whether this movement is composed of rapid shear in basal pure ice or entirely of slide between a pure ice surface and bedrock interface; or, as is more likely, a rapid shear in a mixture of ice, sand and rock, in a basal layer (cf. Hansen 1966). Nye (1959) points out that the effect of an additional small longitudinal stress throughout the ice thickness does not greatly affect the vertical velocity profile.

Certain refinements need to be made to this simple treatment. Robin (1955) showed how the frictional heating of movement can affect the temperature profile. Jenssen and Radok (1963), in their calculations of temperature distributions in ice, adopted Robin's result of simply adding the total frictional heating to the geothermal heat flux at the base. The validity of this approach increases as the thickness of the layer in which it is produced decreases. It will be shown in the following section that this method is a good approximation for all but the basal layer.

Lliboutry (1963) gave a more detailed treatment considering the heat produced over an extended section. This is taken up in the next section which treats the effect of movement on the temperature and the consequent positive feedback process.

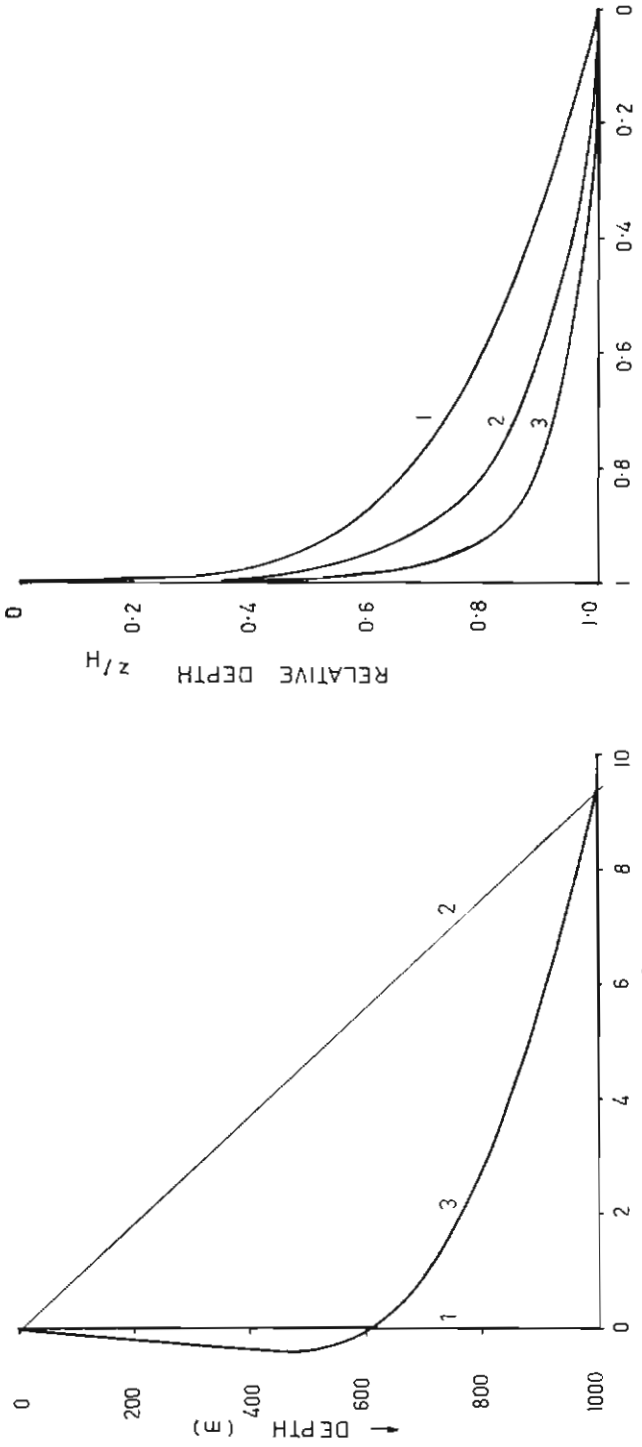

FIG. 4.3. Typical relative velocity profiles calculated in a 1,000 m-thick ice cap, where the basal shear stress is 1 bar for three different temperature profiles (1) isothermal, (2) linear, (3) as calculated for the Wilkes ice cap (cf. Fig. 4.16), using a flow law of the form $\dot{\gamma} = (\tau/B)^n e^{v\theta}$.

4.4. INTERNAL FRICTIONAL HEATING AND ICE MOTION

Already Lagally (1932-3) had considered the frictional heating produced internally in a glacier subject to *viscous* flow, and concluded that the most heat is produced where the shear is greatest, i.e. near the glacier bed. It seems plausible from the study of the ice flow law (Section 2) that frictional heating producing higher temperatures in the ice will produce higher shear rates and hence more internal heating, with the consequence of a strong positive feedback. This argument is relevant to the contexts of glacier-sliding and catastrophic glacier-advances, which are not treated here (cf. Weertman 1957, 1962, 1964 and Lliboutry 1959, 1965).

We shall now try to determine the heating produced by friction within an ice mass and the consequent effect on the ice flow. We need only deal here with "cold" ice masses with temperatures throughout below the pressure melting point. In temperate glaciers, with temperatures everywhere near melting point, the friction caused by motion produces only melting and no temperature changes.

Robin (1955) and Jenssen and Radok (1961, 1963) incorporated the friction heating into the basal gradient by adding the heat produced by friction to the geothermal heat flux. In view of the calculations of the velocity profiles of the previous section (4.3) this procedure appears to be a reasonable approximation and should apply more closely as the ice motion approaches block-sliding. Robin (1955) pointed out that the average geothermal flux of 38 cal $cm^{-2}yr^{-1}$ is equivalent to the energy released by friction below an ice mass, with basal shear stress 0·88 bars, and moving with a speed of about 18 m yr^{-1}. This result comes from the general equation for frictional heat produced by sliding, viz.,

$$\frac{dE}{dt} = \frac{\tau V}{J} \tag{4}$$

where $\frac{dE}{dt}$ is the amount of heat energy (E) produced per unit area per unit time (t) at the base,

τ is the basal shear stress,

V is the velocity of the ice above the thin basal layer in which the shear is assumed to take place,

J is the mechanical equivalent of heat.

Lliboutry (1963) found for the total heat flux (ϕ) produced by the geothermal heat flux (G) and frictional (Γ) the expression

$$\phi = \sqrt{G^2 + \Gamma^2}.$$

For the temperature θ at depth z, Lliboutry used the differential equation

$$K\frac{d^2\theta}{dz^2} - c\rho w\frac{d\theta}{dz} + \frac{\dot{\gamma}\tau}{2J} = 0 \tag{5}$$

where K is the ice conductivity,

$c\varrho$ is the heat capacity per unit volume,

w is the vertical velocity of the ice,

J is the mechanical equivalent of heat,

γ, τ are the effective shear strain rate and shear stress for laminar flow.

From this he deduced for the temperature profile in a cold ice mass corresponding to Robin's (1955) steady-state model

$$\theta = \theta_s + b\sqrt{G^2 + \Gamma^2}\,\frac{\sqrt{\pi}}{2}\left(\operatorname{erf}\frac{H}{b} - \operatorname{erf}\frac{z}{b}\right) \tag{6}$$

where θ_s is the surface temperature,

H is the ice thickness,

$b = \sqrt{2H\kappa/A}$,

A is the accumulation rate at the surface,

κ is the thermal diffusivity.

Lliboutry (1963) considers in detail two special cases of equation (5): (i) firstly, for a basal layer (in which most of the internal friction is produced) where w is small and hence the term with $c\varrho w$ can be neglected: and (ii) for the upper layers of the glacier where the heat from the internal friction may be considered just as additional flux from below, so that the third term can be omitted, and its effect incorporated into an increased basal gradient.

In case (i) Lliboutry takes the shear stress constant (its value at the base) throughout the deformation layer. In this case the strain rate and resultant heat production decreases upwards simply due to the lower temperatures. It is shown below, however, that the decrease in stress above the base must also be considered in calculating the heat dissipation.

In the following we extend Lliboutry's work to cover the heat produced by an extended source of internal friction from the base well into the medium. This is the case applicable to slowly moving ice caps without a high basal temperature gradient (cf. Hansen 1966). The following procedure will be adopted.

We consider a cold ice mass, very wide, of constant thickness H, moving down an inclined plane, α, in laminar flow such that the only velocity is longitudinal and the only velocity gradient is in the direction perpendicular to the bed.

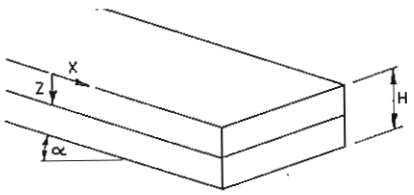

We take orthogonal axes, x in the line of motion and z downwards from the glacier surface. We adopt the following symbols:

ρ ice density,

g gravity acceleration,

θ ice temperature at depth z,

t time,

Q the quantity of heat per unit volume,

K ice conductivity (thermal),

E energy per unit volume of ice,

c thermal capacity for ice (per unit mass),

κ thermal diffusivity of ice.

To obtain a clear insight into the various factors influencing the temperature distribution we shall treat several simple cases separately first, before we study the complex result for a more general ice cap in which the various factors act together. For the moment, zero surface accumulation and a steady-state temperature distribution are assumed, and the effects of the surface warming as the ice moves down the slope are neglected.

Temperatures and the velocities in an ice mass where heat is produced by internal friction will be derived for the following three cases:

(i) *Assuming an ice flow law of Newtonian type (constant viscosity).* This case has been treated in detail by Lagally (1932) and for low stresses and strain rates (less than 0·5 bar shear stress, cf. Section 2.3) represents a close approximation to reality. The flow law is assumed independent of temperature.

(ii) *Assuming a power law for ice flow.* This will illustrate the effect of the non-linearity of the flow. The variation of the flow law with temperature is again neglected.

(iii) *Assuming a temperature-dependent power law for ice flow.* This produces a more complex differential equation with the strong positive feedback, high shear producing higher temperatures which then produce even higher shear rates.

4.4.1. *Internal friction heating and ice motion—constant viscosity.*

For ice of constant viscosity μ (independent of stress and temperature) equation (17) of Section 3.4.1. shows that, for the simple model described above, the velocity u at depth z is given by

$$u = u_s - \frac{\rho g \alpha}{2\mu} z^2 \tag{7}$$

where u_s is the velocity of the surface and

$$\frac{du}{dz} = -\frac{\rho g \alpha}{\mu} z \tag{8}$$

Since there are no other velocities, the rate of energy dissipated per unit volume due to the viscous friction is given by

$$\frac{dE}{dt} = \frac{\partial E}{\partial t} + u \frac{\partial E}{\partial x} \quad \text{and} \quad \frac{\partial E}{\partial t} = \mu \left(\frac{du}{dz}\right)^2 \tag{9}$$

But since there is to be no variation in the rate of energy, dissipation along the direction of flow $\partial E/\partial x = 0$. Hence,

$$\frac{dE}{dt} = \frac{\partial E}{\partial t}$$

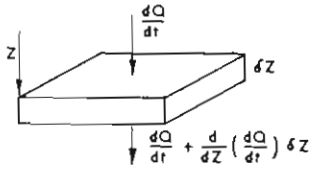

Consider a small element of ice, thickness δz, at depth z (cf. figure above). The heat flux through the ice is given by

$$\frac{dQ}{dt} = -K\frac{d\theta}{dz}.$$

Hence, for steady-state we obtain

$$\frac{\partial E}{\partial t} = J\frac{d}{dz}\left(\frac{d\theta}{dz}\right) = -JK\frac{d^2\theta}{dz^2} \tag{10}$$

So if the temperature profile is to be such that the heat produced by friction is conducted away, leaving the temperature profile constant in time at a point (x, z) fixed in space, we must have

$$\mu\left(\frac{du}{dz}\right)^2 = -JK\frac{d^2\theta}{dz^2} \tag{11}$$

i.e.,

$$\mu\left(\frac{\rho g\alpha}{\mu}\right)^2 z^2 = -JK\frac{d^2\theta}{dz^2} \tag{12}$$

Integrating with respect to z, this becomes

$$\frac{d\theta}{dz} = \frac{-(\rho g\alpha)^2}{3JK\mu}z^3 + c_1 \tag{13}$$

Now, if for $z = H$ (at the glacier bed) we have

$$\frac{d\theta}{dz} = \gamma_b$$

as determined by the geothermal flux ($\simeq$ 38 cal $cm^{-2}yr^{-1}$), then

$$\frac{d\theta}{dz} = \frac{(\rho g\alpha)^2}{3JK\mu}(H^3 - z^3) + \gamma_b \tag{14}$$

and

$$\theta = \frac{(\rho g\alpha)^2}{12JK\mu}z(4H^3 - z^3) + \gamma_b z + c_2.$$

At the surface ($z = 0$), θ equals θ_s, the annual mean surface temperature; then

$$\theta = \frac{(\rho g\alpha)^2}{12JK\mu}z(4H^3 - z^3) + \gamma_b z + \theta_s \tag{15}$$

So far it has been assumed that the temperature everywhere has remained well below pressure melting.

The basal temperature is the highest and is obtained by taking

$$z = H, \qquad \theta = \theta_b$$

as

$$\theta_b = \frac{(\rho g \alpha)^2}{4JK\mu} H^4 + \gamma_b H + \theta_s \tag{16}$$

The condition that the base of the ice remains below melting point is

$$\theta_b < 0°\text{C} \qquad \text{(or the pressure melting temperature)}$$

i.e.,

$$\theta_s \leqslant -\frac{(\rho g \alpha)^2}{4JK\mu} H^4 - \gamma_b H \tag{17}$$

If the base does reach melting (θ_m), then part of the heat is used for melting, viz. (Robin 1955),

$$q_b = K\gamma_b = q_G \frac{\theta_m - \theta_{b,c}}{\theta_s - \theta_{b,c}} \tag{18}$$

where q_G is the geothermal flux

$\theta_{b,c}$ is the calculated basal temperature (from equation (16)).

The temperature gradient at the base then becomes:

$$\gamma_b = \frac{q}{K} \frac{\theta_s - \theta_m}{\theta_s - \theta_{b,c}} \tag{19}$$

The results of this section may be summarised as follows:

(1) The tempeature is highest at the base.

(2) The positive temperature—depth gradient is highest at the surface.

(3) In absence of melting, the heat flux at the surface is equal to the geothermal flux plus the total heat produced by motion. The latter equals the loss of potential energy of the ice during motion.

(4) The rate of change of temperature gradient with depth is greatest at the base.

(5) The most important result is that the internal friction produces an upward convex curvature in the temperature—depth profile near the base. This has not yet been observed in measured profiles (cf. Fig 4.1) which suggests that other factors are more important in the profiles to bedrock measured so far, or that the internal heat produced may be negligible for these cases.

Few profiles, however, go right to the bedrock and, for those that do, the movement of the ice is not well known. Hence, it will be most valuable to obtain temperature profiles right to the bedrock in regions where the velocity is measured and also the velocity—depth profile there. In this way a check can be made on both the internal heating and the geothermal flux as well as the properties of the ice—rock interface.

To illustrate the magnitude of the internal heat production in the ice we take typical values of the parameters for an ice mass and evaluate the difference between the basal and surface gradients from equation (14), with $z = 0$.

$$\gamma_s - \gamma_b = \lambda_1 \frac{H^3}{3}$$

where

$$\lambda_1 = \frac{(\rho g \alpha)^2}{JK\mu}.$$

As typical values of the various parameters we take the following:

$\rho = 0{\cdot}917$ g cm^{-3},
$g = 0{\cdot}98 \times 10^3$ cm sec^{-2}
$\alpha = 10^{-2}$,
$J = 4{\cdot}2 \times 10^7$ erg/cal,
$K = 5 \times 10^{-3}$cal cm^{-2} sec^{-1} °C^{-1},
$\mu = 10^{15}$ poise,
$H = 10^3$ m.

Then $\gamma_s - \gamma_b = 1{\cdot}16$ °C/100 m, which is equivalent to about $0{\cdot}53 \times$ the basal heat flux. Fig. 4.4 shows a typical temperature profile for a simple model of this type.

The ratio q_z/Q %, of the heat flux q_z produced below a certain level z to the total heat flux at the surface Q, is shown in the following table.

TABLE 4.2.a

PROPORTION q_z/Q PRODUCED BELOW DEPTH z OF TOTAL HEAT.

Depth z m	0	500	800	900	1000
q_z/Q %	100	87·5	49	27	0

4.4.2. *Internal friction and power flow law*

We next consider the case of a power flow law of the form

$$\dot{\varepsilon} = \left(\frac{\tau}{B}\right)^n \tag{20}$$

where $\dot{\varepsilon}$ is the shear strain rate,
τ is the shear stress,
B and n are constants, as discussed in Section 2.

In this case, for the simple model described above (Section 4.4), we still have τ_{xz} as the only shear stress and du/dz as the only shear strain rate. Thus the rate of energy dissipation is given by

$$\frac{dE}{dt} = \tau_{xz}\dot{\varepsilon}_{xz} = \frac{(\tau_{xz})^{n+1}}{B^n} \tag{21}$$

and since

$$\tau_{xz} = \rho g \alpha z,$$

we obtain

$$\frac{dE}{dt} = \frac{(\rho g \alpha)^{n+1}}{B^n} z^{n+1} = -JK\frac{d^2\theta}{dz^2} \tag{22}$$

and the differential equation becomes

$$\frac{d^2\theta}{dz^2} + \lambda z^{n+1} = 0 \tag{23}$$

where

$$\lambda = \frac{(\rho g \alpha)^{n+1}}{B^n JK} \tag{24}$$

From this we obtain by integration

$$\frac{d\theta}{dz} = \frac{\lambda}{n+2}(H^{n+2} - z^{n+2}) + \gamma_b \tag{25}$$

and

$$\theta = \theta_s + \gamma_b z + \frac{\lambda}{n+2}\left(H^{n+2}z - \frac{z^{n+3}}{n+3}\right) \tag{26}$$

In particular, if $n = 3$, we obtain

$$\frac{d\theta}{dz} = \frac{(\rho g \alpha)^4}{5B^3 JK}(H^5 - z^5) + \gamma_b \tag{27}$$

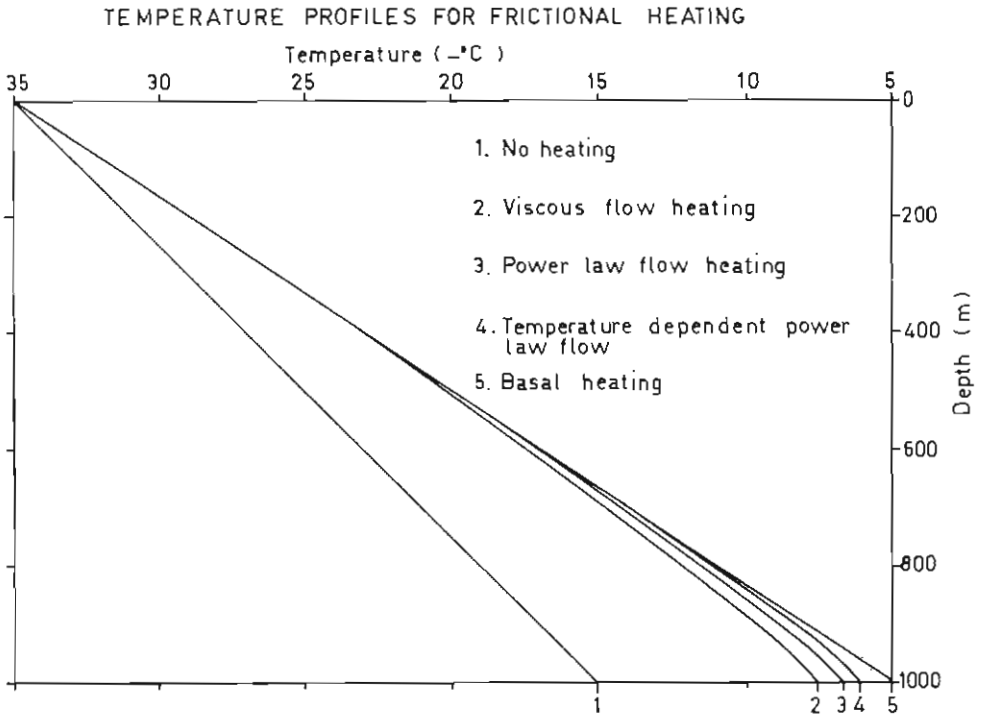

FIG. 4.4. Steady-state temperature profiles showing the effect of frictional heating for various types of flow laws, in absence of other effects.

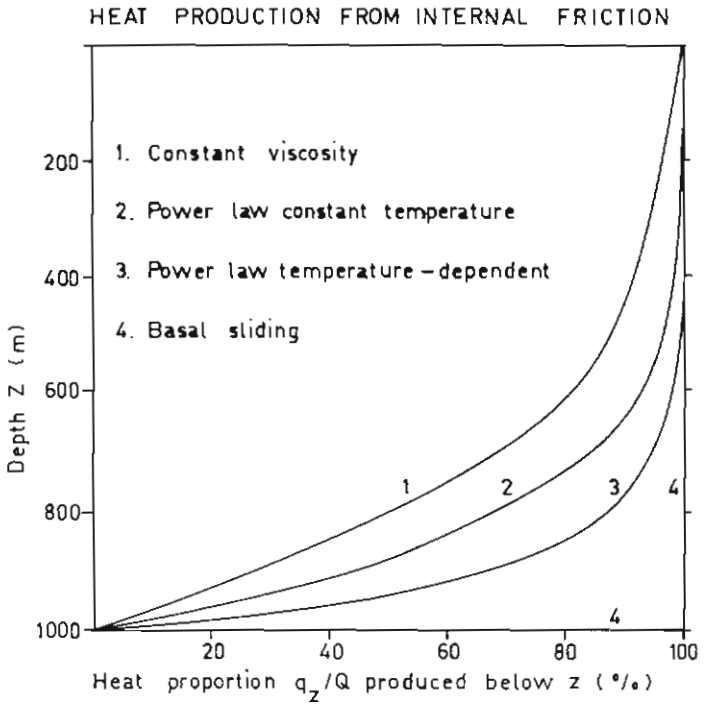

FIG. 4.5. The proportion of the internal steady-state heat flux produced below various levels is shown for the types of flow laws of Fig. 4.4.

and

$$\theta = \frac{(\rho g\alpha)^4}{5B^3JK}\left(H^5 z - \frac{z^6}{6}\right) + \gamma_b z + \theta_s \tag{28}$$

Similar qualitative conclusions apply as in Section 4.4.1 above but, in this case, since $d^2\theta/dz^2$ is proportional to the higher power of z, more of the heat produced for the same potential energy loss is concentrated in the lower layers, i.e.,

$$\frac{d^2\theta}{dz^2} = -\lambda z^{n+1} = \frac{(\rho g\alpha)^4}{B^3JK} z^4.$$

Hence, the temperature gradient changes much less in the upper layers than in the basal layers. The temperature at the base is now given by

$$\theta_b = \theta_s + \gamma_b H + \frac{(\rho g\alpha)^4}{6B^3JK} H^6 \tag{29}$$

The third term on the right-hand side gives the increase in temperature of the base due to the movement.

We write

$$\lambda_2 = \frac{(\rho g\alpha)^4}{B^3JK}.$$

Then, taking the same values of the parameters in λ as Section 4.1, with the exception that $\mu = 10^{15}$ poise now corresponds to $B = 10^9$ bars sec $^{1/3}$ [cf. Budd 1966a, equation (21)], we obtain for the temperature increase due to motion

$$\theta_b - \theta_s - \gamma_b H \simeq \frac{(\cdot 917 \times \cdot 98 \times 10^3 \times 10^{-2})^4}{4 \cdot 2 \times 10^7 (10^9)^3 \, 5 \times 10^{-3}} \frac{(10^5)^6}{6} \, ^\circ\mathrm{C}$$

$$\simeq 5 \cdot 2^\circ\mathrm{C}.$$

The increased flux at any level caused by the movement is given by

$$K\left(\frac{d\theta}{dz} - \gamma_b\right) = \frac{(\rho g \alpha)^4}{5B^3 J}(H^5 - z^5).$$

The total heat produced amounts to a flux corresponding to a gradient in ice of 0·63 °C/100 m, or 0·39 times the geothermal flux. Owing to the high power of z present in equation (27), most of the increased flux is in the lower layers. Table 4.2b gives for a 1000m-thick ice cap the percentage of the total flux which is produced below that level. Fig. 4.4 shows a typical temperature profile.

TABLE 4.2b

z: depth below surface 1,000m-thick ice mass.
q_z/Q: fraction of total heat flux caused by internal friction produced below level z.

z (m)	0	500	800	900	950	990	1000
$q_z/Q\%$	100	97	67	41	23	5	0

From this we see that the upper half of the ice mass contributes only 3% to the frictional heating, the bottom 1/5 (200 m) contributes 67%, and the bottom 100 m still over 40%. Comparing this with Table 4.2a it becomes clear that the presence of a high power flow law is very effective in concentrating the heat production at the base.

4.5. POSITIVE FEEDBACK BETWEEN TEMPERATURE AND VELOCITY AT THE BASE OF A MOVING ICE MASS.

We now consider the case of a flow law which is temperature-dependent. From the results of the measurement of ice flow at stresses of the magnitude which we are dealing with (Mellor and Smith 1966, and Butkovitch and Landauer (1960), it was shown (cf. Section 2.4) that the flow law of ice can be represented by

$$\dot{\varepsilon} = \left(\frac{\tau}{B}\right)^n e^{\nu\theta} \tag{30}$$

where θ is the temperature in °C
and $\nu \simeq 0 \cdot 1$ to $0 \cdot 3$ °C^{-1}.

The differential equation (23) now becomes:

$$\frac{d^2\theta}{dz^2} = -\lambda z^m e^{\nu\theta} \tag{31}$$

where

$$\lambda = \frac{(\rho g \alpha)^m}{B^n J K} \tag{32}$$

and

$$m = n + 1.$$

The presence of θ on the right-hand side now makes the equation much less tractable than previously.

A solution in series for this equation has been found and has the following form:

$$\theta = \theta_s + \gamma_s z + \lambda e^{\nu\theta_s} z^6 \left[\frac{1}{5.6} + \frac{\nu\gamma_s z}{7.6} + \frac{(\nu\gamma_s z)^2}{8.7.2!} + \frac{(\nu\gamma_s z)^3}{9.8.3!} + \ldots \right] \tag{33}$$

$$\frac{d\theta}{dz} = \gamma_s + \lambda e^{\nu\theta_s} z^5 \left[\frac{1}{5} + \frac{\nu\gamma_s z}{6} + \frac{(\nu\gamma_s z)^2}{7.2!} + \frac{(\nu\gamma_s z)^3}{8.3!} + \ldots \right] \tag{34}$$

where θ_s, γ_s are the temperature and the temperature gradient at the surface ($z = 0$).

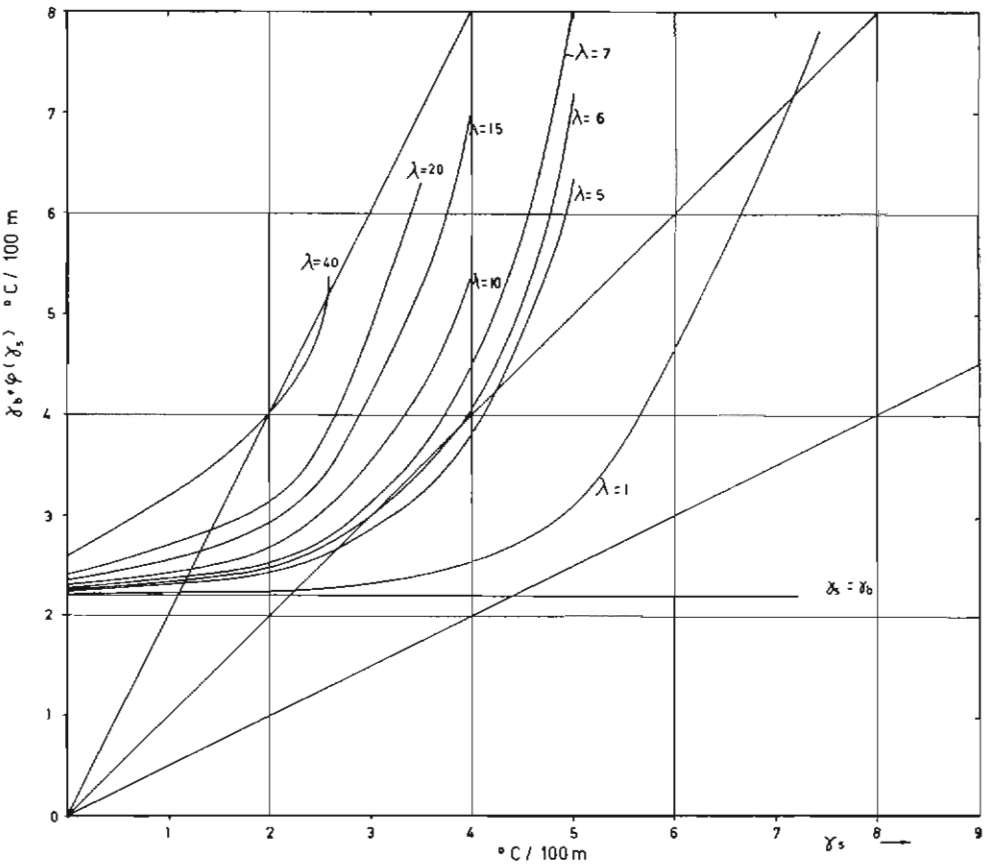

FIG. 4.6. Graphical solution for the increase in surface temperature gradient γ_s above the basal gradient γ_b, by internal friction from a temperature θ dependent power flow law of the form $\dot{\varepsilon} = (\tau/B)^n e^{\nu\theta}$ for different ice thicknesses H, and velocities (implicit in λ) $\gamma_s = \gamma_b + \lambda\Phi(\nu\gamma_s H)$.

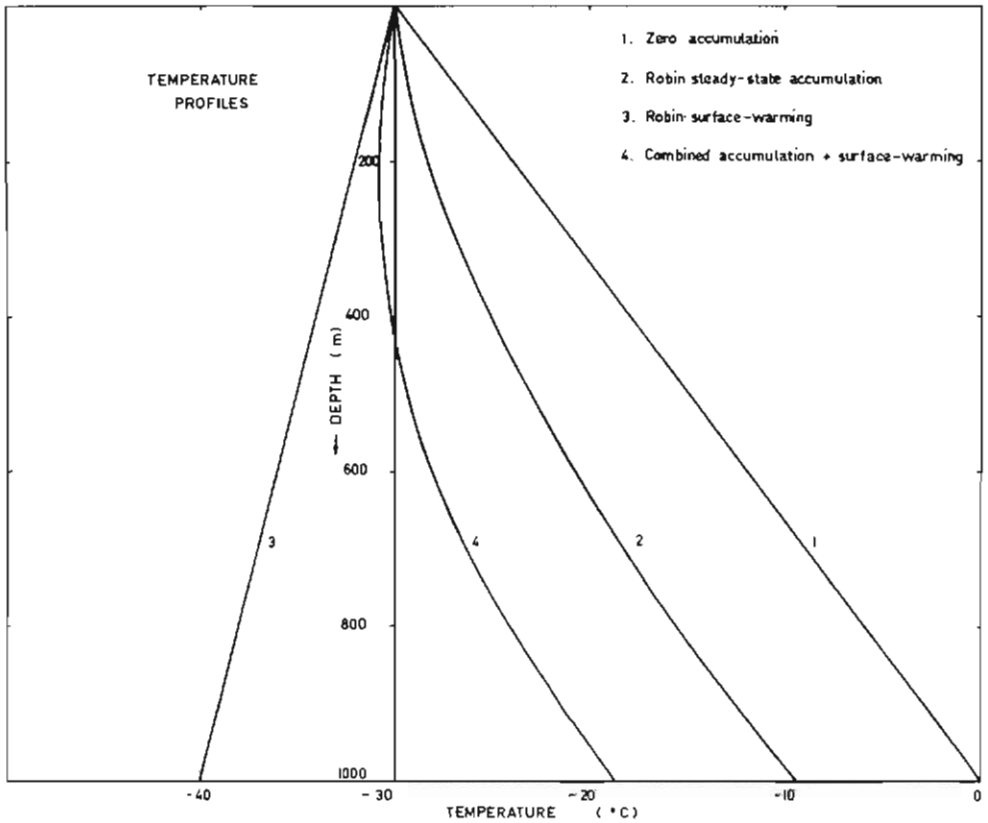

FIG. 4.7. Temperature—depth profiles for a 1,000 m ice cap determined by (1) surface temperature θ_s, and basal gradient γ_b; (2) θ_s, γ_b and accumulation rate A; (3) θ_s, A, surface-warming $\alpha V\lambda$ but no conduction; (4) θ_s, γ_b, A and $\alpha V\lambda$.

To obtain the value of γ_s in terms of γ_b—the temperature gradient at the base—which is generally the known boundary condition, a graphical solution can be found as illustrated in Fig. 4.6. Hence, we obtain γ_s from

$$\gamma_s = \gamma_b + \Phi(\gamma_s) \tag{35}$$

where $\Phi(\gamma_s)$ is the increased flux due to internal friction and has been evaluated for a range of surface gradients. Hence, by plotting

$$\gamma_b + \Phi(\gamma_s) \text{ versus } \gamma_s,$$

the intersection of these curves with $\gamma_s = \gamma_s$ gives the appropriate solution for γ_s. It is now discerned that, because of the rapidly increasing function Φ, instability may be reached such that the heat produced by an increase in γ_s cannot be conducted away by that increase in γ_s. In this case there is no solution. For small values of λ, two solutions exist, in general the lower γ_s value being stable, whereas the higher is unstable. Where there is no solution it means that no steady-state temperature profile exists for the prescribed boundary conditions.

Taking typical values as before we may find the critical values of heat from internal friction, above which the solution becomes unstable. For a shear stress, at the base, of 1 bar this corresponds to a certain velocity as determined from equation (36) below. The value of the critical velocity decreases as the ice thickness increases.

The instability is *not* caused by the temperature of the ice reaching melting but by the increase in internal heat production (proportional to $d^2\theta/dz^2$) becoming too large, by an increase in temperature gradient, to be conducted away by that increase in temperature gradient.

The velocity gradient in the ice mass is given by

$$\frac{du}{dz} = 2\left(\frac{\rho g \alpha}{B}\right)^n e^{\nu\theta} = 2\,\frac{JK}{\rho g \alpha z}\,\frac{d^2\theta}{dz^2}. \tag{36}$$

From equation (34) this may be written

$$\frac{du}{dz} = \frac{2\lambda e^{\nu\theta_s} JK}{\rho g \alpha}\, z^3\left[1 + \nu\theta_s z + \frac{(\nu\theta_s z)^2}{2!} + \ldots\right] \tag{37}$$

since

$$\frac{d^2\theta}{dz^2} = \lambda e^{\nu\theta_s} z^4\left[1 + \nu\theta_s z + \frac{(\nu\theta_s z)^2}{2!} + \ldots\right] \tag{38}$$

Hence, integrating, we find

$$u_s - u = \frac{2\,.\,JK\lambda e^{\nu\theta_s}}{\rho g \alpha}\, z^4\left[\frac{1}{4} + \frac{\nu\theta_s z}{5} + \frac{(\nu\theta_s z)^2}{6\,.\,2!} + \ldots\right] \tag{39}$$

From this equation and the values of the parameters above we find the velocity at the surface of the 1,000 m ice mass as approximately 8 m yr^{-1}.

It should be pointed out here that the temperature curves (cf. Fig. 4.4) do not agree at all with the only temperature profiles so far measured down to bedrock in cold ice caps (Bogoslovski 1958, Hansen 1966). The measured profiles show comparatively constant gradients in the lower layers. This suggests that internal heat produced in these cases is negligible or counteracted by upward curvature by other factors, such as accumulation. However, the movement rate at these positions is also believed to be small. In order to evaluate fully the influence of movement on the temperature of the ice mass, it will clearly be necessary to obtain temperature profiles into the bedrock beneath *moving* ice masses. Fig. 4.4 shows that there is only a slight difference between the temperature profiles for basal heating (all the heat produced at the base) and for internal heating from motion with a temperature-dependent power flow law. This difference is only apparent very near the base.

The preceding discussion is in agreement with the conclusions of Lliboutry (1963) that the problems of

(1) heat production by internal friction, and

(2) accumulation with vertical motion,

can largely be treated separately. This is because the internal friction is produced mainly in the basal layers where the vertical motion is negligible, whereas the accumulation and vertical motion are mainly associated with the upper layers where the frictional heating is negligible. In the next section we examine the effect of surface accumulation and vertical movement on the temperature profile; neglecting internal friction, or by considering it as incorporated in an increased basal temperature gradient, (γ_b^*), i.e.,

$$\gamma_b^* = \gamma_G + \frac{\tau V}{JK},$$

where γ_G is the geothermal gradient in ice,
τ is the shear stress at the base,
and V is the average downslope velocity through the ice.

4.6 THE EFFECT OF ACCUMULATION AND VERTICAL MOVEMENT OF THE ICE ON THE TEMPERATURE PROFILE

This problem has been discussed in detail, first by Robin (1955), and later by Zotikov (1963), who have both given useful theoretical solutions for the profiles of temperature and temperature gradient. Jenssen and Radok (1961, 1963) obtained numerical solutions to fit particular cases, taking account of ice thickness, surface slope, vertical movement, horizontal movement and accumulation rate.

Measured temperature gradients in the Antarctic [Bogoslovski 1958, Mellor 1960, Crary 1961, Gow 1963, Budd 1966, Battye (unpublished)] indicate that the physical assumptions made in the theoretical calculations seem to be at least partly valid. However, at this stage there exists no detailed set of surface temperature gradients going inland from the coast in regions where the associated movement parameters are also known. The temperature gradient values obtained by Budd (1966) at Wilkes are sufficiently close to the movement line of McLaren (1967) to allow a close estimate to be made of the velocities there. However, these measured velocities are small and, though quite compatible with the velocities considered in the analysis of the temperature gradients there, they do not provide a full test of the theory.

In this and the following sections the temperature profiles in moving, accumulating ice masses will be considered from cases representing the most simple situations to those typical of regions in the Antarctic. The main advance over previous work is believed to be the removal of the assumption of steady-state ice cap profiles. The rise or fall of the surface in time may be more important than other effects associated with steady-state conditions. For instance, it may explain the positive temperature gradients measured in thick ice in inland Antarctic by Battye (unpublished). Furthermore, the study of temperature profiles is found to throw new light on the state of balance of the ice masses.

The high negative temperature gradients measured at different sites in the top 50 m (Robin 1955), have been ascribed partly to climatic change over recent times. However, climatic changes would in general be expected to be of fairly wide geographical extent and so would not explain different warming rates in different

neigbouring locations over the same period. It will be shown here that short-distance fluctuations in surface topography and slope (cf. Section 6) on an ice mass surface are also associated with fluctuations in strain rates and accumulation. As a result, different warming rates can occur at the surface of an ice mass over short distances ($\simeq$ 5-10 km) which can persist for short periods ($\simeq$ 1,000 yrs) and cause different temperature gradients in the upper surface layers, compared with the deeper layers. These fluctuations would be quite independent of climatic change and so, before the latter can be deduced, the effects of the ice motion must first be fully investigated.

To begin with, consider a simple model not involving accumulation or horizontal movement.

1. For an ice mass with constant thickness H, constant surface temperature θ_s, and a constant basal temperature gradient γ_b, (corresponding to the geothermal heat flux) we have for the temperature gradient at depth z

$$\frac{d\theta}{dz} = \gamma_b \qquad \text{constant}$$

and hence

$$\theta_z = \theta_s - \gamma_b z.$$

The basal temperature is given by

$$\theta_b = \theta_s - \gamma_b H \tag{40}$$

i.e., the temperature profile is simply determined by the surface temperature θ_s and the basal geothermal gradient γ_b, and is shown in Fig. 4.7. This situation should be approached when the net accumulation rate is close to zero and the horizontal velocity is small. Since the geothermal heat flux is so important in determining the temperature profile, it is necessary to know how it varies from place to place. Lee and Uyeda (1965) summarize all available data to 1964. The general smoothed world variation is shown in Fig. 4.8 from their report. It is notable that data are virtually non-existent for Greenland and the Antarctic. However, Lee and Uyeda found a high correlation between heat flux and major geological features which may be summarized as

Major geological feature	Geothermal heat flux Mean and standard deviation μ-cal cm^{-2}sec^{-1}
Over land	
Precambrian shields	$0{\cdot}92 \pm 0{\cdot}17$
Palcozoic orogenic areas	$1{\cdot}23 \pm 0{\cdot}4$
Post-Precambrian non-orogenic arcas	$1{\cdot}54 \pm 0{\cdot}38$
Mesozoic-Cainozoic orogenic areas	$1{\cdot}92 \pm 0{\cdot}49$
Over sea	
Ocean trenches	$0{\cdot}99 \pm 0{\cdot}61$
Ocean basins	$1{\cdot}28 \pm 0{\cdot}53$
Ocean ridges	$1{\cdot}82 \pm 1{\cdot}56$

This correlation of heat flux with major geological features suggests that the heat flux in Greenland and East Anarctica is close to 0·9 μ-cal cm^{-2}sec^{-1} typical of the old Precambrian shields, whereas West Antarctica, of more recent origin, may have higher geothermal heat flux.

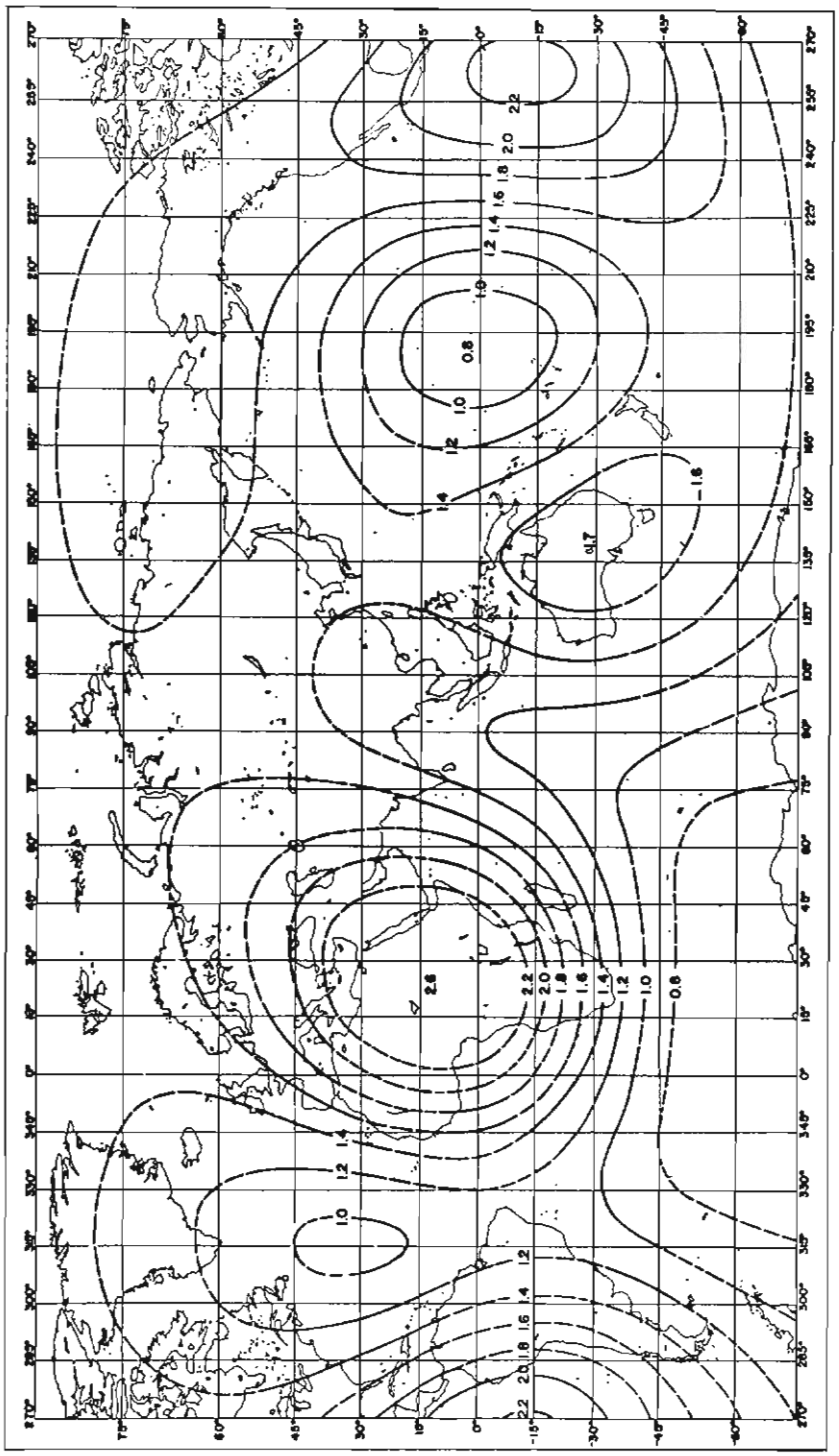

Orthogonal function representation (to third-order spherical harmonics) of 987 heat flow values. Contour lines are in μcal/cm² sec and are dashed over regions where no data exist.

FIG. 4.8. The range of measured geothermal heat flux rates over different parts of the earth is illustrated by this figure from Lee and Uyeda (1965). No values for Greenland and Antarctica are included.

(If $\theta_b \to 0$ the amendment of Section 4.4.1. will apply.)

2. For the second case we still have no horizontal movement but introduce an accumulation rate A at the surface. We assume that the ice thickness is constant with time and the longitudinal strain rate is constant with depth, so that the vertical movement at height z above the base is given by

$$v = A\frac{z}{H}.$$

This is Robin's (1955) steady-state model for which he found the following solution:

$$\kappa\frac{d^2\theta}{dz^2} = \frac{d\theta}{dz}\frac{dz}{dt}$$

$$= \frac{d\theta}{dz}A\frac{z}{H}$$

$$\frac{d\theta}{dz} = \gamma_b e^{-\frac{A}{2H\kappa}z^2} \tag{41}$$

and

$$\theta_z = \theta_s + \gamma_b\sqrt{\frac{2H\kappa}{A}}\operatorname{erf}\sqrt{\frac{A}{2H\kappa}}z\Bigg|_H^z \tag{42}$$

where

$$\operatorname{erf} x = \int_0^x e^{-y^2}\,dy \tag{43}$$

In particular, the temperature gradient at the surface is given by

$$\left.\frac{d\theta}{dz}\right)_s = \gamma_b e^{-AH/2\kappa} \tag{44}$$

This solution is expected to apply closely in regions of low horizontal movement (such as on a dome summit or ice divide) and if steady-state is maintained and no climatic temperature change is occurring.

We notice that, since $\frac{1}{y}\operatorname{erf} y \to 1$ as $y \to 0$, the solution equation (42) reduces to our previous results of model 1 as the accumulation rate becomes small. To examine some typical values of surface gradient over the Antarctic, consider Tables 4.3 and 4.4 below and Figs. 4.9 and 4.10.

TABLE 4.3

ROBIN STEADY-STATE GRADIENTS $\gamma_b e^{-AH/2\kappa}$

$AH/2\kappa$	0·1	0·5	1	2	3	4	5	6
exp $AH/2\kappa$	1·1	1·65	2·72	7·4	20	54	150	400
γ_s °C/100 m, $\gamma_b = 2{\cdot}2$	2·0	1·3	0·81	0·30	0·11	0·04	0·015	0·005
γ_s °C/100 m, $\gamma_b = 4{\cdot}4$	4·0	2·6	1·6	0·60	0·22	0·081	0.030	0·01

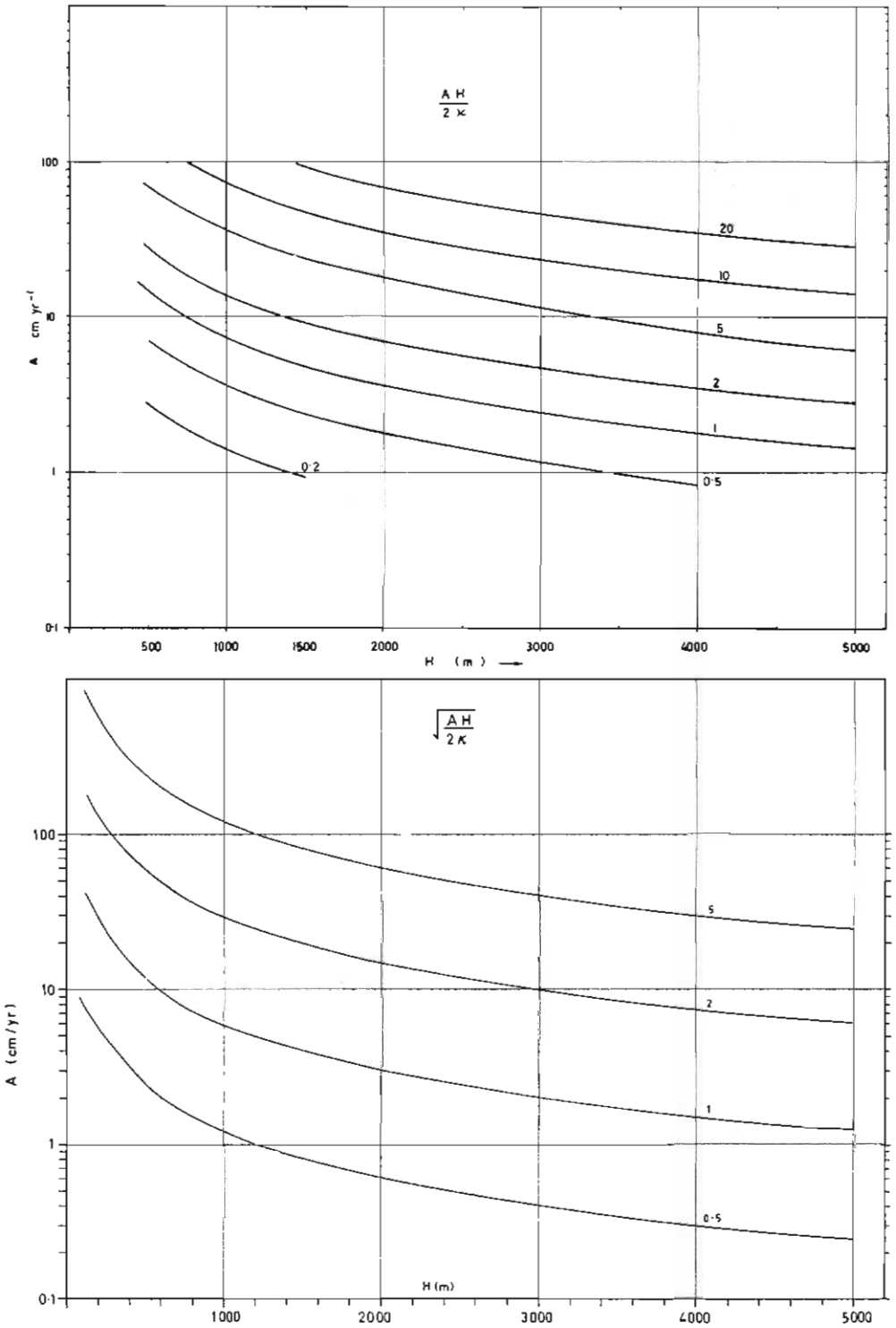

FIG. 4.9. Dimensionless quantities $AH/2\kappa$ and $\sqrt{AH/2\kappa}$ for typical values of A and H and constant $\kappa \sim 1{\cdot}16 \times 10^{-2}$ cm^2 sec^{-1}.

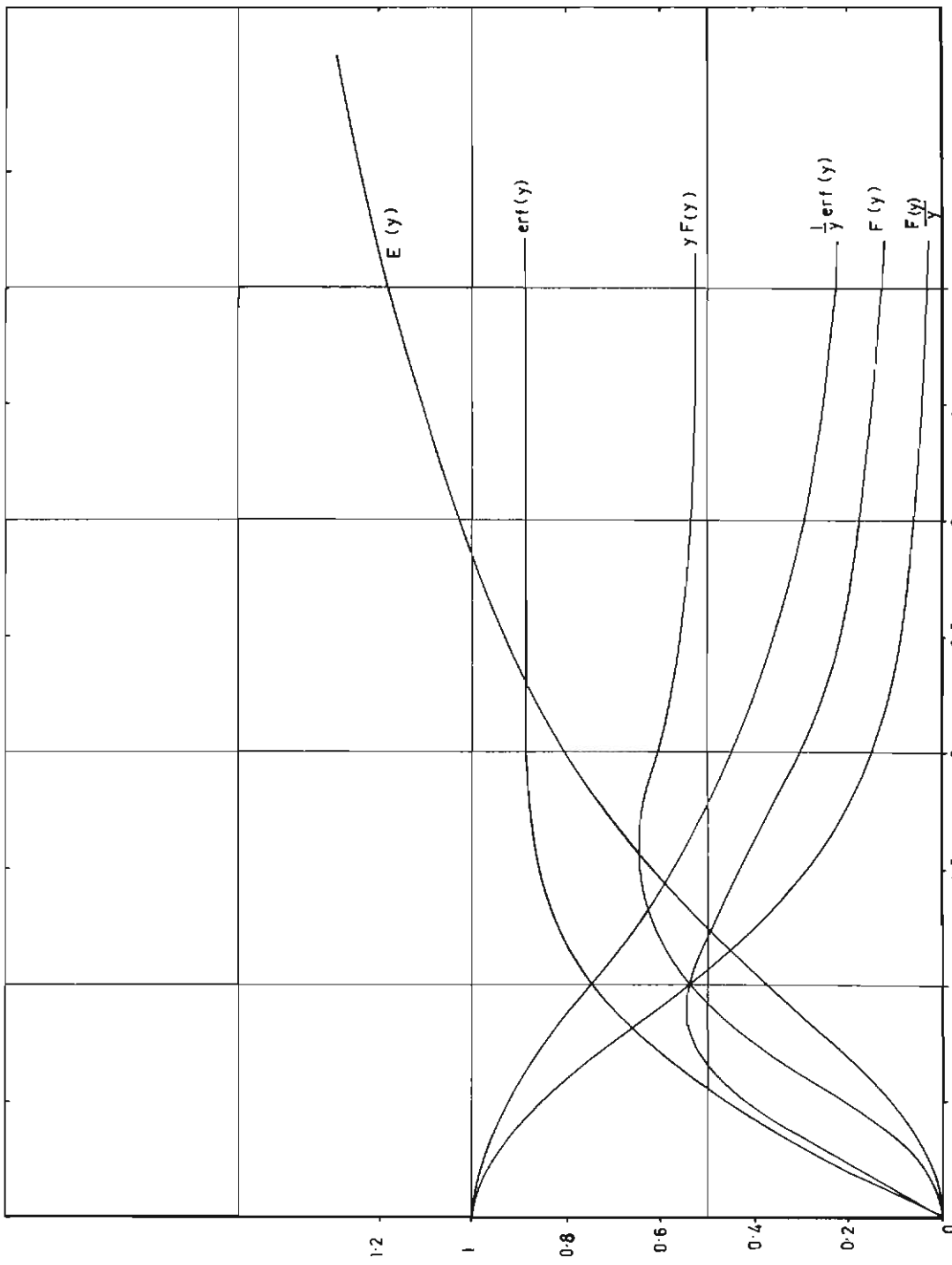

FIG. 4.10. The error function erf y, Dawson's integral $F(y)$ and its integral $E(y)$, as commonly occurring functions in the solution of the

Over most of the Antarctic the surface temperature gradient corresponding to Robin's steady-state model is less than 1°C/100 m. Over a large part of the inland region we can expect the gradient to be less than 0·1°C/100 m.

TABLE 4.4

	$AH/2\kappa$						
A cm yr $^{-1}$ / H_m	1	5	10	20	40	50	100
500	0·07	0·34	0·69	1·38	2·8	3·4	6·9
1000	0·14	0·69	1·38	2·75	5·4	6·9	13·8
1500	0·21	0·95	1·64	4·13	8·1	10·4	20·7
2000	0·28	1·38	2·75	5·30	11·3	13·8	27·5
3000	0 41	2·08	4·13	7·90	17·0	20·6	41·3
5000	0·69	3·40	6·90	13·80	28·0	34·0	69·0

Values of temperature gradient calculated by means of equation (44) along the Wilkes—Vostok line, from the data of Battye (unpublished) and Walker (1966) are given in Table 4.5 below. It is clear that the temperature gradient calculated from the Robin steady-state formula is negligible along most of the route in contrast to the measured gradients which are predominantly negative. Even inland, where the measured gradients are positive, it appears that the calculated gradients from the present model are still too small to account for the measured results. We now consider in the next section the effect of horizontal motion and surface warming.

4.7. EFFECT OF HORIZONTAL AND VERTICAL MOVEMENT ON THE TEMPERATURE PROFILE

Robin (1955) was the first to consider the combined effects of horizontal movement and accumulation on temperature profiles in ice caps. Firstly, if conduction is neglected (i.e., for high rates of movement and accumulation), the negative temperature gradient at the surface $\frac{d\theta}{dz}$, is given by

$$\frac{d\theta}{dz} = \frac{\alpha V \lambda}{A} \tag{45}$$

where the velocity is V, down a slope α (small), with vertical air temperature gradient of λ ($\simeq$ 1°C/100 m in the coastal region of Antarctica) and accumulation rate A.

Radok (1959) pointed out that the temperature gradient at the surface also approaches $\frac{\alpha V \lambda}{A}$ asymptotically, as $t \to \infty$, with conduction, in a semi-infinite medium accumulating at the surface at the rate A, and constantly warming at the rate $\alpha V \lambda$, irrespective of the conductivity.

Negative temperature gradients measured inland of Wilkes and inland of Mirny (Bogoslovski 1958) are shown in Fig. 4.11. The magnitude of the gradient in both cases decreases when going inland. For the Wilkes region further inland they even become positive.

TABLE 4.5

WILKES—VOSTOK TEMPERATURE DATA.

Distance inland x (km)	178	280	370	463	516	570	720	820	920	1020	1120	1206	1312	
Elevation h (m)	855	1475	2115	2515	2650	2740	2910	3015	3180	3280	3380	3530	3640	
Ice thickness H (m)	3200	2055	2500	2890	2690	3700	4600	4560	4320	3380	3460	2890	3140	
Surface temperature (15 m depth) θ_s (—°C)	19·7	27·0	32·5	37·8	40·4	43·6	52·7	54·8	57·2	57·5	59·3	59·6	60·4	
Accumulation A (g cm^{-2}yr^{-1})	35	35·0	17·0	5·2	12·0	9·1	10·5	8·8	8·8	5·2	10·5	7·0	5·2	
Observed surface temperature gradient γ_s (°C/100 m)	—0·2	1·9	—1·7	—1·1	—1·2	—0·7	+0·4	—0·7	+0·3	—0·2	+1·1	+0·6	+0·6	
Robin steady-state surface gradient γ_R (°C/100 m)	10^{-6}	10^{-4}	10^{-4}	0·17	0·01	0·1	10^{-4}	10^{-3}	10^{-3}	0·4	10^{-3}	0·07	0·17	

Typical values of αV and $\frac{\alpha V\lambda}{A}$ are shown in Figs. 4.13 and 4.14, to show the expected magnitudes of this effect over the Antarctic.

If we assume a velocity V for the Vostok—Wilkes line, such that the outward mass flux just balances the accumulation, we can calculate the corresponding temperature gradients due to this effect alone. The results are shown in Table 4.6. Measured gradients inland of Wilkes, together with other relevant data, are shown in Fig. 4.12.

TABLE 4.6

WILKES—VOSTOK ROBIN SURFACE WARMING GRADIENT

x	H	A	V	α	$\frac{\alpha V\lambda}{A} = \frac{d\theta}{dz}$ calc.	$\frac{d\theta}{dz}$ obs.
km	m	cm yr^{-1}	m yr^{-1}	$\times 10^{-3}$	°C/100m	
54	3015	6·1	2·1	1·05	—0·05	+0·6
148	3175	8·8	3·2	1·26	—0·06	+0·6
243	3420	7·9	4·0	1·25	—0·08	+1·1
341	3850	7·0	4·4	1·22	—0·10	—0·2
441	4440	8·8	4·9	1·23	—0·09	+0·3
542	4580	9·7	6·0	1·27	—0·10	—0·7
667	4150	9·8	8·9	1·30	—0·15	+0·4
768	3195	10·6	11·8	1·57	—0·23	—0·7
816	2790	8·6	14·7	2·61	—0·56	—1·2
895	2695	11·0	17·7	4·40	—0·88	—1·1
987	2277	26·0	29·4	5·89	—0·77	—1·7
1083	2627	35·0	36·8	6·32	—0·77	—1·9
						—0·2

Here the agreement between the calculated gradients and the measured gradients is quite close in the region of the coast where high negative gradients are encountered. The discrepancies here may be due to errors in the estimated velocities or in the effect of conduction. This model does not account for the positive gradients inland.

We next consider the effect of movement down the slope with *conduction* but *without accumulation*. Here the movement will be assumed to be so slow that steady state is maintained, i.e., the temperature profile in the ice is constant with time over a given point on the bedrock. As the ice moves down the slope it warms as a whole at the same rate as the surface.

In this case we have for the change in temperature with time of a column moving with the ice

$$\frac{d\theta}{dt} = \alpha V\lambda \tag{46}$$

Hence,

$$\frac{d^2\theta}{dz^2} = \frac{\alpha V\lambda}{\kappa} \tag{47}$$

$$\frac{d\theta}{dz} = \frac{\alpha V\lambda}{\kappa} z + \gamma_s \tag{48}$$

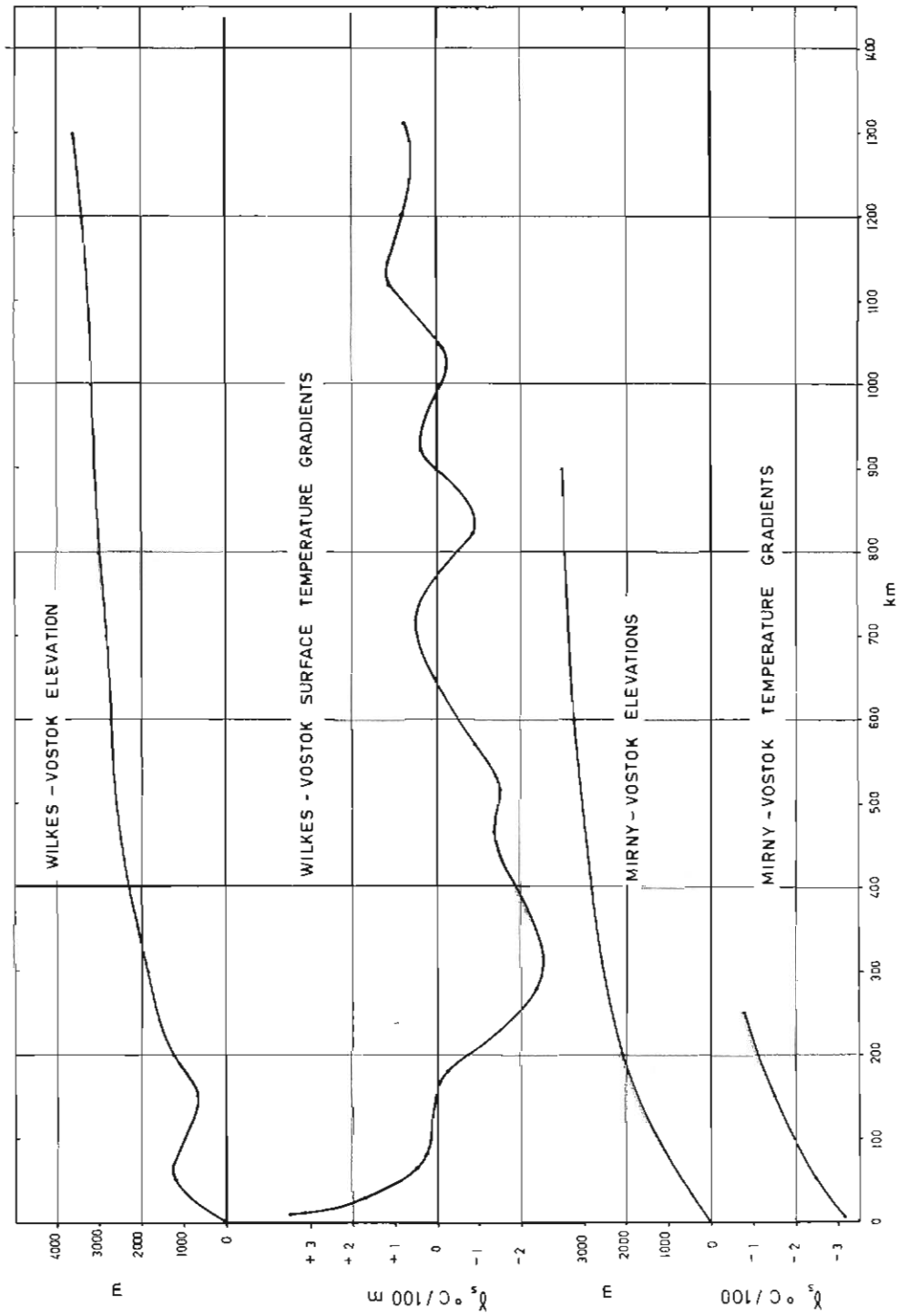

FIG. 4.11. Measured temperature gradients in East Antarctica inland of Wilkes and Mirny. In both cases the magnitude of the high negative gradient decreases in the interior, and inland of Wilkes the gradients even become positive.

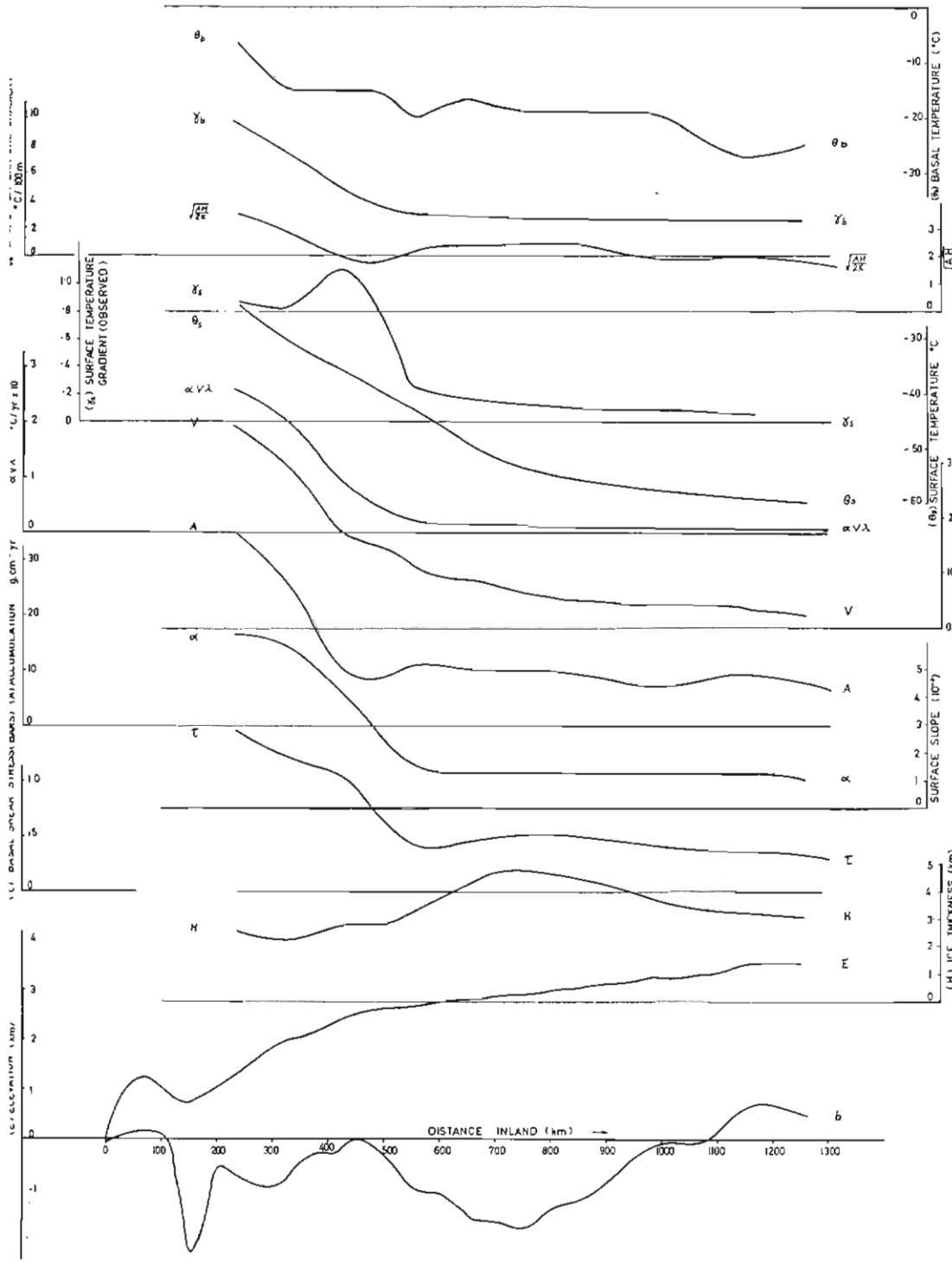

FIG. 4.12a. Various physical parameters inland of Wilkes measured: H, α, A, V, θ_s, γ_s and calculated: τ, $\dot{V}$, γ_b, θ_b, from the data of Walker (1966) and Ballye (unpublished).

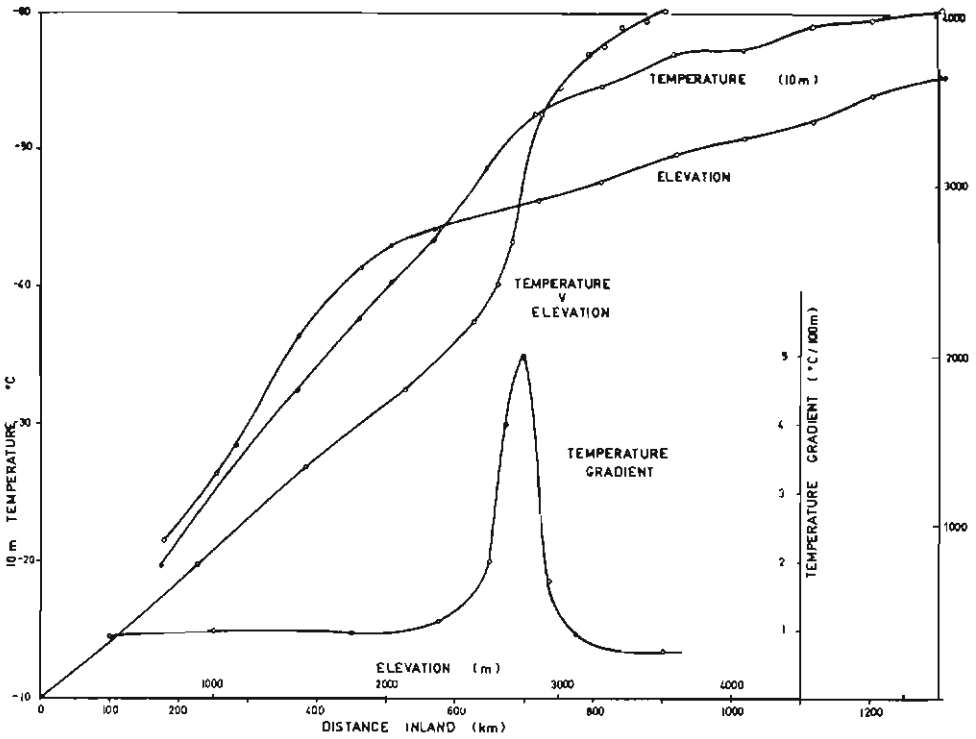

FIG. 4.12b. Elevation and mean surface temperature inland of Wilkes show that about 600 km inland the temperature continues to decrease while the elevation levels off, giving rise to very high temperature elevation gradients there.

$$\theta_z = \frac{\alpha V \lambda}{2\kappa} z^2 + \gamma_s z + \theta_s \tag{49}$$

The surface gradient may be expressed in terms of the basal gradient by

$$\gamma_s = \gamma_b - \frac{\alpha V \lambda}{\kappa} H \tag{50}$$

$$\therefore \frac{d\theta}{dz} = \gamma_b - \frac{\alpha V \lambda}{\kappa}(H - z) \tag{51}$$

and

$$\theta = \theta_s + \gamma_b z - \frac{\alpha V \lambda}{\kappa}\left(Hz - \frac{z^2}{2}\right) \tag{52}$$

Typical values of the temperature gradient at the surface that would arise from this effect in different ice masses may be judged from the tables below (4.7, 4.8). Since λ the vertical air temperature gradient is about 1°C/100 m, the table and Fig. 4.14 for the dimensionless parameter $\frac{\alpha V H}{\kappa}$ give the surface temperature gradient in °C/100 m.

The formula $\gamma_s = \alpha V \lambda / A$ implies that the temperature gradient at the surface becomes large as the accumulation rate becomes small. The formula $\gamma_s = \alpha V H / \kappa$

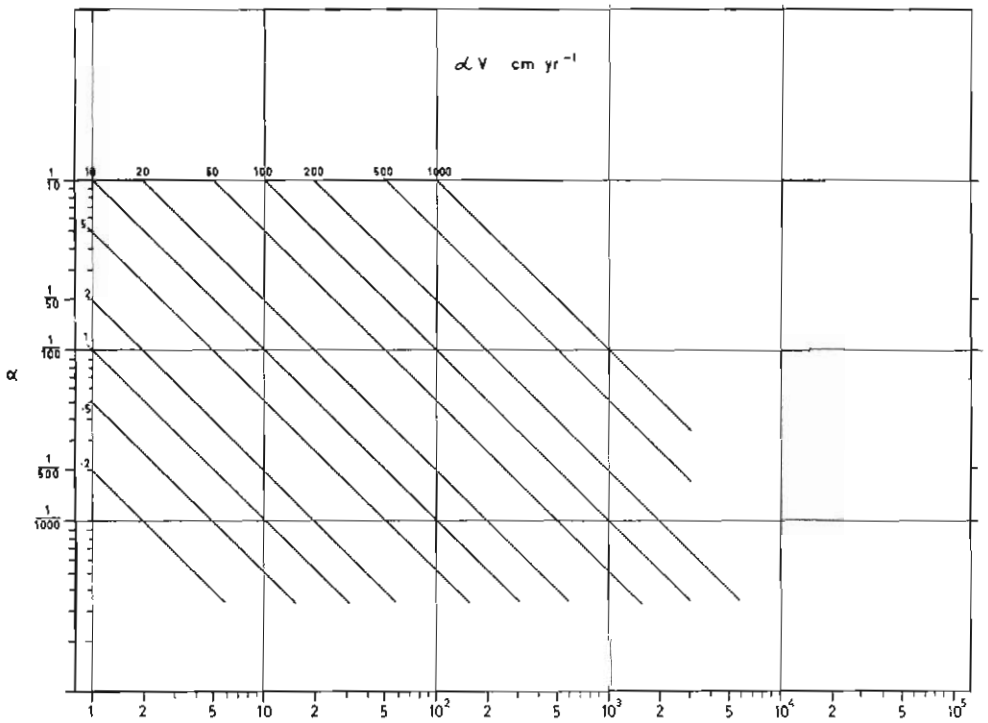

FIG. 4.13. The rate of steady-state surface lowering αV is shown for typieal valucs of velocity V and surface slope α for the large ice masses.

shows that, for a medium of finite thickness, the steady-state surface gradient has a maximum limit even with zero accumulation. By comparing the tables for the dimensionless parameters $\alpha V/A$ *and* $\alpha VH/\kappa$ (Figs. 4.13 and 4.14), the magnitudes of these two effects may be compared. It is clear that, for typical values over the Antarctic, they are of comparable magnitudes. The next stage is to examine the combined effects of surface warming with both conduction and accumulation for a finite slab.

TABLE 4.7

αV cm yr^{-1}

V / α	1	5	10	50	100	m yr^{-1}
1/1000	0·1	0·5	1	5	10	
1/5000	0·2	1	2	10	20	
1/100	1	5	10	50	100	
1/50	2	10	20	100	200	
1/10	10	50	100	500	1000	

TABLE 4.8

$\alpha VH/\kappa$ (DIMENSIONLESS)

αV cm yr^{-1} / H_m	0·10	0·50	1·00	5·00	10·00	50·0	100·0
500	0·01	0·07	0·14	0·68	1·36	6·8	13·6
1000	0·03	0·14	0·27	1·36	2·72	13·6	
1500	0·04	0·21	0·41	2·00	4·08	20·0	
2000	0·05	0·27	0·54	2·70	5·40	27·0	
3000	0·08	0·41	0·82	4·10	8·15	41·0	
4000	0·10	0·54	1·08	5·40	10·80	54·0	

TABLE 4.9

$\alpha V/A$

αV / A	0·1	0·5	1·0	5·0	10	50	100
100	0·01	0·017	0·01	0·05	0·1	0·5	1
50		0·017	0·02	0·10	0·2	1·0	2
20		0·025	0·05	0·25	0·5	2·5	5
10	0·01	0·050	0·10	0·50	1·0	5·0	10
5	0·02	0·100	0·20	1·00	2·0	10·0	20
1	0·10	0·500	1·00	5·00	10·0	50 0	100

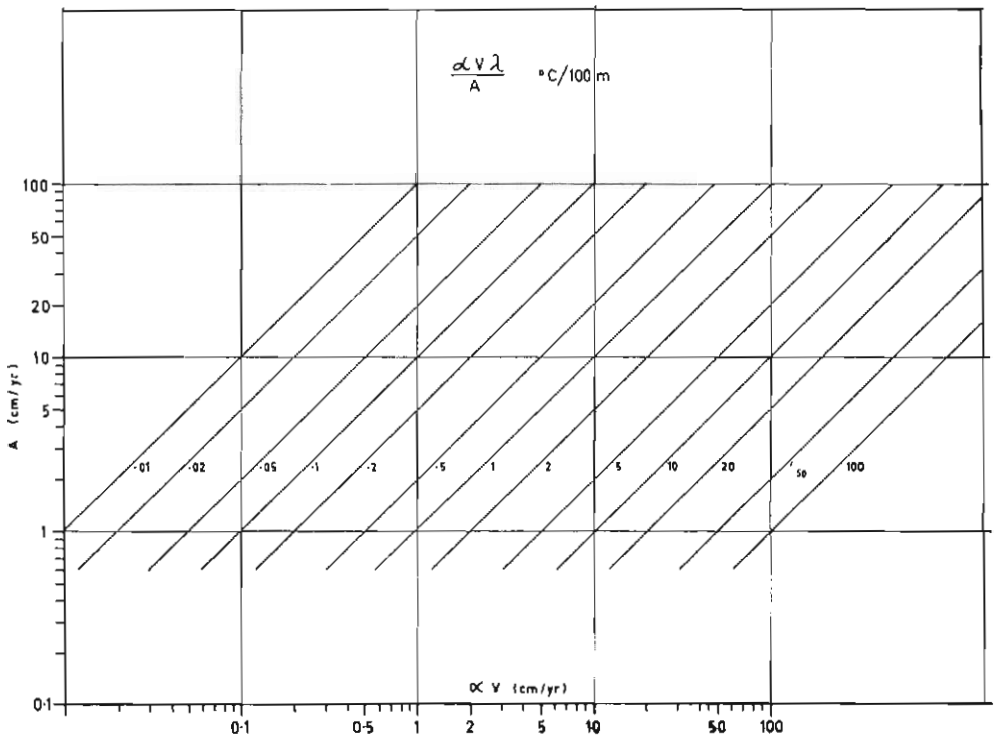

FIG. 4.14. Negative surface temperature gradient due to surface warming αV with accumulation A in absence of conduction.

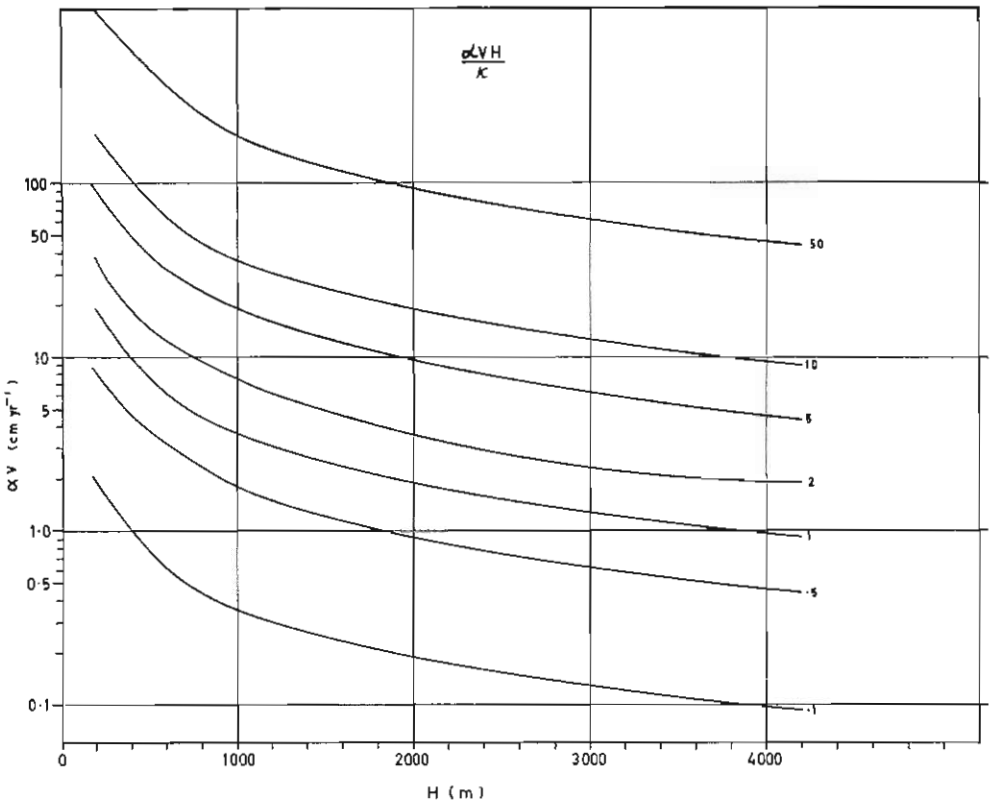

FIG. 4.15. Negative surface temperature gradient for surface warming and conduction in absence of accumulation for different ice thicknesses H.

We now incorporate the *effect of accumulation* on this same model. It is assumed that the ice thickness H remains constant with an accumulation rate A at the surface and a longitudinal extension corresponding to a vertical velocity of $A(H-z)/H$ at depth z. This case was considered by Robin (1955). For ice moving slowly down a slope α, such that the ice thickness remains constant and a steady state temperature profile is maintained, we have the differential equation, analogous to (47), as

$$\frac{d^2\theta}{dz^2} + \frac{A}{\kappa H} z \frac{d\theta}{dz} = \frac{\alpha V \lambda}{\kappa} \tag{53}$$

This model assumes that, as the ice flows outwards, the whole column from surface to base is warming at a constant rate, viz., $\alpha V\lambda$. In many cases this may be a realistic assumption, in others it may be more appropriate to take the warming rate as some other function of depth, e.g., varying linearly from surface to base. For the ease in which the base has reached melting, the warming rate there would be zero and the appropriate equation corresponding to (53) would be

$$\frac{d^2\theta}{dz^2} + \frac{A}{\kappa H} z \frac{d\theta}{dz} = \frac{\alpha V \lambda}{\kappa} \frac{z}{H} \tag{53a}$$

Since in general, however, we do not know how the lower layers are warming (or cooling) we consider first equation(53). After several steady-state profiles have been calculated along a flow line it may then be possible to replace the right-hand side of (53) by a more realistic function of depth.

Robin (1955) fitted equation (53) numerically to observed temperature profiles to determine appropriate values of the velocity V.

Here we solve the equation for the temperature gradient as follows. Writing

$$a = \frac{A}{\kappa H}, \qquad b = \frac{\alpha V \lambda}{\kappa} \tag{54}$$

(53) takes the form

$$\frac{d^2\theta}{dz^2} + az \frac{d\theta}{dz} - b = 0.$$

This equation is linear in $\frac{d\theta}{dz}$ with integrating factor $e^{+(a/2)z^2}$.

Hence,

$$\frac{d\theta}{dz} = e^{-(a/2)z^2}\left[\gamma_b + b \int_0^{\sqrt{(a/2)}z} e^{+(a/2)z^2}\, dz\right],$$

where γ_b is the temperature gradient at the base $(z = 0)$.

At the surface, $(z = H)$ $\frac{d\theta}{dz} = \gamma_s$.

Hence,

$$\gamma_s = \gamma_b e^{-(a/2)H^2} + bH \frac{F(\sqrt{(a/2)}H)}{\sqrt{(a/2)}H} \tag{55}$$

where $F(x)$ is the Dawson integral defined by

$$F(x) = e^{-x^2} \int_0^x e^{+t^2}\, dt \tag{56}$$

This function is tabulated in Abramowitz and Stegun (1964).

Hence, the temperature gradient at depth z is given by

$$\frac{d\theta}{dz} = \gamma_b e^{-(a/2)z^2} + bH \frac{F(\sqrt{(a/2)}z)}{\sqrt{(a/2)}H} \tag{57}$$

(Note that in the present context the direction of z is upwards from the base and so in this notation γ_b is negative.)

In particular, the temperature gradient at the surface $(z = H)$ becomes

$$\left(\frac{d\theta}{dz}\right)_s = \gamma_b e^{-AH/2\kappa} + \frac{\alpha V \lambda}{\kappa} H \sqrt{\frac{2\kappa}{HA}}\, F\left(\sqrt{\frac{AH}{2\kappa}}\right) \tag{58a}$$

which is the generalized form of equation (50) or, to correspond to Robin's formula, equation (45)

$$\left(\frac{d\theta}{dz}\right)_s = \gamma_b e^{-AH/2\kappa} + \frac{\alpha V\lambda}{A}\sqrt{\frac{2HA}{\kappa}}\,F\left(\sqrt{\frac{AH}{2\kappa}}\right) \tag{58b}$$

TABLE 4.10

TABLES FOR DAWSON'S INTEGRAL $F(y), \frac{F(y)}{y}, yF(y), E(y)$, erf $y, \frac{1}{y}$erf y.

y	0·00	0·1000	0·500	1·000	1·500	2·000	3·000	4·000
$F(y)$	0·00	0·0993	0·424	0·538	0·428	0·301	0·178	0·129
$\frac{F(y)}{y}$	1·00	1·0080	0·850	0·540	0·286	0·150	0·059	0·032
$yF(y)$	0·00	0·0100	0·212	0·538	0·642	0·602	0·534	0·517
$E(y)$	0·00	0·0100	0·140	0·390	0·640	0·830	1·040	1·200
erf (y)	0·00	0·0100	0·461	0·748	0·856	0·883	0·886	0·886
$\frac{1}{y}$erf (y)	1.00	1·0000	0·922	0·748	0·578	0·441	0·295	0·222

The corresponding solution for (53a) in which the warming rate decreases linearly to zero at the base is

$$\frac{d\theta}{dz} = \gamma_b e^{-\frac{Az^2}{2\kappa H}} + \frac{\alpha V\lambda}{A}\left[1 - e^{-\frac{A}{2\kappa H}z^2}\right] \tag{57a}$$

We write equation (58) in the form

$$\left(\frac{d\theta}{dz}\right)_s = \gamma_b e^{-AH/2\kappa} + \frac{\alpha V\lambda}{\kappa} H\,\frac{F(y)}{y} \tag{58a'}$$

where $y = \sqrt{AH/2\kappa}$. Now $\frac{F(y)}{y} \to 1$ as $y \to 0$, and $\frac{F(y)}{y} \to 0$ as y becomes large.

Hence, this solution approaches the previous one, equation (50), as $A \to 0$, and the effect of the accumulation is simply to reduce the *magnitude* of the surface gradient.

Typical values of $\sqrt{AH/2\kappa}$, $F(y)$, $\frac{F(y)}{y}$, for inland Antarctica are shown in Tables 4.10 and 4.12. Also shown are the net calculated temperature gradients along the Wilkes—Vostok trail (Table 4.11). These gradients are remarkably close to the values calculated (Table 4.5) for the case where conduction was neglected. This is essentially a consequence of the non-dimensional parameter $\sqrt{AH/2\kappa}$ being large.

We also note that equation (58) can be written in the form

$$\left(\frac{d\theta}{dz}\right)_s = \gamma_b e^{-AH/2\kappa} + \frac{\alpha V\lambda}{A}\,2yF(y) \tag{58b'}$$

Furthermore, $yF(y) \to \frac{1}{2}$ as $y \to \infty$. Hence, as $H \to \infty$, $A \neq 0$,

$$\left(\frac{d\theta}{dz}\right)_s \to \gamma_b e^{-AH/2\kappa} + \frac{\alpha V\lambda}{A} \tag{59}$$

We thus conclude that for a thick ice mass (H large) where the accumulation rate is not too small (A not zero) the steady-state surface temperature gradient approaches the simple sum of Robin's (1955) results for

(1) steady-state accumulation and subsidence with no downslope movement, and (2) downslope movement and accumulation with no conduction.

TABLE 4.11

WILKES—VOSTOK CALCULATED SURFACE TEMPERATURE GRADIENTS FROM COMBINED EFFECTS OF ACCUMULATION AND SURFACE WARMING

$$\left(\frac{d\theta}{dz}\right)_s = \gamma_b e^{-AH/2\kappa} + \frac{\alpha V \lambda}{A} 2yF(y)$$

Distance towards coast	Balance velocity	Dynamics veloeity	Calculated gradient		Observed gradient
x km	V_b m/yr	V_d m/yr	from V_b °C/100 m	from V_d	$\gamma 0$ °C/100 m
101	2·7	1·6	—0·04	—0·02	+0·6
196	3·6	2·7	—0·07	—0·05	+0·6
292	4·2	3·7	—0·10	—0·09	+1·1
391	4·6	5·6	—0·12	—0·14	—0·2
492	5·4	8·1	—0·13	—0·20	+0·3
605	7·4	7·8	—0·34	—0·35	—0·7
718	10·3	8·2	—0·71	—0·56	+0·4
792	13·2	10·1	—1·04	—0·79	—0·7
855	16·2	28·5	—1·15	—2·03	—1·2
941	23·5	51·6	—0·79	—1·74	—1·1
1035	33·1	87·4	—0·73	—1·93	—1·9

From Table 4.10 we see that, for $y > 1$, $yF(y)$ does not vary greatly (less than 25%) from 0·5, and for $y > 3$ the difference is less than 7%. The values of $\sqrt{AH/2\kappa} = y$ in Table 4.12 show that most of the Antarctic ice cap comes into this category of large H, i.e., $\sqrt{AH/2\kappa} > 0{\cdot}8$. Since the term $\gamma_b e^{-AH/2\kappa}$ is also small in most of inland Antarctica, the close agreement between the Robin surface warming gradients, and those obtained from equation (58) along the Wilkes —Vostok line, is thus explained.

Equation (58) implies some general conclusions concerning the dependence of the surface gradient on the accumulation rate and the ice thickness.

The negative gradient required to maintain the steady-state increases as the vertical velocity (αV) of the thickness (H) becomes large. The gradient also becomes more negative as the diffusivity becomes small (e.g., as the firn density decreases in the upper layers). This corresponds to increasing accumulation (in cm snow. The decrease in κ has a similar result to the increase in AH. It can be seen from equation (58b) that, in the upper firn layers, where the diffusivity is small, the surface temperature gradient more closely approaches the Robin non-conduction formula $\gamma_s = \frac{\alpha V \lambda}{A'}$, provided that the A' value is taken as the accumulation rate in cm of *firn* over the appropriate depth. These results support the application of Robin's formula (e.g., Mellor 1960, Budd 1966) in associating surface temperature gradients and velocities. But it should be emphasized that, except for steady-state ice cap, αV is not the *true vertical velocity* (cf. Section

4·8) because, in general, this includes also terms involving basal slope and vertical strain rate, which may result in the ice-cap surface rising or sinking with time.

We next obtain the temperature profile by integration of equation (57) as follows:

$$\theta_z = \theta_b + \gamma_b \int_0^z e^{-(a/2)z^2} dz + b\frac{2}{a}\int_0^z F\left(\sqrt{\frac{a}{2}}\, z\right) dz$$

$$= \theta_b + \gamma_b \frac{2}{a} \operatorname{erf} \frac{a}{2} z + b\frac{2}{a} E\left(\sqrt{\frac{a}{2}}\, z\right) \tag{60}$$

where $E(x)$ is defined by $E(x) = \int_0^x F(y)\,dy$, and has been evaluated for $0 < x < 3$ by Zotikov (1963). It may also be obtained easily from the tables of Dawson's Integral of Abramowitz and Stegun (1964), and a plot of this function $(E(x))$ is shown for values up to $x = 4$ in Fig. 10.

The temperature at the base is given by

$$\theta_b = \theta_s - \gamma_b H \frac{\operatorname{erf}\sqrt{(a/2)H}}{\sqrt{(a/2)H}} - b\frac{2}{a} E\left(\sqrt{\frac{a}{2}}\, H\right) \tag{61}$$

i.e.,

$$\theta_b = \theta_s - \gamma_b H \frac{\operatorname{erf}\sqrt{(AH/2\kappa)}}{\sqrt{(AH/2\kappa)}} - \frac{\alpha V\lambda}{\kappa}\frac{2\kappa H}{A} E\left(\sqrt{\frac{AH}{2\kappa}}\right) \tag{61a}$$

or

$$\theta_b = \theta_s - H\left[\gamma_b \frac{\operatorname{erf} y}{y} - \frac{\alpha V\lambda}{A} 2E(y)\right] \tag{62}$$

where $y = \sqrt{AH/2\kappa}$ is non-dimensional and is given in Table 4.12.

Hence, we find for the temperature profile

$$\theta_z = \theta_s - \gamma_b H \frac{\operatorname{erf}\sqrt{(AH/2\kappa)} - \operatorname{erf}(\sqrt{(AH/2\kappa)}\, z/H)}{\sqrt{(AH/2\kappa)}}$$

$$+ \frac{\alpha V\lambda H}{A} 2[E\sqrt{AH/2\kappa} - E\sqrt{AH/2\kappa}\, z/H] \tag{60a}$$

or

$$\theta_z = \theta_s - H\left[\gamma_b \frac{1}{y}(\operatorname{erf} y - \operatorname{erf}\zeta y) - \frac{\alpha V\lambda}{A} 2(Ey - E\zeta y)\right] \tag{63}$$

where $\zeta = z/H$ is the fractional ice thickness.

Typical temperature profiles are shown in Fig 4.16 for the Wilkes ice cap. From these profiles we notice that the effect of increased velocity as the coast is approached is to increase the negative gradient at the surface and the positive gradient at the base. As a consequence of this, the average temperature through the ice is lower than the surface temperature.

The depth of the temperature minimum is given by $d\theta/dz = 0$ which, from (57), gives

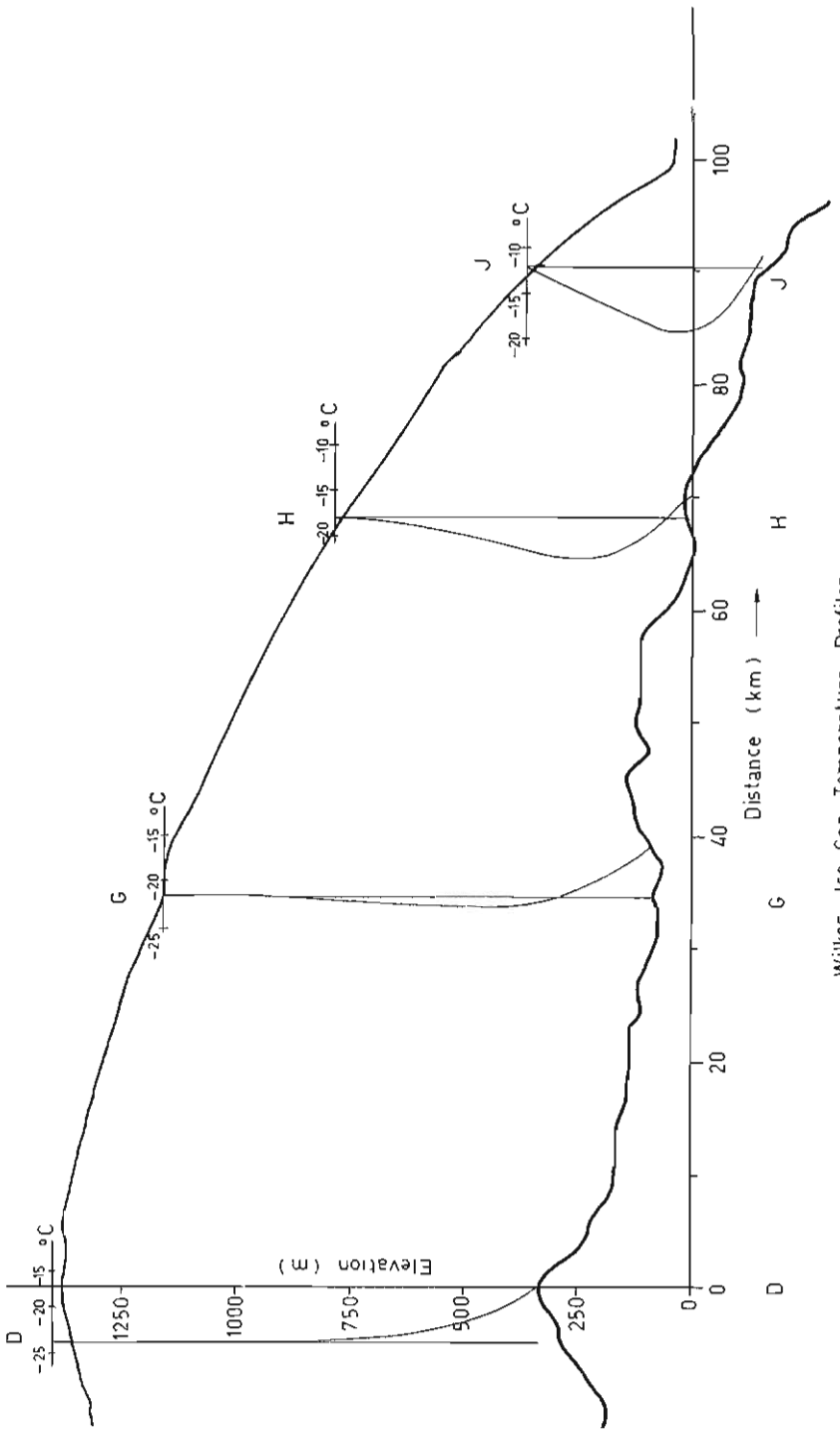

FIG. 4.16. Calculated steady-state temperature profiles, for part of the Wilkes ice cap, from measured velocities, surface warming, ice thickness, and balanced accumulation rates.

$$\frac{bHF(\sqrt{a/2}z)}{\sqrt{a/2}\,H} = \gamma_b e^{-(a/2)z^2} \tag{64}$$

$$e^{(a/2)z^2}F(\sqrt{a/2}z) = \frac{\gamma_b\, a/2H}{bH} \tag{65}$$

or, using (54),

$$\frac{z}{H} = \sqrt{AH/2\kappa}\; G^{-1}\left(2\frac{\alpha V\lambda}{A\gamma_b}\sqrt{AH/2\kappa}\right) \tag{66}$$

where $G(y) = 1/\int_0^y e^{t^2}\,dt$, and is shown in Fig. 4.17.

Finally, it might be mentioned that the differential equation (53) can also be solved in series for temperature and temperature gradient. These series can also be obtained from the series for the analytical functions erf y, $F(y)$ etc. (Ahramowitz *and* Stegan 1964).

TABLE 4.12

$\sqrt{AH/2\kappa}$

$\frac{A}{H}$	1	5	10	20	40	50	100
500	0·26	0·59	0·83	1·13	1·66	1.84	2·62
1000	0·37	0·83	1·18	1·66	2·23	2·62	3·70
1500	0·41	0·98	1·28	2·04	2·86	3·24	4·54
3000	0·64	1·43	2.04	2·36	3·33	3·70	5 25
2000	0·52	1·18	1·67	2·86	4·10	4·54	6·42
4000	0·83	1·84	2·62	3·70	5·25	5·84	8·30

4.8 TEMPERATURE PROFILE FOR GROWING ICE CAP

Crary (1961) showed that, for a slowly increasing thickness H of an ice shelf, with the remaining boundary conditions constant, the form of the steady-state temperature profile $\theta = f(H)$ remained the same with just the new H replacing the old.

Crary used the differential equation for temperature θ at depth z,

$$\kappa\frac{d^2\theta}{dz^2} - \left[A + \frac{z}{H}(M - A)\right]\frac{d\theta}{dz} = 0 \tag{67}$$

where κ = thermal diffusivity, A = surface accumulation rate and M = basal melt rate.

From this he established the solution

$$\frac{\theta_z - \theta_0}{\theta_s - \theta_0} = \frac{\int_0^z e^{-(1/\kappa)[Az + (z^2/2H)(M - A)]}dz}{\int_0^H e^{-(1/\kappa)[Az + (z^2/2H)(M - A)]}dz} \tag{68}$$

which he evaluated numerically.

Here we write

$$z' = \sqrt{\frac{M - A}{2H\kappa}}\,z, \qquad \alpha = \frac{A}{2\kappa}\left(\frac{M - A}{2H\kappa}\right)^{-\frac{1}{2}}$$

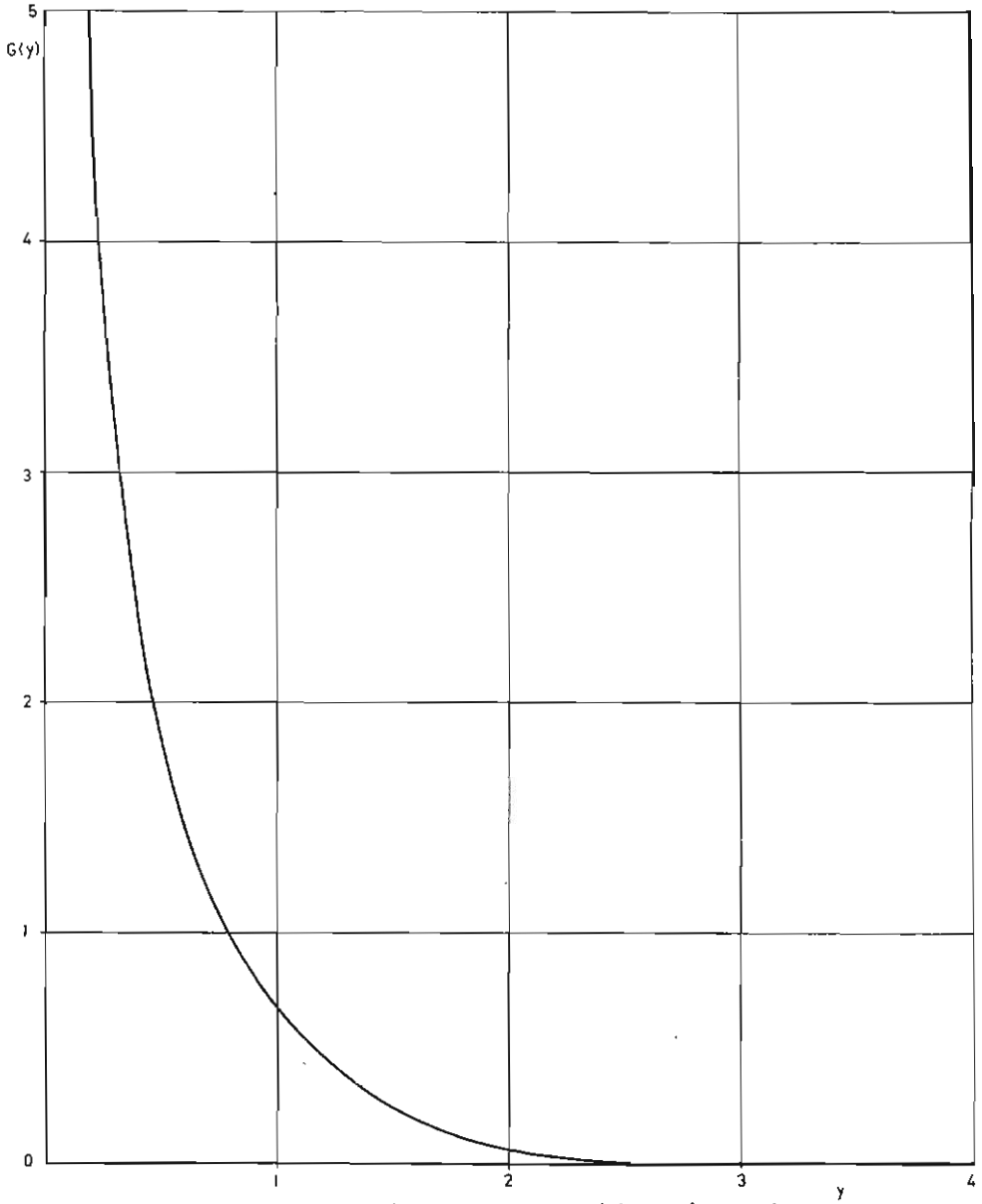

FIG. 4.17. The relative depth z/H of the temperature minimum for steady-state temperature distributions in ice is given by $z/H = y\ G^{-1}(\{2\alpha V\lambda\}/\{A\gamma_0\}\ y)$ where $y = \sqrt{AH/2\kappa}$.

to obtain

$$\frac{\theta_z - \theta_0}{\theta_s - \theta_0} = \frac{\int_{0+\alpha}^{z'+\alpha} e^{-(z'+\alpha)^2} d(z' + \alpha)}{\int_{0+\alpha}^{H'+\alpha} e^{-(z'+\alpha)^2} d(z' + \alpha)}$$
$$= \frac{\operatorname{erf}(z' + \alpha) - \operatorname{erf}\alpha}{\operatorname{erf}(H' + \alpha) - \operatorname{erf}\alpha}.$$

Reverting to our original parameters this becomes

$$\frac{\theta_z - \theta_0}{\theta_z - \theta_0} = \frac{\operatorname{erf}\left(\sqrt{\frac{M - A}{2H\kappa}}\, z + \frac{A}{2\kappa}\sqrt{\frac{2H\kappa}{M - A}}\right) - \operatorname{erf}\frac{A}{2\kappa}\sqrt{\frac{2H\kappa}{M - A}}}{\operatorname{erf}\left(\sqrt{\frac{M - A}{2H\kappa}} + \frac{A}{2\kappa}\sqrt{\frac{2H\kappa}{M - A}}\right) - \operatorname{erf}\frac{A}{2\kappa}\sqrt{\frac{2H\kappa}{M - A}}} \tag{69}$$

where θ_s is the temperature at the surface,
and θ_0 is the temperature at the base.

This result suggests that a steady-state solution for a slowly rising (or subsiding) ice cap may be found simply as a function of the surface warming or cooling, with the vertical velocity and the existing physical parameters of the ice mass at that point.

For an ice mass with thickness H, elevation E, accumulation rate A, surface slope α, and basal slope β, which is moving with horizontal velocity V and has a vertical strain rate $\dot{\epsilon}_z$, the rate of change in thickness over a point of the bedrock is given by

$$\frac{\partial H}{\partial t} = V(\alpha - \beta) + \dot{\epsilon}_z H + A \tag{70}$$

The vertical velocity at height z above bedrock is given by

$$w_z = \frac{\partial H}{\partial t}\frac{z}{H}.$$

Now, with the same model as in Section 4.7, we obtain for the differential equation, for a column moving with the medium and co-ordinates z varying with H, such that z/H remains constant,

$$\frac{d^2\theta}{dz^2} - \frac{A}{\kappa}\frac{z}{H}\frac{d\theta}{dz} = \frac{\lambda}{\kappa}\frac{DE}{Dt} \tag{71}$$

or

$$\frac{d\gamma}{dz} - az\gamma = b' \tag{72}$$

where

$$\gamma = \frac{d\theta}{dz} \qquad a = \frac{A}{\kappa H} \qquad b' = \frac{\lambda}{\kappa}\frac{DE}{Dt} \tag{73}$$

The surface warming is given by the rising or lowering of the surface elevation, E, of the ice cap following the motion,

i.e.,

$$\frac{DE}{Dt} = \frac{DH}{Dt} + V\beta = \frac{\partial H}{\partial t} + V\frac{\partial H}{\partial x} + V\beta = \frac{\partial H}{\partial t} + V\alpha$$
$$= -V\beta + \dot{\varepsilon}H + A,$$

since

$$\frac{\partial H}{\partial x} = (\alpha - \beta) \qquad \text{and} \qquad \frac{\partial H}{\partial t} = V\frac{\partial H}{\partial x} + \dot{\varepsilon}H + A.$$

For a balanced ice cap $\partial H/\partial t = 0$, and hence $DE/Dt = V\alpha$, as used by Robin. As before (Section 4.7), the differential equation (72) has a solution

$$\gamma_z = \gamma_b e^{-(a/2)z^2} - b'H\frac{F(\sqrt{(a/2)}z)}{\sqrt{(a/2)}H} \tag{74}$$

and, in particular, the surface gradient is given by

$$\gamma_s = \gamma_b e^{-(a/2)H^2} - b'H\frac{F(\sqrt{(a/2)}H)}{\sqrt{(a/2)}H} \tag{75}$$

$$= \gamma_b e^{-AH/2\kappa} - \frac{\lambda}{\kappa}[A + \dot{\varepsilon}H - \beta V]H\frac{F(\sqrt{(AH/2\kappa)})}{\sqrt{(AH/2\kappa)}} \tag{75'}$$

Hence, we can see that, even for very thick ice and high accumulation rates, the surface temperature gradient can be *positive or negative* depending on whether DE/Dt is positive or negative; i.e., for a growing ice cap the surface gradient would be positive if the accumulation rate is sufficiently large for $(A + \varepsilon H - \beta V)$ to be positive.

Now, positive surface temperature gradients have been observed in inland Antarctica by Battye in 1963 and, since the Robin steady-state term $e^{-AH/2\kappa}$ is small there, it appears that the cause of the positive gradient may be that the ice cap surface is rising. We can calculate the required growth rate $(\partial H/\partial t)$ to cause such a positive gradient γ_s from (75) in the form

$$\gamma_s = \gamma_b e^{-AH/2\kappa} - \frac{\lambda}{A}\frac{DE}{Dt}2\sqrt{\frac{AH}{2\kappa}}F\left(\sqrt{\frac{AH}{2\kappa}}\right) \tag{75''}$$

or, since

$$2\sqrt{\frac{AH}{2\kappa}}F\left(\sqrt{\frac{AH}{2\kappa}}\right) \simeq 1$$

$$\gamma_s \simeq \frac{\lambda}{A}\frac{DE}{Dt} \rightarrow \frac{DE}{Dt} \simeq \frac{A\gamma_s}{\lambda},$$

or

$$\frac{\partial H}{\partial t} = \frac{A\gamma_s}{\lambda} + \alpha V. \tag{76}$$

Typical values of observed γ_s and λ along the Wilkes—Vostok route of Fig. 4.12 suggest that the rise of the surface in the interior of Antarctica may be 20-50% of the accumulation rate (i.e., $\simeq$ 2-5 cm yr^{-1}), which is a general confirmation of the net positive budget in inland Antarctica (cf. Loewe 1967, Bardin and Suyetouo 1967, Giovinetto 1964, 1966, Budd 1967). This general result has

some very important consequences. If we know the climatic temperature change over a period, equation (76) can tell us the rate of lowering of the surface. On the other hand, if we know the rate of surface lowering, say from flux divergence measurements, then equation (76) will provide a guide for determining the recent changes in surface temperature. This means that the surface temperature gradient may well provide a useful means of gauging mass budgets of inland regions of large ice masses. As another example, we consider the surface temperature gradient to $\simeq$ 150 m at Station Centrale in Greenland (cf. Heuberger 1954, also Mellor 1964). Here the temperature gradient from 100 to 150 m is $\simeq 0{\cdot}26$ °C/100 m, the accumulation rate $\simeq$ 40 cm yr^{-1} (ice equivalent) and the estimated velocity and slope (Haefeli 1961) $\simeq$ 2 m yr^{-1} and $\simeq$ ·002 respectively.
Hence,

$$\frac{\alpha V}{A} \simeq 0{\cdot}1,$$

with the consequence that the expected temperature gradient is 0·1 °C/100 m. This suggests that the surface lowering (or net negative budget) is about 150% of the accumulation rate, assuming negligible effect of climatic change. On the other hand, if the effect were due entirely to climatic change, a temperature warming of about 0·06°C/100 years would be required. This figure is also compatible with estimated recent climatic changes, cf. Fairbridge (1967).

In the calculations carried out so far, a constant diffusivity has been assumed. Actually, ice conductivity, capacity, and diffusivity appear to be quite temperature-dependent. This is shown in Table 4.13 and Fig. 4.18.

To introduce temperature dependence into the thermal diffusivity makes the heat conduction equation much more non-linear. This complication is better treated numerically and the results of such a treatment will be published elsewhere. Here we simply adopt the mean value of diffusivity over the particular temperature range we are concerned with in a given context, but note that such a value may be in error up to about $\pm$ 20%, depending on the temperature range.

The problem so far dealt with has also assumed steady-state temperature conditions. For very thick ice which is changing rapidly this steady state may not be achieved. Such time dependence makes the problem much more complex and the numerical approach of Jenssen and Radok (1963) appears to be the most useful

TABLE 4.13

THERMAL PARAMETERS FOR ICE [FROM DORSEY (1940); CF. ALSO POWELL (1964)]

Temperature	Conductivity K	Capacity c	Diffusivity $\kappa = \frac{K}{\rho c}$
°C	cal $cm^{-2}sec^{-1}°C^{-1}$	cal g^{-1}	cm^2sec^{-1}
0	5·35	0·506	1·15
—10	5·54	0·486	1·24
—20	5·81	0·469	1·35
—30	6·10	0·450	1·47
—40	6·35	0·431	1·60
—50	6·64		
—60	6·95	0·394	1·93

technique to solve this problem for any particular region. If the time dependence is significant, however, it is not sufficient to determine the temperature distribution from the values of the present parameters of the ice cap (velocity, accumulation, strain, etc.) at a certain position, as has been done here. The motion and changes of the ice cap must then be followed over a considerable time as the ice moves outwards from the centre, accumulates, strains and either builds up or subsides.

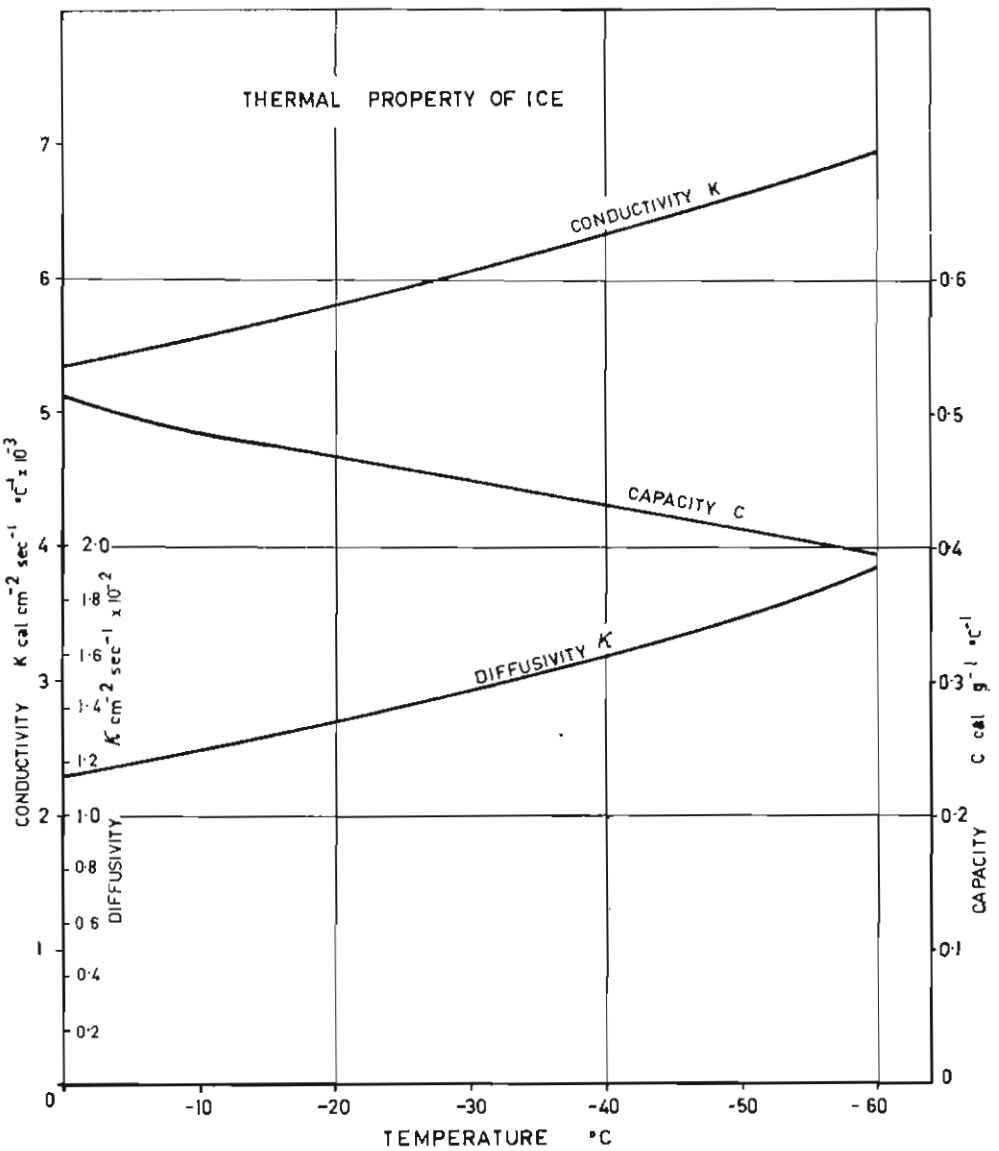

FIG. 4.18. The thermal properties of ice: conductivity K, diffusivity κ, and capacity C, are shown for the range of temperatures in ice, after Dorsey (1940), Powell (1958), Ratcliffe (1962).

Since the velocities and strains in inland Antarctica are still largely unknown (let alone the extrapolations back in time) a detailed calculation of this sort can only be speculation at this stage.

On the other hand, once all the movement parameters of the ice are known, as well as its temperature distributions, much cane be learned about its past history, and in particular about the possible change in the climate over recent times (last

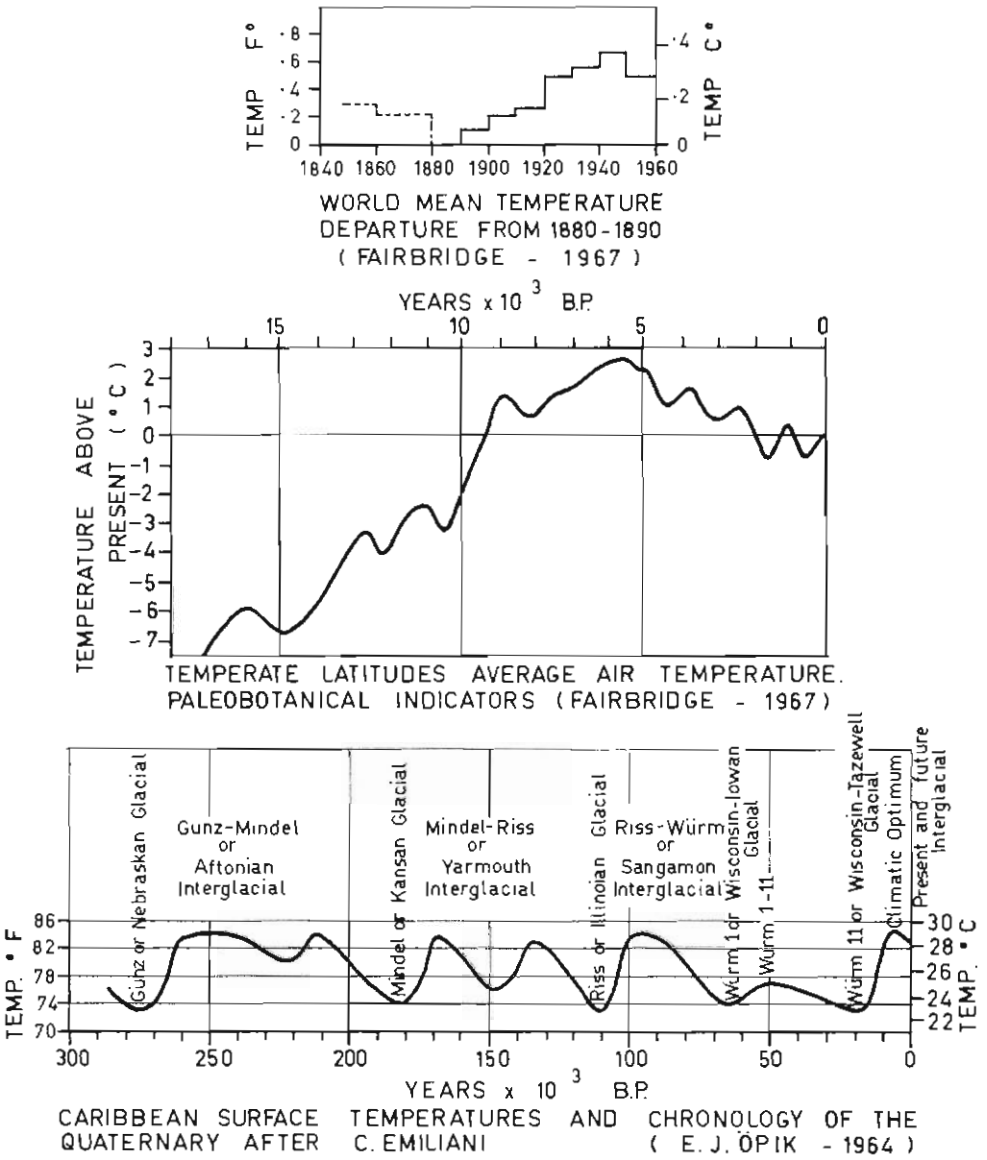

FIG. 4.19. The range of magnitudes of the amplitude and frequency of climatic variations in temperature can be judged from the above estimates of temperature changes over recent periods from 100 years to 300,000 years.

100,000 years). The order of magnitude of such temperature variations may be judged from the estimated temperature variations over the world illustrated in Fig. 4.19.

4.9. THE VALIDITY OF THE ASSUMPTION OF STEADY-STATE TEMPERATURE DISTRIBUTION

The essence of "steady-state" is that something is constant in time. In some cases it may be temperature, in others temperature gradient, or ice thickness. Hence we make the following definitions:

(i) We define a "steady-state temperature-profile" in an ice cap as one that remains the same with time in space over a fixed point in the bedrock as the ice moves past. In this case the ice cap itself must also be in steady-state there, i.e., not rising or sinking.

(ii) For a rising or sinking ice cap surface we may define a "thickness-relative steady-state temperature-profile" where the temperature may be expressed as a constant function (with time) of the ice thickness, H, even though H is changing slowly with time. This definition may also be applied to a moving column, with expanding co-ordinates.

(iii) If the whole column is warming at a constant rate (or, more generally, at a rate which is a constant function of depth) then we may define a "steady-state temperature-gradient-profile" as one in which the temperature gradient remains constant in time.

(iv) Similarly, for a growing (or sinking) ice-cap column which is warming at a constant function of its relative depth, we call a "relative steady-state temperature-gradient-profile" one whose temperature gradient is a constant function of ice thickness H, which may be changing with time. This is the more general case required for the moving column.

In all cases, the final result is temperature or temperature-gradient as a function of depth but not time. We now examine under what conditions the ice cap may have profiles approaching the various types of steady-state.

To maintain a steady-state temperature gradient throughout the whole ice thickness, the ice mass must be able to warm up at the rate at which the surface is warming.

The question arises as to whether, as the column of ice flows outwards in an ice cap and warms at the surface, the rest of the ice column also warms up to keep in steady state, or whether the basal temperature lags the surface temperature. The rate of warming is not constant but increases rapidly as the velocity and slope increase towards the coast. As a result of this, it may be expected that the temperature profile does not remain in the steady state defined for constant warming rate. However, as the coast is approached, the decrease in ice thickness and the increased heat due to increased friction at higher velocities tend to assist the ice mass in maintaining steady state. In order to determine a criterion to judge whether steady-state temperature profiles are realistic, and can be maintained in a moving ice cap, we now consider time-dependent solutions of the heat conduction equation for a finite slab, and investigate the time required to reach stability.

4.9.1. *An ice cap with a constant surface warming rate*

Firstly, we consider the simple model of an ice-cap column warming, as it moves downwards and outwards, as the case of the finite slab $-H < z < H$, with zero accumulation and a constantly rising surface temperature. This problem was considered by Carslaw and Jaeger (1959, p. 105 (i)). We take zero initial temperature for the whole column for the time $t > 0$ the surfaces are kept at temperature $\theta_0 = kt$, where k is a constant. The temperature θ at depth z and time t is given by

$$\theta = kt + \frac{k(z^2 - H^2)}{2\kappa} + \frac{16kH^2}{\kappa\pi^2} \sum_{n=0}^{\infty} \frac{(-1)^n}{(2n+1)^3} e^{-\frac{\kappa(2n+1)^2\pi^2}{4H^2}t} \cos\frac{(2n+1)\pi z}{2H} \tag{76}$$

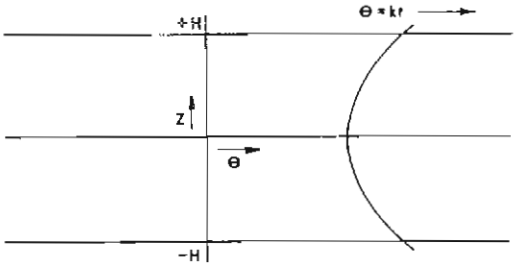

This equation can be used to simulate the temperature distribution in the ice column of constant thickness H, with the bedrock at $z = 0$. The temperature gradient at the base in this case is zero; for the case of the ice cap with constant basal flux γ_b we simply need to add the term $\gamma_b z$ to the above solution.

The first and second terms in the above solution are the steady state solution as obtained in Section 4.7. The series is the time-dependent part which tends to zero as $t \to \infty$ and converges quite rapidly with increasing n, which implies that high frequency variations are quickly damped out.

For $n = 0$ we have

$$\theta(t) = \frac{16kH^2}{\kappa\pi^3} e^{-\frac{\kappa\pi^2}{4H^2}t} \cos\frac{\pi z}{2H} + kt + \frac{k(z^2 - H^2)}{2\kappa} \tag{77}$$

We can see that the basal temperature ($z = 0$) takes longest to reach stablility. For the temperature at the base we have

$$\theta_b(t) = \frac{16kH^2}{\kappa\pi^3} e^{-\frac{\kappa\pi^2}{4H^2}t} - \frac{kH^2}{2\kappa} + kt \tag{78}$$

$$\theta_b(t) = kt - \frac{kH^2}{2\kappa}\left(1 - \frac{32}{\pi^3} e^{-\frac{\kappa\pi^2}{4H^2}t}\right) \tag{79}$$

$\left(\text{Note: } \frac{32}{\pi^3} \simeq 1\right)$

We now consider the magnitude of the exponent

$$-\frac{\kappa\pi^2}{4H^2}t = \psi, \text{ say,} \tag{80}$$

In order to have the basal temperature within 90% of its final value we require $t = 2{\cdot}2(4H^2/\kappa\pi^2)$.

For $H = 3{,}000$ m, $t = \dfrac{4(3 \times 10^5)^2}{10^{-2}\pi^2} \simeq 4 \times 10^{12}$ sec or $1{\cdot}3 \times 10^5$ yrs.

$H = 1{,}000$ m, $t = \dfrac{4(10^5)^2}{10^{-2}\pi^2} \simeq 4 \times 10^{11}$ sec or $1{\cdot}3 \times 10^4$ yrs.

Hence, provided the warming rate for the ice cap is constant over this length of time (for a given ice thickness), we could expect the temperature profile to remain in steady state. If the velocities of the ice in inland Antarctica are of the order of 1 m/yr, this may be possible. If they are closer to 10 m/yr, steady state under these conditions would not be maintained.

Our problem is that, as an ice column moves outwards, the warming rate may be expected to increase. Hence, we examine the variation of k with time:

taking

$$\theta(t) = \frac{15kH^2}{\kappa\pi^2} e^{-\frac{\kappa\pi^2}{4H^2}t} \cos\frac{\pi x}{2H}$$

$$= ake^{-bt},$$

where $a = \dfrac{15H^2}{\kappa\pi^2}\cos\dfrac{\pi x}{2H}$ and $b = \dfrac{\kappa\pi^2}{4H^2}$,

$$\frac{d\theta}{dt} = ae^{-bt}\left(-bk + \frac{dk}{dt}\right) \tag{81}$$

For steady state, dk/dt must be small compared to bk, or $\dfrac{1}{k}\dfrac{dk}{dt} \ll b$. If $k = \alpha V\lambda$, we can estimate values of $\dfrac{1}{k}\dfrac{dk}{dt}$, assuming constant λ, from $\dfrac{1}{k}\dfrac{dk}{dt} = \dfrac{1}{\alpha}\dfrac{d(\alpha V)}{dx}$. Typical values of $\dfrac{1}{k}\dfrac{dk}{dt}$ and values of $b = \dfrac{\kappa\pi^2}{4H^2}$ for different ice thickness are given below:

H m	$b = \dfrac{\kappa\pi^2}{4H^2}$ yr^{-1}	$\dfrac{1}{k}\dfrac{dk}{dt}$ yr^{-1}
3000	$0{\cdot}75 \times 10^{-5}$	$0{\cdot}5 \times 10^{-5}$
2000	$1{\cdot}70 \times 10^{-5}$	$2{\cdot}0 \times 10^{-5}$
1000	$7{\cdot}00 \times 10^{-5}$	$15{\cdot}0 \times 10^{-5}$

It is apparent that, far from being smaller, the values of $\dfrac{1}{k}\dfrac{dk}{dt}$ are comparable to, or even greater than, values of b. This means that, in absence of accumulation, the increase in warming rate of the ice as it moves outwards is too rapid for such thick ice to remain in the steady state for constant warming rate.

If stability is not reached, in the inland region, there may be a lag of $\simeq$ 30,000 years between the surface and basal layers reaching steady states. This time lag may correspond to a distance travelled $\simeq 100$ km, i.e., the basal temperatures may reflect the steady-state conditions upstream of the point in question.

The temperature gradient is given approximately by

$$\frac{\partial\theta}{\partial z} = \frac{kz}{\kappa} - \frac{8kH}{\kappa\pi^2}\, e^{-\frac{\kappa\pi^2}{4H^2}t} \sin\frac{\pi z}{2H} \tag{82}$$

At the surface $(z = H)$ the temperature gradient is given by

$$\left(\frac{\partial\theta}{\partial z}\right)_{z=H} = \frac{kH}{\kappa}\left(1 - \frac{8}{\pi^2}\, e^{-\frac{\kappa\pi^2}{4H^2}t}\right) \tag{83}$$

and at the base, $(z = 0)$,

$$\left(\frac{\partial\theta}{\partial z}\right)_0 = 0.$$

Hence, it may be expected that the surface gradient would take the same time to reach stability as the basal temperature, while the basal temperature gradient remains constant. The magnitude of the temperature gradient at the surface is always less than its final value, but gradually approaches it.

4.9.2. *Ice mass with exponentially increasing warming rate*

Since, for ice caps, the surface warming rate is not constant but increases rapidly towards the coast, we now consider the case of the slab $-H < z < H$ whose surfaces are kept at temperature $Ve^{\nu t}$, i.e., warming at the rate $\nu Ve^{\nu t} = \nu T$, say where T is the temperature at time t. This problem has also been considered by Carslaw and Jaeger (1959, p. 105).

For small ν, $e^{\nu t} \simeq 1 + \nu t$, and $\nu e^{\nu t} \simeq \nu$. Hence we may expect for very small warming rates that the solution of this problem approaches our previous result for constant warming rate $V\nu = k$, and as a consequence the steady-state temperature profiles for constant warming rate are maintained. We wish to determine the values of ν that are sufficiently small. The solution to this problem, given by Carslaw and Jaeger, is

$$\theta = Ve^{\nu t}\frac{\cosh x\sqrt{\nu/\kappa}}{\cosh H\sqrt{\nu/\kappa}} - \frac{4V}{\pi}\sum_{n=0}^{\infty}\frac{(-1)^n e^{-\kappa(2n+1)^2\pi^2 t/4H^2}}{(2n+1)[1 + \{4\nu H^2/(2n+1)^2\pi^2\kappa\}]}\cos\frac{2n+1}{2H}\pi x \tag{84}$$

The asymptotic solution, neglecting the the terms that die out with time, for the temperature at the base is given by

$$\theta_b = Ve^{\nu t}\frac{1}{\cosh H\sqrt{\nu/\kappa}} \tag{85}$$

In the previous case of constant warming kt we had

$$\theta_b' = kt + \frac{kH^2}{2k} \tag{86}$$

For $|H\sqrt{\nu/\kappa}| < \pi/2$

$$\theta_b = Ve^{\nu t}\left(1 - \frac{\nu H^2}{2\kappa} + \frac{5}{24}\frac{\nu^2}{\kappa^2}H^4 - \frac{61}{720}\frac{\nu^3}{\kappa^3}H^6 + \ldots\right) \tag{87}$$

$$\theta_s - \theta_b = \frac{T\nu H^2}{2\kappa} + \frac{5T}{24}\left(\frac{\nu}{\kappa}\right)^2 H^4 \ldots \tag{88}$$

The first term on the right corresponds to the previous result for constant warming rate $k = \nu T$. For the remaining terms to be negligible

$$\frac{5}{24}\left(\frac{H^2\nu}{\kappa}\right)^2 \ll \frac{H^2\nu}{2\kappa} \tag{89}$$

i.e., $$\frac{H^2\nu}{2{\cdot}4\kappa} \ll 1 \quad \text{or} \quad \nu \ll \frac{2{\cdot}4\kappa}{H^2} \tag{90}$$

To examine this condition in practice we consider the following values typical for a thick ice and thin ice position:

Ice thickness H	$T\frac{2{\cdot}4\kappa}{H^2}$	Slope α	Velocity V	Temperature gradient λ	Warming rate $\alpha V\lambda$
m	°C yr^{-1}		cm yr^{-1}	°C cm^{-1}	°C yr^{-1}
3000	$1{\cdot}10 \times 10^{-5}$	10^{-3}	10^{2}	$0{\cdot}7 \times 10^{-4}$	$0{\cdot}7 \times 10^{-5}$
1000	$0{\cdot}99 \times 10^{-4}$	$0{\cdot}5 \times 10^{-2}$	$2 \times 10^{+2}$	1×10^{-4}	$1{\cdot}0 \times 10^{-4}$

With these values of velocity and surface slope, the rates of surface warming $\alpha V\lambda$ are of comparable magnitude to $T\frac{2{\cdot}4\kappa}{H^2}$, which means that the higher terms in equation (88) cannot be neglected.

Hence, it appears that the warming rates of the present ice caps are too great (relative to the thicknesses) for steady-state temperatures to be maintained in the absence of accumulation and vertical velocity,

The effect of the accumulation may be judged from equation (71), with internal heating incorporated from equation (31) written as

$$\frac{d^2\theta}{d\zeta^2} + \frac{AH^2}{\kappa}(1 - \zeta)\frac{d\theta}{d\zeta} + \mu H^6\zeta^4 e^{\nu\theta} - \frac{H^2\lambda}{\kappa}\frac{DE}{Dt} = 0 \tag{91}$$

where $$\zeta = 1 - \frac{z}{H}$$

and $$\mu = \frac{(\rho g\alpha)^{n+1}}{B^n Jk}.$$

For typical values we may take $A \simeq 10$ cm/yr, $H \simeq 10^3$ m, $K \simeq 10^{-2}$cm^{2}sec^{-1}, $\frac{DE}{Dt} \simeq 10$ cm/yr, $\mu H^6 \simeq 50$, $\theta_s \simeq -30°$C, $\lambda \simeq 1°$C/100 m. Using these values, we find that at the surface the first and third terms are negligible, while the other two are each about 30°C in magnitude. Near the base the third term reaches $\simeq 50°$C and becomes dominant, but elsewhere may be neglected.

Hence, we see that the term in the accumulation at the surface is of similar magnitude as the surface warming but of opposite sign for negative surface gradients (typical of high warming rates) and hence diminishes the effect of the warming. As the depth increases the vertical velocity decreases but so does the effective remaining thickness. Hence, we may establish, as an approximate criterion for steady-state, profiles with accumulation, analogous to inequality (89) for no accumulation.

$$\frac{\lambda}{\kappa}\frac{DE}{Dt} - \frac{A}{\kappa}\frac{d\theta}{dz} \ll \frac{2{\cdot}4\kappa}{H^2} \tag{92}$$

For a balanced-state ice cap, $\frac{DE}{Dt} \simeq \alpha V$.

From equation (58) we can expect that the temperature gradient at the surface is given approximately by

$$\frac{d\theta}{dz} = \frac{\alpha V \lambda}{A}.$$

Hence, the above inequality becomes

$$\frac{\lambda}{\kappa}\alpha V - \frac{A}{\kappa}\frac{\alpha V \lambda}{A} \ll \frac{12\kappa}{H^2} \tag{93}$$

This brings the left-hand side to zero.

Therefore we conclude that, for accumulation rates high enough for an ice mass to be close to balance (within 10%), we may expect that the effect of the warming at the surface is sufficiently compensated by the accumulation rate so as to make the net warming of the ice mass low enough to remain in steady state as it flows outwards towards the coast.

4.10. PENETRATION OF TEMPERATURE VARIATIONS AT THE SURFACE INTO AN ACCUMULATING MEDIUM

For the long periods of time involved in setting up steady-state temperature profiles in ice masses we wish to know how long-term changes in the temperature at the surface affect the temperatures within the ice mass. The reaction of the temperatures inside an accumulating snow-cover to temperature variations at the surface has been treated by Benfield (1949, 1951, 1953). A similar study for periodic annual sine-wave temperature variations was made by Budd (1966). This latter can be extended in principle to much longer periods and by harmonic analysis be extended to cover other forms of temperature variation at the surface.

For the case of zero accumulation rate, a temperature wave at the surface of amplitude A_0 and frequency ω, defined by

$$\theta_0 = A_0 \cos \omega t,$$

generates a temperature wave at depth z given by

$$\theta_z = A_0 e^{-\sqrt{\omega/2\kappa}\, z} \cos(\omega t + \sqrt{\omega/2\kappa}\, z) \tag{94}$$

where κ is the diffusivity of the ice.

It was shown (Budd 1966) that, for an accumulating medium, i.e., moving downwards from the surface at a constant velocity u, the amplitude A_z of the corresponding temperature wave at depth z was related to the amplitude at the surface by

$$A_z = A_0 \exp - z\left[\frac{u}{2\kappa} - \frac{1}{\sqrt{2}}\left[\sqrt{\left(\frac{u^2}{4\kappa^2}\right)^2 + \frac{\omega^2}{\kappa^2}} + \frac{u^2}{4\kappa^2}\right]^{\frac{1}{2}}\right] \tag{95}$$

The phase lag at depth z is given by

$$\psi_z = z\left[\frac{1}{\sqrt{2}}\left[\sqrt{\left(\frac{u^2}{4\kappa^2}\right)^2 + \frac{\omega^2}{\kappa^2}} - \frac{u^2}{4\kappa^2}\right]^{\frac{1}{2}}\right] \tag{96}$$

The speed of downward travel of the temperature wave for zero accumulation is given by

$$\frac{dz}{dt} = \sqrt{2\kappa\omega} = \sqrt{\frac{4\pi\kappa}{p}} \tag{97}$$

where $p = 2\pi/\omega$ is the period of the wave.

From equation (95) we note that for high accumulation rates or low frequency temperature changes, i.e., $u \gg \sqrt{2\kappa\omega}$, the amplitude of the wave passes through the medium undiminished, its speed of travel being equal to the vertical velocity of the ice. For low accumulation rates or high frequency changes $u \ll \sqrt{2\kappa\omega}$, the wave is dissipated as usual for a medium with zero accumulation rate.

Table 4.14 shows the orders of magnitudes of accumulation rates and wave periods for equivalent diffusion velocity.

Table 4.15 shows the effects of penetration of temperature waves with periods from 1 to 10^6 years for zero accumulation (or accumulation rates significantly less than the penetration velocity).

TABLE 4.14

ACCUMULATION RATES AND DIFFUSION VELOCITIES

Accumulation rate	Ice thickness		Period with diffusion velocity A	Time for surface ice to reach 90% of depth	Distance travelled in ½ period
A cm yr^{-1}	H m	$\frac{H}{A}$ yrs	$p = \frac{16\pi\kappa}{A^2}$ yrs	t_{90} yrs	z_p m
1	4,000	400,000	4,600,000	920,000	11,500
5	3,000	60,000	183,000	138,000	2,380
10	2,000	20,000	46,000	46,000	1,150
50	1,000	2,000	1,800	4,600	238
100	500	200	460	460	115

TABLE 4.15

PENETRATION OF TEMPERATURE WAVES IN ICE CAPS WITHOUT ACCUMULATION

Period	Pentration velocity	Depth pentrated per period	Depth for 1/10 amplitude of surface	Depth for ½ period phase lag	Time taken to reach 1/10 amplitude
$p = \frac{2\pi}{\omega}$	$u = \sqrt{2\omega\kappa}$	$z_p = up$	$z_{0.1} = \sqrt{\frac{\kappa p}{\pi}} ln10$	$z_{\frac{1}{2}p} = \sqrt{\pi\kappa p}$	$t = \frac{ln10}{2\pi} p$
yrs	m yr^{-1}	m	m	m	yrs
10^6	0·020	20,000	7,000	10,000	360,000
10^5	0·065	6,500	2,300	3,000	36,000
10^4	0·200	2,000	730	1,000	3,600
10^3	0·650	650	230	300	360
10^2	2·000	200	73	100	36
10	6·500	65	23	30	3 60
1	20·000	20	7·3	10	0·36

The parameters listed are the penetration velocity, the depth penetrated over a time length of one period, the depth at which the amplitude is reduced to 10% of its value at the surface, the depth corresponding to a phase lag of ½ a period, and the time taken to reach the depth at which the amplitude is reduced to 1/10. For the waves of shorter period, i.e. $p < 10^3$ years, the accumulation rate is generally negligible and so this table gives an accurate prediction of their depths of penetration. These short period waves die out very quickly in the top few hundred metres and so cannot affect the temperatures in the deep layers of the ice caps. Only the very long waves penetrate into the deep layers. Table 4.16 shows times taken to reach various depths from 100 to 4,000 m and the amplitude decrease of the waves of various periods in absence of accumulation. Even the longest waves (10^6 years) are substantially damped out by the 4,000 m depth and are only slightly greater at 3,000 m. However, for these long waves, the effect of the accumulation is the dominating feature.

The time taken for the ice deposited at the surface to reach the height z above the surface for an ice mass in balance is given by

$$\frac{dz}{dt} = -A\frac{z}{H} \tag{98}$$

where H is the ice thickness
and A is the accumulation rate at the surface.

The average velocity through the ice mass is $A/2$.

Integrating equation (98) we obtain

$$\frac{z}{H} = e^{-At/H} \tag{99}$$

or

$$t = \frac{H}{A}\ln\frac{H}{z} \tag{100}$$

In particular, the time taken to reach 90% of the depth below the surface is

$$t_{90} \simeq \frac{H}{A}2{\cdot}3.$$

The time taken to reach this depth for various ice thicknesses and accumulation rates is shown in Table 4.17.

In effect, for accumulation rates of 10 g $cm^{-2}yr^{-1}$ or greater, temperature variations of periods of 50,000 years or more are carried to the base of ice by the internal convection of the ice. Over this period, with a horizontal velocity of between 1 and 5 m yr^{-1}, the ice would have moved along between 50 and 250 km. For lower accumulation rates we may conclude that ice masses 3,000-4,000 m thick are virtually unaffected in their lower layers by temperature fluctuations of periods less than 100,000 years.

The warming of the ice at its upper surface as it flows outwards to the coast may be considered as a very long period variation and, hence, where the accumulation rates are high enough, the increased warming passes relatively quickly through the ice mass, and the temperature profile will tend to stay the "steady-

TABLE 4.16

DAMPING OF TEMPERATURE VARIATIONS IN ICE CAPS

Time t (yrs) taken to reach depth z, and amplitude decrease A/A_0

Period yrs \ Depth z m	100		500		1000		2000		3000		4000	
	t	A/A_0	t	A/A_0	t	A/A_0	t	A/A_0	t	A/A_0	t	A/A_0
10^6	5,000	$\frac{1}{1{\cdot}03}$	25,000	$\frac{1}{1{\cdot}17}$	50,000	$\frac{1}{1{\cdot}4}$	100,000	$\frac{1}{1{\cdot}9}$	150,000	$\frac{1}{2{\cdot}7}$	200,000	$\frac{1}{3{\cdot}7}$
10^5	1,820	$\frac{1}{1{\cdot}1}$	9,100	$\frac{1}{1{\cdot}65}$	18,200	$\frac{1}{2{\cdot}7}$	36,400	$\frac{1}{7{\cdot}3}$	54,500	$\frac{1}{27}$	72,600	$\frac{1}{52}$
10^4	500	$\frac{1}{1{\cdot}4}$	2,500	$\frac{1}{5}$	5,000	$\frac{1}{27}$	10,000	$\frac{1}{740}$	15,000	$\frac{1}{22{,}000}$	20,000	
10^3	182	$\frac{1}{2{\cdot}7}$	910	$\frac{1}{150}$	1,820		3,640		5,450		7,260	
10^2	50	$\frac{1}{27}$	250		500		1,000		1,500		2,000	
10	18	$\frac{1}{22{,}000}$	91		182		364		545		726	
1	5		25		50		100		150		73	
											200	

TABLE 4.17

$$t = \frac{H}{A} \ln \frac{H}{z}$$

Time t years taken for surface snow to reach various depths z m, for various accumulation rates A cm/yr, and ice thickness Z m

$Z = 4{,}000$ m

z	100	500	2,000	3,600	3,960
A					
1	10,100	53,200	277,000	920,000	1,840,000
5	2,020	10,610	55,400	192,000	364,000
10	1,010	5,320	27,700	92,000	184,000
20	506	2,660	13,800	46,000	92,000

$Z = 2{,}000$ m

z	100	500	1,000	1,800	1,980
A					
5	2,060	11,500	27,700	92,000	184,000
10	1,030	5,760	13,800	46,000	92,000
20	514	2,880	6,920	23,000	46,000
50	206	1,150	2,770	9,200	18,400

$Z = 1{,}000$ m

z	100	500	900	990
A				
10	1,040	6,920	23,000	46,000
20	520	3,460	11,500	23,000
50	208	1,380	4,600	9,200
100	104	692	2,300	4,600

state" asymptotic profile—with perhaps a slight phase lag at the base. This phase lag at the base would imply that the basal temperature corresponded to that for steady state of the ice several tens of km upstream—depending on the horizontal velocity. It must be kept in mind, also, that over such long periods the ice cap shape and size could change greatly due to only a slight imbalance in the net budget. Over 50,000 years a net imbalance between 1 and 5 cm yr^{-1} would result in an ice thickness change of 500 to 2,500 m. This surface rising or lowering may then be the controlling element for the temperature changes at the surface.

Again, it is emphasized that the problem for non-steady state temperature gradients is very complex because we have to incorporate the change in the boundary conditions with time, as well as their present values. Hence, a general solution cannot be given for the temperature profile in an ice mass for a specified ice thickness, accumulation rate, velocity, surface and basal slopes, strain rates, etc., i.e., a solution of the form

$$\theta_z = f(H, A, V, \alpha, \beta, \dot{\varepsilon}_x, \ldots) \tag{101}$$

because the solution will also involve the rates of change of these variables with time over the period of time taken for the ice to move to its present position. In other words, the temperature profile is also a function of the terms $\frac{dH}{dt}, \frac{dA}{dt}, \frac{dV}{dt}, \frac{d\alpha}{dt}, \frac{d\dot{\varepsilon}_z}{dt}, \ldots$ which will generally vary with both time and position. This means

that, to interpret a measured temperature profile, at a certain position, firstly all the relevant movement, accumulation, etc., data must be obtained up and down stream along the flow line. Then, if the the flow rate is sufficiently low and the ice thickness sufficiently small for steady state to be maintained, the profiles can be interpreted by the theory outlined here. On the other hand, if the ice mass is not in steady state the numerical method of Jenssen and Radok (1963) may be used to follow a column along the flow line, integrating the heat conduction equation and incorporating the actual boundary conditions, over a long enough time for the ice cap to reach its temperature distribution from some assumed value. If the time intervals are not too long, perturbation techniques applied to the steady-state profile may be appropriate.

On the experimental side, the emphasis should be on obtaining temperature profiles at a large number of key positions, especially along a flow line, where all the other relevant data are available. Other key positions include the tops of domes and ice divides, where the horizontal movement is negligible and climatic variations can be most easily discerned. The importance of the basal flux, in expressions for the temperature profile, makes it essential for the temperature gradient near the base, and preferably right into the bedrock, to be known at a number of places, to ascertain how the geothermal flux varies from place to place. In conjunction with the deep drilling programmes, accurate inclinometer measurements may be made to reveal the velocity distribution in the vertical. This is important for the calculation of the internal heat produced by viscous friction, and its effect on the temperature profiles.

Since a large amount of data on temperature and velocity with depth in the ice masses is required, new techniques such as the Philberth meltsonde probe (Philberth 1967), may be very useful in supplementing the data provided by the deep drill holes.

4.11. CONCLUSIONS

Having found in Section 2 that the flow law of ice is highly temperature-dependent, it becomes necessary to know how the temperatures vary throughout the body of an ice mass in order to calculate the velocity distribution. In this section it was first shown how the vertical temperature profile affected the velocity—depth profile, and it was found that the typical temperature profiles tended to enhance the concentration of the shear in the basal layers.

Secondly, it was found that the high shear in the basal layer produces heat from viscous friction which substantially affects the temperature profile. This process has high positive feedback which can cause a rapid rise in the basal temperatures as the velocity is increased.

Two factors, sometimes an order of magnitude greater in their effect on the temperature profile than the internal friction (except in the basal layer), are the accumulation rate and the rate of surface warming as the ice flows out to the coast. The temperature conduction equation has been solved, taking these effects into account, and as a result steady-state temperature profiles have been calculated for various ice masses.

This study of "steady-state" temperature profiles has been extended to the case of rising or sinking ice masses. As a result of this it is found that the temperature gradient near the surface can throw light on the state of balance of an ice mass or the recent climatic changes. In particular, the temperature gradients measured in inland East Antarctica are consistent with a positive balance and a rising ice cap surface in that region, provided that climatic change over the period is negligible.

We next found, by an examination of the conditions required for steady-state temperatures, that we may expect the temperatures in the large ice masses to be close to the calculated steady-state profiles—except for the case of a rapidly sinking ice mass. A criterion has been established to determine whether the temperatures may be expected to approach steady state.

Finally, an examination of the penetration of temperature variations at the surface into ice masses has revealed that short-period fluctuations (less than 10^3 years die out within the top few hundred metres. Long-term variations travel through the ice mass at the rate of the ice itself, but still do not reach the base except for high accumulation rates (greater than 20 cm/yr) and for periods comparable to the turnover time of the ice mass. As a consequence, we may expect climatic changes over recent times to affect only the regions of thin ice of the large ice masses or those regions with high accumulation rates and high turnover rates. Thus the steady-state temperature profiles may still be expected to be close approximations to the actual temperature profiles. Hence, for interpreting the measured longitudinal velocities at the surface of ice masses in the following sections, we shall incorporate the effects of the steady-state temperature profiles developed here.

5. LONGITUDINAL VELOCITY PROFILES IN ICE MASSES

So far, we have been concerned with how the velocity profile in a moving ice mass varies transversely to the direction of motion (horizontally and vertically) and how the flow varies with temperature and stress. We shall now study how the velocity varies along the line of motion. In practice we find that the longitudinal velocity depends on all these parameters (width, depth, transverse strain rate, cross-section shape, temperature, etc.), but in general these only vary slowly along the line of motion, and so their higher derivatives with respect to distance (x) along the ice mass can, in many cases, be neglected.

We will hence proceed firstly with a simple two-dimensional model (zero transverse strain), with slowly varying thickness, and then later study the effects of varying transverse strain, temperature, shape factors and different forms of the boundary conditions.

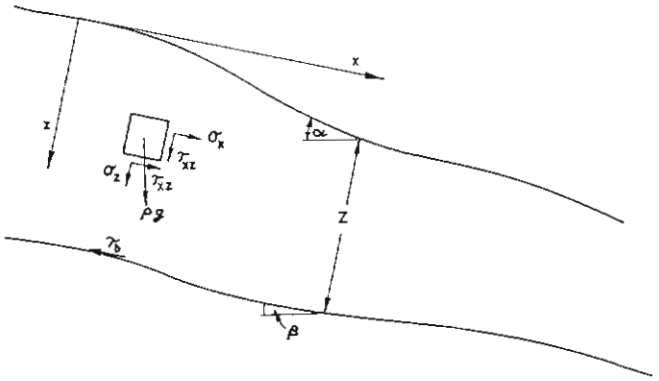

5.1. TWO-DIMENSIONAL FLOW

We consider a vertical section through an ice mass along a flow line where there are no transverse strain rates—typical of, say, the central flow line of a very wide glacier (compared to its thickness), with parallel sides, or of a flow line in an ice cap where horizontal divergence is negligible. We wish to determine the longitudinal profile of velocity and strain rate from the dimensions of the ice mass and the flow law of ice. The following approach is similar to that of Shoumsky (1961, 1963), but with several major modifications and with particular emphasis on the application to the study of measurements made on the ice masses.

An outline of this present work, showing the effect of longitudinal stresses on the strain rates was presented at the IUGG IASH Berne Symposium, September 1967 (Budd, 1968). Other writers, e.g., Lliboutry (1965), Shoumsky (1967), Robin (1967) have also shown the importance of the longitudinal stresses in the ice motion. Collins (1968) has derived a similar result to investigate the conditions under which Robin's approximate equation for longitudinal strain rate applies.

Nye (to be published) shows that, by choosing the longitudinal axis parallel to the surface, the exact equation for longitudinal stress gradient is simplified.

Here the original approximate presentation (Budd 1968) is followed. This is accurate for ice masses with small slopes. A precise derivation of the basic equation, with arbitrary axes orientation, which holds for slopes of any magnitude is presented in Appendix I. A major result of this generalized study is that, for small surface and bed slopes, the basic equation for the longitudinal strain-rate gradient is the same for the longitudinal axis taken horizontal, or parallel to the surface, or parallel to the bed.

Here we take orthogonal axes, x parallel to the average bed and in the direction of motion, and z downwards, from the surface.

The following symbols are introduced:

α—surface slope, at position x,
β—basal slope, at position x,
Z—ice thickness, at position x,
ρ—ice density (assumed constant),
g—gravitational acceleration,
τ_b—the basal shear stress,
$(\sigma_x, \tau_{xz}, \sigma_z)$—the stress components, and
$(\dot{\varepsilon}_x, \dot{\varepsilon}_{xz}, \varepsilon_z)$—the strain rate components.

From the results of Section 2 we have the following empirical relation for the flow law of randomly orientated polycrystalline ice:

$$\dot{\varepsilon}_{ij} = \frac{\sigma'_{ij}}{A_{1,\theta}} + \frac{\tau_0^{n-1}}{A_{2,\theta}^n}\,\sigma'_{ij} \tag{1}$$

where $\dot{\varepsilon}_{ij}$ is the strain rate tensor,

σ'_{ij} is the stress deviator tensor,

τ_0 is the octahedral shear stress defined by

$$\tau_0 = [\tfrac{1}{3}(\sigma'^2_1 + \sigma'^2_2 + \sigma'^2_3)]^{\frac{1}{2}} \tag{2}$$

where σ'_1, σ'_2, σ'_3 are the principal stress deviators.

$$\begin{aligned} A_{1,\theta} &= A_{1,0}e^{k\theta} \qquad A_{1,0} \simeq 5 \times 10^{14} \text{ dynes cm}^{-2} \text{ sec}^{-1} \\ A_{2,\theta} &= A_{2,0}e^{k\theta} \qquad A_{2,0} \simeq 3 \times 10^{8} \text{ dynes cm}^{-2} \text{ sec}^{1/3.5} \\ n &\simeq 3.5, \end{aligned} \tag{3}$$

where θ is the ice temperature in °C,

$$\text{and} \qquad k \simeq \tfrac{1}{10}{}^{\circ}\text{C}^{-1}.$$

The flow law can be expressed in terms of the "effective shear stress"

$$\tau_e = \sqrt{3/2}\ \tau_0$$

just by taking the appropriate value of A_2. This being understood, we leave τ unsubscripted. We note that over a limited range of stress we can represent the flow law by

$$\dot{\varepsilon}_{ij} = \frac{\tau^{n-1}}{B^n}\,\sigma'_{ij} \tag{4}$$

where the n and B values are chosen to match the curve of Fig. 2.2 over the appropriate range. This is the form af the flow law which we shall generally adopt

in this section, although it may be convienient on occasions to refer to a generalized flow law simply as

$$\dot{\varepsilon}_{ij} = \frac{1}{\eta}\sigma'_{ij},$$

where η (τ, θ) is a "generalized viscosity function" dependent on both stress and temperature defined by $\eta = \frac{\tau}{\dot{\varepsilon}}$ where τ, and $\dot{\varepsilon}$ are the octahedral shear stress and strain rate, at a particular temperature, determined empirically from stress-strain rate curves, e.g., Fig. 2.2.

We assume that the bedrock and surface slopes are sufficiently small so that we may take

$$\sin\beta \simeq \tan\beta \simeq \beta \qquad \text{and} \qquad \cos\beta \simeq 1$$
$$\sin\alpha \simeq \tan\alpha \simeq \alpha \qquad\qquad \cos\alpha \simeq 1.$$

The equations of motion can then be written as

$$\frac{\partial\sigma_x}{\partial x} + \frac{\partial\tau_{xz}}{\partial z} + \rho g\beta = 0 \tag{5}$$

$$\frac{\partial\sigma_z}{\partial z} + \frac{\partial\tau_{zx}}{\partial x} + \rho g = 0 \tag{6}$$

We integrate these equations with respect to z to obtain approximately

$$\frac{\partial F_x}{\partial x} = -\rho g Z\beta + \tau_b \tag{7}$$

$$\sigma_z = -\rho g z - \frac{\partial \int_0^z \tau_{xz}\, dz}{\partial x} \tag{8}$$

where F_x is the total longitudinal force over the section, and τ_b is taken positive in the negative x direction.

We require as the basic quantity governing the longitudinal strain rate, the mean longitudinal stress deviator $\bar{\sigma}'_x = \frac{1}{2}(\bar{\sigma}_x - \bar{\sigma}_z)$ (9)
where the bar denotes the average over the vertical section.

Now,

$$\bar{\sigma}_x = \frac{F_x}{Z} = -\frac{1}{Z}\int \rho g Z(\beta - f)\, dx \tag{10}$$

(where we write f for the basal friction coefficient defined by

$$f = \frac{\tau_b}{\rho g Z}, \tag{11}$$

and

$$\bar{\sigma}_z = \frac{1}{Z}\int_0^z \sigma_z\, dz \tag{12}$$

$$= -\frac{1}{2}\rho g Z - \frac{1}{Z}\frac{\partial \int_0^z \int_0^z \tau_{xz}\, dz\, dz}{\partial x} \tag{13}$$

We now obtain

$$\frac{\partial Z\bar{\sigma}'_x}{\partial x} = -\frac{1}{2}\left[\rho g Z(\beta - f) - \rho g Z\frac{\partial Z}{\partial x} - \frac{\partial^2 \iint \tau_{xz}\,dz\,dz}{\partial x^2}\right] \tag{14}$$

We note that

$$-\frac{\partial Z}{\partial x} = \alpha - \beta \tag{15}$$

and hence equation (14) becomes

$$\frac{\partial(Z\bar{\sigma}'_x)}{\partial x} = -\frac{1}{2}\left[\rho g Z(\alpha - f) - \frac{\partial^2 \iint \tau_{xz}\,dz\,dz}{\partial x^2}\right] \tag{16}$$

If we consider a flow law of the type

$$\dot{\varepsilon}_x = \frac{\tau^{n-1}}{B^n}\sigma'_x \tag{17}$$

where

$$\tau = \tfrac{1}{2}\sqrt{(\sigma_x - \sigma_z)^2 + 4\tau_{xz}^2} \tag{18}$$

we note that with a linear flow law ($n = 1$) the longitudinal strain rate is directly related to the longitudinal stress deviator independent of the vertical shear stress τ_{xz}. When a higher power operates, however, the vertical shear becomes important.

We write the flow law as

$$\sigma'_x = B\dot{\varepsilon}_x^{1/n}(1 + \gamma^2)^{-(n-1)/2n} \tag{19}$$

where

$$\gamma = \frac{2\tau_{xz}}{(\sigma_x - \sigma_z)} \tag{20}$$

and we see that the effect of vertical shear τ_{xz} is negligible when it is significantly smaller than $\frac{\sigma_x - \sigma_z}{2}$, or when $n \simeq 1$. It will be found in Section 6.3 that indeed, for the longitudinal strain rates measured in the Wilkes ice cap, $n \simeq 1$ in this context.

More recent work, however, by Carter (in preparation), involving higher stresses, makes it necessary to consider the effect of the vertical shear stresses. The procedure for doing this is outlined in Appendix II. The net result of this procedure simply indicates that a different interpretation is required for the flow parameter B_1. Here the following discussion is restricted to small stresses, and the generalization to areas of appreciable vertical shear may be readily carried out by a re-interpretation of B_1.

Hence, we make the *assumption* that, vertically averaged, the flow law can be written

$$\dot{\varepsilon}_x = \left(\frac{\bar{\sigma}'_x}{\bar{B}_1}\right)^n \tag{21}$$

where $\dot{\varepsilon}_x$ is the longitudinal strain rate at the surface and $\bar{B}_1$ is the simple linear average of B over the section, and the error given by the integral of equation (19).

Equation (16) now becomes

$$\frac{\partial Z\overline{B_1\dot{\varepsilon}_x^{1/n}}}{\partial x} = -\frac{1}{2}\left[\rho g Z(\alpha - f) - \frac{\partial^2 \iint \tau_{xz}\, dz\, dz}{\partial x^2}\right] \tag{22}$$

The term on the right-hand side containing τ_{xz} was considered by Shoumsky (1961) to be negligible.

For laminar flow $\frac{\partial \tau_{xz}}{\partial x}$ is zero and, in general, it depends on the variations in vertical velocity along the flow line. Hence, we estimate its importance with regard to flow over undulations. If the surface traction is zero the shear stress τ_{xz} at the surface, τ_s say, is related to the longitudinal stress deviator and surface slope α_s by

$$\tau_s = \tfrac{1}{2}(\sigma_x - \sigma_z)_s \tan 2\alpha_s \approx (\sigma_x - \sigma_z)\alpha_s.$$

Now, if the longitudinal strain rate does not vary greatly with depth through the ice mass, except in the basal layer, we may make the following *assumption* for the variation of shear stress with depth

$$\tau_{xz} = \rho g Z(\alpha_s - \bar{\alpha}) + \rho g z(2\bar{\alpha} - \alpha_s) \tag{23}$$

Here the shear stress τ_{xz} has the value $\rho g(\alpha_s - \alpha)Z$ at the surface, where α_s, $\bar{\alpha}$ are the local and regional surface slopes, and varies linearly with depth to the value $\tau_b = \rho g \alpha Z$ at the base, which we assume constant with x.*

Using equation (23) we find

$$\frac{\partial^2 \int_0^Z \int_0^z \tau_{xz}\, dz\, dz}{\partial x^2} = \frac{\rho g}{3}\frac{\partial^2 \alpha Z^3}{\partial x^2} \tag{24}$$

We now examine how the this term affects the variation in strain, first in surface undulations over comparatively short distances x where Z can be considered constant, and secondly on the large scale when the general curvature of the ice cap is taken into account.

(i) Local ice cap undulations

Consider a short section of the ice cap with small fluctuations of wave-length λ, in surface elevation, compared with the ice thickness Z. We can write for the surface elevation H

$$H = H_0 + \bar{\alpha}x + A\cos\frac{2\pi}{\lambda}x \qquad (\bar{\alpha}x, A \ll Z) \tag{25}$$

The surface slope may then be written

$$\alpha = \bar{\alpha} - \frac{2\pi}{\lambda}A\sin\frac{2\pi}{\lambda}x \tag{26}$$

and

$$\frac{\partial^2 \alpha}{\partial x^2} = -\left(\frac{2\pi}{\lambda}\right)^2(\alpha - \bar{\alpha}) \tag{27}$$

* Other assumptions besides $\tau_{xz} = \rho g\,(\alpha_s - \bar{\alpha})\,Z + \rho g z\,(2\bar{\alpha} - \alpha_s)$

such as (ii) $\tau_{xz} = \rho g\,(\alpha_s - \bar{\alpha})\,z$

or (iii) $\tau_{xz} = \rho g\,(\alpha_s - \bar{\alpha})\,Z$

lead to similar results, but with, instead of the factor $p_1 = \frac{2\pi}{\sqrt{3}}$ in equation 29, the factor is $p_2 = \frac{2\pi}{\sqrt{6}}$ or $p_3 = \frac{2\pi}{\sqrt{2}}$ respectively.

Using (24) and assuming Z, B remain constant over the section, equation (22) can then be written approximately

$$\frac{\partial \dot{\varepsilon}_x^{1/n}}{\partial x} = -\frac{\rho g}{2B}\left[(\alpha - f) - \frac{Z^2}{3}\frac{\partial^2 \alpha}{\partial x^2}\right] \tag{28}$$

$$= -\frac{\rho g}{2B}\left[(\alpha - f) + \left(\frac{2\pi}{\sqrt{3}}\frac{Z}{\lambda}\right)^2(\alpha - \bar{\alpha})\right] \tag{29}$$

Since $\frac{2\pi}{\sqrt{3}} \simeq 3.63$ we find that for short surface wavelengths ($\lambda \simeq 3.6Z$ or less) the second term ($\partial^2\alpha/\partial x^2$) becomes important. If $f \simeq \bar{\alpha}$ (as inferred from the Wilkes data, cf. Section 6) we see that the effect of the second derivative of slope for short undulations is to amplify the relative maximum extension on the crests of the waves and the comparative compression in the troughs.

(2) Large scale ice cap curvature

In order to estimate the magnitude of the second term on the right of equation (22), on the larger scale, if we put for an ideal case $\alpha = f$ in equation (22), integrate and divide by $2B$ to obtain from (24)

$$\dot{\varepsilon}_x^{1/n} = \frac{\rho g}{6B}\frac{1}{Z}\frac{\partial \alpha Z^3}{\partial x} \tag{30}$$

By considering ice cap shapes of the form $Z = x^m$ with $m = 1, \frac{1}{2}, \frac{1}{3} \ldots$ it can be shown that, although strain rates and velocities deduced from this relation are compatible with the velocities calculated in Section 6, from the assumption that the basal shear stress is proportional to the large scale surafce slope of the ice cap, the magnitudes are quite small. We shall examine the terms of equation (30) later in this section for various hypothetical ice caps, after finding a relation for the large scale velocity. Here it suffices to state that, on the scale of about 10 to 20 times the ice thickness this term may be neglected, but for short undulations $\lambda \simeq 3{\cdot}6Z$ it becomes important and this is discussed with reference to ice flow over undulations in Section 5.4.

Hence for the present, we write the basic equation for longitudinal strain rate as

$$\frac{\partial Z B_1 \dot{\varepsilon}_x^{1/n}}{\partial x} = -\frac{1}{2}\rho g Z(\alpha - f) \tag{31}$$

Equation (31) suggests that fluctuations in slope over short distances, where Z, f and B can be considered constant, give rise to corresponding fluctuations in longitudinal strain rate according to

$$\bar{B}\frac{\partial \dot{\varepsilon}_x^{1/n}}{\partial x} = -\frac{1}{2}\rho g(\alpha - f) \tag{31a}$$

This immediately suggests a means of determining f, i.e., by measuring the small-scale variations of surface strains and slope along the ice mass. If the *net* strain rate over long distances is very small or relatively constant or, more precisely from equation (31), if

$$\frac{\partial Z B_1 \dot{\varepsilon}^{1/n}}{\partial x} = 0$$

we find $f \rightarrow \bar{\alpha}$. This means that, over larger distances, with smoothed values, the formula for basal stress, Nye (1952),

$$\tau_b = \rho g Z \bar{\alpha} \tag{32}$$

is a reasonable approximation. The actual distance over which the smoothing is taken is discussed in Section 5.4.3.

From equation (31) we can determine the values of n and B by comparing the stress variations resulting from the slope changes with the resultant strain rate variations, i.e., from the equation

$$\dot{\varepsilon}_x^{1/n} = -\frac{\rho g}{2B} \int (\alpha - \bar{\alpha})\, dx \tag{33}$$

where the integral is taken over a half wave. The use of this equation is elaborated in Section 6.

We next consider the longitudinal *velocity* profile which, on the larger scale, is determined by the general ice cap curvature rather than the minor fluctuations in slope. To do this we first see how the velocity at the surface is related to the basal shear stress. Nye (1957, 1959) has shown that the presence of a small longitudinal strain rate does not significantly affect the velocity—depth profile.

We can express $f = \dfrac{\tau_b}{\rho g Z}$ in terms of the velocity at the surface. Taking $\tau_{xz} = \rho g \bar{\alpha} z$ and a flow law

$$\dot{\varepsilon}_{xz} = \frac{1}{2}\frac{dV_x}{dz} = \left(\frac{\tau_{xz}}{B}\right)^n \tag{34}$$

we deduce

$$V_{xz}\Big|_0^z = 2\int_0^z \left(\frac{\rho g \bar{\alpha} z}{B}\right)^n dz \tag{35}$$

or

$$V_s - V_b = \frac{2(\rho g \bar{\alpha})^n}{(n+1)B_2^n} Z^{n+1} \tag{36}$$

where V_s, V_b are the velocities at the surface and base respectively and $\bar{B}_2$ is the weighted integrated average dependent on the temperature distribution and defined by

$$\bar{B}_2 = \left[\frac{n+1}{Z^{n+1}} \int_0^z \frac{1}{B^n} z^n\, dz\right]^{-1/n} \tag{37}$$

$\bar{B}_2$ is, in effect, the average value of B in the basal layers. With isothermal conditions, 94% of the value of the integral for $\bar{B}$ is determined by the lower half of the ice mass. Moreover, the typical positive temperature gradient ($\simeq$ 2-4°C/100 m) near the base gives smaller values of B which enhances this so that $\bar{B}_2$ is effectively determined by the temperature in the lowest 10-20% of the ice. Hence, the subscript 2 will be adopted for these B and n values to distinguish them from those of equation (31) which apply to an average through

the column. From equations (36) and (23) we can write for the basal stress

$$\tau_b = \overline{B}_2 \left[\frac{n_2 + 1}{2Z} (V_s - V_b) \right]^{1/n_2} \tag{38}$$

For a cold ice mass (basal temperature well below zero) we may expect $V_b = 0$. Hence, equation (22) can be written using (38) and (11) as

$$-\frac{\partial Z B_1 \dot{\epsilon}_x^{1/n}}{\partial x} = \frac{1}{2}\rho g Z \alpha - \frac{1}{2} B_2 \left(\frac{n_2 + 1}{2Z} V_s \right)^{1/n_2} - \frac{\rho g}{6} \frac{\partial^2 \alpha Z^3}{\partial x^2} \tag{39}$$

This is now a second-order differential equation in velocity and the flow law parameters and the boundary dimensions of the ice mass (viz., ice thickness and surface slope). If we knew the flow parameters precisely, we could use this equation to calculate the velocity and strain rate along the ice mass, provided boundary values of velocity and strain rate are known at an end-point. On the other hand, if the strain rates and velocities can be measured, along with the ice mass thickness and elevation profiles, then the effective flow parameters can be calculated.

We note that, since the power flow law only holds over a small range of stress, the n and B values on the left-hand-side and right-hand-side may be quite different, since they refer to quite different regions of the ice mass with different stresses and temperatures. The values on the left are associated with the longitudinal strain right through the ice mass, while those on the right refer to the high shear in the basal layers. In the particular cases, where either

$$\frac{\partial Z B \dot{\epsilon}_x^{1/n}}{\partial x} = 0 \quad \text{and} \quad \frac{\partial^2 \alpha Z^3}{\partial x^2} = 0, \quad \text{or} \quad \frac{\partial Z B \dot{\epsilon}_x^{1/n}}{\partial x} = -\frac{\rho g}{6} \frac{\partial^2 \alpha Z^3}{\partial x^2},$$

we have the result $f = \overline{\alpha}$ which leads to the following relation for longitudinal velocity

$$\frac{V}{Z} = \frac{2}{n_2 + 1} \left(\frac{\rho g}{B_2} \overline{\alpha} Z \right)^{n_2} \tag{40}$$

This relation is equivalent to the result deduced by Haefeli [1961 equation (12)] for constant B and used by him to determine the velocity along a flow line in Greenland.

We may expect this formula for velocity in terms of the ice thickness, surface slope and the flow law parameters to hold for smoothed values on the large scale, provided the mean longitudinal strain rate is small, as distinct from the small-scale fluctuations in slope, and strain rates described by equation (33). Since the parameter B is dependent on temperature it is necessary to know also the temperature distribution through the ice mass.

We now examine the variation with the large scale ice-cap curvature of the term

$$\frac{\partial^2}{\partial x^2} \iint \tau_{xz} \, dz \, dz = \frac{\rho g}{6} \frac{\partial^2 \alpha Z^3}{\partial x^2}.$$

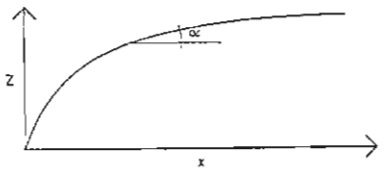

Consider an ice cap profile represented by $Z \propto x^m$ (41), where Z is the ice thickness at distance x inland from the edge. Note that x here is taken in the reverse direction to the previous.

If we assume the bedrock is horizontal we have

$$\alpha = \frac{dZ}{dx} \propto x^{m-1}.$$

Then equation (30) gives us for the strain rate

$$\dot{\varepsilon}_x^{1/n_1} \propto x^{-m} \frac{\partial x^{4m-1}}{\partial x} \propto x^{3m-2} \tag{42}$$

provided B is constant.

On the other hand, if equation (40) holds, we have

$$\begin{aligned} V &\propto \alpha^{n_2} Z^{n_2+1} \\ &\propto x^{n_2(m-1)+m(n_2+1)} \\ \therefore\ \dot{\varepsilon}_x &\propto x^{2n_2m-n_2+m-1} \end{aligned} \tag{43}$$

Equating these expressions for strain rate, we must have the same exponents, i.e.,

$$n_1(3m - 2) = m(2n_2 + 1) - n_2 - 1 \tag{44}$$

or

$$m = \frac{n_2 - 2n_1 + 1}{2n_2 - 3_1 + 1} \tag{45}$$

For $n_1 = 1$ $\quad m = \frac{1}{2}$ for all n_2

For $n_1 = 2$ and $n_2 = 3$ $\quad m = 0$

3.5 $\quad \frac{1}{4}$

4 $\quad \frac{1}{3}$

Also, if $n_2 \to \infty$ $\quad m \to \frac{1}{2}$

The parabola $Z = x^{\frac{1}{2}}$ was found by Nye (1952) to be equivalent to the relation $\tau_b = \rho g \alpha Z$ for a plastic solid. This form is also approached for high values of n_2. Many existing ice caps (cf. Section 7) approach this in shape. For the higher values of $1/m$ calculated above, we see that slightly different values of n_1 and n_2 are required to maintain compatibility between the relations

$$V \propto \alpha^{n_2} Z^{n_2+1} \quad \text{and} \quad \dot{\varepsilon}_x^{1/n_1} = \frac{1}{2} \frac{\partial^2 \alpha Z^3}{\partial x^2}.$$

Actual values of these parameters will be discussed in Section 6.

Although variations in bedroek slope and the parameter B require modification

cation of these general considerations, it appears that the presence of the term $\frac{\partial^2}{\partial x^2}\int\int \tau_{xz} dz dz$ in equation (22) does not conflict with the use of the longitudinal velocity and strain rate equations (40) and (33), for determining the flow parameters. This will be found to be the case in Section 6.

The results of this two-dimensional analysis are applicable to ice sheets where transverse strain rates are negligible. An extension to certain simple three-dimensional models will now be carried out in Section 5.2 to cover the cases of glaciers, where transverse *shear* is important, by considering averages over the cross-section and appropriate shape factors (cf. Nye 1965). Transverse extension and compression will be discussed in Section 5.3.

5.2. THREE DIMENSIONS

The analogous equations of motion for a ice mass moving slowly down a slope under its own weight for three dimensions to equations 5.1 (4) and (5) are

$$\frac{\partial \sigma_x}{\partial x} + \frac{\partial \tau_{xy}}{\partial y} + \frac{\partial \tau_{xz}}{\partial z} = \rho g \beta \tag{1}$$

$$\frac{\partial \sigma_z}{\partial z} + \frac{\partial \tau_{zx}}{\partial x} + \frac{\partial \tau_{zy}}{\partial y} = -\rho g \tag{2}$$

$$\frac{\partial \sigma_y}{\partial y} + \frac{\partial \tau_{yx}}{\partial x} + \frac{\partial \tau_{yz}}{\partial z} = 0 \tag{3}$$

(1*) We now assume that the ehanges in cross-section shape and width of the ice mass along the line of flow are sufficiently small to be neglected. Then the main changes in the ice mass along the line of flow are just in the thickness Z and the surface slope α.

Since the channel is non-diverging, we have no velocity components perpendicular to the flow lines, and therefore

$$\tau_{yz} = 0,$$

and

$$\tau_{yx} \propto sy,$$

where s is a shape factor which is constant across the section for the special shapes of

(1) semi-circular cross-section,
(2) infinitely wide cross-section,
(3) infinitely deep cross-section,

but is generally a function of y and z. Here we shall assume s is independent of x.

Hence,

$$\frac{\partial \tau_{yx}}{\partial x} = 0$$

and from equation (3)

$$\frac{\partial \sigma_y}{\partial y} = 0.$$

Equation (2) reduces to the equivalent equation of two dimensions, 5.1 (6).

We integrate equation (1) over the cross-section area to obtain

$$\frac{\partial F_x}{\partial x} = -\rho g A\beta + p\bar{\tau}_b \tag{4}$$

where F_x is the total force over the cross-section in the line of flow, p is the length of the boundary perimeter and $\bar{\tau}_b$ is the mean shear stress around the boundary defined by

$$\bar{\tau}_b = \frac{1}{p}\int_0^Y \int_0^{Z(y)} \left(\frac{\partial \tau_{xy}}{\partial y} + \frac{\partial \tau_{xz}}{\partial z}\right) dz\, dy \tag{5}$$

Integrating (2) over the cross-section and using assumption (1*) we obtain

$$\begin{aligned}\bar{\sigma}_z &= \frac{1}{A}\int_0^Y \int_0^{Z(y)} \sigma_z(z)\, dz\, dy \\ &= -\frac{\rho g}{A}\int_0^Y \int_0^{Z(y)} z\, dz\, dy - \frac{1}{A}\frac{\partial \int_0^Y \int_0^{Z(y)} \int_0^z \tau_{xz}\, dz\, dz\, dy}{\partial x}\end{aligned} \tag{6}$$

(2*) We assume to a first approximation here that, similarly to equation 5.1 (23),

$$\tau_{xz} = s_2 \rho g Z(\alpha_s - \bar{\alpha}) + s_2 \rho g z(2\bar{\alpha} - \alpha_s) \tag{7}$$

where s_2 is a second shape factor constant over the cross-section.

It was shown in Section 3 that, although this approximation generally only holds near the centre line, it is close for rectangular cross-sections and also ice masses wide compared to their depth. For other cross-sections it is necessary to consider variation in s_2 across the glacier. We also consider only the case for α constant over the cross-section.

Equation (6) now may be written

$$\bar{\sigma}_z = -\frac{1}{2}\rho g \bar{Z} - \frac{s_3 \rho g}{2A}\frac{\partial \alpha A \bar{Z}^2}{\partial x} \tag{8}$$

where the bar denotes the mean value over the section, i.e.,

$$\tfrac{1}{2}\bar{Z} = \frac{1}{A}\int_0^Y \int_0^{Z(y)} z\, dz\, dy,$$

and

$$s_3 = s_2 \frac{\overline{Z^2}}{\bar{Z}^2}.$$

The mean longitudinal stress is given by

$$\bar{\sigma}_x = \frac{F_x}{A}$$

which from (4) becomes

$$\bar{\sigma}_x = -\frac{1}{A}\int_0^x \rho g A(\beta - \bar{f})\, dx \tag{9}$$

where we define the friction coefficient $\bar{f}$ by

$$\bar{f} = \frac{p}{A}\frac{\bar{\tau}_b}{\rho g} \tag{10}$$

We now find for the mean stress deviator from (8) and (9)

$$\bar{\sigma}'_x = -\frac{1}{2}\left[\frac{1}{2}\rho g\bar{Z} - \frac{\rho g}{A}\int_0^x A(\beta - \bar{f})\,dx - \frac{s_3\rho g}{2A}\frac{\partial \alpha A\bar{Z}^2}{\partial x}\right] \tag{11}$$

Hence

$$\frac{\partial A\bar{\sigma}'_x}{\partial x} = -\frac{1}{2}\left[\frac{1}{2}\rho g\frac{\partial A\bar{Z}}{\partial x} - \rho g A(\beta - \bar{f}) - \frac{s_3\rho g}{2}\frac{\partial^2 \alpha A\bar{Z}^2}{\partial x^2}\right] \tag{12}$$

Adopting a flow law of the form

$$\dot{\varepsilon}_x = \left(\frac{\bar{\sigma}'_x}{\bar{B}}\right)^n \tag{13}$$

analogous to our case for two dimensions, where $\dot{\varepsilon}_x$ is the strain rate on the centre-line and $\bar{\sigma}'_x$ and $\bar{B}$ are averages over the section, and defining $\bar{Y}$ *by* $A = \bar{Y}\,\bar{Z}$ (14) equation (12) becomes

$$\frac{\partial A\bar{B}\dot{\varepsilon}_x^{1/n}}{\partial x} = -\frac{1}{2}\left[\frac{1}{2}\rho g\bar{Y}\frac{\partial \bar{Z}^2}{\partial x} - g\bar{Y}\bar{Z}(\beta - \bar{f}) - \frac{s_3\rho g}{2}\bar{Y}\frac{\partial^2 \alpha \bar{Z}^3}{\partial x^2}\right] \tag{15}$$

or for constant $\bar{Y}$

$$\frac{\partial \bar{Z}\bar{B}\dot{\varepsilon}_x^{1/n}}{\partial x} = -\frac{1}{2}\left[\rho g\bar{Z}\left(\frac{\partial \bar{Z}}{\partial x} + \beta - \bar{f}\right) - \frac{s_3\rho g}{2}\frac{\partial^2 \alpha \bar{Z}^3}{\partial x^2}\right] \tag{16}$$

Finally, with $\dfrac{\partial \bar{Z}}{\partial x} = \bar{\alpha} - \beta$ and assuming the last term on the right negligible under similar conditions to those discussed for two dimensions, we may write

$$\frac{\partial \bar{Z}\bar{B}\dot{\varepsilon}_x^{1/n}}{\partial x} = -\frac{1}{2}\rho g\bar{Z}(\alpha - \bar{f}) \tag{17}$$

which is analogous to the result for two dimensions, with some of the parameters having more generalized meanings in terms of averages over the section. Similarly, we can express $\bar{f}$ in terms of the average velocity or the velocity of the centre-line, using approximate shape factors—as calculated for particular cross-sections by Nye (1965). These results then allow the results for two dimensions of section (3) to be extended to ice masses bounded at their sides—such as typical glaciers or ice shelves—provided the transverse extension or compression is negligible. The effect of such diverging or converging flow on the longitudinal strain rate and velocity profile will now be examined.

5.3. EFFECT OF TRANSVERSE STRAIN $\dot{\varepsilon}_y$ ON THE LONGITUDINAL VELOCITY PROFILE

Weertman (1957 appendix), considered a special case of three-dimensional strain in an ice shelf. For the two-dimensional case, i.e., with zero lateral strain $\dot{\varepsilon}_y = 0$:

$$\dot{\varepsilon}_x = -\dot{\varepsilon}_z,$$

Weertman obtained

$$\dot{\varepsilon}_x = (2A)^{-n}|\sigma_x - \sigma_z|^{n-1}(\sigma_x - \sigma_z) \tag{1}$$

whereas, for the case of an ice shelf expanding equally in all (horizontal) directions (three dimensions), he obtained

$$\dot{\varepsilon}_x^* = \dot{\varepsilon}_y = -\frac{1}{2}\dot{\varepsilon}_z = A^{-n}\left|\frac{\sigma_x - \sigma_z}{\sqrt{3}}\right|^{n-1}\left(\frac{\sigma_x - \sigma_z}{3}\right) \tag{2}$$

We note that

$$\dot{\varepsilon}_x^* = \dot{\varepsilon}_x \frac{1}{\sqrt{3}}\left(\frac{2}{\sqrt{3}}\right)^n \tag{3}$$

and, since

$$\frac{1}{\sqrt{3}}\left(\frac{2}{\sqrt{3}}\right)^n = 1 \qquad \text{for } n \approx 4,$$

we obtain the interesting result that the longitudinal strain rate for a given stress deviator is *decreased* with the presence of an equal lateral expansion for *low* values of n (< 4), but for *high* values of n it would be increased.

We shall now consider the effect on the longitudinal strain rate ($\dot{\varepsilon}_x$) of an arbitrary transverse strain rate ε_y.

We adopt a flow law of the form

$$\dot{\varepsilon}_x = \lambda\sigma_x'$$

$$\text{where} \quad \sigma_x' = \sigma_x - \tfrac{1}{3}\sigma_{ii} \tag{4}$$

where $\sigma_{ii} = \sigma_x + \sigma_y + \sigma_z$

and $\lambda = A^{-n}\tau^{n-1}$ (6)

and $2\tau^2 = \sigma_x'^2 + \sigma_y'^2 + \sigma_z'^2$ (7)

where τ is the "effective shear stress" (equal to $\sqrt{3/2}$ times the octahedral shear stress. A, and n are parameters of the power law for flow.

Now, we require the longitudinal strain rate $\dot{\varepsilon}_x$ in terms of the longitudinal terms of the longitudinal and vertical stresses σ_x, σ_z and the transverse strain rate $\dot{\varepsilon}_y$. From (4) and (5) we obtain

$$\dot{\varepsilon}_x = \lambda[\sigma_x - \tfrac{1}{3}(\sigma_x + \sigma_y + \sigma_z)]$$

$$= \frac{\lambda}{3}[2\sigma_x - \sigma_y - \sigma_z] \tag{8}$$

We obtain σ_y *from*

$$\dot{\varepsilon}_y = \lambda\sigma_y' \tag{9}$$

$$= \frac{\lambda}{3}[2\sigma_y - \sigma_x - \sigma_z] \tag{10}$$

$$\therefore \quad \sigma_y = \frac{3}{2}\frac{\dot{\varepsilon}_y}{\lambda} + \frac{1}{2}(\sigma_x + \sigma_z) \tag{11}$$

Substituting this in equation (8) above, we obtain

$$\dot{\varepsilon}_x = \frac{\lambda}{3}\left[\frac{3}{2}\sigma_x - \frac{3}{2}\sigma_z - \frac{3}{2}\frac{\dot{\varepsilon}_y}{\lambda}\right]$$

or

$$\dot{\varepsilon}_x = \frac{\lambda}{2}\left[(\sigma_x - \sigma_z) - \frac{\dot{\varepsilon}_y}{\lambda}\right] \tag{12}$$

Next, to obtain λ from (6) we first require τ from (7) for which we require the stress deviators.

From (4) and (12) we see

$$\sigma'_x = \frac{1}{2}(\sigma_x - \sigma_z) - \frac{\dot{\varepsilon}_y}{2\lambda} \tag{13}$$

similarly

$$\sigma'_z = \frac{1}{2}(\sigma_z - \sigma_x) - \frac{\dot{\varepsilon}_y}{2\lambda} \tag{14}$$

and

$$\sigma'_y = \frac{\dot{\varepsilon}_y}{\lambda} \tag{15}$$

Hence from (7) we obtain

$$2\tau^2 = \frac{1}{2}\left[(\sigma_x - \sigma_z)^2 + \left(\frac{\dot{\varepsilon}_y}{\lambda}\right)^2\right] + \left(\frac{\dot{\varepsilon}_y}{\lambda}\right)^2 \tag{16}$$

Now, let us write the lateral strain rate as a certain fraction ($\gamma\lambda$, say) of the stress difference ($\sigma_x - \sigma_y$), i.e.,

$$\frac{\dot{\varepsilon}_y}{\lambda} = (\sigma_x - \sigma_z)\gamma \tag{17}$$

Then from equation (12)

$$\dot{\varepsilon}_x = \frac{\lambda}{2}(\sigma_x - \sigma_z)(1 - \gamma) \tag{18}$$

and from equation (16)

$$\begin{aligned} 2\tau^2 &= \tfrac{1}{2}[(\sigma_x - \sigma_z)^2(1 + \gamma^2)] + (\sigma_x - \sigma_z)^2\gamma^2 \\ &= (\sigma_x - \sigma_z)^2(\tfrac{1}{2} + \tfrac{3}{2}\gamma^2) \end{aligned} \tag{19}$$

or

$$\tau = (\sigma_x - \sigma_z)(\tfrac{1}{4} + \tfrac{3}{4}\gamma^2)^{\frac{1}{2}} \tag{20}$$

We now substitute this for τ in equation (6) to obtain λ which we can substitute in (18) for the longitudinal strain rate to give

$$\dot{\varepsilon}_x = \frac{A^{-n}}{2}(\sigma_x - \sigma_z)^n(1 - \gamma)(\tfrac{1}{4} + \tfrac{3}{4}\gamma^2)^{(n-1)/2} \tag{21}$$

Since we wish to know the relation between the longitudinal strain rate ($\dot{\varepsilon}_x$) and the stress difference ($\sigma_x - \sigma_z$) for a given transverse strain rate ($\dot{\varepsilon}_y$), which is a certain fraction (say, ν) of the longitudinal strain rate, we write,

$$\dot{\varepsilon}_y = \nu\dot{\varepsilon}_x \tag{22}$$

then from (12) we obtain

$$\dot{\varepsilon}_x = \frac{\lambda}{2}(\sigma_x - \sigma_z)\frac{1}{1 + \nu/2} \tag{23}$$

By comparing this with equation (18) we see γ and ν are related by

$$(1 - \gamma) = \frac{1}{1 + \nu/2} \text{ or } \gamma = \frac{\nu}{2 + \nu} \text{ or } \nu = \frac{2\gamma}{1 - \gamma} \tag{24}$$

Finally, then, from (24) and (21) we can write the strain rate as

$$\dot{\varepsilon}_x = (2A)^{-n}(\sigma_x - \sigma_z)^n \phi^{-1} \tag{25}$$

where

$$\phi^{-1} = (1 - \gamma)(1 + 3\gamma^2)^{(n-1)/2} \tag{26}$$

or

$$\phi = \left(1 + \frac{\nu}{2}\right)\left[1 + 3\left(\frac{\nu}{2 + \nu}\right)^2\right]^{(n-1)/2} \tag{27}$$

Hence, as analogous to equation (1) for two dimensions, where the lateral strain rate is zero, we now have for a lateral strain rate, which is ν times the longitudinal strain rate,

$$(\phi\dot{\varepsilon}_x) = (2A)^{-n}(\sigma_x - \sigma_z)^n \tag{28}$$

In other words, if a transverse strain $\dot{\varepsilon}_y = \nu\dot{\varepsilon}_x$ is present, we can incorporate its effect into the association of the longitudinal stress and strain simply by using $\phi^{1/n}\,\dot{\varepsilon}_x^{1/n}$ instead of $\dot{\varepsilon}_x^{1/n}$.

Tables of ϕ and $\phi^{1/n}$ for various values of ν and n are given below. These are illustrated in Figs. 5.1 and 5.2.

From the tables we can see that, for a flow law with $n = 3$ or 4, the presence of a lateral strain rate which is a small fraction of the longitudinal strain rate makes no appreciable difference. Even values of $\nu = +1, +2, +3$ only cause slight variations for large n values. For $n = 1$ or 2 the deviations become more significant.

When the lateral strain is of opposite sign, however, the deviations become very important. In particular for $\nu = -2$, we find that the longitudinal stress difference is zero. This may be easily seen from the continuity condition for an icompressible medium:

$$\dot{\varepsilon}_x + \dot{\varepsilon}_y + \dot{\varepsilon}_z = 0$$

and, if

$$\dot{\varepsilon}_y = -2\dot{\varepsilon}_x,$$

then

$$\dot{\varepsilon}_z = \dot{\varepsilon}_x,$$

i.e., the longitudinal strain rate can exist even with $\sigma_x - \sigma_z = 0$.

This means that, for $\nu = -2$, the longitudinal motion is being dominated by the lateral stress, which causes equal vertical and longitudinal strains simply to conserve volume. For greater negative values of ν (—3, —4 . . .) the longitudinal mean stress difference is of opposite sign to the longitudinal strain rate.

Finally, our general equation of motion for three dimensions may now be written as

$$\frac{\partial \overline{Z}\overline{B}(\phi\dot{\epsilon}_x)^{1/n}}{\partial x} = -\frac{1}{2}\rho g\overline{Z}(\bar{\alpha} - \bar{f}) + \frac{\rho g}{6}\frac{\partial^2 \alpha Z^3}{\partial x^2} \tag{29}$$

and we can relate the longitudinal slope α to the longitudinal strain rate $\dot{\epsilon}_x$ and include the effect of the transverse strain in ϕ. An examination of the consequences of this result for particular ice masses will be carried out in Section 6.

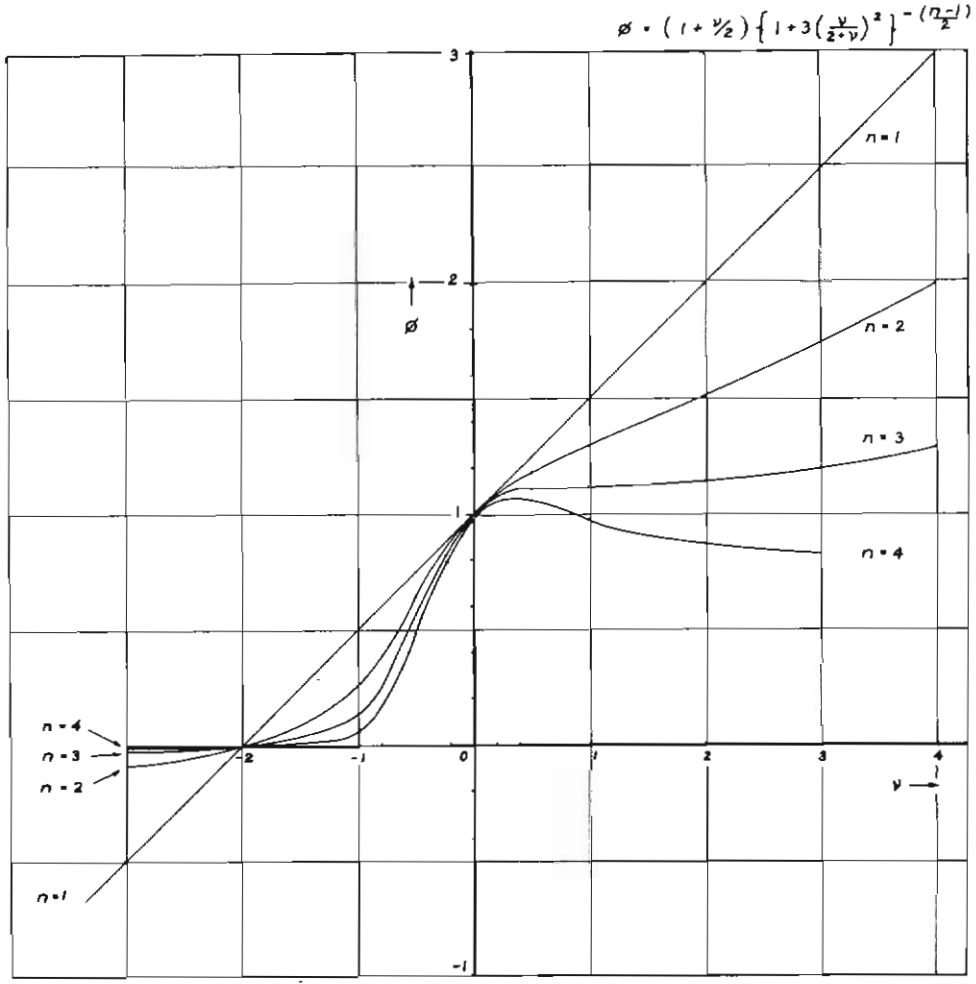

FIG. 5.1. Transverse strain function $\phi(\nu,n)$ where $\nu = \dot{\epsilon}_y/\dot{\epsilon}_x$, such that $\phi\dot{\epsilon}_x = (2A)^{-n}(\sigma_x - \sigma_z)^n$ is shown for different values of ν and n, in order to correct the two-dimension longitudinal strain rate ($\dot{\epsilon}_x$) results to three dimensions, where the transverse strain rate is $\dot{\epsilon}y$.

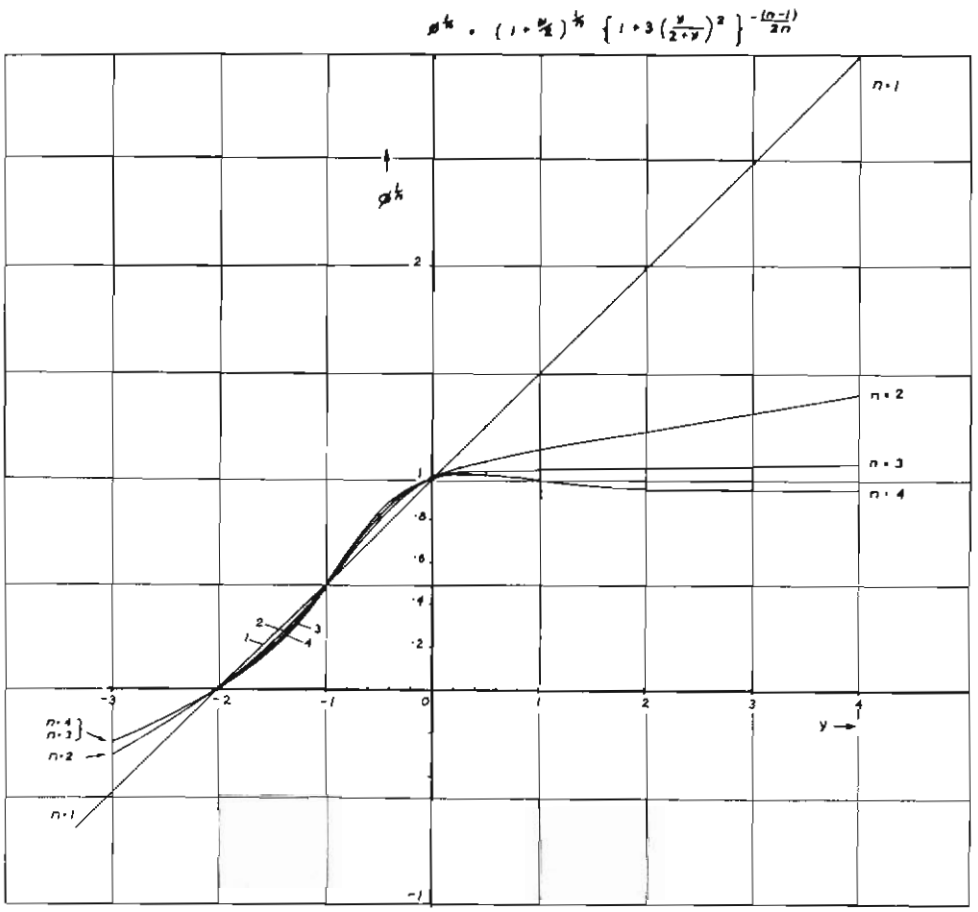

FIG. 5.2. Since the longitudinal strain rate equations involve $(\phi\varepsilon_z)^{1/n}$, the values of $\phi^{1/n}$ are shown against ν and n. For positive values of ν and high values of n there is little effect of the transverse strain on the longitudinal strain. For negative ν values, the transverse strain is very important.

TABLE 5.1.

$$\phi = \left(1 + \frac{\nu}{2}\right)\left\{1 + 3\left(\frac{\nu}{2 + \nu}\right)^2\right\}^{-(n-1)/2}.$$

ν \ n	1	2	3	4
4	3·000	1·990	1·290	
3	2·500	1·740	1·200	0·830
2	2·000	1·490	1·140	0·870
1	1·490	1·300	1·120	0·970
½	1·250	1·180	1·110	1·060
¼	1·120	1·110	1·100	1·060
0	1·000	1·000	1·000	1·000
−¼	0·876	0·853	0·825	0·808
−½	0·751	0·655	0·565	0·488
−1	0·500	0·250	0·125	0·063
−2	0	0	0	0
−3	−0·500	−0·095	−0·018	−0·005

TABLE 5.2.

$$\phi^{1/n} = \left(1 + \frac{\nu}{2}\right)^{1/n}\left\{1 + 3\left(\frac{\nu}{2+\nu}\right)^2\right\}^{-(n-1)/2n}.$$

ν \ n	1	2	3	4
4	3·000	1·410	1·090	0·950
3	2·500	1·320	1·060	0·950
2	2·000	1·220	1·050	0·960
1	1·490	1·140	1·040	0·990
½	1·250	1·080	1·030	1·010
¼	1·120	1·050	1·030	1·010
0	1·000	1·000	1·000	1·000
−¼	0·876	0·924	0·934	0·930
−½	0·751	0·810	0·823	0·835
−1	0·500	0·500	0·500	0·500
−2	0	0	0	0
−3	−0·500	−0·310	−0·260	−0·260

5.4 FLOW OF ICE OVER UNDULATIONS

5.4.1. *Short wavelength undulations*

Many examples have been reported of wave-like features on the surface of cold ice caps by Bentley (1964), Robinson (1966), Budd (1966), Robin (1967) and Mock (1967). The mechanics of waves on the surface of an ice mass have been discussed by Weertman (1958), and Nye (1958, 1959). The general theory of time-dependent waves is quite complex and will not be discussed here but, so far, in the present work the effect of irregularities in the bedrock has not been considered. This has been because the base slope β does not appear explicitly in the final equations for longitudinal strain rate. However, the equations derived for longitudinal velocity and strain rate can be used to study steady-state flow over bedrock undulations.

Consider non-diverging flow (two-dimensional) of an ice cap down a small steady slope β_0. In general, the bedrock is rough and irregular, but here we consider the flow over an undulating base given by

(1*)
$$\beta = \beta_0 + \beta_1 \cos \omega x \tag{1}$$

where β_0 is the regional slope, β_1 is the slope amplitude and ω is the frequency of the undulations along the line of motion x. It may be expected that real bedrock shapes can be approximated by sums of these forms of undulations with different amplitudes and frequencies.

Only the simplest form of steady-state flow is treated first, but several generalizations can be readily carried out, some of which will be given later.

(2*) We assume that the average regional ice thickness varies insignificantly over the undulations with the ice thickness gradient given by

$$\frac{\partial Z}{\partial x} = \alpha - \beta \tag{2}$$

where α is the surface slope.

(3*) It is assumed that the surface slope is given by

$$\alpha = \alpha_0 + \alpha_1 \cos \omega x + \alpha_2 \sin \omega x \tag{3}$$

where α_0 is the constant regional slope,

and α_1 and α_2 are constants to be determined.

(4*) It is assumed that the accumulation rate A is constant over the undulations.

(5*) We also assume that the variations in ice thickness Z, and the average horizontal velocity through the ice thickness V, are small compared to the regional values of thickness and velocity.

(6*) As a result of the last section for low strain rate, we take the strain rate gradient proportional to the surface-slope deviations from the regional slope, i.e., from equation 5.1 (29) viz.,

$$\frac{\partial \dot{\varepsilon}_x^{1/n}}{\partial x} = -\frac{\rho g}{2B}\left[(\alpha - \bar{\alpha}) + \left(\frac{2\pi}{\sqrt{3}}\frac{Z}{\lambda}\right)^2 (\alpha - \bar{\alpha})\right],$$

For low longitudinal strain rates, the results of Section 6 (cf. Fig. 6.7) suggest that we may take $n \simeq 1$

or

$$\frac{d\dot{\varepsilon}_x}{dx} = c(\alpha - \alpha_0)(1 + p^2) \tag{4}$$

where

$$c = -\frac{\rho g}{2B} \quad \text{and} \quad p = \frac{2\pi}{\sqrt{3}}\frac{Z}{\lambda}, \quad \lambda = \frac{2\pi}{\omega} \tag{5}$$

The continuity condition demands

$$\frac{d(VZ)}{dx} = A$$

$$V\frac{dZ}{dx} + Z\frac{dV}{dx} = A \tag{6}$$

From equations (1), (2) and (3)

$$\frac{dZ}{dx} = (\alpha_0 - \beta_0) + (\alpha_1 - \beta_1)\cos \omega x + \alpha_2 \sin \omega x \tag{7}$$

From equations (3) and (4)

$$\frac{d^2V}{dx^2} = c(1 + p^2)(\alpha_1 \cos \omega x + \alpha_2 \sin \omega x) \tag{8}$$

$$\therefore \quad \frac{dV}{dx} = \dot{\varepsilon}_0 + \frac{c(1 + p^2)}{\omega}(\alpha_1 \sin \omega x - \alpha_2 \cos \omega x) \tag{9}$$

since p may be considered constant provided $\alpha \ll \frac{2\pi Z}{\lambda}$.

Substituting (9) and (7) in (6) we see that assumption (3*) is compatible with (1*) and the steady-state continuity condition if

$$V(\alpha_0 - \beta_0) + Z\dot{\varepsilon}_0 = A \tag{10}$$

$$V(\alpha_1 - \beta_1) - \frac{Zc\alpha_2(1 + p^2)}{\omega} = 0 \tag{11}$$

$$V\alpha_2 + \frac{Zc\alpha_1(1 + p^2)}{\omega} = 0 \tag{12}$$

Equation (10) is simply the continuity equation for the regional (smoothed) values independent of the undulations. The remaining equations determine the surface undulations in terms of the basal undulations and the other parameters: ice thickness Z, velocity V, wavelength λ, and the "viscosity" parameter B.

From (12) we obtain

$$\alpha_2 = -\frac{Zc(1 + p^2)}{V\omega}\alpha_1 \tag{13}$$

and from (11)

$$\alpha_1 = \beta_1 + \frac{Zc(1 + p^2)}{V\omega}\alpha_2 \tag{14}$$

Substituting from (13) this becomes

$$\alpha_1 = \beta_1 - \psi^2\alpha_1,$$

$$\text{where} \quad \psi = \frac{Zc(1 + p^2)}{V\omega} \tag{15}$$

$$\therefore \qquad \alpha_1 = \frac{\beta_1}{1 + \psi^2} \tag{16}$$

From this and (13) we find for α_2

$$\alpha_2 = \frac{\psi\beta_1}{1 + \psi^2} \tag{17}$$

$$\simeq \frac{\beta_1}{\psi} \qquad \text{for} \qquad \psi \gg 1.$$

For $\psi > 1$, (16) and (17) show that the surface undulations are out of phase with the bedrock. For $\psi \gg 1$, the waves are $\frac{\pi}{2}$ out of phase and the maximum surface slope occurs over the highest point of the bedrock. This means that the surface *slopes* are in phase with the bedrock *elevations*. It is obvious from (16) and (17) that the surface waves are always smaller than the bedrock waves, i.e., damped by the factor ψ, which we may call the "damping factor".

Expressing ψ in full from (15) and (5)

$$\psi = \frac{Z^2\rho g}{VB4\pi}\left[\frac{\lambda}{Z} + \left(\frac{2\pi}{\sqrt{3}}\right)^2\frac{Z}{\lambda}\right] \tag{18}$$

This function has a minimum for the wavelength

$$\lambda_m = \frac{2\pi}{\sqrt{3}}Z \tag{19}$$

$$\simeq 3.63\,Z$$

This implies that bedrock undulations of wavelength about three to four times the ice thickness tend to be less damped out than other wavelengths. Table (5.3) below, however, shows that ψ is not a rapidly changing function of λ, especially

for larger values than λ_m. Shorter wavelengths appear to be rapidly damped out but the longer waves only slightly more damped. This gives rise to scope for harmonics, i.e., waves of $2\lambda_m$, $3\lambda_m$, or $4\lambda_m$ may also prevail, particularly where they are superimposed on the shorter waves.

TABLE 5.3.

WAVELENGTH FACTOR $\psi(\lambda) = \left[\frac{\lambda}{Z} + \left(\frac{2\pi}{\sqrt{3}}\right)^2 \frac{Z}{\lambda}\right]$

λ/z	$\frac{1}{4}$	$\frac{1}{2}$	1	2	4	8	16	32
$\psi(\lambda)$	53·3	26·9	14·2	8·6	7·3	9·7	16·8	32·3
$\psi/(\gamma)\psi(\lambda_m)$	7·31	3·69	1·95	1·18	1·002	1·33	2·30	4·32
$\psi(\lambda_m)/\psi(\lambda)$	0·136	0·270	0·513	0·846	0·998	0·750	0·445	0·232

From equations (17) and (18) it is apparent that increased iee thickness causes greater damping of the undulations. For other effects held constant, there is less damping for higher velocities and also higher "viscosity" parameters B. It is possible to estimate B from the relative amplitudes of the bedrock and surface undulations as follows:

$$B \simeq \frac{\alpha_2}{\beta_1} \frac{Z^2 \rho g}{V 4\pi} \left[\frac{\lambda}{Z} + \left(\frac{2\pi}{\sqrt{3}}\right)^2 \frac{Z}{\lambda}\right] \tag{20}$$

An estimate of the order of magnitude of the damping may be obtained by recalling from equation 5.1 (40)

$$\frac{V}{Z} = \frac{2}{n+1} \left(\frac{\rho g}{\overline{B}_n} \alpha Z\right)^n \tag{21}$$

For $n = 1$

$$V = \frac{\rho g Z^2 \alpha}{\overline{B}},$$

or

$$\frac{\rho g Z^2}{V \overline{B}} = \frac{1}{\alpha}$$

If we denote by $\overline{B}_1$ the value of $\overline{B}_n$ of (21) converted to the units with $n = 1$ by means of the general equation (cf. Budd 1966)

$$\left(\frac{B_1}{\tau}\right)^{n_1} = \left(\frac{B_2}{\tau}\right)^{n_2} \tag{22}$$

then (21) may be written

$$\frac{\rho g Z^2}{V} = \frac{\overline{B}_1}{\alpha}.$$

Hence, from (18) ψ becomes

$$\psi = \frac{\overline{B}_1}{\alpha_0 B 4\pi} \left[\left(\frac{\lambda}{Z} + \left(\frac{2\pi}{\sqrt{3}}\right)^2 \frac{Z}{\lambda}\right]\right. \tag{23}$$

Here α_0 is the regional slope and typical values range from 10^{-3} to 10^{-1}. The value of B in the denominator is the value from equations (4) and (5) appropriate for

the longitudinal strain through the whole ice thickness. The value B_1 in the numerator is effectively the value in the basal layers and (in units with $n = 1$) may be an order of magnitude smaller because of the higher temperatures there. Hence, we may expect typical damping from 2 to 100 times decreasing towards the coast as the average surface slope increases. The damping factors from the bedrock and surface undulations for the Wilkes ice cap will be discussed in Section 6.3.5. and used to calculate the flow parameter B.

Extensions to three-dimensional bedrock perturbations may be estimated by introducing the transverse strain factor ϕ of equation 5.4 (28) and generalizing the continuity equation. The net result for an equal transverse strain rate is an increased damping by a factor of 4/3 for low strain rates ($n = 1$). Across the line of flow the surface and bedrock undulations are in phase. Hence, for directions between the line of flow and across the line of flow, the phase difference between surface slope and bedrock elevation varies from 0 to $-\frac{\pi}{2}$.

Similarly, the above analysis can be extended to the case of variable accumulation rate over the undulations, as was found to be the case by Black and Budd (1963). In this case we may write

$$A = A_0 + A_1 \cos \omega x + A_2 \sin \omega t.$$

In this case we obtain, instead of (16) and (17),

$$\alpha_1 = \frac{\beta_1 + \psi A_2/V - A_1/V}{1 + \psi^2} \tag{16'}$$

$$\alpha_2 = \frac{\psi\beta_1 + \psi^2 A_2/V - \psi A_1/V}{1 + \psi^2} - \frac{A_2}{V} \tag{17'}$$

For $\psi \gg 1$ $\alpha_2 \simeq \frac{\beta_1}{\psi} - \frac{A_1}{\psi V}$, and $\alpha_1 \simeq \frac{A_2}{\psi V}$.

From this, it appears that for large ψ—resulting from large strain rates, or small B—the accumulation variation is not very significant. Black and Budd (1963) found that accumulation maxima tended to occur near the positions of minimum surface slope (downhill). This effect becomes important for small ψ (or large B causing small strain rates). Putting $\psi \to 0$ in (16') and (17') gives

$$\alpha_1 = \beta_1 - \frac{A_1}{V} \tag{16''}$$

and

$$\alpha_2 = -\frac{A_2}{V} \tag{17''}$$

showing that, for low strain rate, the accumulation pattern can become very important in determining the steady-state surface configuration.

5.4.2. *Long wavelength undulations*

On the larger scale, taking smooth values over $\simeq 20$ times the ice thickness, then instead of equation (4) the relevant relation for velocity V, ice thickness Z

and surface slope α may be taken from 5.1 (40) as

$$V = k\alpha^n Z^{n+1} \tag{18}$$

where $k = \dfrac{2}{n_2 + 1}\left(\dfrac{\rho g}{B_2}\right)^{n_2}$

and $n_2 \simeq 3$

and k may be taken as constant, provided the temperatures change insignificantly over the distances involved.

Similarly to the analysis in Section 5.4.1, take

$$\frac{dVZ}{dx} = A \tag{19}$$

$$\left.\begin{aligned} \frac{dZ}{dx} &= \alpha - \beta \\ \beta &= \beta_0 + \beta_1 \cos \omega x \\ \alpha &= \alpha_0 + \alpha_1 \cos \omega x + \alpha_2 \sin \omega x \end{aligned}\right\} \tag{20}$$

Then the substitution of equations (20) in (19) leads to the results

$$\alpha_1 = \frac{\beta_1}{1 + \psi_2^2} \tag{21}$$

$$\alpha_2 = \frac{\psi_2 \beta_1}{1 + \psi_2^2} \tag{22}$$

As before, the surface and base undulations are out of phase by $\pi/2$.
In this case the damping factor ψ_2 is given by

$$\psi_2 = \frac{n}{n + 2} \frac{2\pi Z}{\bar{\alpha}\lambda} \tag{23}$$

This result implies that the damping increases with ice thickness, decreases with increasing wavelength and is inversely proportional to the surface slope. The following table indicates the magnitudes involved, for $n = 3$.

TABLE 5.4

LARGE SCALE DAMPING FACTOR ψ_2

λ/Z \ α	1/10	1/30	1/100	1/300	1/1000
10	3·80	11·0	38·0	110	380
30	1·10	3·8	11·0	38	110
100	0·38	1·1	3·8	11	38

For a more general form of bedrock variation we substitute equations (18) and (20) into (19) to obtain

$$kVZ\left[\frac{n}{\alpha}\frac{d\alpha}{dx} + \frac{n+2}{Z}(\alpha - \beta)\right] = A \tag{24}$$

or

$$\frac{1}{\alpha^2}\frac{d\alpha}{dx} - \frac{1}{\alpha}\left(\frac{n+2}{nZ}\beta - \frac{A}{nkVZ}\right) = \frac{n+2}{nZ} \tag{25}$$

Now, if it is assumed that the variations in Z and V are small compared to their average values over the region, then this equation can be written as

$$\frac{dy}{dx} + \left(p\frac{\beta}{Z} - q\right)y = r \tag{26}$$

where $y = \frac{1}{\alpha}$ and p, q and r are constants. This equation may then be integrated to give

$$\alpha = \alpha_0 e^{p\,b/Z - qx} + \frac{e^{p\,b/Z - qx}}{\int_0^x e^{p\,b/Z - qx}\,dx} \tag{27}$$

where b is the bedrock elevation above that at $x = 0$. The full import of this equation will not be discussed here but, by considering an undulating bedrock profile of the form $b = b_0 + b_1 \cos \omega x$, it can be shown that equation (27) implies a slightly more cusped surface than a regular sine wave, i.e., it has shorter peaks and longer valleys.

5.4.3. *Distance scales relevant to long and short wave undulations*

On the large scale for smoothed values of velocity V, slope and ice thickness Z we have equation 5.4.1. (21)

$$V = \frac{2Z^{n+1}}{n+1}\left(\frac{\rho g \bar{\alpha}}{B_2}\right)^n \tag{28}$$

For small-scale undulations, where the strain rates are so small that the stress and strain rate are linearly related ($n = 1$), we have, from equation 5.4 (4),

$$\frac{\partial \dot{\varepsilon}_x}{\partial x} = \frac{\rho g}{2B_1}(\alpha - \bar{\alpha})(1 + p^2) \tag{29}$$

where $\bar{\alpha}$ is the average regional slope. We are here concerned with finding the distance over which the $\bar{\alpha}$ of (28) and (29) needs to be smoothed. For the longer waves p can be neglected.

As the wave length λ of the undulations increases, these two relations will interact and equation (29) will be gradually replaced by (28), i.e., as

$$\lambda \to \lambda_T \quad \lambda\alpha \to \bar{\alpha} \quad \frac{\partial \dot{\varepsilon}_x}{\partial_x} \to \sim 0 \quad V \to \frac{2Z^{n+1}}{n+1}\left(\frac{\rho g \bar{\alpha}}{B_2}\right)^n$$

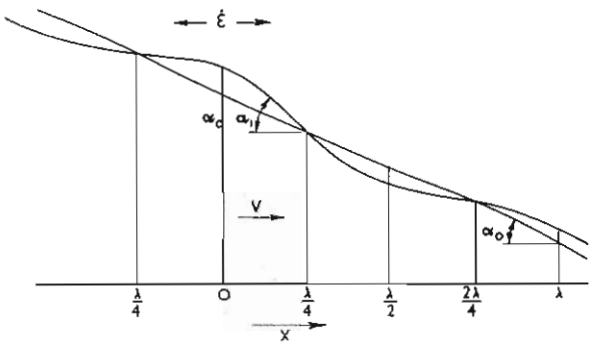

This merging will occur when the velocity increase, from the crest of a wave to the point of maximum slope due to the strain rate by (29), equals the increase in velocity over this interval due to the increase in slope from (28),
i.e.,

$$\int_0^{\lambda/4} \frac{dV}{dx}\,dx \text{ are equal from equations (28) and (29).}$$

We assume that the slope of the undulations is given by

$$\alpha = \bar{\alpha} + \alpha_1 \cos \omega x \tag{30}$$

where $\omega = \dfrac{2\pi}{\lambda}$.

From (28) for the smoothed slope relation

$$\begin{aligned}\int_0^{\lambda/4} \frac{dV}{dx}\,dx &= \frac{2Z^{n+1}}{n+1}\left(\frac{\rho g}{B_2}\right)^n \alpha^n \Big|_{\bar{\alpha}}^{-\alpha+\alpha_1} \\ &= \frac{2Z^{n+1}}{n+1}\left(\frac{\rho g}{B_2}\right)^n [(\bar{\alpha}+\alpha_1)^n - \bar{\alpha}^n] \\ &= \frac{2Z^{n+1}}{n+1}\left(\frac{\rho g \alpha_1}{B_2}\right)^n \chi_n \end{aligned} \tag{31}$$

where $\chi_n(y) = (y+1)^n - y^n \qquad \left(y = \dfrac{\bar{\alpha}}{\alpha_1}\right)$ (32)

From (29) and (30) for the short-wave undulations

$$\int_0^{\lambda/4} \frac{dV}{dx}\,dx = \frac{\rho g \alpha_1}{2B_1\omega^2} \sin \omega x \Big|_0^{\lambda/4} = \frac{\rho g \alpha_1}{2B_1\omega^2} \tag{33}$$

Equating (31) and (33),

$$\frac{\rho g \alpha_1}{2B_1\omega^2} = \frac{2Z^{n+1}}{n+1}\left(\frac{\rho g \alpha_1}{B_2}\right)^n \chi.$$

Now B_1 and B_2 are in units of bars sec and bars $\sec^{\frac{1}{n}}$ respecively.
i.e.,

$$\frac{\rho g Z \alpha_1}{B_1} = \left(\frac{\rho g Z \alpha_1}{B_2}\right)^n,$$

provided $B_1 = B_2$ when converted to the same units, B_c for the column, say, and B_b for the base when $n = 1$. For the case in which they are not equal, as is generally true for typical temperature profiles existing in cold ice caps where $B_c > B_b$, we write

$$\nu = \frac{B_c}{B_b}.$$

Then

$$\frac{1}{2\omega^2} = \frac{2Z^2}{n+1}\chi/\nu \tag{34}$$

Therefore, the transition wavelength is given by

$$\lambda_T = 4\pi Z \sqrt{\frac{\chi}{(n+1)\nu}} \tag{35}$$

For the Wilkes ice cap it is shown in Section 6.3 that $\nu \simeq 4$.

Tables of $\chi_n^{\frac{1}{2}}$ and $\sqrt{\chi/(n+1)}$, $4\pi\sqrt{\chi/(n+1)}$, and $4\pi\sqrt{\chi/(n+1)\nu}$ with ν 4, are given below. For the Wilkes ice cap it was found that $n \simeq 3.4$ and typically $\bar{\alpha}/\alpha_1 \simeq 4$. Hence it can be seen from the table for $\lambda_T/Z = 4\pi\sqrt{\chi_n/(n+1)\nu}$ that the transition wavelength is about 30 times the ice thickness, for this region.

The results of this section indicate that, to avoid discrepancies in the smoothed velocity—slope equation (28), it is necessary to average over distance greater than λ_T. On the other hand, we may expect the equation for the strain and slope fluctuations

$$\frac{\partial \varepsilon}{\partial x} = -\frac{\rho g}{2B}(\alpha - \bar{\alpha})$$

to hold only for $\bar{\alpha}$ taken as smoothed over distance greater than λ_T and slope fluctuations over distances shorter than λ_T.

In Section 6 we next examine the application of the theory developed in this section to measurements on existing ice masses.

TABLE 5.5

TRANSITION WAVELENGTH λ_T

$$\chi_n^{\frac{1}{2}} = \sqrt{(y+1)^n - y^n} \qquad \sqrt{\frac{\chi_n}{n+1}}$$

y	n	1	2	3	4	n	1	2	3	4
0		1	1·00	1·00	1·00		0·71	0·58	0·50	0·45
¼		1	1·22	1·39	1·56		0·71	0·70	0·70	0·70
½		1	1·41	1·80	2·24		0·71	0·81	0·90	1·00
1		1	1·73	2·65	3·87		0·71	1·00	1·33	1·73
2		1	2·24	4·36	8·06		0·71	1·30	2·18	3·60
4		1	3·00	7·80	19·20		0·71	1·73	3·90	8·60

$$4\pi\sqrt{\frac{\chi}{n+1}} \qquad \lambda_T/Z = 4\pi\sqrt{\frac{\chi}{(n+1)\nu}}$$

0	8·9	7·3	6·3	5·7	4·45	3·65	3·15	2·85
¼	8·9	8·8	8·8	8·8	4·45	4·40	4·40	4·40
½	8·9	10·2	11·3	12·6	4·45	5·10	5·65	6·30
1	8·9	12·6	16·7	21·8	4·45	6·30	8·35	10·90
2	8·9	16·3	27·4	45·2	4·45	8·15	13·70	22·60
4	8·9	21·8	49·0	109·0	4·45	10·90	24·50	54.50
8	8·9	30·0	91·2	278·0	4·45	15·00	45·60	139·00

$$y = \frac{\bar{\alpha}}{\alpha_1} \qquad \nu = \frac{B_c}{B_b}$$

$$\chi_n(y) = (y+1)^n - y^n$$

6. APPLICATION OF DYNAMICS THEORY TO DIFFERENT TYPES OF ICE MASSES

In this section the theory developed in the earlier sections will be applied to the three major types of ice masses: ice shelves, glaciers, and ice caps. The scope of the application of the theory to the analysis of measurements on ice masses is very broad but space here prohibits more than a brief outline of two main avenues of investigation. As more detailed measurements become avalaible more refined testing of the theory will be possible. The two major aims here are to

(i) determine longitudinal velocity profiles from the ice mass boundary dimensions and an assumed flow law, and

(ii) determine flow law parameters from the ice mass boundary dimensions and measured velocity and strain rates along a flow line.

6.1. ICE SHELVES

6.1.1. *General equations of motion for determining flow parameters*

The general dynamics theory of Section 5 has been applied to the Amery Ice Shelf by Budd (1966) where it is shown how the theory can be used to determine the flow parameters of the ice from measurements of velocity and strain rate, together with the elevation profile, along the centre-line of the ice shelf.

The main principles of this application are outlined below. If, as for many ice shelves, the range of stress is comparatively small (0 — 3/4 bars) the B, n notation for the power law for ice flow can be used and average values over that range can be obtained. Having determined the n and B values it is then possible to calculate the velocity distribution throughout the rest of the ice shelf.

We consider the general equation for the longitudinal strain rate $\dot{\varepsilon}_x$ at distance x along the centre-line of the ice shelf [cf. Section 5, equations 5.1 (31a), 5.2 (17), 5.3 (29)], where the term $\iint \frac{\partial^2 \tau_{xz}}{\partial x^2}\, dz\, dz$ is neglected, since here we are not considering short-wave slope fluctuations but rather averages over long distances,

$$\frac{\partial \overline{B}(\phi \dot{\varepsilon}_x)^{1/n}}{\partial x} = -\frac{1}{2}\overline{\rho} g(\alpha - f) \tag{1}$$

where $\overline{B}$ is the average value of the flow parameter through the ice thickness,
ϕ is the transverse strain function [cf. Section 5, equation (27)],
α is the longitudinal surface slope averaged across the ice shelf at x, and
f is the "friction coefficient" of the boundary defined by

$$f = \frac{p\tau_b}{sA\rho g} \tag{2}$$

where τ_b is the boundary shear stress,

p/A is the ratio of the cross-section boundary perimeter to the area, and

s is an appropriate shape factor for the cross-section. For an ice shelf the shape factor s for the transverse velocity profile is unity, as for the infinitely deep channel, because there is no shear stress at the base.

Let σ_x be the longitudinal stress and τ_{xy} the transverse shear stress at position x along the ice shelf and distance y from the centre line. We first assume $\frac{\partial \sigma_x}{\partial x}$ is independent of y. Equilibrium for a central element then gives

$$\tau_{xy} = y \frac{\partial \sigma_x}{\partial x}.$$

Hence, for a power law for flow with parameters n and B, the velocity gradient across the ice shelf is given by

$$\frac{1}{2}\frac{dV}{dy} = B^{-n} y^n \left(\frac{\partial \sigma_x}{\partial x}\right)^n.$$

If the half width of the ice shelf is a, then the velocity in the centre V is given by (cf. Section 3.4.1.)

$$V = \frac{2a^{n+1}}{(n+1)B^n}\left(\frac{d\sigma_x}{dx}\right)^n \tag{3}$$

The shear stress at the edge is given by

$$\tau_b = a \frac{d\sigma_x}{dx} \tag{4}$$

From equation (3), this may be written

$$\tau_b = B\left[\frac{n+1}{2}\frac{V}{a}\right]^{1/n} \tag{5}$$

This value of τ_b may now be substituted in equations (2) and (1) to give (noting $p/A = 1/a$ for such an ice shelf)

$$-\frac{\partial B(\phi \dot{\varepsilon}_x)^{1/n}}{\partial x} = \frac{1}{2}\rho g \alpha - \frac{B}{2a}\left[\frac{n+1}{2}\frac{V}{a}\right]^{1/n} \tag{6}$$

Hence, if in addition to the dimensions of the ice shelf the flow parameters, n and B, are known as well as some boundary values of velocity and strain rate, then this equation can be solved iteratively to give the velocity and strain rate along the central flow line. [Note that a correction is made here to Budd (1966) equation (7) in that the surface slope α is used instead of the thickness gradient $-\frac{\partial H}{\partial x}$, which is only applicable for base slope $\beta = 0$.]

On the other hand, if the velocity along the central flow line is known, equation (6) enables the flow parameters to be calculated. Generally, the values n and B have to be obtained by numerical solutions of equation (6), except where special forms of the boundary conditions allow simplifications to be made. These special cases will now be examined.

6.1.2. *Special cases of velocity distribution*

In three special cases Budd (1966) showed that analytical solutions are obtainable. We consider the case of an ice shelf bounded at its sides where the width ($2a$), the flow parameters n and B, and the transverse strain factor ϕ change only slowly along the ice shelf.

For the following context we reverse the direction of the axis x, i.e., we take x horizontal along the centre line directed inwards from the seaward front.

Equation (6) may be written

$$-\frac{d}{dx}\left(\frac{dV}{dx}\right)^{1/n} = \frac{1}{n}\left(\frac{dV}{dx}\right)^{1/n-1}\frac{d^2V}{dx^2} = \frac{\rho g\alpha}{2\phi^{1/n}B} - \frac{1}{2a}\left(\frac{n+1}{2\varphi a}V\right)^{1/n}$$

I. Flat ice shelf ($\alpha \to 0$).

In this case, equation (6) reduces to

$$\frac{d^2V}{dx^2} = \mu\left(\frac{dV}{dx}\right)^{1-1/n}V^{1/n} \tag{7}$$

where

$$\mu = \frac{n}{2a}\left(\frac{n+1}{2\phi a}\right)^{1/n} \tag{8}$$

This has the solution for the particular case of $V = 0$, when $\frac{dV}{dx} = 0$, of

$$V = V_0 e^{-\lambda x} \tag{9}$$

$$\frac{dV}{dx} = -\lambda V_0 e^{-\lambda x} = -\lambda V \tag{10}$$

where

$$\lambda = \mu^{n/(n+1)} = n^{n/(n+1)}\left(\frac{n+1}{\phi}\right)^{1/(n+1)}\frac{1}{2a} \tag{11}$$

and V_0 is the velocity at the front of the ice shelf where $x = 0$. This result implies that both the velocity and longitudinal strain rate in a flat ice shelf decrease exponentially going inland from the front, with rate of decrease depending on the index n, the ice shelf width and the transverse strain rate.

In the more general case when $V = V_0$, when $\frac{dV}{dx} = 0$, the integration is more difficult, but we find the following relation between the longitudinal strain rate and velocity

$$\left(\frac{dV}{dx}\right)^{1+1/n} = -\mu\left[V^{1+1/n} - V_0^{1+1/n}\right].$$

This may also be used to determine the n value from the measured velocity profile along the centre line.

II. For constant viscosity ($n = 1$).

We have $n = 1$ in equation (6)

$$\frac{d^2V}{dx^2} - \frac{V}{2a^2} = -\frac{\rho g}{4B}\alpha \tag{12}$$

In this case. we have for constant surface slope α, and the condition

$$V = \frac{\rho g a^2 \alpha}{2B}, \text{ when } \frac{dV}{dx} = 0, \quad V = V_0 e^{-\lambda x} + \frac{\rho g a^2}{2B}\alpha \tag{13}$$

and we see that the resultant velocity is simply the sum of the velocities due to creep and the pressure gradient acting independently.

Here again the velocity and velocity gradient decrease exponentially going inland from the front until the strain rate is zero, when $V = \frac{\rho g a^2 \alpha}{2B}$, as expected for normal viscous flow with no longitudinal strain. In this case the exponential decrease is governed by $\lambda x = \frac{1}{\sqrt{2\phi}}\frac{x}{a}$ and depends on the ice-shelf width.

III. For a comparatively flat ice shelf, where the slope varies slowly along the centre-line, the following approximate solution may be used.

We write the total velocity at position x as

$$V = V_I + V_c \tag{14}$$

where V_I is the velocity due to the pressure gradient alone, and V_c is the velocity gradient due to varying creep.
Now, if

$$V_c = \beta V_I \tag{15}$$

then, for the region towards the front of the ice shelf, where β only changes slowly along the ice, we obtain the equation

$$\frac{d^2V}{dx^2} = \mu' \left(\frac{dV}{dx}\right)^{1-1/n} V^{1/n} \tag{16}$$

where

$$\mu' = \mu \left[\frac{(\beta + 1)^{1/n} - 1}{\beta^{1/n}}\right] \tag{17}$$

The solution may now be written as

$$V = \frac{\rho g a^2}{2B} + V_0 e^{-\psi(n)x/a} \tag{18}$$

where

$$\psi(n) = \frac{n(n+1)^{1/n}}{\phi^{1/(n+1)} 2^{(n+1)/n}} \left[\frac{(\beta + 1)^{1/n} - 1}{\beta^{1/n}}\right]^{n/(n+1)} \tag{19}$$

This function is plotted in Budd (1966, Fig. 10, where the function ψ is called ϕ) for the transverse strain factor $\phi = 1$.

An exact solution for strain rate $\frac{dV}{dx}$ in terms of velocity V in this case is

$$\left(\frac{dV}{dx}\right)^{1+1/n} = \frac{(1+n)\rho g \alpha}{2\phi^{1/n} B}(V - V_0) - \frac{n}{2a}\left(\frac{n+1}{2\ a}\right)^{1/n} [V^{1+1/n} - V_0^{1+1/n}],$$

where $V = V_0$, when $\frac{dV}{dx} = 0$.

Now, if the parameters α, B, a, only vary slowly with x, then the values of n can be obtained from the second term on the right of equation (18) which governs the exponential decrease of velocity going inland from the front. Far inland this term decreases to zero. The value of B can then be readily determined from the velocity, slope, thickness and width of the ice shelf. By examining equation (18) numerically for the Amery Ice Shelf, a value of $n = 2$ was found by Budd (1966). After applying the correction for basal slope, noted previously, the value of B is determined as

$$B = \cdot 63 \times 10^9 \text{ dyne cm}^{-2} \text{ sec}^{1/3}.$$

This value appears to be somewhat lower than the value expected ($\simeq 1 \cdot 3 \times 10^9$) from the flow law (cf. Fig. 2.2 at $-16°$C, the mean temperature calculated for this region of the ice shelf). The low B value may reflect the lower density of the ice-shelf ice ($\rho \simeq 0 \cdot 85$ g cm^{-3}) which, from Section 2.5.1. could cause the value of B (in these units) to be lower by about a factor of $1 \cdot 6$. However, in view of the inaccuracies in the preliminary data available for the Amery Ice Shelf, more exact agreement cannot be expected at this stage. Phase II of the Amery Ice Shelf project now in operation (1968) aims at providing sufficient data for a complete analysis by measuring the ice thickness and velocity distributions in detail and by core drilling to supply the information on the temperature and density profiles with depth.

6.2. GLACIERS

6.2.1. *General equations of motion*

To examine the longitudinal velocity along a glacier, first with parallel sides where, at distance x along the centre-line the cross-section area is A, the mean thickness is $\bar{Z}$, the basal slope is β, and the mean boundary friction co-efficient is $\bar{f}$, we consider equations 5.2 (12) and (13), neglecting for the moment the final term on the right of equation (12), according to Section 5.1:

$$\frac{\partial A B \dot{\varepsilon}_x^{1/n}}{\partial x} = -\frac{1}{2}\rho g \left[\frac{\partial \frac{1}{2}\bar{Z}A}{\partial x} - A(\beta - \bar{f})\right] \tag{20}$$

In practice, for most glaciers the cross-sectional shape only varies slowly with x. Then the main factor influencing the velocity, as the cross-section area changes, is just the mean thickness $\bar{Z}$. Thus, if we write

$$A = \bar{Z}\bar{Y} \tag{21}$$

and if the mean width $\bar{Y}$ only changes slowly with x, then we may adopt the simpler equation 5.2 (17), analogous to the two-dimensions equation

$$-\frac{\partial \bar{Z} B \dot{\bar{\varepsilon}}^{1/n}}{\partial x} = \frac{1}{2}\rho g \bar{Z}(\bar{\alpha} - \bar{f}) = \frac{1}{2}\rho g \overline{Z\alpha} - \frac{p\bar{Z}}{2A}\tau_b \tag{22}$$

with the generalization that the parameters with bars represent means over the cross-section, and τ_b is defined by equation 5.2 (5), and

$$f = \frac{p\tau_b}{A\rho g} \tag{23}$$

Along the centre-line we can express the velocity difference $(V_s - V_b)$ between the surface and the base in terms of τ_b by using $\tau_{xz} = s_2\rho g\alpha z$ and the flow law, and integrating from 0 to Z, the thickness in the centre.

$$s_2\rho g\bar{\alpha}\bar{Z} = B\left[\frac{n+1}{2}\frac{V_s - V_b}{Z}\right]^{1/n} \tag{24}$$

Here s_2 is a shape factor for the particular cross-section, which can be estimated empirically from Nye's calculations, as outlined in Section 2.

By introducing another shape factor defined by $\frac{1}{s} = \frac{s_2\rho g\bar{\alpha}Z}{\tau_b}\frac{p\bar{Z}}{A}$ we can write

$$\frac{p\bar{Z}}{2A}\tau_b = \frac{B}{2s}\left[\frac{n+1}{2}\frac{V_s - V_b}{Z}\right]^{1/n},$$

so that from (22) the final equation becomes

$$-\frac{\partial\bar{Z}B\dot{\varepsilon}_x^{1/n}}{\partial x} = \frac{1}{2}\rho g\bar{Z}\bar{\alpha} - \frac{B}{2s}\left[\frac{n+1}{2}\frac{V_s - V_b}{Z}\right]^{1/n} \tag{25}$$

The basal velocity is a difficult parameter to obtain. Although several theories have been presented on glacier-sliding, viz., Weertman (1957a, 1964, 1967), Lliboutry (1959, 1965, 1968), the confirmation of these is far from satisfactory (cf. Meier 1968). The empirical measurements to date of glacier-sliding are also inadequate. Measurements of horizontal velocity from vertical boreholes have been limited so far to the depth at which the thermal drill stops. This leaves as unknown the very interesting transition zone at the base of a glacier—which may be a sharp ice rock interface or include sand, moraine, or a mixture of ice and rock. In general, it will be difficult to distinguish between pure sliding, high shear in basal ice, or a combination of high shear and sliding, in a basal layer of an ice-rock mixture. In the present work it is proposed to calculate the effects of differential motion first. This then allows the sliding motion to be analysed by reference to the theories of basal sliding.

If we have no slip at the base, equation (25) becomes (dropping the bars)

$$-\frac{\partial ZB\dot{\varepsilon}^{1/n}}{\partial x} = \frac{1}{2}\rho gZ\alpha - \frac{B}{2s}\left(\frac{n+1}{2}\frac{V}{Z}\right)^{1/n}. \tag{26}$$

This, then, is the fundamental equation for the centre-line longitudinal velocity and velocity gradient in a glacier as a function of the ice thickness, surface slope, shape of cross-section and the flow law parameters of the ice. If the glacier is widening or narrowing, such that the transverse extension or compression is appreciable, then instead of $\dot{\varepsilon}_x$ we use (cf. Section 5.3)

$$\dot{\varepsilon}_x{}^* = \phi\dot{\varepsilon}_x \tag{27}$$

where

$$\phi = \left(1 + \frac{\nu}{2}\right)\left[1 + 3\left(\frac{\nu}{2+\nu}\right)^2\right]^{-(n-1)/2} \tag{28}$$

and ν is the ratio of the lateral to the longitudinal strain rates.

We also note that the n and B values on the left-hand-side and right-hand-side of equation (26) will in general be different because of the different stress ranges

involved. Since the shear at the base may be $\simeq 1$ bar, the longitudinal strain rate would have to be $\simeq \frac{1}{10}\text{yr}^{-1}$ to give comparable values of n and B. Since, in typical glaciers of small slope, mean longitudinal strain rates $> 1{:}30\ \text{yr}^{-1}$ are unusual in undisturbed regions, we may expect lower values of n for the left-hand-side.

Equation (26) can be used as follows:

(i) given the dimensions of an ice mass and the ice flow law parameters to determine its velocity distribution,

(ii) given the ice mass dimensions and its velocity distribution to determine the appropriate flow law parameters.

Since the flow law parameters for naturally deforming ice are still not well known, we examine (ii).

6.2.2. *Observed relation between velocity and slope (smoothed)*

We look at a typical glacier (Athabasca Glacier in Alberta, Canada) that has been measured in detail for ice thickness, slope, cross-section shape and centre-line

TABLE 6.1.

PHYSICAL PARAMETERS OF THE ATHABASCA GLACIER

Stake position L No.	Distance x m	Elevation h m	Slope $\alpha°$	Longitudinal strain rate $-\dot{\varepsilon}_x$ 10^{-3}yr^{-1}	Ice thickness Z m	$\overline{Z_{11}}$ m	$\bar{\alpha}_{10}°$ $\times 10^2$
10	0	458	4·5		310		450
11	82	452	4·0	103	318		376
12	180	447	2·8	74	323		344
13	279	442	2·8	42	320		356
14	380	437	3·1	34	317	317	371
15	477	431	3·6	23	320	316	350
16	618	422	4·1	22	322	316	325
17	761	412	4·3	21	314	313	308
18	910	401	4·2	19	312	309	308
19	1046	392	3·2	22	310	303	312
20	1199	386	1·9	18	310	397	318
21	1362	381	1·7	7	310	290	324
22	1517	376	2·2	1	290	284	334
23	1669	369	2·8	4	273	276	351
24	1811	362	3·2	3	260	264	371
25	1951	353	3·8	1	248	251	395
26	2042	348	4·2	—1	248	237	418
27	2115	342	5·2	2	248	242	448
28	2211	331	6·2	—3	225	221	490
29	2354	315	6·4	7	186	207	543
30	2431	296	5·9	18	170	293	603
31	2711	281	4·4	9	155	178	657
32	2859	270	5·0	4	118	162	752
33	2954	262	6·8	2	115	145	897
34	3049	250	8·6	6	113	129	1132
35	3130	237	9·8	14	100	97	1246
36	3321	206	9·8	17	90	85	1466
37	3450	180	14·6	16	73		1745
38	2560	144	21·2	31	56		2260
39	3603	131	23·0	—10	43		3200

velocity [Paterson and Savage (1963a,b,c), Kanasewich (1963) and Paterson (unpublished)]. Some of these parameters for this glacier are illustrated below, in Fig. 6.1, and also Fig. 3.5, for the cross-section profiles.

We notice the fluctuations in slope and strain rate over a comparatively short distance (0·5 to 1·2 km), which suggest that the basal friction $\bar{f}$ follows the smoothed

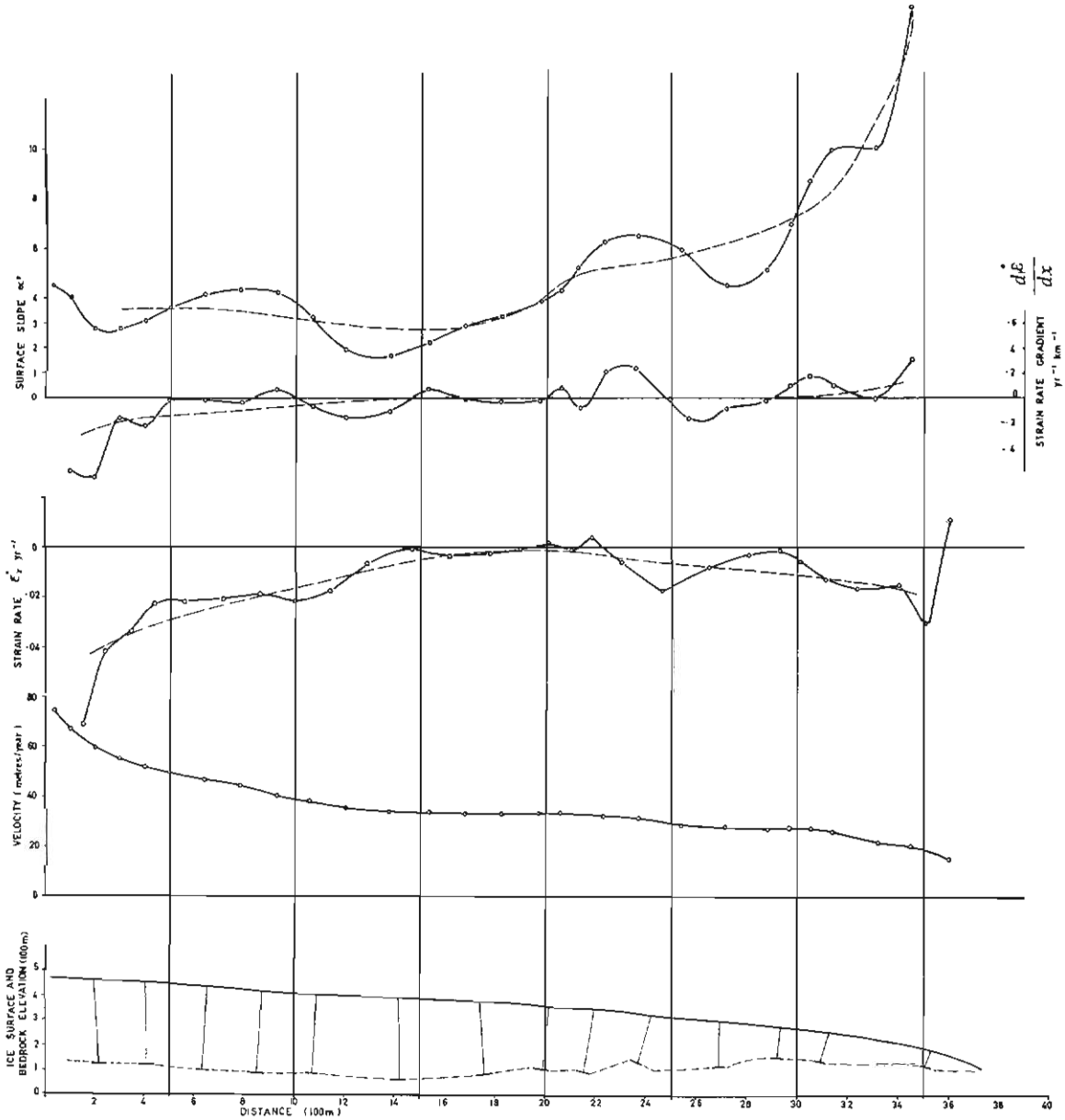

FIG. 6.1. Longitudinal profile of the Athabasca Glacier showing elevation and bedrock, velocity, strain rate, strain-rate gradient, and surface slope. Smoothed 1200 m running means are shown by the fine broken lines. Data from Paterson (unpublished).

surface slope (over 1200 m). Hence, we first examine the relation for smoothed velocity V, thickness Z, and slope α, in the absence of basal sliding, equation (26) with zero strain-rate gradient,

$$\left(\frac{V}{Z}\right)^{1/n} = \left(\frac{2}{n+1}\right)^{1/n} \frac{s\rho g \alpha \overline{Z}}{B} \tag{29}$$

Values for this equation from the Athabasca Glacier are shown plotted on log-log scale in Fig. 6.2. The smoothing has been taken over 1100 m. The value of the shape factor s has been estimated from Nye's (1965) calculations of velocity profiles for various cross-section shapes and the measured cross-sections of the glacier from Paterson (cf. Fig. 3.5).

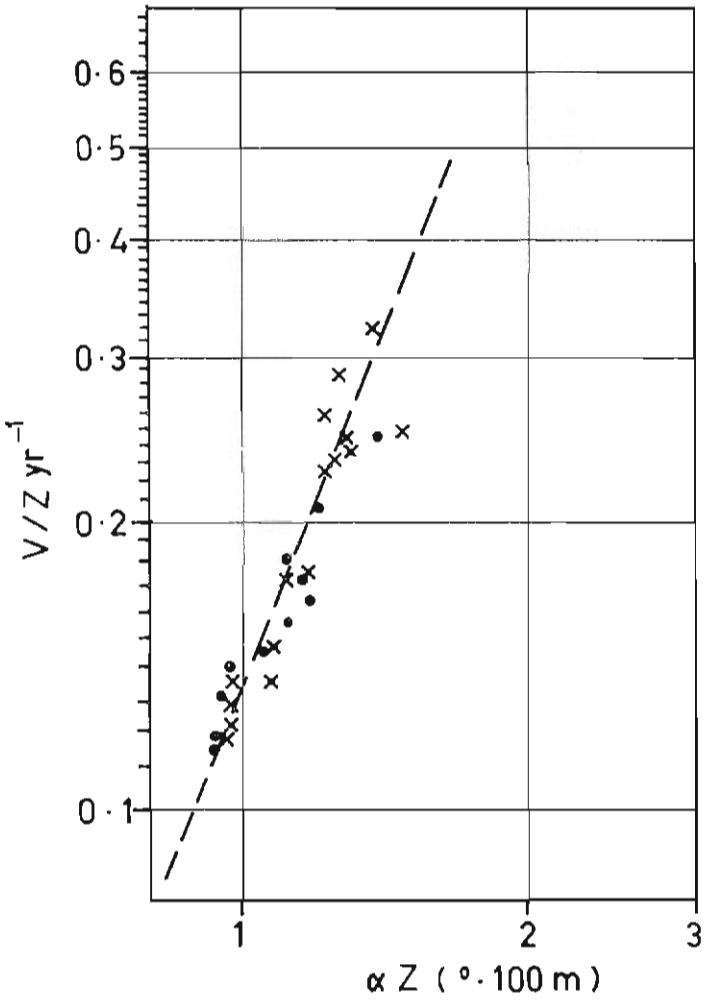

FIG. 6.2. From the values of smoothed-surface slope α, ice thickness H and velocity V, for the Athabasca Glacier from Fig. 6.1, V/Z is plotted against αZ on a log-log scale. The slope of the broken line suggests a value of $n \simeq 2{\cdot}6$ for the power law index.

From this we obtain estimates of n and B as

$n = 2{\cdot}6$,

$B = 0{\cdot}63 \times 10^9$ dynes cm^{-2}sec$^{1/3}$.

These values show reasonable agreement with other measurements of the flow parameters from laboratory and field determinations, for temperatures close to the melting point. The scatter in Fig. 6.2 can be attributed to several factors such as the shorter distance fluctuations, the errors in the measurements, and other effects not considered here, such as basal sliding and variation in the shape factor along the glacier. In spite of these deviations, the results suggest that equation (29) gives a good approximation for the smoothed velocity in terms of the other parameters. For unsmoothed values, however, this relation is completely obscured by the smaller-scale fluctuations in slope shown in Fig 6.1. These are now examined in more detail.

6.2.3. *Strain rate and slope fluctuations*

We consider the short-distance fluctuations of strain rate and slope with reference to the equation

$$\frac{\partial \dot{\varepsilon}_x^{1/n}}{\partial x} = -\frac{\rho g}{2B}(\alpha - \bar{\alpha}) \tag{30}$$

We assume, that for a temperate glacier, the parameter B is constant along the tongue, and from this we obtain, by integrating (30) over the $\frac{1}{2}$ waves, values of strain rate $\Delta\dot{\varepsilon}_x$ and stress $\rho g \Delta\alpha$ deviations for each of the $\frac{1}{2}$ waves. There is not sufficient range of values here to determine the power law index n precisely, but the cluster of values is consistent with a low value of n. Hence, we determine B by averaging the results over the length of the glacier and taking

$n = 1$, to obtain

$B = 0{\cdot}70 \times 10^9$ dynes cm^{-2}sec$^{1/3}$.

These parameters are appropriate for the whole thickness of the ice, whereas the others (from Section 6.2.2) are associated with the region of high shear at the base.

For most temperate glaciers the temperature variation is not very great, so that the B values are not expected to vary widely over the glacier. However, due to the curvature of the flow law of ice, on the log-log scales, near 1 bar the values of B obtained from different ranges of stress may be expected to differ slightly, depending on the distance of the stress ranges from 1 bar.

These two-sub-sections are not meant to be more than a guide to the application of the general results of the theory of longitudinal strain rates developed for ice masses to temperate glaciers. The method of determining the values of the flow parameters from the longitudinal velocity profile provides a supplement to the methods employed by Paterson and Savage (1963) and others who have used the transverse and vertical profiles of velocity to study the flow law of ice.

6.2.4. *Compression and extension*

From the equations developed for longitudinal velocity and strain rate, some general ideas may be obtained as to the shapes of ice masses which will have com-

pressive or extensive flow. Only a simple case is outlined here. Extensions to this treatment to cover effects of variable bedrock elevation, varying shape factor, etc., can readily be carried out in specific cases by numerical techniques.

For a glacier on a flat bed the ice longitudinal thickness gradient equals the surface slope, i.e.,

$$\frac{dZ}{dx} = \alpha \tag{31}$$

where x is directed opposite to the motion. We note that the surface velcoity V, in the absence of sliding, is given by equation (29) for smoothed slope and thickness

$$\frac{V}{Z} = a_1 \left(Z \frac{dZ}{dx}\right)^n \tag{32}$$

where a_1 is constant. This may be written as

$$\int V^{1/n} dx = \int a_1 Z^{1-1/n} dZ,$$

and from this equation we wish to find the forms of the ice-thiekness profile which cause increasing or decreasing velocity along the line of flow. A typical glacier profile $Z(x)$ may be approximated by an equation of the form

$$Z = a_2 x^m \tag{33}$$

where x is the distance from the front, directed opposite to the motion, and a_2 and m are constants ($m = 2,\ 1,\ \frac{1}{2},\ 1/3,\ 1/4\ \ldots$).
Then

$$\frac{dZ}{dx} = m a_2 x^{m-1}$$

$$Z \frac{dZ}{dx} = m a_2^2 x^{2m-1}$$

and

$$\left(Z \frac{dZ}{dx}\right)^n = (m a_2^2)^n x^{(2m-1)n}.$$

From this and equation (32) we find for velocity

$$\begin{aligned} |V| &= a_1 (m a_2^2)^n a_2 x^{(2m-1)n+m} \\ &= A x^p \end{aligned} \tag{34}$$

where

$$p = (2m - 1)n + m, \text{ say.}$$

Now the velocity is constant when p is zero, i.e., when $(2m-1)n + m = 0$, i.e.,

$$m = \frac{n}{2n + 1} \tag{35}$$

i.e., for

$$\begin{aligned} n &= 1 \quad 2 \quad 3 \quad 4 \quad \ldots\ldots \infty \\ m &= 1/3 \quad 2/5 \quad 3/7 \quad 4/9 \ldots\ldots 1/2. \end{aligned}$$

Hence, for an ice mass with a flat base and a surface of the form $H = ax^m$, the velocity decreases inland (extension) for $m < \frac{3}{7}$ for $n = 3$, or $m < \frac{4}{9}$ for $n = 4$. For $m > \frac{3}{7}(n = 3)$, the ice mass velocity increases going inland and compression exists.

We note that, for a perfectly plastic medium ($n = \infty$), the parabolic profile ($m = \frac{1}{2}$) is required for zero longitudinal strain rate. For lower values of n, slightly more curved profiles ($m < \frac{1}{2}$) are required for constant velocity. Also, for extending flow with any n, a slightly more curved profile ($m < \frac{1}{2}$) is required than that corresponding to the zero strain case. In Section 7 we examine more fully the forms of the elevation profiles of ice masses.

6.2.5. *Waves on a glacier surface* (constant ice thickness)

As an application of Section 5.4 we examine the variation in strain rate over ideal surface waves, say, typical of those observed on the Athabasca Glacier..

Suppose we have an undulating glacier surface whose slope can be represented by the equation

$$\alpha - \bar{\alpha} = a \cos \omega x,$$

where $\lambda = \frac{2\pi}{\omega}$ is the wavelength of the undulations.

Equation (30) now becomes

$$B \frac{\partial \dot{\varepsilon}^{1/n}}{\partial x} = -\frac{1}{2} \rho g (a \cos \omega x) \tag{36}$$

or

$$\dot{\varepsilon}^{1/n} = -\frac{\rho g a}{2B\omega} \sin \omega x + \dot{\varepsilon}_0^{1/n} \tag{37}$$

The results of the flow studies of Section 2 suggest, if the strain rates are low, we may take $n \simeq 1$;

then

$$\frac{dV}{dx} = -\frac{\rho g a}{2B\omega} \sin \omega x + \dot{\varepsilon}_0 \tag{38}$$

and

$$V = V_0 + \dot{\varepsilon}_0 x - \frac{\rho g a}{2B\omega^2} \cos \omega x \tag{39}$$

Hence, the velocity maxima tend to occur at the positions of downslope maxima. Maximum extension occurs on the crests of relative elevations (hills) and relative compression occurs as maxima in the valleys. This may be seen to be the case from Fig. 6.1 for the Athabasca Glacier, showing the strain rate gradients and slopes approximately in phase. It is expected that this relation may break down near the front of the glacier where the ice thickness gradient is not negligible.

Similar properties of strain rate and slope fluctuations have been observed on the surface of ice caps which are examined in the next section.

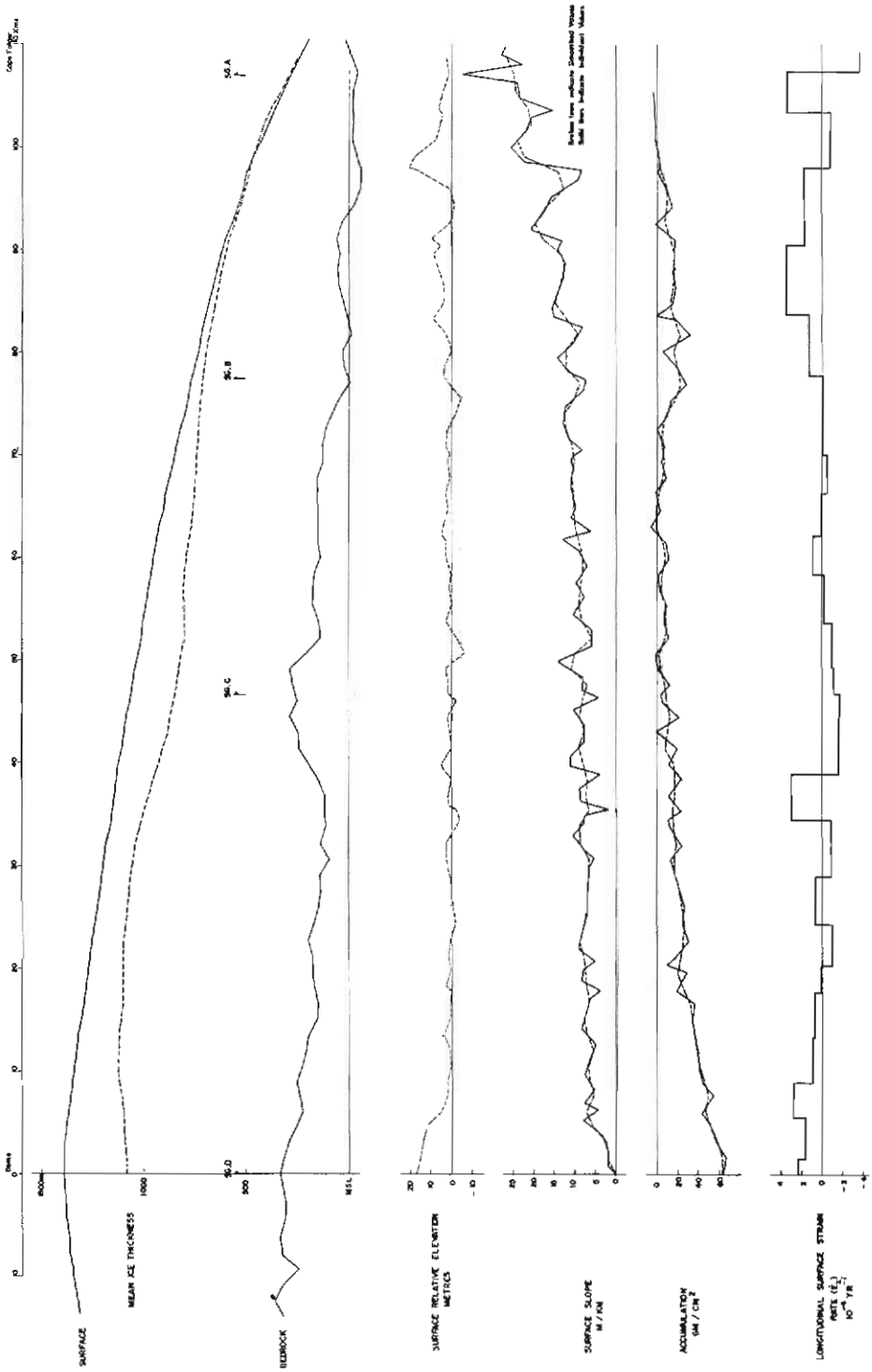

FIG. 6.3. Wilkes ice cap dome—Folger line showing profiles of ice thickness, relative elevation, surface slope, accumulation and strain rates (from McLaren 1968).

6.3. ICE CAPS

In the case of ice caps, the only boundary holding the ice is the bedrock at the base, unless a "stream" of more rapidly flowing ice exists in the main ice mass. The complications of such streams will be neglected for the present. For the ice cap, then, there is no horizontal transverse shear and the dynamics problem becomes similar to that for the ice shelf, except that in the ice cap the velocity varies in the vertical, while for the ice shelf it changes transversely in the horizontal. In both cases the cross-sections to the line of flow correspond to infinite slabs with shape-factor unity.

6.3.1. *Velocity and slope (smoothed)*

Neglecting for the moment the effect of the longitudinal strains, and transverse compression or extension, i.e., provided the term of equation 5.3 (29) $\partial Z B_1 (\phi \dot{\varepsilon}_x)^{1/n}/\partial x \simeq 0$, we may expect the relation for smoothed velocity (V) thickness (Z) and slope ($\bar{\alpha}$) to hold generally:

$$V = \frac{2Z^{n+1}}{(n+1)} \left(\frac{\rho g \bar{\alpha}}{B}\right)^n \tag{40}$$

This corresponds to the equation (3) for ice shelves, with the half width a replaced by the thickness Z, and to equation (29) for glaciers (with the shape factor equal to 1).

As an example to see how well this relation holds for an ice cap along a flow line we consider the 200 km diameter local ice cap near Wilkes and examine the profiles from the Dome to Cape Poinsett and Cape Folger, cf. MeLaren (1968) and Pfitzner (to be published). Figs. 6.3 and 6.4 show the elevation, slope, ice thickness, bedrock and velocity profiles along these two lines. Fig. 6.5 shows the plots of

$$\frac{B_\theta V}{Z} \quad \text{against} \quad \alpha Z$$

for these two lines. From these latter we see that the linear relation on log coordinates seems to hold fairly well and that we can determine n and B as

$$n = 3{\cdot}4,$$
$$B = 0{\cdot}85 \times 10^9 \text{ dynes cm}^{-2} \text{ sec}^{1/3}.$$

The value of B is dependent on temperature and has been taken to vary with temperature θ here according to the equation

$$B_\theta = B_0 e^{-k\theta},$$

where $k \sim 10^{-1}$ °C^{-1}.
From this the value of B has been deduced for different values of basal temperature θ which have been calculated in Section 4 along the profile from the dome to Cape Poinsett. The results of the temperature calculations are illustrated in Fig. 4.16 and suggest that the basal temperatures vary with surface temperature, but are somewhat higher with a mean value, along the line, of about −10°C.

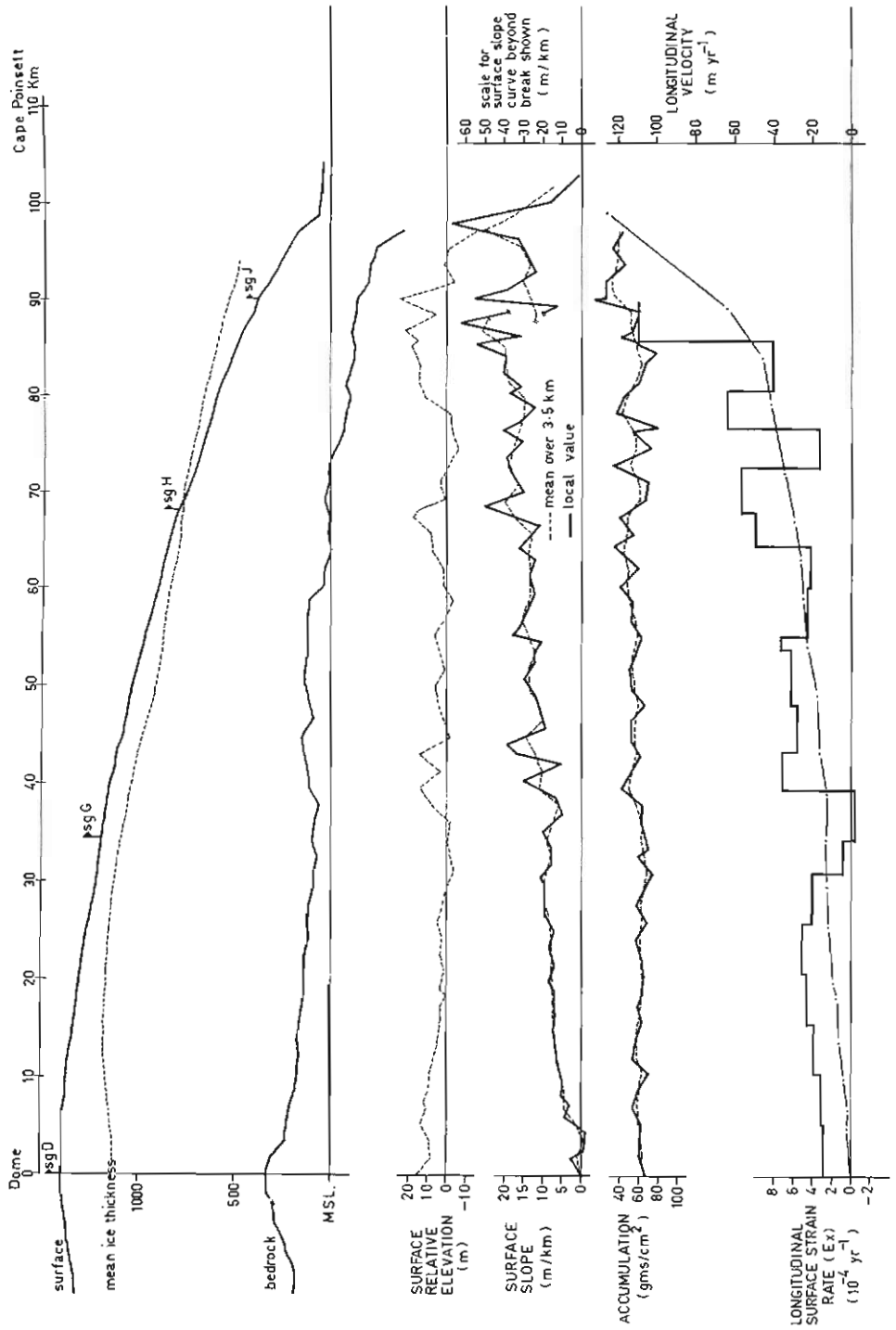

FIG. 6.4. Wilkes ice cap dome—Cape Poinsett line showing ice thickness, relative elevation, surface slope, accumulation, strain rate and velocity. [after McLaren 1968 and Pfitzner (to be published)].

Finally, by plotting the strain rate $\frac{n+1}{2}\frac{V}{Z}$ against the stress $\rho g\overline{Z}\alpha\, e^{k}$, reduced to a constant temperature, on Fig. 2.2, for the flow law of ice it is apparent that these stress and strain rate values correspond to those for temperatures in the range calculated for the basal temperatures along this profile (cf. Fig. 4.16).

Complete confirmation of these temperatures, however, will have to wait for the completion of the drilling and temperature measurement programme in this region.

The formula (40) for smoothed velocity may also be used to estimate the

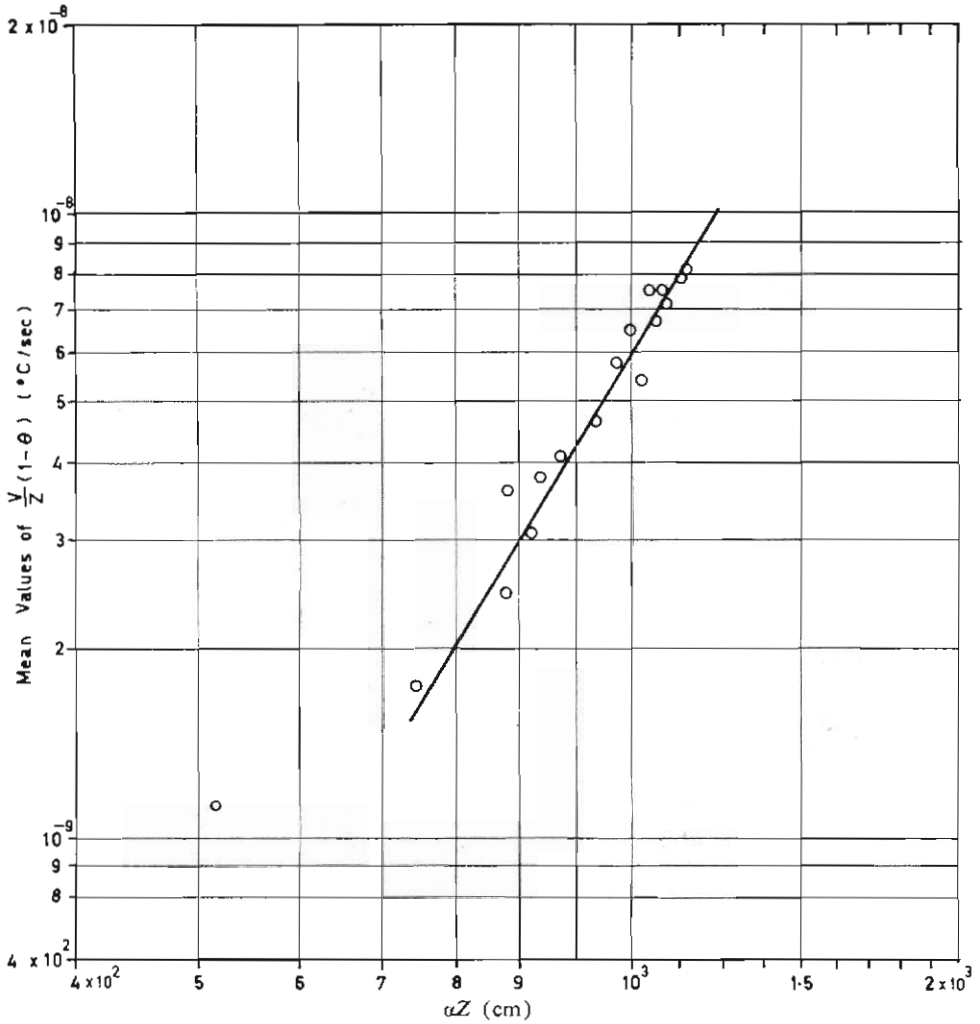

FIG. 6.5. From the Wilkes ice cap dome—Cape Poinsett line for the smoothed values of velocity V, surface slope α, and ice thickness Z, the values V/Z, corrected for calculated basal temperatures θ, have been plotted against αZ. The slope of the line suggests a power law index $n \simeq 3.4$, although lower values may operate for the lower stresses.

velocity inland of a large ice cap if the thickness and slope are known, as well as the velocity at the edge. As an example of the use of this formula in this capacity, we calculate the function $(\alpha Z)^n Z$ for the profile of Antarctica inland of Wilkes. This then allows velocities V_0 to be calculated along the line if the basal temperatures were constant, i.e., by taking a constant B_0, say, 10^9 dyne cm^{-2}sec$^{1/3}$. From Section 4 we obtain estimates of basal temperatures θ_b along this line, calculated from these velocities. Finally, using these basal temperatures, new velocities V_θ may be calculated which take account of the temperature variation along the route. These are shown in Table 6.2. This procedure may be repeated to obtain new temperatures and velocities until convergence is reached. However, since other details in the region, such as transverse strain and curvature of the flow lines, are still unknown, a more advanced two-dimensional analysis is not warranted at this stage.

TABLE 6.2

WILKES—VOSTOK CALCULATED VELOCITIES

Distance inland x km	Ice thickness Z km	αZ m	$V_0 \propto (\alpha Z)^n Z$ m/yr	$V_\theta \propto V_0 \frac{1}{1-\theta_b}$ m/yr
1310	3·02	3·36	0·6	0·5
1205	3·17	3·99	1·0	0·8
1118	3·42	4·28	1·7	1·4
1020	3·85	4·70	2·0	2·0
921	4·44	5·46	3·6	3·8
820	4·58	5·82	4·1	4·8
720	4·15	5·40	3·8	4·2
570	4·00	6·28	5·0	5·5
518	2·79	7·28	5·2	5·7
464	2·70	11·88	24·3	30·1
370	2·28	13·43	27·4	36·0
280	2·63	16·62	60·0	105·0

6.3.2. *Strain rate and slope fluctuations*

We next consider the small variations in slope, causing similar fluctuations in strain rate, superimposed on the smoothed velocity, slope and ice thickness.

Such short-wave fluctuations are governed by the equation

$$\frac{\partial Z B \phi \dot{\varepsilon}^{1/n}}{\partial x} = -\frac{1}{2}\rho g Z(\alpha - f) \tag{41}$$

This equation can also be tested by the Wilkes ice cap data.

First of all, we note that along the dome—Cape Poinsett section beyond strain grid G the lateral strains were smaller than the longitudinal strains and so, by equations 5.3 (27) and (28), they have little influence.

Fig. 6.6 shows the high correspondence between the strain-rate gradient and the slope. By examining the magnitude of these corresponding variations, values of n and B may be obtained from

$$\delta \dot{\varepsilon}^{1/n} = -\frac{\rho g}{2B}(\alpha - \bar{\alpha})\delta x \tag{42}$$

These results are illustrated by Fig. 6.7. This shows that the octahedral shear stress produced by the right-hand-side varies from 0·06 to 0·25 bars.

The values of the parameters n and B are

$$n = 1{\cdot}2,$$
$$B = 1{\cdot}5 \times 10^{9} \text{ dyne cm}^{-2}\text{sec}^{1/3}, \text{ or } 3{\cdot}4 \times 10^{15} \text{ dyne cm}^{-2}\text{sec}.$$

The low value of n reflects the almost Newtonian viscosity at low stresses as reported by other workers (e.g., Butkovitch and Landauer 1960, Mellor and Smith 1966).

The value of B here represents the average value characteristic of the whole column of the ice mass:

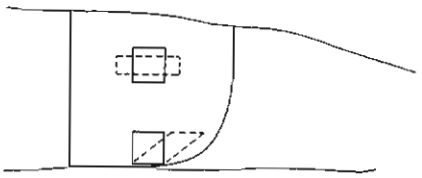

i.e., near the base, simple shear predominates, but for most of the column the deformation is longitudinal extension or compression in the horizontal and vertical, with the maximum shear direction at 45° to the extension and compression.

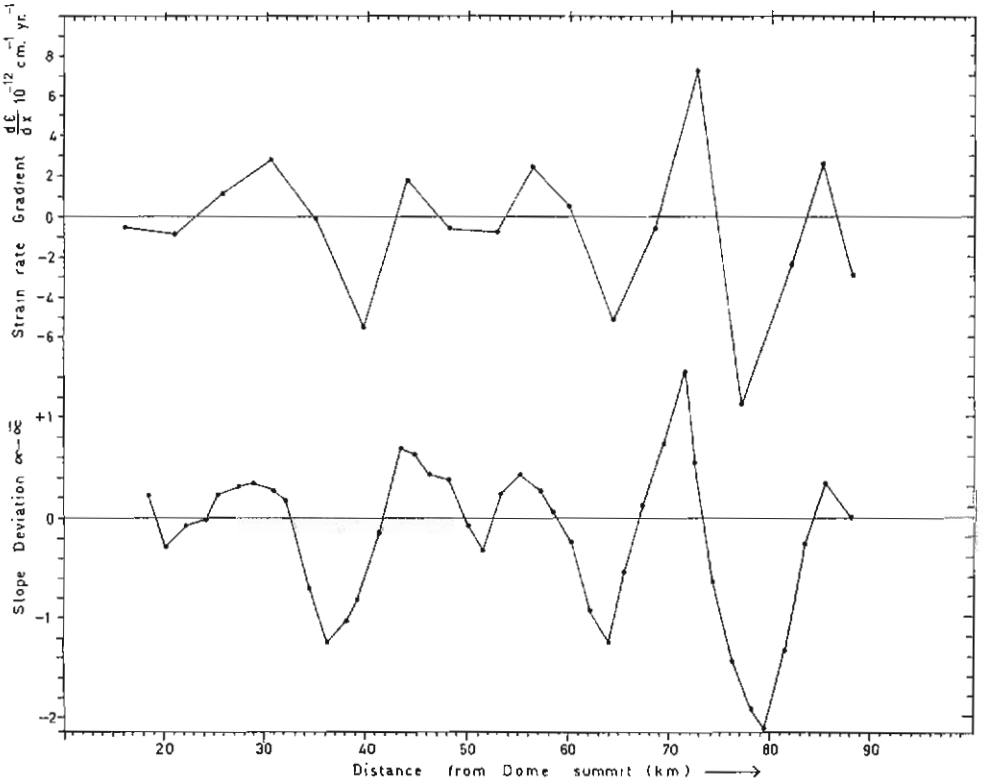

FIG. 6.6. Wilkes ice cap, strain-rate gradient and surface-slope deviations.

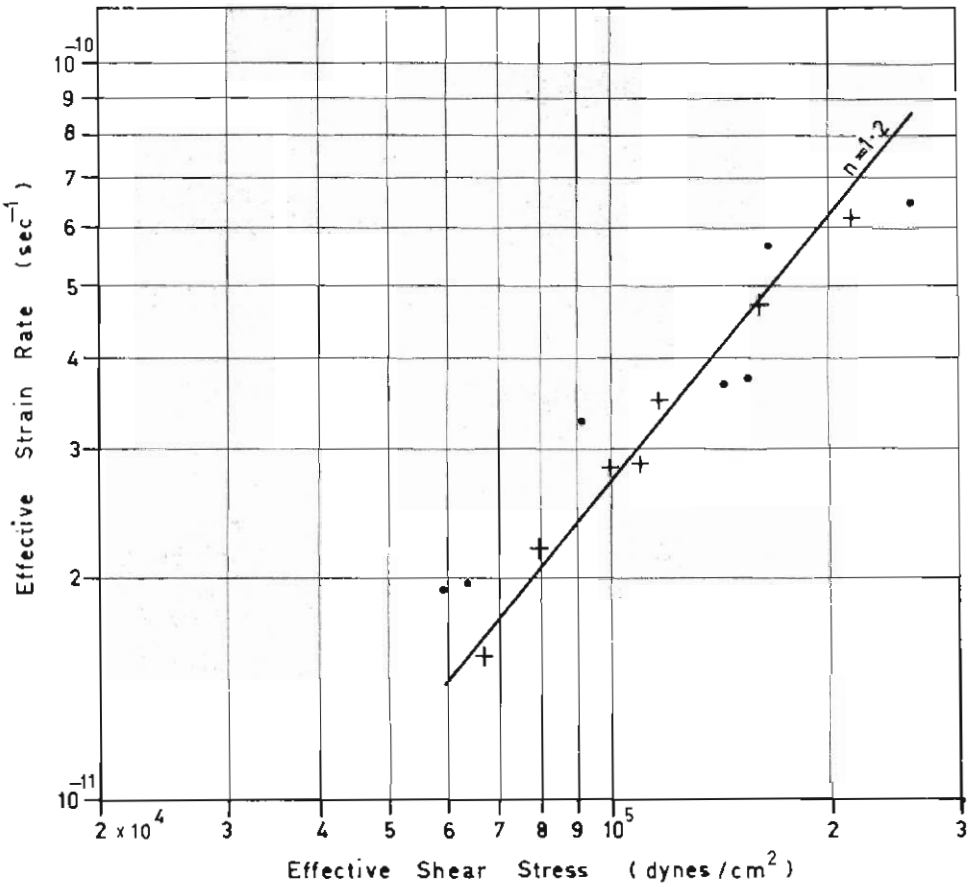

FIG. 6.7. Integrating the curves of Fig. 6.6 over ½-waves, shear-strain rate plotted against shear stress shows an approximately linear relation (after McLaren 1968).

In order to compare the magnitude of B with that of other measurements, it is necessary to convert the longitudinal stresses and strains of equation (42), $(\sigma_x, \dot{\varepsilon}_x)$, to the corresponding octahedral shear stress and strain values, (τ_0, γ_0) by Nye (1953), or cf. Section 2.1:

$$\tau_0 = \sqrt{2/3}\,\sigma'_x \simeq 0{\cdot}816\,\sigma'_x, \text{ for two-dimensions.}$$

$$\gamma_0 = \sqrt{2/3}\,\dot{\varepsilon}_x \simeq 0{\cdot}816\,\dot{\varepsilon}_x \text{ for two-dimensions.}$$

The magnitudes of the δx in equation (42) have not been specified as yet, but to obtain maximum stress variation we require to integrate over a ½-wave, i.e., from

$$\frac{d\dot{\varepsilon}}{dx} = -\frac{\rho g}{2B}(\alpha - \bar{\alpha}),$$

if we have undulations of wavelength λ at the surface given by

$$Z = Z_0 - \bar{\alpha}x - \alpha_1 \cos \omega x,$$

where $$\omega = \frac{2\pi}{\lambda},$$

and hence $$\alpha = \bar{\alpha} - \alpha_1 \sin x\omega.$$

Then $$\int_0^{\lambda/2} \frac{d\dot{\varepsilon}}{dx}\, dx = -\frac{\rho g}{2B}\alpha_1 \int_0^{\lambda/2} \sin \omega x\, dx;$$

hence $$\dot{\varepsilon}_0 - \dot{\varepsilon}_{\lambda/2} = -\frac{\rho g}{2B}\frac{\alpha_1}{\omega} 2,$$

or $$2\dot{\varepsilon}_1 = \frac{\rho g \alpha_1 \lambda}{B 2\pi},$$

where ϵ_1 is the amplitude of the strain-rate variations.

In octahedral shear values

$$\frac{1}{\sqrt{2}}\varepsilon_1 = \frac{\sqrt{2}}{3}\frac{\rho g}{B}\frac{\alpha_1 \lambda}{2\pi},$$

or $$B = \frac{\rho g \lambda}{3\pi}\frac{\alpha_1}{\dot{\varepsilon}_1}.$$

It is also interesting to note that the *maximum* variation in otachedral shear stress at the base is

$$\sqrt{\frac{2}{3}}\rho g Z \alpha_1.$$

Hence, the wavelength over which the shear stress produced by longitudinal stress equals the increase in basal shear stress is given by

$$\sqrt{\frac{2}{3}}\frac{\rho g \alpha_1 \lambda}{4\pi} = \sqrt{\frac{2}{3}}\rho g Z \alpha_1,$$

i.e., $$\lambda = 4\pi Z.$$

This result suggests that greater wavelengths would tend to be absorbed by the smoothed velocity relation (equation 40).

From Fig. 6.7 of the octahedral shear stress versus strain ratc, and Fig. 2.2 for the flow law of ice, we can see that the value of B determined above would correspond to an average temperature of the column of $-15°C$, with variations from this temperature, along the flow line, according to the variation in average temperature. This temperature seems compatible with the average temperature in the ice mass as may be estimated from the calculations of Section 4, Fig. 4.16. Again, a more precise analysis will have to await the results of temperature measurements through the ice cap. For large strain rates the value of n may well be much greater than 1. In this case it is necessary to follow the more general analysis of Appendix II, in which the effect of the horizontal shear must be taken into consideration for a non-linear flow law.

6.3.3. *The effect of transverse strain on the longitudinal velocity profile in ice caps*

We can see from equations 5.3 (27) and (28) how the presence of a transverse strain affects the relation between longitudinal stress and strain. We note that a

small transvere strain of the same sign has little effect on the longitudinal strain in equation (41). For large transverse strain, especially of opposite sign, the relation between longitudinal stress and strain is greatly affected.

As a first example of the effect of the transverse strain, consider the results of the strain grid measurements over the Wilkes dome region as set out in the table below, from Pfitzner (to be published).

TABLE 6.3

WILKES STRAIN GRIDS

	A	B	C	D_A	D_J	G	H	J	K	L
$\dot{\varepsilon}_x yr^{-1} \times 10^3$	0·97	0·39	0·15	1·12	0·28	0·05	3·52	10·70	−0·48	0·06
$\dot{\varepsilon}_y yr^{-1} \times 10^3$	0·89	0·47	0·72	0·75	1·52	1·77	1·18	5·10	−0·18	0·88
$\nu = \dot{\varepsilon}_y/\dot{\varepsilon}_x$	0·92	1·20	4·80	0·67	5·40	35·00	0·34	0·48	0·25	14·60
$\phi_1 = 1 + \frac{\nu}{2}$	1·40	1·60	3·40	1·34	1·27	18·50	1·17	1·24	1·13	8·30
$\phi_1\dot{\varepsilon}_x = \dot{\varepsilon}_x + \frac{\dot{\varepsilon}_y}{2}$	1·41	0·62	5·10	1·50	0·36	0·92	4·10	13·40	−0·54	0·50

It is noted here that, from McLaren (1968), these strain grids were small, rosettes with three 100m arms. Equation 5.1 (29) indicates that strain-rate variations over short distances (wavelengths $\lambda \ll \frac{2\pi}{\sqrt{3}} Z$) may be very high. A comparison of the strain-grid values with long-distance tellurometer measurements (cf. Figs. 6.3, 6.4, 6.8) shows this to be the case for this region.

For those strain grids in which the transverse strain dominates, there is little direct relation between longitudinal slope and strain rate unless the strain factor ϕ is taken into consideration. This result shows the importance of the transverse strain rate in ice cap dynamics. Since the only transverse strain rates available, so far, for the Wilkes flow line profiles *DJ*, *DA* are the spot values at the strain grids, we cannot adequately test at this stage the effect of the transverse strain and the equations derived in Section 5.3. However, from Table 6.3 it appears that the value of the "viscosity" parameter B, calculated from equation (42) for this line, could be in error by a factor of 2 if the transverse strain were neglected. The coastal line *JA* (cf. Fig. 6.9) is largely across the line of flow, and the high correlation between the relative elevations and strain rates (cf. Fig. 6.8) indicate that the equation (42) operates across the line of flow as well as longitudinally, thus justifying the consideration of the transverse strain factor. To overcome the difficulty of transverse strain, an additional set of large strain grids have recently been established by D. Carter in 1967 at intermediate positions around the triangle. We conclude that a trilateration traverse, which obtains continuous transverse strains along the route, is more valuable than the line traverse where only distances and angles are measured.

Secondly, the transverse strain rate may also affect the smoothed longitudinal velocity profile. However, the effect is generally small and may be considered

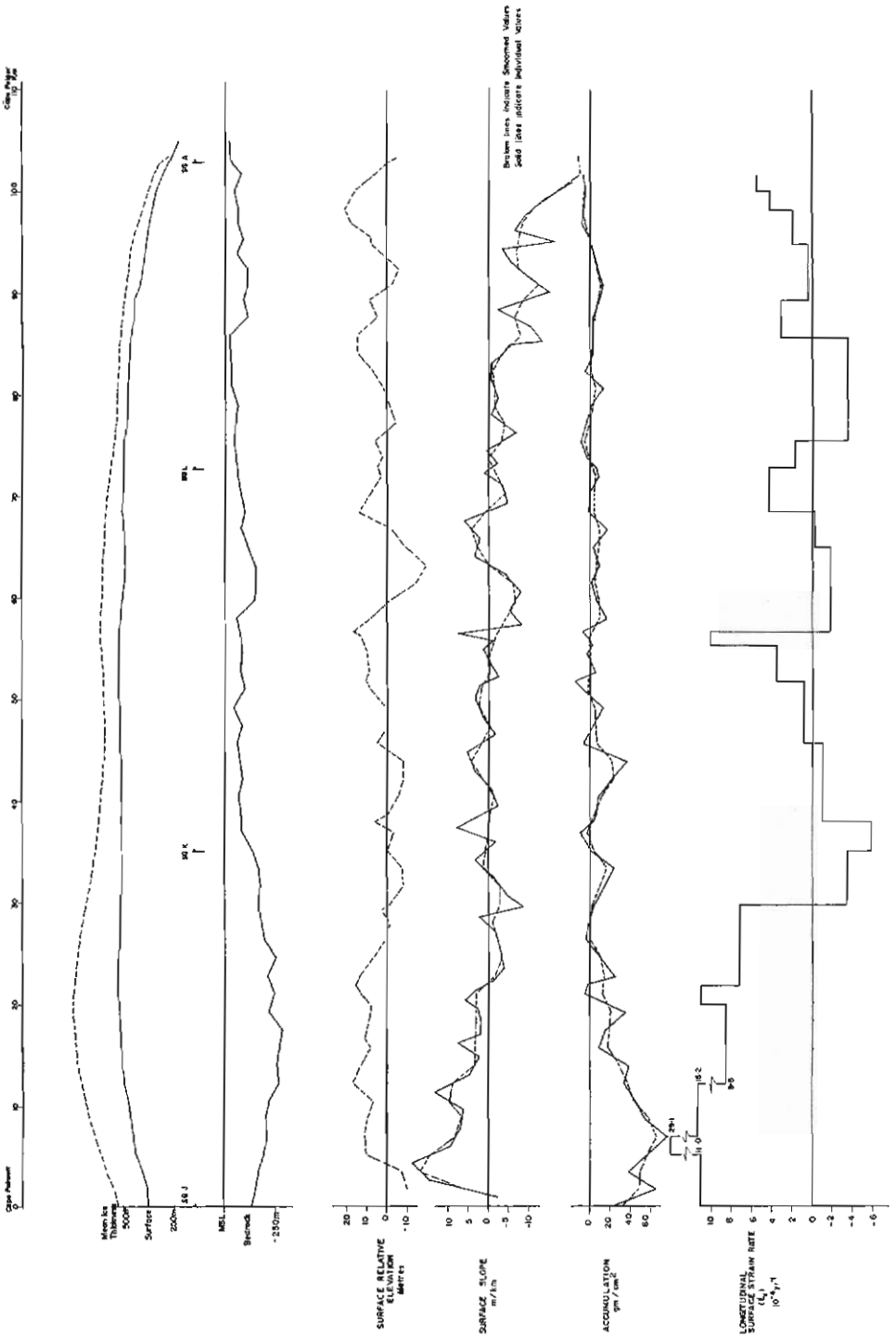

FIG. 6.8. Wilkes ice cap transverse line Cape Poinsett to Cape Folger (from McLaren 1968).

generally with the effect also of the longitudinal strain rate. From the general equation 5.1 (39), neglecting the last term on the right and including the factor ϕ,

$$-\frac{\partial ZB_1(\phi\dot{\varepsilon}_x)^{1/n}}{\partial x} = \frac{1}{2}\rho gZ\alpha - B_2\left(\frac{n_2+1}{2Z}V\right)^{1/n_2} \tag{43}$$

By taking smoothed values over distance $x \simeq 15Z$ it was found that the term on the left was small, giving the smoothed velocity relation

$$\frac{n_2+1}{2\bar{Z}}\bar{V} = \left(\frac{\rho g\bar{Z}\bar{\alpha}}{2B}\right)^n \tag{44}$$

When, however, the first term, which we can write as

$$-\frac{\partial ZB_1(\phi\dot{\bar{\varepsilon}}_x)^{1/n}}{\partial x} = \frac{1}{2}\rho gZ(\delta\alpha), \quad \text{say,} \tag{45}$$

is not negligible, then the smoothed velocity relation becomes

$$\frac{n_2+1}{2\bar{Z}}\bar{V} = \left(\frac{\rho g\bar{Z}\bar{\alpha}^*}{2B_2}\right)^n = \left(\frac{\tau^*}{2B}\right)^n, \tag{46}$$

where $\bar{\alpha}^* = \bar{\alpha} + \delta\alpha$ and $\tau^* = \rho g\alpha^* Z$ (47)

This allows corrections to be made to the smoothed velocity profile for high longitudinal and transverse strain rates. Table 4 shows the magnitude of the corrections calculated from transverse strains, due to flow line divergence, which are appropriate to the Wilkes ice cap on the dome—Cape Poinsett and dome—Cape Folger lines. The value of B_1 used here was that found for the variation of strain rate over undulations. These corrections have been incorporated into the calculations of the flow parameters described earlier in the section. The highest correction is less than 10% but is still important in the determination of the flow law parameter n_2.

TABLE 6.4

STRAIN RATE CORRECTION TO SHEAR STRESS

Line	Distance	Shear stress			Line	Distance	Shear stress		
$D\rightarrow A$	from D	τ	$\delta\tau$	τ^*	$D\rightarrow J$	from D	τ	$\delta\tau$	τ^*
	km		bars			km		bars	
D	0-23	0·52	—0·05	0·47	D	0-18	0·28	0	0·28
C	23-63	0·68	0	0·68	G	18-50	0·70	—0·01	0·69
B	63-92	0·77	0·01	0·78	H	50-75	0·85	0·02	0·87
A	92-110	0·92	0·02	0·93	J	75-101	1·20	0·60	1·26

6.3.4. *Strain rate and flow lines*

For an ideal circular ice cap, flowing out in straight lines from the centre, a transverse strain rate $\dot{\varepsilon}_\theta$ exists as a result of the velocity V and divergence angle θ, depending on the distance r from the centre. If we write $y = r\theta$, the transverse strain rate is given by

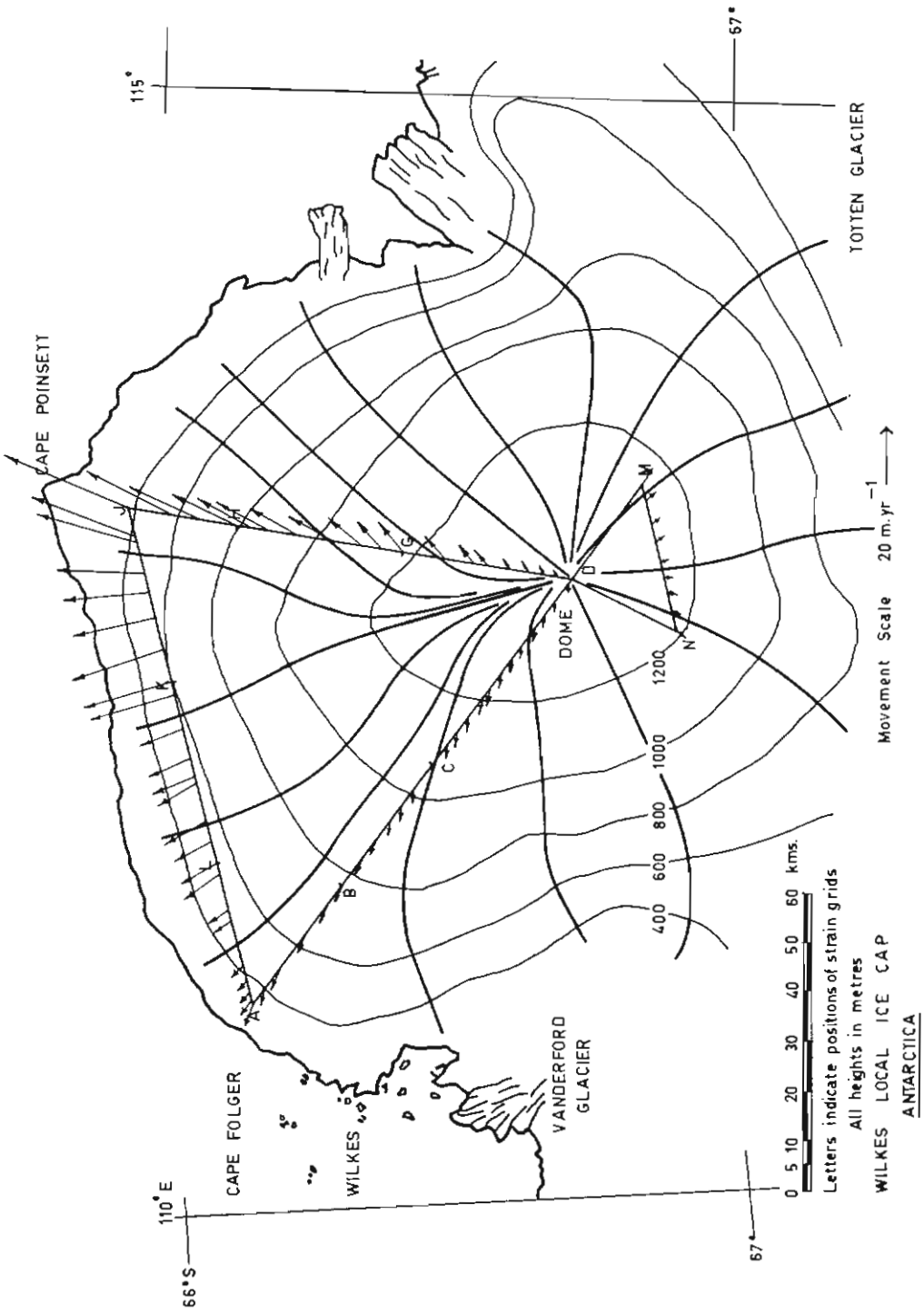

FIG. 6.9. Measured velocities and surface contours show agreement with flowlines drawn as orthogonals to contours [after Pfitzner (to be published)].

TABLE 6.5

TRANSVERSE STRAIN RATES FOR WILKES ICE CAP

$10^{-4}yr^{-1}$

	Strain grids	Flow divergence	Angle to line
A	5·0	2·8	21°
B	4·5	2·0	8°
C	8·0	2·2	34°
D_A	7·5	3·5	
M	10·0	3·7	5°
N	5·7	2·3	13°
D_J	15·2	3·6	
G	7·5	2·1	41°
H	12·0	6·9	16°
J	44·0	14·7	13°
K	—0·2	—3·0	0°
L	0·9	3·5	0°

$$\dot{\varepsilon}_\theta = \frac{V\theta}{y} = \frac{V}{r} \tag{48}$$

or

$$\theta = \frac{y\dot{\varepsilon}_\theta}{V}.$$

Such an ideal ice cap is characterized by a circular symmetry about its centre, and is approached by an ice cap with a smooth flat base and concentric circular contours. For real ice caps the irregular surface contours and varying bedrock profiles cause divergence and convergence of flow lines (cf. Fig. 6.9).

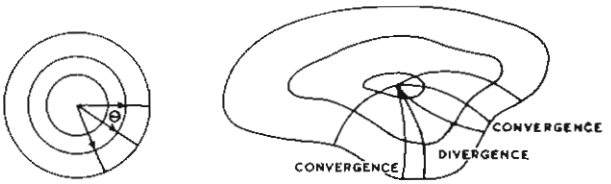

IDEAL ICE CAP
CIRCULAR CONTOURS
SIMPLE RADIAL FLOW

IRREGULAR ICE CAP

If the strain rates and velocity are known, the divergence angle θ between two flow lines distance y apart may be calculated from

$$\theta = \frac{y\dot{\varepsilon}_\theta}{V}.$$

The effect of the curvature of the flow lines (and the resulting transverse strain) on the longitudinal velocity distribution may then be calculated from equations (45) and (46).

Fig 6.9 shows flow lines over the Wilkes local ice cap drawn from orthogonals to the contours. The actual measured velocity directions are shown to be in close agreement with these. Table 6.5 lists the values of transverse strain rate calculated from the flow line divergences and those actually measured at the strain grid positions. There is general agreement between the two, but the measured strain

rates are on a much smaller scale and show considerably greater fluctuations. This implies that very large scale strain grids ($\simeq$ 15 km) are required to obtain the general flow line divergences.

6.3.5. *Ice flow over undulations*

At this stage only a preliminary analysis has been made of the Wilkes ice cap data in regard to the implications of the theory of ice flow over bedrock undulations developed in Section 5.4. The main conclusions reached there can be summarized as follows:

(1) Bedrock undulations cause similiar but damped undulations on the ice-cap surface.

(2) Along the line of flow, for large damping factors ($\psi \simeq 10$), the surface undulations are out of phase with the base undulations by $\pi/2$, such that the surface-slope maxima occur over bedrock-elevation maxima.

(3) Across the line of flow the surface and bedrock undulations are in phase. For other directions of flow the phase shift varies between 0 and $\pi/2$.

(4) The damping factor ψ depends on the ice thickness Z, the forward velocity V, the ice flow "viscosity" parameter B, and the wavelength of the undulations λ,

$$\psi = \frac{\rho g Z^2}{4\pi B V}\left[\frac{\lambda}{Z} + \frac{4\pi^2}{3}\frac{Z}{\lambda}\right] \tag{49}$$

(5) There is a characteristic wavelength λ_m, for a given ice thickness, for which the damping is a minimum. This implies that much shorter or longer waves are more readily damped out and, as a consequence, surface undulations of wavelength $\lambda \simeq 2$ to 10 times the ice thickness may tend to be predominant, although harmonics of λ_m may also be apparent:

$$\lambda_m = \frac{2\pi}{\sqrt{3}} Z \simeq 3{\cdot}63Z \tag{50}$$

(6) From detailed measurements of surface and bedrock elevations (or slopes α_2 and β_1) the values of the flow parameter B may be determined from the magnitudes of the damping factor together with the ice thickness and velocity, i.e.,

$$B \simeq \frac{\alpha_2}{\beta_1}\frac{\rho g Z^2}{4\pi V}\left(\frac{\lambda}{Z} + \frac{4\pi^2}{3}\frac{Z}{\lambda}\right) \tag{51}$$

(7) Three-dimensional bedrock protrubences will be slightly more damped than the corresponding two-dimensional ones.

To test these conclusions, an accurate profile of both surface and bedrock elevations, as well as the velocity vector, are required along a flow line and preferably with also some data across the flow line. Continuous profiles are ideal but in practice it is generally necessary to concede to closely spaced discrete values. In this case, wave lengths down to about 4 times the discrete distance interval are as short as can be expected to be studied precisely. A further limitation in studying short wave undulations is that ice-thickness measurements from gravity readings, no matter how closely spaced, severely damp out wavelengths shorter than several times the ice thickness. Even the radio echo sounder will start to damp out hollows of wavelengths shorter than a critical value λ_c such that the radius of curvature

at the bottom of a hollow equals the ice thickness, i.e., for a bedrock profile of the form $b = b_0 + b_1 \cos \frac{2\pi}{\lambda} x$,

$$Z^{-1} = b_1 \left(\frac{2\pi}{\lambda_c}\right)^2$$

or

$$\lambda_c = 2\pi\sqrt{b_1 Z} \quad \text{or} \quad \frac{\lambda_c}{Z} = 2\pi \sqrt{\frac{b_1}{Z}} \tag{52}$$

With this limitation in mind we now look at some preliminary data from the Wilkes ice cap.

D. Carter in 1967 obtained continuous bedrock profiles of ice thickness from a SPRI-designed radio echo sounder around the three arms of the northern triangle, *ADJ* of the Wilkes ice cap (cf. Fig. 6.9). For the line *DJ*, surface slopes and bedrock elevations from the radio echo sounder results have been plotted for each 1·5 km. The bedrock elevations from the earlier gravity and seismic results [cf. Morgan (unpublished)] are also shown (Fig. 6.10).

It is immediately clear that, although there is a very close agreement between the two profiles on the broad scale, the short wave undulations have been greatly damped out in the gravity survey.

The following qualitative points are noted:

(1) Although the broadness of the 1·5 km point spacing prohibits the analysis of the very short wave undulations ($\lambda < 5$ km), there does appear to be a predominant surface wavelength between 5 and 10 km. A detailed amplitude-frequency spectrum would be required to confirm this.

(2) It also appears that the surface undulations do reflect the bedrock and, as predicted by the theory, the surface slopes are generally in phase with the bedrock elevations. From Fig. 6.9 it is clear that the actual flow direction does depart from the profile line, particularly in the region of strain grid *G*. This leads to a phase shift such that surface and basal slopes are out of phase by less than $\pi/2$.

(3) The high slope variations near the coast indicate that the damping is less here, where the ice thickness is smaller, and the forward velocity is greater.

L. Pfitzner (to be published) has made a preliminary quantitative analysis of these results by reference to the theory of Section 5.4, in particular formula (51) above.

In Table 6.6 are shown the values of λ, Z, λ/Z, V, α_1, β_1, ψ, B for the predominant obvious waves along the line. From this the mean wave length was found to be $\lambda = 7{\cdot}31\ Z$.

The damping factor (ψ) (mean $\psi^{-1} = 0{\cdot}086$), did tend to decrease approaching the coast.

From this table a mean value of B was calculated as $5{\cdot}4 \times 10^{13}$ dyne $\text{cm}^{-2}\text{sec}^{1/3}$. The B value also decreased towards the coast as expected from the temperature distributions.

This mean value of B differs only slightly from the value of B obtained along this line by McLaren (1968) from the variation in strain rate over the undulations. In units of dynes $\text{cm}^{-2}\text{sec}^{1/3}$: strain rates $B = 1{\cdot}5 \times 10^9$,
damping factor $B = 1{\cdot}7 \times 10^9$.

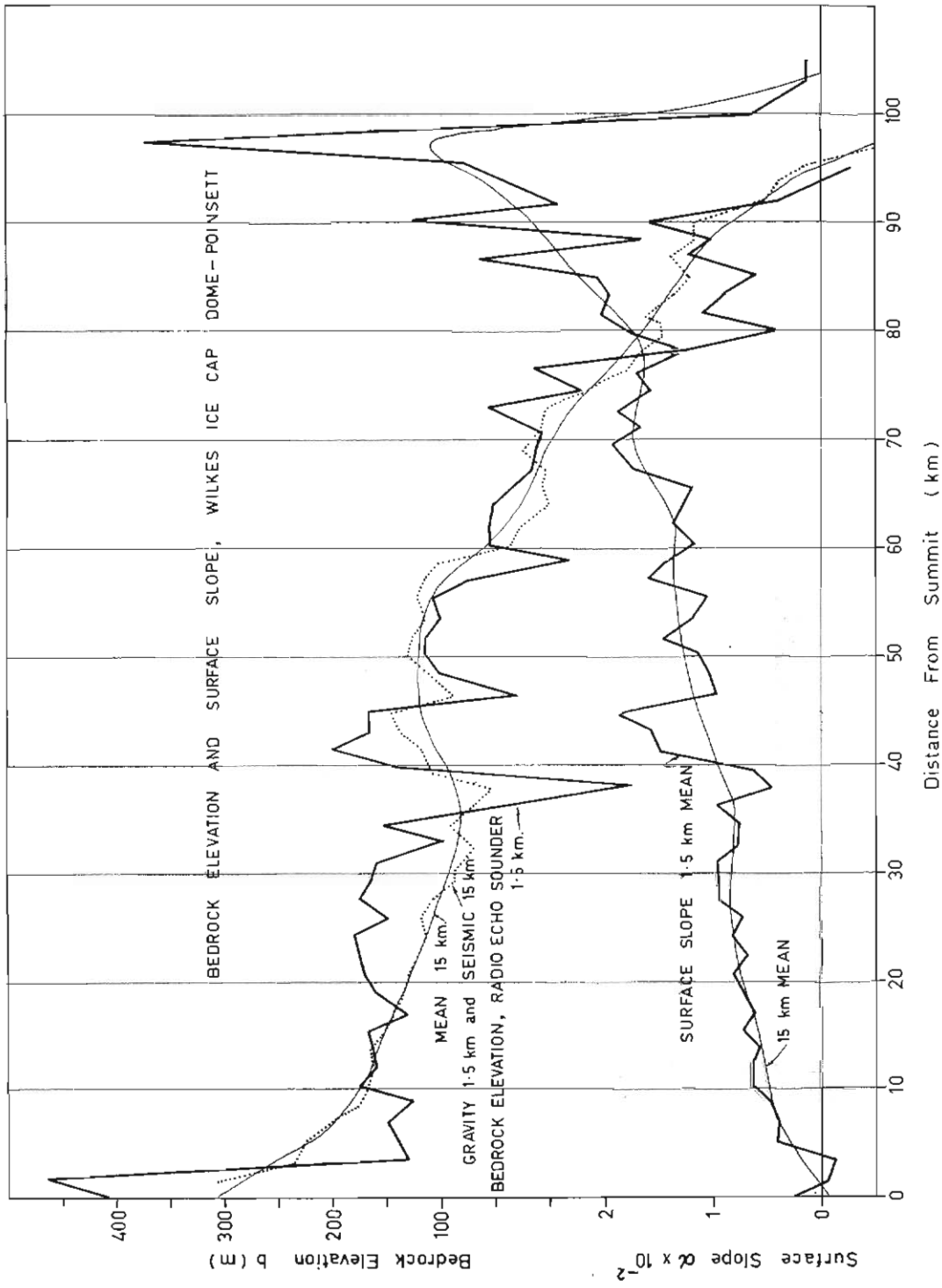

FIG. 6.10. Surface slopes and bedrock elevations (1·5 km spot values) show reasonable correlation and, near the coast where the flow direction is close to this profile, they tend to be in phase.

TABLE 6.6

FLOW PARAMETER FROM DAMPING FACTOR

$$B = \frac{\rho g Z^2}{4\pi V}\left[\frac{\lambda}{Z} + \frac{4\pi^2 Z}{3\lambda}\right]\frac{\alpha_2}{\beta_1}$$

Distance from dome x km	Wavelength λ km	Ice thickness Z km	Bedrock variation $2b_1$ m	λ/Z	$\left[\frac{\lambda}{Z} + \frac{4\pi^2 Z}{3\lambda}\right]$	Velocity V m yr^{-1}	Slope variation $2\alpha_2$ 10^{-2}	Damping $\psi^{-1} = \frac{\lambda\alpha_2}{2\pi b_1}$	Flow law parameter B 10^{15}dynes cm^{-2}sec$^{1/3}$
6	5·0	1·16	20	4·3	7·4	1·3	0·35	0·139	24·10
13	8·0	1·16	40	6·9	8·8	4·0	0·15	0·048	32·20
22	9·0	1·14	40	7·9	9·6	8·3	0·10	0·036	12·30
30	7·5	1·10	40	6·8	8·7	12·0	0·25	0·075	14·90
37	4·5	1·05	90	4·3	7·4	12·0	0·40	0·032	4·90
43	8·5	1·00	230	8·5	10·0	14·0	1·00	0·059	9·54
50	8·0	0·93	50	8·6	10·1	18·0	0·35	0·089	9·76
57	5·5	0·86	50	6·4	8·5	22·0	1·00	0·175	11·30
65	10·0	0·80	75	12·5	13·6	26·0	0·40	0·085	6·45
72	4·5	0·72	60	6·3	8·4	33·0	0·45	0·054	1·61
77	5·0	0·69	90	7·3	9·1	37·0	0·25	0·022	0·57
81	6·0	0·66	50	9·1	10·5	40·0	0·45	0·086	2·21
87	4·0	0·59	40	6·8	8·7	47·0	1·25	0·199	2·91
90	3·5	0·53	83	6·6	8·6	54·0	1·70	0·114	1·15
Means	6·36	0·885	68·4	7·31	9·02	23·5	0·579	0·0857	5·40

For the dome—Cape Folger line (D/A), the wavelengths are similar but the velocities are much lower. The damping factor is also much lower and, as a consequence, the value of B determined for this line only differs slightly from that for the other, thus confirming the previous results from strain measurements.

This analysis is only preliminary but suggests that variations in surface and bedrock elevations over undulations and damping factors provide a valuable further means of investigating the flow properties of the ice masses. A more detailed analysis is being carried out by Carter, using more closely spaced intervals of 400 m and performing spectral analyses of the surface and bedrock elevations, as well as the cross-spectra to test more thoroughly the ice flow predictions.

7. MASS BALANCE AND STATE OF CHANGE

7.1 INTRODUCTION

This section deals with the problem of whether or not the existing pattern of accumulation over an ice mass exactly balances everywhere the change in the ice mass due to movement. In the case of exact balance, the shape and size of the ice mass remains constant in time. If exact balance does not exist everywhere, parts of the ice mass will be changing thickness in time. In this analysis we wish to devise means of answering the following types of questions:

(1) Given a fixed accumulation pattern over a certain area, and constant temperature and ice flow parameters, will an ice cap develop with a shape and size which remain constant, provided all other parameters are constant with time?

(2) What is this "steady-state" shape for the given parameters, and how does it depend on the accumulation pattern and flow law parameters of the ice?

(3) How does an ice mass change when it is not in steady state? What is the steady state corresponding to its present accumulation profile? Is the shape tending towards the steady-state shape or not?

(4) How can the history of an ice cap, i.e., its build-up and decay, be related to the changes in accumulation patterns and the ice flow parameters, which are temperature-dependent?

Hence, to obtain answers to these questions in the following sections we examine the conditions for balance over an ice cap, imbalance and the resultant state of change, the elevation profiles of existing ice caps and their dependence on accumulation, bedrock topography and the flow law parameters; and, finally, the paths of particles with time through the ice cap and the age of the ice.

7.2. CONDITIONS FOR BALANCED STATE

We consider a generalized sector of an ice cap between two flow lines which are a small distance s apart at distance r from the centre (cf. Fig. 7.1, above).

Let V be the average forward velocity at position r where the ice thickness is H and the accumulation rate A.

Then the condition for balance state is that the flow across the area sH equals the accumulation over the area between the flow lines inland of the section at distance r,

i.e., $$d(sVH) = sAdr \tag{1}$$

or $$sVH = \int_0^r sAdr \tag{2}$$

Now, we define $\overline{A}_r$ as the mean accumulation rate over the sector between the flow lines from the centre to distance r, by

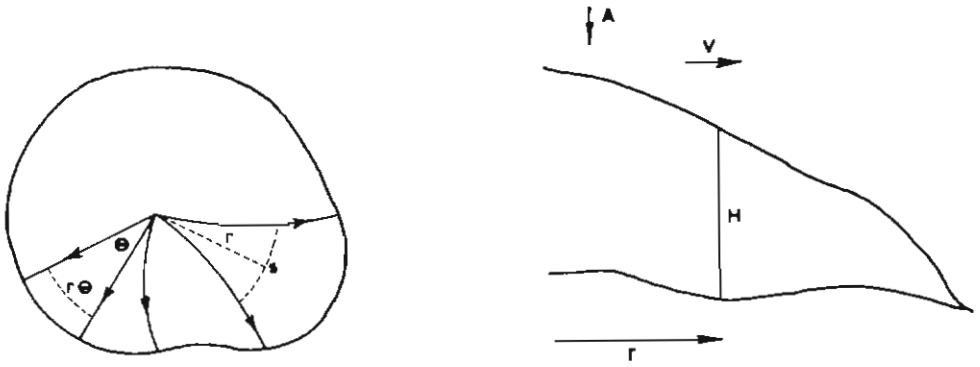

FIG. 7.1.

$$\bar{A}_r = \frac{\int_0^r sAdr}{\int_0^r sdr} = \frac{\int_0^r sAdr}{S_r} \tag{3}$$

where S_r is the area between the flow lines to distance r.

Equation (2) may then be written:

$$sHV = S_r\bar{A}_r \tag{2'}$$

For the special case where the angle of divergence (θ) of the flow lines is constant, we have the corresponding equations:

$$d(rVH) = rAdr \tag{1b}$$

$$rVH = \int_0^r Ardr \tag{2b}$$

and

$$VH = \tfrac{1}{2}\bar{A}_r r, \tag{2'b}$$

where

$$\bar{A}_r = \frac{2\int_0^r Ardr}{r} \tag{3b}$$

When the divergence angle θ is zero this result reduces to that for two dimensions or a cylindrical cross-section, i.e.,

$$d(VH) = Adx \tag{1c}$$

or

$$VH = \bar{A}_x x \tag{2'c}$$

..here

$$\bar{A}_x = \frac{1}{x}\int_0^x Adx \tag{3c}$$

For the case of the ice cap above, with constant divergence angle, we note the balance velocity is obtained from equation (2'b) as

$$V^* = \frac{\bar{A}_r r}{2H} \tag{4}$$

For the case of zero divergence the balance velocity corresponding to (4) is given by

$$V_x^* = \frac{\bar{A}_x x}{H} \tag{4c}$$

Differentiating (4), we obtain the balance longitudinal strain rate as given (dropping the subscript $_r$ on $\bar{A}$) by

$$\dot{\varepsilon}_r^* = \frac{\bar{A}}{2H} - \frac{\bar{A}r}{2H}\frac{dH}{dr} + \frac{r}{2H}\frac{d\bar{A}}{dr} \tag{5}$$

An alternative form for the strain rate may be obtained in terms of the velocity V from equation (1b) as

$$\dot{\varepsilon}_r = \frac{V}{H}\frac{dH}{dr} + \frac{V}{r} + \frac{A}{H} \tag{6}$$

These equations may be used to answer questions (2) and (3) of Section 7.1. Specifically, they permit the derivation of the required veloeities and strain rates for balance from given profiles of ice thickness and accumulation along a flow line. If, in addition, the velocities and strain rates are measured, then a check can bc made on the state of balance of the ice mass along the flow line.

In the case where balance does not occur, equation (2′b) may be also considered as defining the required accumulation profile A^* to balance the actual velocity and thickness profile, i.e.,

$$\bar{A}^* = \frac{2VH}{r} \tag{7}$$

or, for the case of zero divergence,

$$\bar{A}_x^* = \frac{VH}{x} \tag{7c}$$

i.e., half the accumulation for the same velocity and thickness profile as that required for an ideal circular ice cap.

Similarly, we can use (1b) to obtain for the balance accumulation

$$A^* = \frac{1}{r}\frac{d(rVH)}{dr} \tag{8}$$

7.3. IMBALANCE AND STATE OF CHANGE

In general, for an ice mass where the accumulation does not everywhere balance the change due to movement, there will be a resultant net change in form (given by the variation in elevation, or ice thickness, contours with time). The net change in ice thickness in time $\frac{\partial H}{\partial t}$ over a fixed point of the bedrock, depends on the accumulation rate A, the basal melt rate M, the ice thickness H and mean vertical strain rate $\dot{\varepsilon}_z = (\dot{\varepsilon}_x + \dot{\varepsilon}_y)$, the horizontal velocity V and the surface and basal slopes, α, β, according to the relation.

$$\frac{\partial H}{\partial t} = A - M + H\dot{\varepsilon}_z + V(\alpha - \beta) \tag{9}$$

All terms are calculated in units of cm of ice per year, and we neglect the variation in density in the surface layers of the ice mass.

If all the parameters on the right-hand-side of equation (9) are known over the ice cap, then the change in shape can be calculated. The change in thickness with time can also be computed from generalizations of (7) and (8) from

$$\frac{\overline{\partial H}}{\partial t} = \overline{A}_r - \frac{\overline{2VH}}{r} \tag{10}$$

or

$$\frac{\partial H}{\partial t} = A - \frac{1}{r}\frac{d(rVH)}{dr} \tag{11}$$

for a circular ice cap of constant divergence angle. For the more general case from (1)

$$\frac{\partial H}{\partial t} = A - \frac{1}{s}\frac{d(sHV)}{dr} \tag{12}$$

and for the mean rate of surface-lowering $\frac{\overline{\partial H}}{\partial t}$ over the total area S between two flow lines we have

$$\frac{\overline{\partial H}}{\partial t} = \overline{A} - \frac{\overline{sHV}}{S} \tag{13}$$

Using the equations (11) and (13) the surface-lowering at each point of the surface of the ice cap can be calculated where the accumulation rate, ice thickness and velocity are known. From equations (10) and (12) the average lowering over a sector may be calculated. These results should agree with those obtained from equation (9) and thus provide a check on the accuracy and validity of the method.

For the Wilkes ice cap the results of these calculations by L. Pfitzner (to be published) for the surface-lowering are shown in Fig. 7.2. It can be seen from this figure that the ice cap is not stationary. The western side is remaining fairly stationary but the north-eastern section is lowering rapidly, thus changing the ice-cap shape. This section of the ice cap is already lower than other parts of the same distance from the centre and extrapolation back in time suggests that, if the present rate of change has been constant, then the ice cap was close to symmetrical about 400 years ago.

A direct check on the state of change of an ice mass can be carried out by making precise measurements of the elevation profile, and the rate of change of this elevation profile with time. Several methods are commonly used to determine elevation or elevation change of an ice mass:

(i) Precise optical levelling traverses over the ice-cap surface can determine elevations to within a fraction of a metre over 100 km. This is generally a laborious and slow process, and to detect vertical change the whole line must be relevelled at a later date. A 100 km optical levelling profile from Wilkes to the summit of the local ice cap and back was carried out by Pfitzner in 1966. The round trip closure error was less than ± 30 cm.

(ii) Repeated aerial photogrammetry. Provided there is sufficient ground control and at the same time adequate markers and features exist on the ice mass

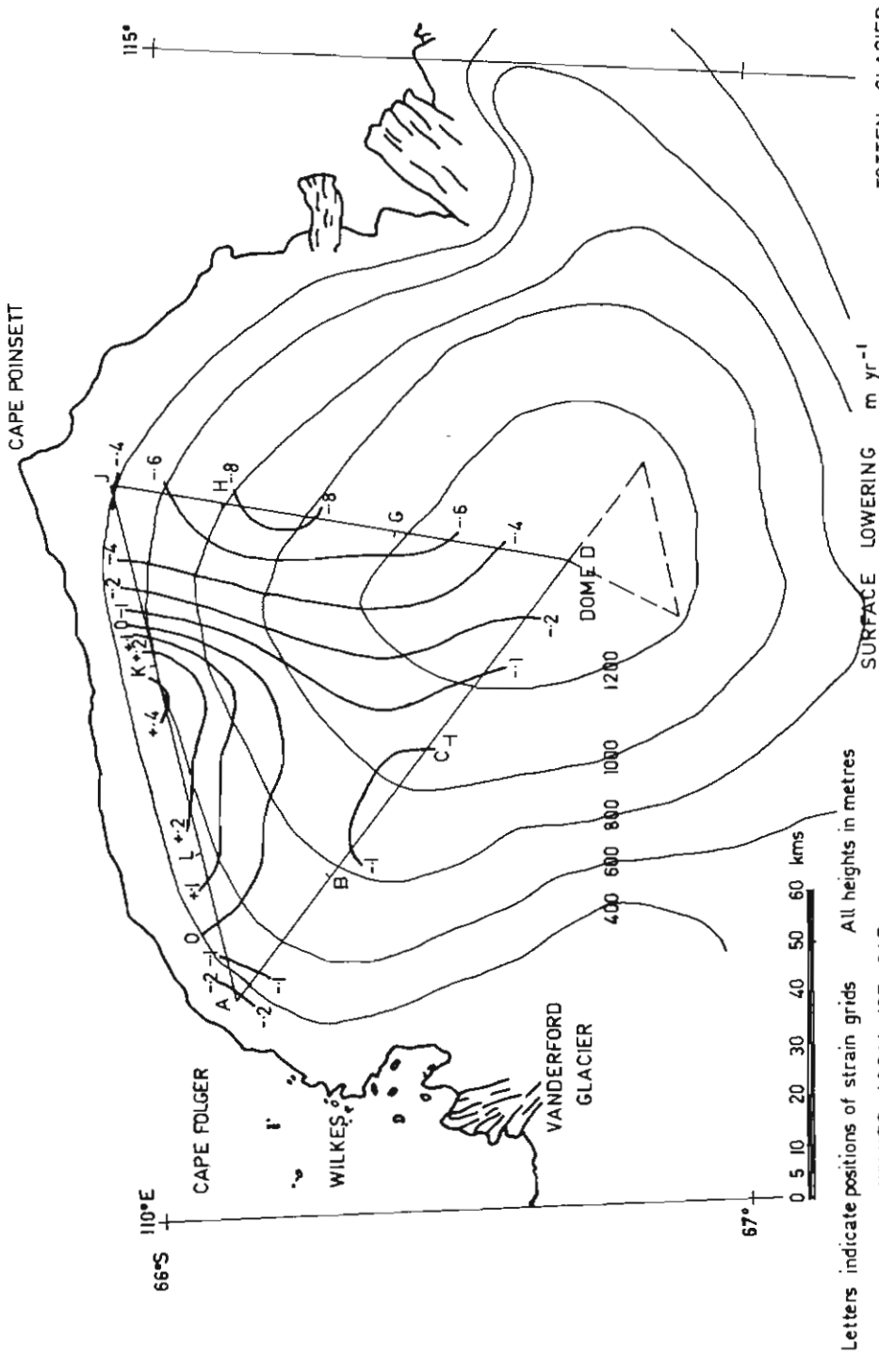

FIG. 7.2. Annual net surface-lowering rates from flux divergence calculations using measured velocities, strains and accumulation rates [after Pfitzner (to be published)].

surface, an accuracy of 1 metre or better may be achieved for vertical heighting with present high order cameras and plotting machines (cf. Blachut and Müller 1966, Konecny 1966, Kick 1966).

(iii) Repeated gravity readings at a marker on the ice surface can reveal its height change. Ideally, the remeasurements should be over the same point of the bedrock. If the horizontal movement of the ice is small compared to the ice thickness, then the change in gravity (Δg) at a marker on the surface depends only on the lowering of the elevation (ΔE) and the change in ice thickness (ΔH), assuming the density profile remains constant, i.e.,

$$\Delta g = \lambda \Delta E + \mu \rho \Delta H \tag{14}$$

where λ is the variation in gravity with elevation ($\simeq -0{\cdot}31$ mgal/m) (cf. Dobrin 1960),

ρ is the ice specific gravity $\simeq 0{\cdot}917$,

μ is the attraction coefficient of an infinite slab of unit thickness and of unit density contrast ($\simeq 0{\cdot}042$ mgal/m).

For a lowering or rising ice cap following a point on the surface of a column of ice where the accumulation rate is A, the basal melt rate M, the ice thickness H, vertical strain rate $\dot{\varepsilon}_z$, velocity V, and basal slope β the change in elevation in time Δt is given by

$$\Delta E = (A - M + H\dot{\varepsilon}_z - V\beta)\Delta t \tag{15}$$

and the change in ice thickness by

$$\Delta H = (A - M + H\dot{\varepsilon}_z)\Delta t \tag{16}$$

Hence, we obtain for the gravity change (Δg)

$$\Delta g = (\lambda + \mu\rho)\Delta E + \mu\rho V\beta\Delta t,$$

or

$$\Delta E = \frac{\Delta g}{(\lambda + \mu\rho)} - \frac{\mu\rho V\beta\Delta t}{(\lambda + \mu\rho)} \tag{17}$$

$$= -3{\cdot}7\Delta g + {\cdot}10V\beta\Delta t \text{ m}.$$

The change in ice thickness over a fixed point in the bedrock is given by

$$\delta H = \Delta E + V\alpha\Delta t.$$

Table (1) shows the preliminary repeated gravity measurements by D. Carter in 1967 at the strain grid positions over the Wilkes ice cap and the calculated elevation changes. Also shown are the elevation changes calculated by L. Pfitzner from the measurements of strains, movement, ice thickness, slopes, and accumulation rates, at each of the strain grids for the surface of the column of ice moving with the surface marker down the slope.

TABLE 7.1

ICE CAP LOWERING FROM (g) GRAVITY VARIATION (f) FLUX DIVERGENCE

Strain grid		A	B	C	D	G	H	J	K	L
Lowering rate m yr^{-1}	f	0·4	0·5	0·5	1·5	2·0	2·4	(5)	0·4	0·6
	g	0·5	0·6	0·6	1·3	1·3	2·2	3·0	1·5	0·9

It can be seen that the lowering deduced from the gravity results (in spite of still large errors at this stage) agrees fairly well with that calculated from the flux

divergenee. Precise measurements of this kind can be used to detect the difference between $\dot{\varepsilon}_z$ the mean strain rate through the ice and $\dot{\varepsilon}_z$ the strain rate at the surface. Since, from Sections 5 and 6, the strain rates can be very local it is important to obtain regional averages over a considerable area, rather than single spot values.

7.4. ICE CAP SURFACE ELEVATION PROFILES

We found in Section 6 that the velocity profile from the centre to the edge of an ice cap was largely governed by the ice thickness, surface slope, and the flow parameters of the ice. We have also seen above that, for certain values of the parameters V, H, A, α, β, the ice cap surface remained stationary in time. If the accumulation is too large for balance, then the ice cap increases in thickness. This increases the velocity and outward flow and so at some stage the point of balance may be reached. We now examine the shape of the ice cap profile for the stationary state. This question has been treated by many workers including Nye (1959), Weertman (1961 a and b, and 1964), Haefeli (1961), Shoumsky (1963), Lliboutry (1965). The following approach is similar to Haefeli's, since the velocity —slope—thickness law used here is similar to his, except that the variation of the flow parameter B with temperature is included here.

For the case in which the longitudinal thickness—strain rate gradient is small,

i.e., $$\frac{\partial H B \dot{\varepsilon}_x^{1/n}}{\partial x} \to 0.$$

A simple power relation holds between velocity V, ice thickness H and surface slope α, and the flow law parameters n and B, viz., 5(40),

$$V = \frac{2H^{n+1}}{n+1}\left(\frac{\rho g \alpha}{B}\right)^n \tag{18}$$

Now, for the balanced state we see that equation (2′b) gives a relation between velocity, ice thickness and accumulation rate (for an ice cap of constant divergence angle).

$$VH = \tfrac{1}{2}\bar{A}_r r$$

Hence, we can obtain a balanced state profile by equating these two velocities, viz. (dropping the subscript r),

$$\frac{\bar{A}r}{2H} = \frac{2H^{n+1}}{n+1}\left(\frac{\rho g \alpha}{B}\right)^n \tag{19}$$

For zero divergence the analogous equation is

$$\frac{\bar{A}_x}{H} = \frac{2H^{n+1}}{n+1}\left(\frac{\rho g \alpha}{B}\right)^n$$

which corresponds to a similar profile to (19), but with double the accumulation rate. It is shown below that this only makes a small difference in the shape.

For the more general ice cap, where the flow line divergence angle is not constant, the corresponding relation is found from (2′) as

$$\frac{S_r \bar{A}_r}{sH} = \frac{2H^{n+1}}{n+1}\left(\frac{\rho g \alpha}{B}\right)^n \tag{19′}$$

7.4.1. *Effect of bedrock slope*

We note that the equation

$$\alpha = -\frac{dH}{dr} + \beta \tag{20}$$

relates the surface slope to the ice-thickness gradient and the bedrock slope.

Hence, from (19) and (20),

$$\overline{A}r = \frac{4}{n+1} H^{n+2} \left[\frac{\rho g}{B}\left(-\frac{dH}{dr} + \beta\right)\right]^n \tag{21}$$

or

$$\left(\frac{n+1}{4} Ar\right)^{1/n} = -H^{1+2/n} \frac{\rho g}{B}\left(\frac{dH}{dr} - \beta\right).$$

We may express the bedrock slope as $-\frac{db}{dr}$, where b is the bedrock elevation.

Equation (21) may then be integrated, assuming for the moment A, and B are constant, to give:

$$-\left(\frac{n+1}{4}\overline{A}\right)^{1/n} r^{1+1/n} = \frac{\rho g}{2B} H^{2+2/n} + \left(\frac{n+1}{n}\right)\frac{\rho g}{B}\int H^{1+2/n} db + C \tag{22}$$

In many cases the height of the bedrock b is small compared to the ice thickness H, and so may be neglected. In general, this equation can be integrated numerically from the irregular functions of $b(r)$ and $H(r)$, as pointed out by Nye (1959).

To obtain an idea on the general effect of the bedrock on the steady-state surface profile, we consider the particular case where the bedrock height is everywhere a certain constant small proportion (ν) of the ice thickness.

We then have $db = \nu dH$, and so from (22)

$$-\left(\frac{n+1}{4}\overline{A}\right)^{1/n} r^{1+1/n} = \frac{\rho g}{2B} H^{2+2/n}(1+\nu) + C \tag{23}$$

In this case, the basic "shape" of the surface is unchanged and, since ν is generally less than 25%, only a slight change is made to the profile. The net effect is equivalent to having a smaller value of B given by

$$B^* = \frac{B}{1+\nu}.$$

Furthermore, we notice from equation (23), in answer to questions 1 and 2 of Section 7.1, that, given constant conditions (of accumulation A and flow law parameters n and B), then a steady-state profile will develop, but this profile is not unique since the boundary value C is determined by a ratio of H/r. Hence, for a profile to be unique, the extent r_0 must also be specified. In practice, the extent is generally determined by such external factors as bedrock height, sea-water action, air temperature and ablation rates.

From equations (10) and (18)

$$\frac{\partial H}{\partial t} = \overline{A}_r - \frac{4H^{n+2}}{(n+1)r}\left(\frac{\rho g \alpha}{B}\right)^n \tag{24}$$

This result indicates that, if $\overline{A}_r$ or B change from the balance values, the ice thickness will change in such a way as to tend back towards steady-state. However, the possibility of uneven distributions of A and $\partial H/\partial t$ exists which could give rise to waves, surges and oscillations with phase delays and consequent "hunting", without actually reaching equilibrium more than momentarily.

We now examine in more detail the profile on a flat base, i.e., for $\beta = 0$. If we write

$$r = r_0 \quad \text{when} \quad H = 0,$$

and

$$H = H_0 \quad \text{when} \quad r = 0,$$

we may write equation (23) as

$$\left(\frac{H}{H_0}\right)^{2+2/n} + \left(\frac{r}{r_0}\right)^{1+1/n} = 1 \tag{25}$$

This is the equation derived by Haefeli (1961) and differs from that of Nye (1959) viz.,

$$\left(\frac{H}{H_0}\right)^{2+1/m} + \left(\frac{r}{r_0}\right)^{1+1/m} = 1 \tag{26}$$

in the exponent of $\left(\frac{H}{H_0}\right)$ (i.e., $2 + 1/m$ compared to $2 + 2/n$) and that Nye's m is the exponent of an assumed relation between stress τ and velocity V of the form

$$V \propto \tau^m,$$

where $m = \dfrac{n+1}{2}$ for sliding, i.e., for $n = 1 \quad 2 \quad 3 \quad 4,$

$$m = 1 \quad 1{\cdot}5 \quad 2 \quad 2{\cdot}5.$$

Hence, we see that for $n \simeq 3$ or 4 the two profiles of Haefeli and Nye do not differ very greatly. Nye (1959) pointed out that the profile (26) tended to a parabola as $m \to \infty$, the case of perfect plasticity. Ths also holds for the profile (25).

7.4.2. *Effect of flow parameter B*

In general, the flow parameter B varies with temperature. The average temperature (θ) through the ice cap may be expected to decrease as tbe surface elevation increases. Thus, if the value of B typical of the ice mass depended on the average temperature through the ice, then it might be expected that B increases with H. In this case it can be seen from equation (21) that, if

$$B \propto (1 - \theta)^{1/n},$$

as used by Shoumsky (1961), and if

$$\theta \propto H,$$

then

$$\frac{H^{1+2/n}}{B} \simeq kH^{1+1/n},$$

where k is constant. The profile (25) then reduces to that of Nye, with m replaced by n.

But, since most of the shear occurs in the basal layers, the temperature there, rather than the average through the ice, is most relevant for the value of B. From the results of Section (4) on the temperature distributions in ice caps, it appears that the basal temperatures may typically decrease inland, but depend on the ice thickness accumulation, velocity, etc., so that a detailed general discussion of the temperature effects on the profile is too extensive to be included here.

From equations (23) and (25) we obtain the following relation between the maximum height, H_0, width, r_0, accumulation rate A, and flow parameters n and B (assumed constant here),

$$\frac{H_0^2}{r_0} = \left(\frac{2B}{\rho g}\right)^{n/n+1} \left(\frac{n+1}{4}\bar{A}^*\right)^{1/n+1} (1+\bar{v}) \tag{27}$$

where for balance $\bar{A}^* = \bar{A}$,

and for non-balance $\bar{A}^* = \bar{A} - \dfrac{\partial H}{\partial t}$.

From this we obtain an estimate for B as

$$\bar{B} = \frac{\rho g}{2}\left(\frac{4}{(n+1)\bar{A}^*}\right)^{1/n} \left(\frac{H_0^2}{r_0}\right)^{(n+1)/n} (1+\bar{v}) \tag{28}$$

Hence, if we know the value of n, the value of B can be estimated from the size of the ice mass and the accumulation rate.

The value of n may first be determined from the velocity—slope—thickness law, equation (18), provided we know a velocity profile.

It can be seen that the parameter B (if constant over the region) only affects the size and not the shape. The shape is then determined primarily by the parameter n. Haefeli (1961) shows the profiles of equation (25) for several values of n and shows how different ice masses compare with them. The results suggest that the appropriate values of n lie between 3 and 4, as found for the Wilkes ice cap.

If B is not constant and is known as a function of r, equation (21) can be written as

$$\frac{n+1}{4} A^{1/n} B r^{1/n} = H^{1+1/n} \rho g \frac{dH}{dr},$$

and integrated to give the new shape.

Table 7.2 shows estimated mean values of $\bar{B}$ from equation (28) for various ice-cap profiles.

For Roosevelt Island and Greenland, zero divergence has been assumed while, for the remainder, ideal circular divergence has been assumed.

The values of accumulation listed for Wilkes are the balance accumulation $\bar{A}^*$. For the other ice caps the actual accumulation is used. If Greenland were sinking and the Antarctic rising, then using balance accumulations would bring their values closer together. The errors in the value of B are about $\pm 0{\cdot}2 \times 10^9$, and so we conclude that the effective average values of B do not differ by more than the estimated error for the different ice caps. This means that the calculated values are not sufficiently accurate to differentiate between different average basal temperatures

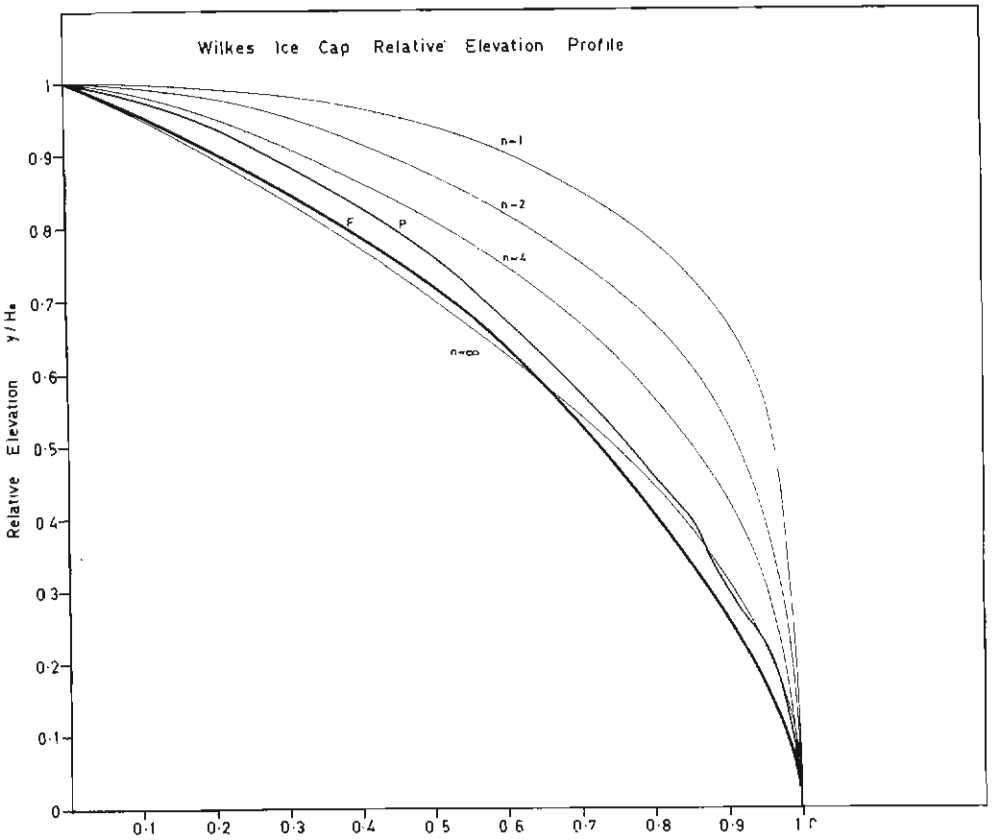

FIG. 7.3a. The relative elevation profiles for the dome—Cape Folger line (F) and the dome—Cape Poinsett line (P) only differ slightly from the parabola ($n = \infty$).

TABLE 7.2

FLOW PARAMETER $\bar{B}$ FOR STEADY-STATE PROFILES FOR ICE CAPS

Ice cap	r_0 km	H_0 m	A g cm^{-2}	$\bar{\nu}$	B dynes cm^{-2}sec$^{1/3}$	Comments	Data
Drygalski I.	10	426	70	0·05	$0{\cdot}75 \times 10^9$	Average whole island	Bakayev 1967
Roosevelt I.	40	760	20	0·10	$0{\cdot}71 \times 10^9$	Central E-W section	Clapp 1965
Wilkes (a)	96	1200	(100)	0·20	$0{\cdot}75 \times 10^9$	Dome to Poinsett	McLaren 1968
Wilkes (b)	115	1200	(30)	0·42	$0{\cdot}75 \times 10^9$	Dome to Folger	McLaren 1968
Greenland	560	3200	45	0	$0{\cdot}73 \times 10^9$	EGIG profile	Bader 1961
Antarctica	1200	3700	15	0	$0{\cdot}68 \times 10^9$	Inland of Wilkes and Mirny	Bakayev 1967 Battye (unpublished)

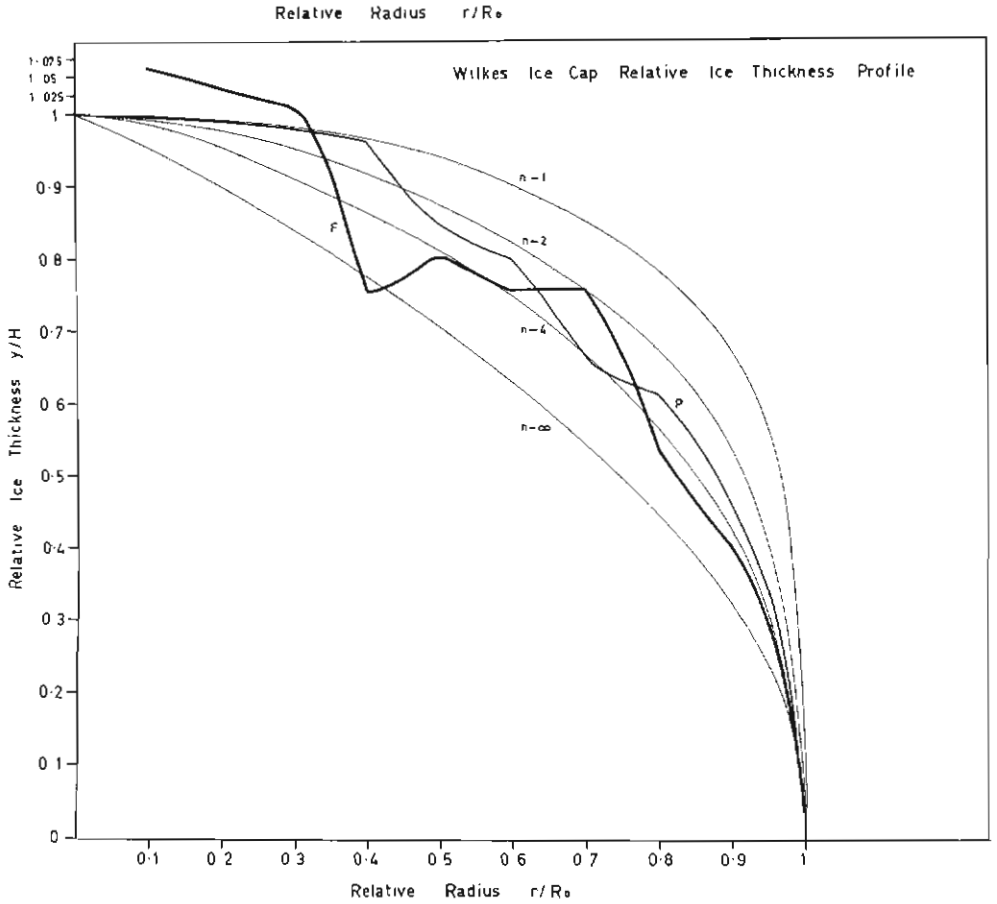

FIG. 7.3b. Relative ice-thickness profiles conform more closely to $n = 3$ to 4.

for the ice caps. The values found for Wilkes are close to the values obtained from the velocity—slope thickness profiles of equation (18) ($0{\cdot}85 \times 10^9$ dynes cm^{-2} sec$^{-\frac{1}{3}}$) and indicate a mean basal temperature of about $-10°$C, (cf. Section 6.3.1). For a more precise anaysis the variation in the bedrock elevation, according to equation (22), should be considered.

From equation (27) it is also evident that, with other parameters constant, the variation of maximum ice-thickness with the average value of the flow parameter B is given by

$$H_0 \propto B^{n/2(n+1)} \text{ or, for } n = 3, H_0 \propto B^{3/8}$$

7.4.3. *Effect of accumulation*

From equations (24) and (25)—assuming *constant accumulation* over the area, and constant flow parameters—we see how the general steady-state ice cap *size* depends on the accumulation. The actual *shape* is dependent only on the n value (or the variation with r in the various parameters), but the ratio of the

maximum height to the width depends on the accumulation rate. From equation (27) we see that for a given radius r_0 the maximum thickness is proportional to the $\frac{1}{2(n+1)}$th power of the accumulation,

i.e., $H_0 \propto A^{1/2(n+1)}$, or for $n = 3$ $H_0 \propto A^{1/8}$

For the same extent and flow parameters, with $n = 3$, the rectangular-type ice cap (with zero divergence) is $2^{\frac{1}{8}}$ 1·04 times the height of the corresponding circular ice-cap.

A similar conclusion for the low power of the accumulation rate was reached by Nye (1959). As Haefeli (1961) pointed out, the consequence of this general relation is that the accumulation rate has only slight effect on the maximum height of an ice mass. However, this conclusion is only valid for the radius r_0 held constant. If the accumulation rate were to increase, the ice mass would generally expand laterally as well as increase in thickness. In reality, the limit of the extent of the ice mass may more often be governed by the basal topography, sea water, and the prevailing temperatures.

For a constant height in the centre, and constant flow parameters, the extent of an ice cap is related to the accumulation rate as follows:

$$r_0 \propto \frac{1}{A^{1/n+1}}.$$

As a particular example of this, we notice for the Wilkes ice cap the different extents r_1 and r_2 on the sides of different accumulation rates: A_1 for the dome—Cape Poinsett line and A_2 for the dome—Cape Folger line, shown in Table 2. Although $A_1 = .3A_2$ the resultant B values only differ slightly.

In the case of zero divergence, it is evident from (27), (7) and (7c) that the extent of an ideal circular ice-cap is $2^{\frac{1}{n+1}}$, or $\simeq 1{\cdot}19$ for $n = 3$, times the extent of the corresponding rectangular or two-dimensional model. For regions of convergence the reduction in extent is even more pronounced.

A further point noted by Haefeli was that the larger the ice mass, the smaller is the ratio of ice thickness to radius (provided the other parameters are the same). Table 7.3 lists the radius R_0 and maximum ice thickness H_0 (above the zero bedrock) and the ratios H_0/R_0 and H_0^2/R_0 for a range of ice-cap sizes.

TABLE 7.3

RELATIVE DIMENSIONS OF VARIOUS ICE CAPS

Ice cap	Mean Radius or width R_0 km	Height H_0 m	H_0/R_0 $\times 10^2$	H_0^2/R_0 10 m
Drygalski	10	426	5·30	1.80
Roosevelt	40	760	1·90	1·40
Wilkes	115	1200	0.96	1·26
Greenland	560	3200	0·17	1·35
Antarctic	1200	3700	0·03	1·15

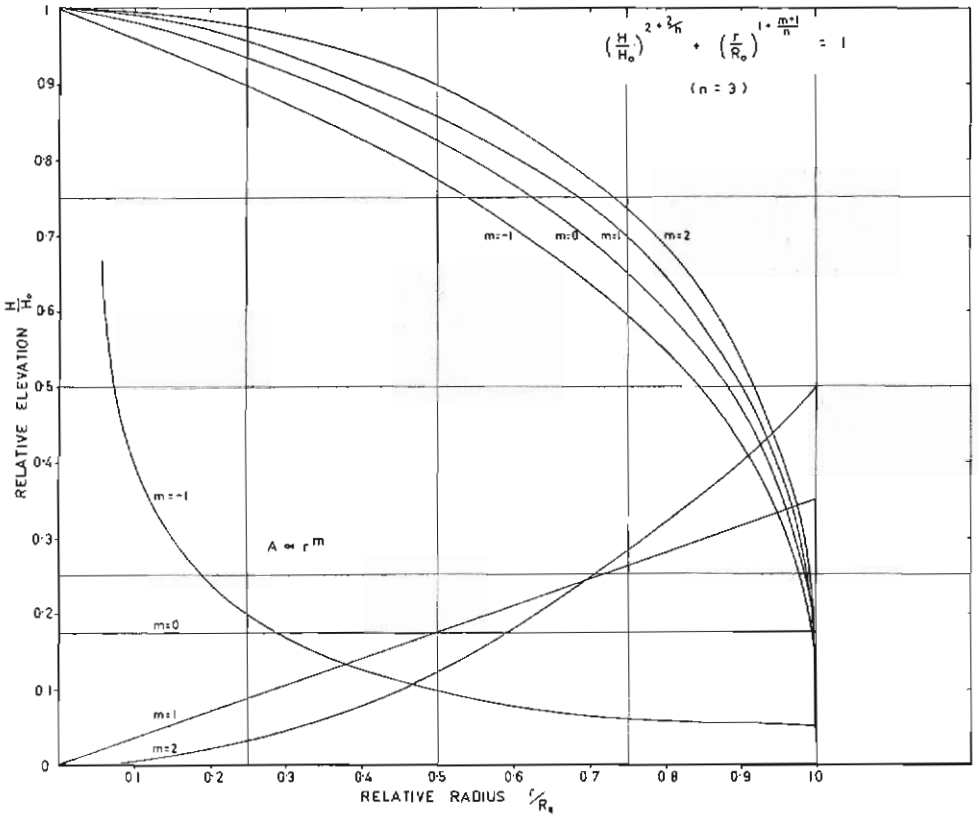

FIG. 7.3c. The effect of the form of the accumulation profile on the steady-state shape of an ice cap is illustrated for four types of accumulation profiles $A \propto r^m$ for the ice cap profile, with power law flow B constant and $n = 3$.

The table confirms Haefeli's qualitative prediction and, furthermore, shows that the ratio H_0^2/R_0 remains remarkably stable. Table 7.2 shows that part of the residual variation in H_0^2/R_0 is due to the different divergence and accumulation rates.

In general, it is unusual to find the accumulation rate constant from the centre to the edge. However, if we know $\bar{A}(r)$ as a function of r, then equation (21) can be readily integrated to give the appropriate steady-state profile.

As an example, suppose $\bar{A}(r) = ar^m$, where a, m are constant, and further, for the present, $\beta \simeq 0$, B is constant. Then equation (21) reduces to

$$\left(\frac{n+1}{4} a r^{m+1}\right)^{1/n} = -H^{1+2/n} \frac{\rho g}{B} \frac{dH}{dr} \tag{29}$$

Integrating, we obtain similarly as before

$$\left(\frac{H}{H_0}\right)^{2+2/n} + \left(\frac{r}{r_0}\right)^{1+(m+1)/n} = 1 \tag{30}$$

This indicates that, although the magnitude of a constant accumulation rate over the area does not affect the shape of the profile, the *pattern* of the accumulation

rate does. Fig. 7.3c shows how different typical patterns of accumulation rate affect the steady-state shape of the ice mass.

7.5. PARTICLE PATHS AND AGE OF THE ICE

In studying the history of an ice mass the main task is to extrapolate forward or backward in time the positions of each particle of the ice along its flow path. In general, as the surface rises or falls at a rate depending on the degree of imbalance of the budget, there will be a change in the ice cap boundary as well. This change of form of the ice masses causes the velocity distribution to change, which makes the extrapolation, in time, of the ice particle positions very complex. Hence, to begin with, we study the particle paths for an ice cap in steady-state.

This problem has been discussed by several workers, including Crary, *et al.* (1962) for the Ross Ice Shelf, Haefeli (1963) for Greenland, Meier (1960) for the Saskatchewan Glacier, and Shoumsky (1963) and Lliboutry (1967) for glaciers generally.

Here this earlier work is reviewed and generalized to examine the import of the various parameters, first for steady-state and then for non-steady-state ice masses.

7.5.1. *Equations of trajectories*

Let V be the horizontal velocity of an element of ice at distance x from the centre at time t, and depth z below the surface. Denote the accumulation rate at x by A and vertical strain rate $_z$ assumed constant from surface to base).

Now, if we know V, ε_z, and A as functions of x, we can determine the paths of the particles, or the positions of the particles at any time.

The time δt to travel distance δx is given by

$$\delta t = \frac{\delta x}{V} \tag{31}$$

and hence the time taken to reach x is given by

$$t = \int \frac{dx}{V} \tag{32}$$

Similarly, the distance travelled in time t is given by

$$x = \int V\,dt \tag{33}$$

The increase in depth z of the particle below the surface in time δt is given by

$$\delta z = A\delta t - \dot{\varepsilon}_z z \delta t \tag{34}$$

Hence,

$$\frac{dz}{dt} + \dot{\varepsilon}_z z = A \tag{35}$$

Crary (1961) showed that this equation had the solution

$$z = e^{-\int \dot{\varepsilon} dt}\left[z_0 + \int_0^t A e^{\int \dot{\varepsilon} dt} dt\right] \tag{36}$$

If we define

$$\bar{\dot{\varepsilon}}_t = \frac{1}{t}\int_0^t \dot{\varepsilon} dt \tag{37}$$

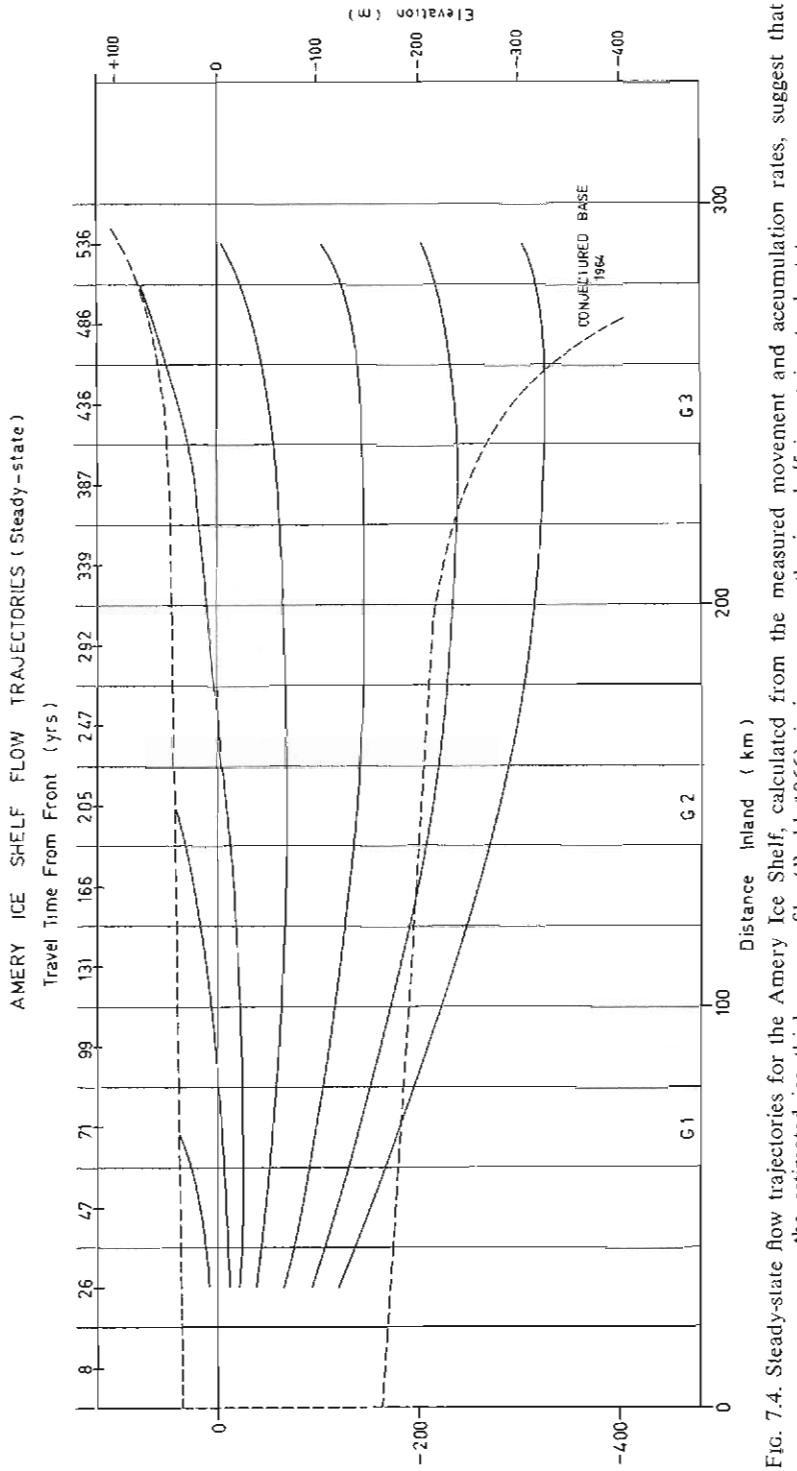

FIG. 7.4. Steady-state flow trajectories for the Amery Ice Shelf, calculated from the measured movement and accumulation rates, suggest that the estimated ice thickness profile (Budd 1966) is in error or the ice shelf is not in steady-state.

equation (36) becomes

$$z = e^{-\bar{\dot{\varepsilon}}t}\left[z_0 + \int_0^t Ae^{-\bar{\dot{\varepsilon}}t}dt\right] \tag{36'}$$

We may also express these relations in terms of x from equation (31)

i.e., $$\delta z = \frac{A}{V}\delta x - \frac{\dot{\varepsilon}_z z \delta x}{V} \tag{37}$$

and $$\frac{dz}{dx} - \frac{\dot{\varepsilon}_z}{V}z = \frac{A}{V} \tag{38}$$

Hence, $$z = e^{-\int(\dot{\varepsilon}/V)dx}\left[z_0 + \frac{A}{V}e^{\int(\dot{\varepsilon}/V)dx}dx\right] \tag{39}$$

The particle paths in some cases may be more easily calculated in terms of the distance from the base (ξ, say). If M is the basal melt rate, the relevant equations corresponding to (37) and (39) are

$$\delta\xi = -\frac{\dot{\varepsilon}_\xi \xi}{V} + \frac{M}{V}\delta x \tag{37'}$$

and $$\xi = e^{-\int(\dot{\varepsilon}/V)dx}\left[\xi_0 - \int\frac{M}{V}e^{\int(\dot{\varepsilon}/V)dx}dx\right] \tag{39'}$$

For many ice caps the basal melt is negligible and this then reduces to

$$\xi = \xi_0 e^{-\overline{(\dot{\varepsilon}/V)}x}.$$

The results of the calculation of particle paths from these equations for the centre line of the Amery Ice Shelf, and two profiles of the Wilkes ice cap, are shown in Figs. 7.4, 7.5, and 7.6. The age isolines of the ice are indicated and show up as approximately parallel layers in the ice cap, but gradually becoming closer together approaching the base and the ice front. It can be seen that the age of 90% of the dome—Cape Poinsett profile of the Wilkes ice cap under 5,000 years.

7.5.2. *Effect of various parameters on particle trajectories*

Haefeli (1963) calculated steady-state streamlines for the central regions of ideal ice masses of strip shape (two-dimensional) and circular shape, where the ice thickness and accumulation are assumed constant and the bedrock flat. The following approach generalizes this to allow for flow lines, curved in the horizontal, variable ice thickness, accumulation, and bedrock slope, and also non-steady state.

Let V be the horizontal velocity of a particle distance r from the ice cap centre and z above the bedrock at time t. Let v_z be the corresponding vertical velocity (relative to the bedrock, which may be flat or irregular).

The area between two flowlines, which are distance s apart at distance r from the centre, is denoted by S_r. We define the variable coefficient λ by

$$\frac{S_r}{s} = r\lambda \tag{40}$$

Then, for the particular cases of the strip ice sheet $\lambda = 1$, and for the ideal circular ice cap $\lambda = \frac{1}{2}$. In general, however, λ will be a function of r.

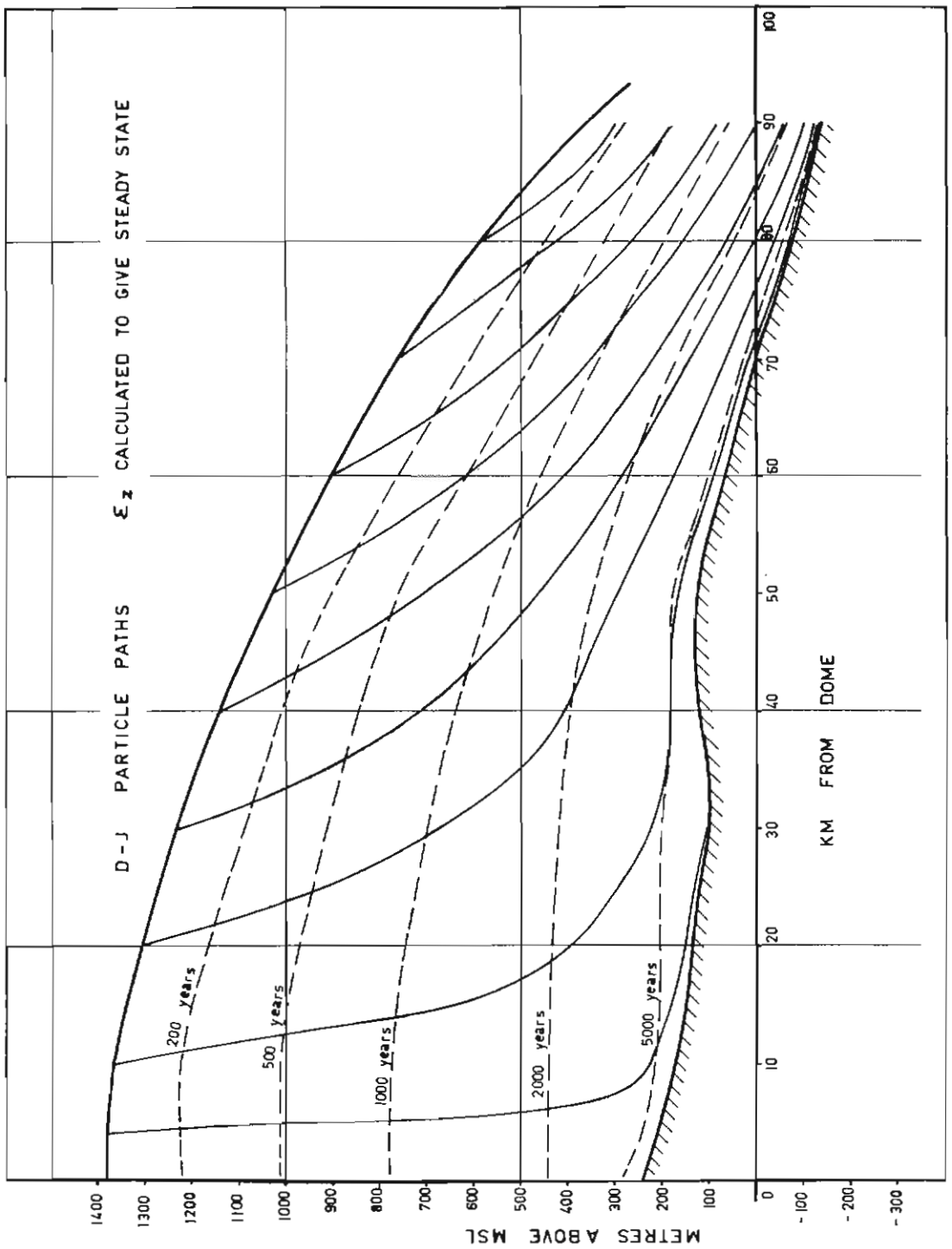

FIG. 7.5. Steady-state particle paths and isotimes, using "balance" accumulation, suggest that most of the ice in this line is less than 5,000 years old.

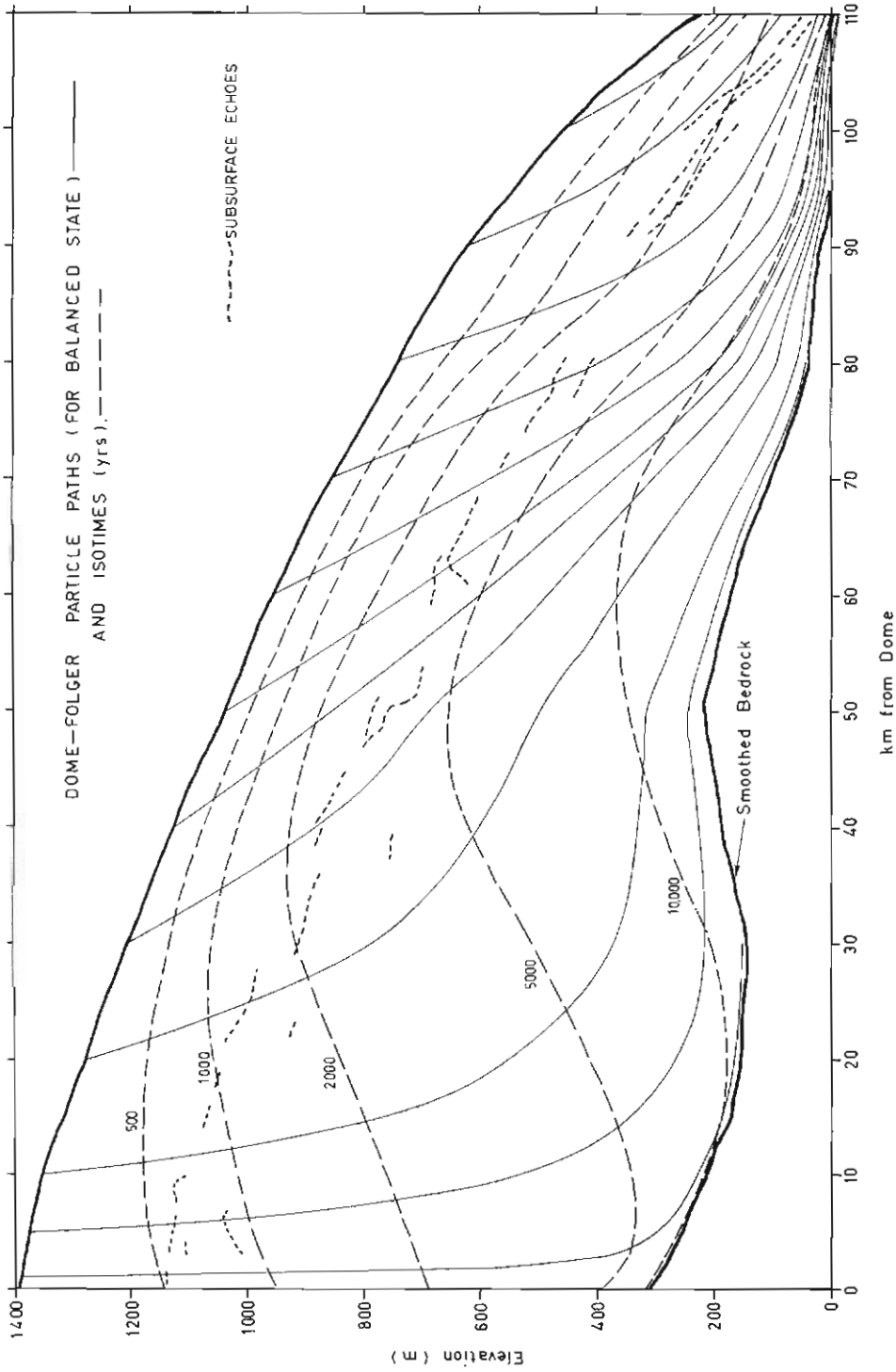

FIG. 7.6. Steady-state particle paths and isotimes show that the much slower moving dome—Cape Folger line contains much older ice than in Fig. 7.5. The scattered dots show observed subsurface layering from a radio echo-sounder profile [after Carter (to be published)].

Let $\bar{A}$ be the accumulation rate at distance r from the centre and $\bar{A}_r$ the mean accumulation over the area between the two flowlines to distance r.

Let the ice thickness at r be H.

Equation (13) expresses the continuity condition

$$sHV = S\left(\bar{A}_r + \frac{\overline{\partial H}}{\partial t}\right)$$
$$= S\bar{A}_r^* \tag{41}$$

where $\bar{A}_r^*$ is the "balance" accumulation rate.

Hence, the horizontal velocity is obtained as

$$\frac{dr}{dt} = V = \frac{S\bar{A}_r^*}{sH} = \frac{\lambda r\bar{A}_r^*}{H} \tag{42}$$

The vertical velocity is given by

$$\frac{dz}{dt} = \dot{\varepsilon}_z z \tag{43}$$

where $\dot{\varepsilon}_z$ is the vertical strain rate.

From equation (9) this may be written

$$\frac{dz}{dt} = \frac{z}{H}\left(A - V\frac{\partial H}{\partial x} + \frac{\partial H}{\partial t}\right)$$
$$= \frac{z}{H}\left(A_r^* - \frac{V\partial H}{\partial x}\right) \tag{44}$$

Consequently, the equation of the flow lines is obtained from (42) and (44) as

$$\frac{dz}{dr} = \frac{z\left(A_r^* - V\frac{\partial H}{\partial x}\right)}{\lambda r\bar{A}_r^*}$$
$$= \frac{z}{\lambda r}\left(\frac{A_r^*}{\bar{A}_r^*} - \frac{V}{\bar{A}_r^*}\frac{\partial H}{\partial x}\right) \tag{45}$$

Hence,
$$\frac{dz}{z} = \frac{1}{\lambda}\left(\frac{\dot{\varepsilon}_z H}{\bar{A}_r^*}\right)\frac{dr}{r},$$

or
$$\frac{dz}{z} = \frac{1}{\lambda}\left(\frac{A_r^*}{\bar{A}_r^*} - \frac{V}{\bar{A}_r^*}\frac{\partial H}{\partial r}\right)\frac{dr}{r} \tag{46}$$

Provided S/s, A, H, $\partial H/\partial t$ are known as functions of r, the trajectories can be calculated using stepwise increments of δr. It should be noted that for non-steady state this equation gives the instantaneous trajectories only. In order to trace the paths of actual particles, H and V must be varied in time along with $\frac{\partial H}{\partial t}$, even if A_r is constant. The procedure for calculating non-steady state trajectories is indicated in the final section. Here we merely note that the non-steady trajectories are obtained by using the balance accumulation rate A_r^* and $\bar{A}_r^*$ rather than the actual

values. Now, to examine the effect of the various parameters, we consider steady-state, dropping the asterisks from equation (46).

(1) *Divergence of flow lines.* The trajectories of equation (46) reduce to those of Haefeli (1963), if we consider the inland region of an ice cap where the accumulation rate can be taken constant (and hence $\bar{A}_r = A_r$) and the thickness gradient neglected (i.e., $V \frac{\partial H}{\partial x} \ll A$). Equation (46) then integrates to

$$z = Z_0 r^{-1/\lambda} \tag{47}$$

This corresponds to Haefeli's strip ice sheet and circular ice sheet where $\lambda = 1$ and $\frac{1}{2}$ respectively and z is the height above the bedrock at distance r, and $z = Z_0$ when $r = 1$. More generally, λ can be estimated from the convergence or divergence of the flow lines. For a circular ice cap, relative divergence (compared to radial) gives $\lambda < \frac{1}{2}$, while convergence gives $\lambda > \frac{1}{2}$.

(2) *Variable accumulation along profile.* The effect of variation in accumulation rate along the profile can be examined by considering the variation in accumulation given by a relation of the form

$$A_r \propto r^m \tag{48}$$

In this case the average accumulation rate from o to r is given by

$$\bar{A}_r = \frac{1}{m+1} A_r \qquad (m > -1) \tag{49}$$

Then, taking $\lambda = 1$ and $\frac{\partial H}{\partial x} \simeq 0$, equation (46) integrates to

$$z = Z_0 r^{-(m+1)} \tag{50}$$

Thus, it appears that a linear increase in accumulation rate away from the centre ($m = 1$) has the same effect on the particle trajectories as a constant circular divergence ($\lambda = \frac{1}{2}$).

Decreasing accumulation from the centre to the edge ($m < 0$) results in the trajectories converging less rapidly than for the constant accumulation.

(3) *Effect of thickness gradient.* From equation (46), for constant λ, and $A_r \propto r^m$, we obtain

$$z = Z_0 e^{-\int (m+1)/\lambda \, dr/r} + \int \frac{V}{A\lambda} \frac{\partial H}{\partial r} \frac{dr}{r} \tag{51}$$

$$= Z_0 r^{-(m+1)/\lambda} e^{\int \frac{V}{\lambda A} \frac{\partial H}{\partial r} \frac{dr}{r}} \tag{52}$$

Hence, any decrease in thickness from the centre outwards ($\partial H/\partial r$ negative) causes higher convergence rates of the trajectories in the vertical profile. Typical ice masses decrease in thickness towards the edge, and at the same time the velocity generally increases so that $V \frac{\partial H}{\partial r}$ becomes large compared to A. As a result, in this region of the ice mass the thickness gradient is as important as the accumulation rate in determining the particle trajectories, and its magnitude can be calculated from equation (52).

7.5.3. *Non-steady-state trajectories*

To trace the particle paths in an ice mass that is not in steady-state we must first calculate the ice thickness change δH of the surface over a time δt from

$$\delta H = (A - \bar{\dot{\varepsilon}}_z H + V(\alpha - \beta))\delta t \tag{53}$$

This allows us to calculate the new elevation profile.

Then we can still refer the depth to the new surface and use equations (37) and (39) to calculate the position of the particle for the first step.

But we note that, as the thickness changes, so will the slope and the velocity. From the relation for velocity

$$V = k\alpha^n H^{n+1} \tag{54}$$

where

$$k = \frac{2}{n+1}\left(\frac{\rho g}{B}\right)^n,$$

we can obtain the change in velocity, provided the temperatures (and therefore B) remain the same, as

$$\delta V = nk\alpha^{n-1}H^{n+1}\delta\alpha + (n+1)k\alpha^n H^n \delta H \tag{55}$$

or

$$\frac{\delta V}{V} = n\frac{\delta\alpha}{\alpha} + (n+1)\frac{\delta H}{H} \tag{56}$$

With the new velocity profile the position of the ice particles after the next time step can now be calculated. $\frac{\partial H}{\partial t}$ will change as V and H change and, in some cases, may tend to zero, giving steady-state. But a steady-state will not be reached in general and so the above *extrapolation* technique will have to be continued.

The process becomes very tedious for lengthy extrapolation but, because of its feedback properties, it lends itself very readily to iterative computer techniques. However, we note that the accumulation rate and ice flow properties have been taken as constant. For lengthy extrapolation with large changes in the ice cap dimensions, this may well not be valid. So, without detailed information on the variation of accumulation and temperature (and hence the ice mass flow parameters) over a long period, lengthy calculations to study the growth or decay of large ice masses remain premature.

As an example of the use of the technique Fig. 7.7 shows the results of a comparatively short-term non-steady state extrapolation to show the expected positions of the Wilkes ice cap surface several hundred years in the past and also into the future.

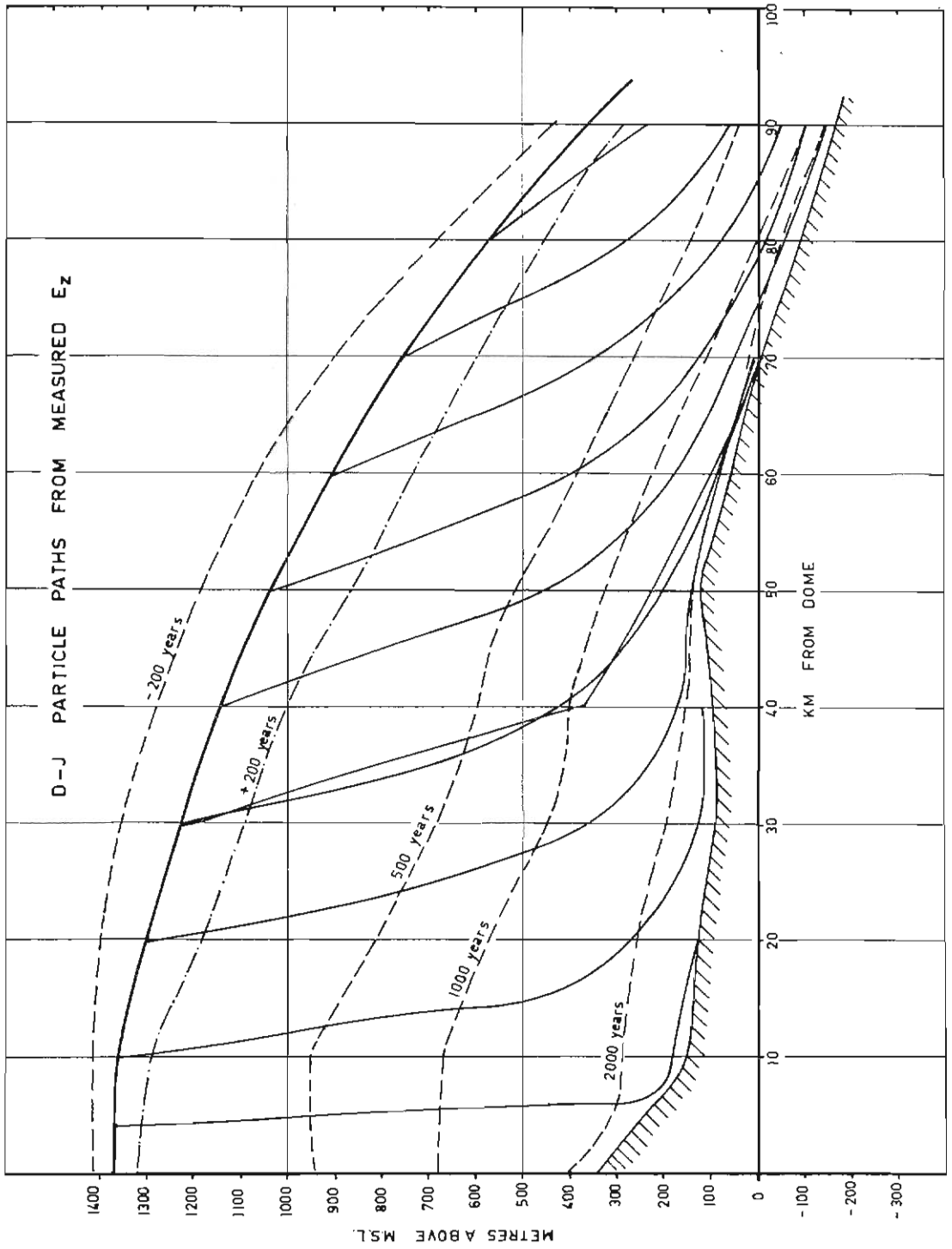

FIG. 7.7. Non-steady state particle paths calculated from the measured parameters show the estimated surfaces 200 years ago and in 200 years' time.

8. SUMMARY AND CONCLUSIONS

8.1. INTRODUCTION

Although the general equations of motion for an ice mass, of density ρ, where σ_{ij} is the stress at x_i, and X_i is the external force,

$$\frac{\partial \sigma_{ij}}{\partial x_i} = \rho X_i \tag{1}$$

is difficult to solve in general for moving ice masses, solutions for velocity and velocity gradient can be obtained in certain cases, because of the special types of symmetry encountered in the moving ice, by separately considering the stress gradients and velocity gradients:

(1) laterally across the line of motion,
(2) vertically from surface to bedrock,
(3) longitudinally in the line of motion.

The reason for this is that the respective velocity gradients are greatest in different parts of the moving ice mass, i.e., the transverse gradients (vertically and horizontally) are maximum near the boundary and least at the surface and centre, while the reverse is true of the longitudinal gradients. Appreciable direct interaction of the velocity gradients only occurs in some cases which are not considered here.

Given a flow law of ice, i.e., if we know the relation between the stress deviator and strain rate for ice, say,

$$\dot{\varepsilon}_{ij} = 1/\eta \, \sigma'_{ij} \tag{2}$$

where η is a funcion of temperature and the stress invariants, then the equations of motion can be written in terms of strain rates and solved (numerically) to give velocities throughout the ice mass in terms of the boundary conditions, viz., the shape and size of the ice mass and the velocity and strain rate at some position.

8.2. THE FLOW LAW OF ICE

The flow law of ice, however, is not a simple one and depends on the stress, temperature, ice type (crystal orientation, size, density, etc.). In natural deforming ice masses the crystal sizes and orientations are not random but tend to adopt certain common features. Although the precise nature of these features has still to be determined, the result is that the stress and temperature are the main variables that need to be considered in moving ice masses. The experimental results to date suggest that the flow law can be represented approximately by the empirical relation

$$\dot{\gamma} = a_1 e^{k\theta}\tau + a_2(e^{k\theta}\tau)^n \tag{3}$$

where $\dot{\gamma}$ is the octahedral shear strain rate $\sec^{-1}$,

τ is the octahedral shear stress in bars,

θ is the temperature in °C,

$a_1 \simeq 4 \times 10^{-9}$ bars^{-1}sec^{-1}, approximately depending on the ice type,

$a_2 \simeq 2 \times 10^{-8}$ bars^{-n}sec^{-1}, approximately depending on the ice type,

$n \simeq 3 - 4$,

$k \simeq 1/10$ °C^{-1}.

The experimental data so far, however, still leaves the strain rate in doubt by about a factor of 2, depending on the ice type. With the above values of a and n, the first term ($a_1\tau$) predominates at low stresses, up to 0·5 bars, (the two terms are equal at $\tau = 0{\cdot}6$ bars for $n = 4$) where the stress-strain relation is Newtonian and the ice reacts as if of constant viscosity. At stresses above 0·6 bars the second term ($a_2\tau$) becomes predominant, and above 1 bar the first term is negligible, giving a simple power law for the flow relation. Over any limited range of stress, equation (3) can be approximated by a simple power law whose parameters will vary with the stress range.

8.3. CROSS-SECTION PROFILES OF FLOW

8.3.1. *The tranverse velocity profile, glaciers, ice shelves*

When the longitudinal strain rate is small (less than 1% yr^{-1}) it can be generally neglected in the calculation of the transverse and vertical profiles of horizontal velocity (u). For a typical symmetrical glacier, flowing down a uniform slope α with zero horizontal divergence, the general equations reduce to

$$\frac{\partial \tau_{xy}}{\partial y} + \frac{\partial \tau_{xz}}{\partial z} = \rho g \alpha \tag{4}$$

$$\frac{\partial u}{\partial y} = 2B^{-n}\tau^{n-1}\tau_{xy}; \qquad \frac{\partial u}{\partial z} = 2B^{-n}\tau^{n-1}\tau_{xz} \tag{5}$$

$$\tau^2 = \sqrt{\tau_{xy}^2 + \tau_{xz}^2} \tag{6}$$

where B and n are the power flow law parameters, assumed constant here.

These equations can be solved numerically for a given cross-section or to a fair degree of accuracy may be extrapolated from the results obtained by Nye (1965) for velocity profiles across sections of rectangular, elliptic and parabolic shapes. For glaciers much wider than they are deep the cross-section shape has only a slight effect on the *shape* of the vertical profile of velocity at the centre, but does affect the *magnitude*.

For the special case of an ice shelf of width 2a bounded at the sides, we have for the velocity V_y at distance y from the centre where the velocity is V_c

$$V_c - V_y = \frac{1}{n+1}\left(\frac{\rho g \alpha}{2B}\right)^n y^{n+1} \tag{7}$$

8.3.2. *The vertical velocity profile: ice caps*

For the simple power law for flow the vertical velocity—depth profile is given by

$$V_s - V_z = \frac{1}{n+1}\left(\frac{\rho g \alpha}{B}\right)^n z^{n+1} \tag{7'}$$

This, however, does not consider the effect of the temperature dependence on the flow law and the variation of temperature with depth in ice caps.

In typical ice caps the temperature increases near the base, i.e., in the region where the shear stress is greatest. This leads to a vertical velocity profile which is very temperature-dependent. Hence, it is necessary to adopt the generalized flow law

$$\dot{\gamma} = a_{1,\theta}\tau + a_{2,\theta}\tau^n, \qquad \text{with} \qquad a_\theta = a_0 e^{-k\theta},$$

and also to know the vertical temperature profile to calculate the vertical profile of velocity.

8.4. TEMPERATURE PROFILES IN ICE MASSES

8.4.1. *Effect of frictional heating on the temperature profile*

The temperature θ at depth z in an ice mass of thickness of H, in the absence of accumulation or movement, is governed by the temperature at the surface θ_s, and the basal temperature gradient $\gamma_b = \gamma_G$ (the geothermal heat flux).

$$\theta = \theta_s + \gamma_b z \tag{8}$$

Horizontal movement causes heat production by energy dissipation $\frac{dQ}{dt}$ from internal friction, depending on the shear stress τ_{xz} and the strain rate $\dot{\varepsilon}_{xz}$, as

$$\frac{dQ}{dt} = \tau_{xz}\dot{\varepsilon}_{xz} \tag{9}$$

Since the strain rate is temperature-dependent

$$\text{i.e.,} \qquad \dot{\varepsilon} = \left(\frac{\tau}{B}\right)^n e^{v\theta}, \qquad \text{with} \qquad v \simeq \cdot 1 \qquad \text{to} \qquad \cdot 3^\circ\text{C}^{-1} \tag{10}$$

the energy dissipation affects both the temperature and velocity profiles.

Neglecting other effects, the temperature variation in the basal layers is given by

$$\frac{d^2\theta}{dz^2} = -\lambda z^{n+1} e^{v\theta} \tag{11}$$

where

$$\lambda = \frac{(\rho g \alpha)^{n+1}}{B^n J K} \tag{12}$$

with ρ the ice density, g gravity acceleration, α the slope in the line of motion, J the mechanical equivalent of heat, and K the ice conductivity.

From this, the temperature variation may be evaluated from the series solution

$$\theta = \theta_s + \gamma_s z + \lambda e^{v\theta_s} z^6 \left(\frac{1}{5\cdot 6} + \frac{v\gamma_s z}{7\cdot 6} + \frac{(v\gamma_s z)^2}{8\cdot 7\cdot 2!} + \ldots\right) \tag{13}$$

With this form of flow law it is found that almost 90% of the heat production in a typical 1000 m-thick ice mass occurs in the lowest 200 m. Since most of the

heat production is in the basal layers, the effect of the frictional heating can be approximately accounted for in most of the ice mass by simply taking the basal gradient as

$$\gamma_b = \gamma_G + \frac{\tau_b V}{JK} \tag{14}$$

where V is the average forward velocity of the ice, and τ_b is the basal stress.

8.4.2. *Effect of accumulation and movement on the temperature profile*

The "Robin" steady-state temperature profile for an ice mass in balanced state with an accumulation rate A at the surface, constant surface temperature, and negligible horizontal transfer is

$$\theta = \theta_s - \gamma_b H \frac{\operatorname{erf} y - \operatorname{erf} \zeta y}{y} \tag{15}$$

where

$$y = \sqrt{\frac{AH}{2\kappa}} \quad \text{and} \quad \zeta = \frac{z}{H} \tag{16}$$

The temperature gradient at the surface for these conditions is

$$\left(\frac{d\theta}{dz}\right)_s = \gamma_b e^{-y^2} \tag{17}$$

The effect of horizontal motion may be estimated by the steady-state negative surface temperature gradient due to downslope movement and consequent surface warming in the absence of conduction

$$\left(\frac{d\theta}{dz}\right)_s = -\frac{\alpha V \lambda}{A} \tag{18}$$

where λ is the vertical annual mean air temperature gradient.

Alternatively, the steady-state temperature profile for an ice mass moving outwards and downwards, and warming at the surface, with conduction, but with zero accumulation rate, is

$$\theta = \theta_s + \gamma_b z + \frac{\alpha V \lambda}{\kappa}\left(Hz - \frac{z^2}{2}\right) \tag{19}$$

with surface gradient

$$\left(\frac{d\theta}{dz}\right)_s = \gamma_b - \frac{\alpha V \lambda}{\kappa} H \tag{20}$$

When both accumulation rate and conduction are present the steady-state profile for an ice cap column moving outwards and downwards in a balanced state, and consequently warming at the surface at the rate $\alpha V \lambda$ is given by

$$\theta_z = \theta_s + \gamma_b H \frac{\operatorname{erf} y - \operatorname{erf} \zeta y}{y} - \frac{\alpha V \lambda}{A} H\, 2(Ey - E\zeta y) \tag{21}$$

where

$$E(x) = \int_0^x F(y)dy \quad \text{and} \quad F(y) = e^{-y^2}\int_0^y e^{t^2}dt \tag{22}$$

The surface gradient is

$$\left.\frac{d\theta}{dz}\right)_s = \gamma_b e^{-AH/2\kappa} + \frac{\alpha V\lambda}{A} 2y\, F(y) \tag{23}$$

$$= \gamma_b e^{-AH/2\kappa} + \frac{\alpha V\lambda}{\kappa} H \frac{F(y)}{y} \tag{23'}$$

which is approximately the sum of the results for (17) and (18) or (20).

8.4.3. *Temperatures in a growing or sinking ice cap*

For a growing or sinking ice cap, where the elevation E is changing at the constant rate $\frac{DE}{Dt}$ as the column moves outwards, the result is similar to the previous result, equation (23), but in this case expanding (or contracting), moving coordinates are chosen and $\frac{DE}{Dt}\lambda$ must be used—as the warming rate instead of $\alpha V\lambda$ which is appropriate for steady state ice masses. The surface gradient in this case is

$$\left.\frac{d\theta}{dz}\right)_s = \gamma_b e^{-AH/2\kappa} - \frac{\lambda}{A}\frac{DE}{Dt} 2y\, F(y) \tag{24}$$

From this last result, for those cases where climatic changes are negligible, the state of balance or rate of change of ice thickness may be estimated from the surface temperature gradient, the ice thickness and the accumulation rate as

$$\frac{\partial H}{\partial t} = \alpha V - \frac{A}{\lambda}(\gamma_s - \gamma_b e^{-AH/2\kappa}) \tag{25}$$

8.4.4. *Non-steady-state temperatures in ice caps*

When the boundary conditions have not remained constant for a long enough time the steady-state temperature profiles may not be realized.

The time lag t of the basal temperature in reaching steady-state may be estimated from

$$\theta_b(t) = \mathrm{k}t - \frac{\mathrm{k}H^2}{2\kappa}\left(1 - \frac{32}{\pi^3} e^{-k\pi^2/4H^2\, t}\right) \tag{26}$$

where k is the rate of constant surface-warming, for zero accumulation at the surface. For accumulation at the surface the criterion for approach of the temperature profile to steady-state is

$$\frac{\lambda}{\kappa}\frac{DE}{Dt} - \frac{A}{\kappa}\frac{d\theta}{dz} \ll \frac{2\cdot 4\kappa}{H^2} \tag{27}$$

This condition appears to be realized in most ice masses that are in a balanced state.

Sinusoidal temperature variations at the surface in the absence of motion or accumulation are conducted into the medium with velocity

$$\frac{dz}{dt} = \sqrt{2\kappa\omega} \tag{28}$$

where ω is the frequency of the variation.

Long-period temperature changes penetrate by means of the accumulation A and movement, travelling with the ice which at distance z above the base has the vertical velocity

$$\frac{dz}{dt} = -A\frac{z}{H} \tag{29}$$

When both these velocities (28) and (29) are comparable, the decrease of amplitude with depth may be estimated from

$$\theta_z = \theta_0 \exp\left\{ z\left[\frac{A}{2\kappa} - \frac{1}{\sqrt{2}}\left(\sqrt{\left(\frac{A^2}{4\kappa^2}\right)^2 + \frac{\omega^2}{2\kappa^2}} + \frac{A^2}{4\kappa^2}\right)\right]^{\frac{1}{2}}\right\} \tag{30}$$

Calculations from these equations suggest that, for ice caps near balance, the temperature profiles in natural cold ice masses will be close to the steady-state profile corresponding to a constant warming rate at the surface but, in those cases where the rate of warming increases rapidly, the basal temperatures may lag the surface temperatures. Short-term climatic changes die out quickly in the top layers, while long-term changes are carried by the ice with decreasing speed towards the base, with the rate depending on the accumulation and strain rates.

8.5. LONGITUDINAL VELOCITY PROFILE

8.5.1. *Glaciers*

The general equation for the longitudinal velocity at the surface of an ice mass (V_s) and the strain rate ($\dot{\varepsilon}$) along a flow line, equation 6.2 (25), adjusted for transverse strain:

$$\frac{\partial(ZB_1(\phi\dot{\varepsilon})^{1/n_1})}{\partial x} = \frac{1}{2}\rho g\bar{Z}\alpha - sB_2\left(\frac{n_2+1}{2}\frac{V_s - V_b}{Z}\right)^{1/n_2} \tag{31}$$

where ϕ is the transverse strain rate factor,
V_b is the basal velocity,
s is a shape factor for the cross-section,
expresses these in terms of the glacier dimensions, ice thickness Z and surface slope α, and the ice flow law, parameters n and B.

If the mean (smoothed) value of the left-hand-side over a certain distance is sufficiently close to zero, then we obtain the relation for smoothed slope, velocity and thickness, and the flow parameters as 6.2 (29)

$$\left(\frac{\bar{V}}{Z}\right)^{1/n} = \left(\frac{2}{n+1}\right)^{1/n}\frac{s\rho g\bar{\alpha}Z}{B} \tag{32}$$

where $\bar{B}$ is highly dependent on the temperature profile, especially in the basal layers and is given by 5.1 (37)

$$\bar{B} = \left[\frac{n+1}{Z^{n+1}}\int_0^Z \frac{1}{B^n} z^n dz\right]^{-1/n}$$

Equation (32) may be used to evaluate the flow parameters of the ice (relevant to the high shear layer at the base), when the velocity and thickness profiles are known. Alternatively, if the flow parameters and thickness profiles are known, then the longitudinal velocity may be estimated.

The longitudinal strains, however, are generally more influenced by the slight variations in slope from the mean slope, i.e.,

$$\frac{\partial(ZB\phi\dot{\varepsilon}^{1/n})}{\partial x} = \frac{1}{2}\rho g(\alpha - \bar{\alpha}) \tag{33}$$

By measuring the strains and the associated slope deviations along the centre-line, estimates can be made of the flow parameters, n and B, which are appropriate to the whole thickness and generally for much lower shear stresses than the basal shear above.

8.5.2. *Ice shelves*

The general equation for velocity and strain rate along the centreline is given by

$$B\frac{\partial(\phi\dot{\varepsilon})^{1/n}}{\partial x} = \frac{1}{2}\rho g\alpha - B\left(\frac{n+1}{2}\right)^{1/n}\frac{V^{1/n}}{a^{1+1/n}} \tag{34}$$

For the cases in which the parameters a, B, n, ϕ, only change slowly along the line of motion, the solution of this general equation may be obtained as

$$V = \frac{\rho g a^2}{2B}\alpha + V_0 e^{-f(n)x/a} \tag{35}$$

where

$$f(n) = \frac{n(n+1)^{1/n}}{2^{(n+1)/n}}\left[\frac{(\beta+1)^{1/n} - 1}{\beta^{1/n}}\right]^{n/n+1} \tag{36}$$

and β is the ratio of the two terms on the right-hand-side of equation (34), i.e., the ratio of the stress gradient due to slope α and that due to varying creep rate.

We can use this equation to calculate the velocity profile from the dimensions of the ice shelf and the flow parameters, or to calculate the flow parameters from the velocity profile.

8.5.3. ICE CAPS

Similarly to the result for glaciers, we have the general equation

$$\frac{\partial ZB_1\phi\dot{\varepsilon}^{1/n}}{\partial x} = \frac{1}{2}\rho gZ(\alpha - f) - \frac{\rho g}{6}\frac{\partial^2\alpha Z^3}{\partial x^2} \tag{37}$$

The final term on the right is only relevant for short distance wavelengths $\lambda \simeq 2\pi/\sqrt{3}\ Z$. We find for the smoothed velocity, slope, and ice thickness (if the left-hand-side average $\rightarrow$ 0)

$$V = \frac{2\bar{Z}^{n_2+1}}{n_2+1}\left(\frac{\rho g\bar{\alpha}}{\bar{B}_2}\right)^{n_2} \tag{38}$$

which can be used to calculate the velocity or flow parameters from the slope and thickness.

These values of the parameters n_2 and B_2 are those appropriate for the high shear layer at the base. For the fluctuations in longitudinal strain rate associated with the variations in slope from the mean, we have

$$\delta B_1\phi\varepsilon^{1/n_1} = \tfrac{1}{2}\rho g(\alpha - \bar{\alpha})\delta x \tag{39}$$

This equation gives the flow parameters associated with the extension and compression right through the ice cap — generally at much lower shear stresses than for the basal shear.

With ice caps, the temperature dependence of the B values is very important: in general, B_2 for the basal layer is much lower (due to the higher temperatures) than B_1 for the body of the ice. Furthermore, there is variation in temperature (and hence B) along the line of flow. This means that an accurate idea of the ice cap temperature profiles is required before accurate velocity profiles may be obtained.

Over undulations on the ice cap, surface maximum extension occurs on the crests and minima over the troughs.

8.5.4. *Transverse strain*

The effect of a transverse extension $\dot{\varepsilon}_y$ on the longitudinal velocity profile is to reduce the longitudinal strain rate $\dot{\varepsilon}_x$ for a given slope gradient, according to

$$\dot{\varepsilon}_x = (2A)^{-n}(\sigma_x - \sigma_z)\phi^{-1} \tag{40}$$

where
$$\phi^{-1} = \left(\frac{2}{2+v}\right)\left[1 + 3\left(\frac{v}{2+v}\right)^2\right]^{(n-1)/2} \quad \text{and} \quad v = \frac{\dot{\varepsilon}_y}{\dot{\varepsilon}_x} \tag{41}$$

This means that the general equations applying in three dimensions have $(\phi\dot{\varepsilon}^{1/n})$ replacing $\dot{\varepsilon}^{1/n}$ in the case of two dimensions, where $\dot{\varepsilon}_y = 0$.

Now since the longitudinal strain rates are low, we are generally concerned here with the region of the flow law where $n \simeq 1$, i.e., we have

$$\phi \simeq 1 + \frac{v}{2} \quad \text{or} \quad \phi\dot{\varepsilon}_x = \dot{\varepsilon}_x + \frac{\dot{\varepsilon}_y}{2} \tag{42}$$

and see that small strains (especially of the same sign) have little effect on the longitudinal profile, but large lateral strains of the same order as the longitudinal strain (especially if of opposite sign) can dominate the deformation process. But provided the divergence or convergence of the flow lines is known, the effects of the lateral strain can be calculated and incorporated into the equations for both longitudinal velocity and strain rate.

8.5.5. *Ice flow over undulations*

For a two-dimensional bedrock slope profile in the line of motion of the form

$$\beta = \beta_0 + \beta_1 \cos \omega x$$

an ice mass adopts a steady-state surface with undulations given by

$$\alpha = \alpha_0 + \alpha_1 \cos \omega x + \alpha_2 \sin \omega x,$$

where
$$\alpha_1 = \frac{\beta_1}{1+\psi^2} \quad \text{and} \quad \alpha_2 = \frac{\psi\beta_1}{1+\psi^2} \simeq \frac{\beta_1}{\psi},$$

where
$$\psi = \frac{\rho g Z^2}{4\pi V B}\left[\frac{\lambda}{Z} + \frac{4\pi^2}{3}\frac{Z}{\lambda}\right] \tag{43}$$

where Z is the ice thickness,

V is the ice velocity,

B is the ice "viscosity" parameter,
$\lambda = 2\pi/\omega$ is the wavelength of the undulations.

The damping factor ψ is a minimum for $\lambda_m = \frac{2\pi}{\sqrt{3}}Z$. Equation (43) can be used to determine values of the flow parameter B from the damping factor and the velocity .

8.6. APPLICATION TO PARTICULAR ICE MASSES

The general equations of longitudinal velocity and strain rate have been examined by studying actual ice masses whose longitudinal velocity and dimensions have been measured. Since the flow law parameters from laboratory measurements show considerable variation, rather than calculating velocities for the ice masses from these parameters, the measured velocity profiles have been used to calculate the flow parameters.

(1) Ice shelves

Near the front of an ice shelf the strain rate becomes high while the surface slope is small. This means that the smoothed velocity—slope relation is not satisfactory but the combined equation (34) can be used to determine the flow parameters n and B. The values of n and B determined from the velocity profile of the Amery Ice Shelf are of the right order of magnitude and confirm the application of the general equations. To determine these parameters more accurately, higher precision is required for the ice thickness and velocity profiles, and also the temperature and density distribution with depth.

(2) Glaciers

The general equations (31), (32), (33) applied to the longitudinal velocity profile of the Athabasca Glacier give reasonable confirmation. The flow parameters were calculated from both the smoothed velocity, slope and thickness, and also from the variations over undulations. If unsmoothed values are used in equation (32), the short distance variations over undulations almost completely mask the broad effects. The calculated flow parameters from the two methods show reasonable agreement with each other, as well as with values obtained from transverse and vertical velocity profiles, as would be expected for a temperate glacier. To study the effect of the short-distance undulations in more detail, a more closely spaced profile of ice thickness and strain rates is required.

(3) Ice caps

An analysis of the longitudinal velocity, strain rate, surface slope, and ice thickness over the Wilkes ice cap provides an extensive set of data to test equations (37), (38), (39). Flow parameters were calculated from both the smoothed velocities (38) and the deviations (39). The results of Section 4 on the temperature distributions in ice masses had to be used to incorporate the effect of the variation in temperature on the flow parameters.

The equation (38) for smoothed velocities had to be generalized, using equation (37) to include the effect of significant longitudinal and transverse strain rate. The transverse strain factor ϕ of equation (40) was used successfully to incorporate the effect of transverse strain in botb equations (38) and (39). It was found

that the flow parameters for a given temperature are much the same over the area. The values of the flow parameter B from the smoothed velocity profile correspond to the basal layers of the ice and are generally lower than that for the body of the ice calculated from the strain over the undulations. This is as one would expect from the temperature calculations showing higher temperatures at the base. Final confirmation will not come, however, until the temperature profiles can be measured.

8.7. MASS BALANCE, STATIONARY STATE AND CHANGE IN FORM

Once the longitudinal velocity (V) of the ice mass is known, as well as the flow lines, surface accumulation rate (A), basal melt rate (M) and ice thickness profile (H), then the rate of change in the ice-cap thickness in time over each point of bedrock ($\frac{\partial H}{\partial t}$) can be calculated from

$$\frac{\partial H}{\partial t} = \dot{\varepsilon}_z H + V\frac{\partial H}{\partial x} + A - M \tag{43}$$

where $\dot{\varepsilon}_z$ is the vertical strain rate, given approximately by the sum of the two horizontal strain rates (longitudinal and transverse).

From this formula, evaluated over the ice mass, a new shape over a given period can be calculated, provided the parameters do not change significantly over that period. As the ice mass changes shape and size, a new velocity distribution will develop: this can be calculated from the results of the smoothed velocity relation (38) above. In this way the past and future histories of the ice cap can be calculated. The further the extrapolation in time the less accurate is the result. It can be seen that for long-term extrapolation it is also necessary to know the long-term variation in accumulation rate.

The very special case in which $\frac{\partial H}{\partial t} = 0$ all along the flow line is the "stationary state" in which case the ice-cap shape and size remains constant with time. In general, the condition for balance for an ice cap of thickness H, velocity V at distance r from the centre, where for flow lines distance s apart at r the area enclosed by them is S_r and the average accumulation rate over this area is $\bar{A}_r$, may be written

$$sHV = S_r\bar{A}_r \tag{44}$$

Using equation (38) for the velocity in terms of the flow parameters, ice thickness and surface slope allows equation (44) to give a surface profile required for balance.

i.e.,
$$\frac{S_r\bar{A}_r}{sH} = -\frac{2H^{n+1}}{n+1}\left[\frac{\rho g}{B}\left(\frac{dH}{dr} - \beta\right)\right]^n \tag{45}$$

where $\beta = \frac{dH}{dr} - \alpha$ is the bedrock slope.

Provided all these parameters are known as functions of r, then this equation can be numerically integrated to give the steady-state profile corresponding to the existing parameters.

Alternatively, equations (44) and (45) may be used to determine which values of these various parameters, in particular A, V, B, would be required for the existing profile to be in steady-state.

Steady-state particle paths, or trajectories tracing the paths of ice deposited on the surface as it moves through the ice mass, may be calculated from

$$\frac{dz}{z} = \frac{1}{\lambda}\left(\frac{A_r}{\bar{A}_r} - \frac{V}{\bar{A}_r}\frac{\partial H}{\partial r}\right)\frac{dr}{r}$$

where z is the depth of the parcel of ice at distance r,

A_r is the accumulation rate at distance r,

$\bar{A}_r$ is the average accumulation rate to distance r,

and $\lambda = \frac{1}{r}\frac{S_r}{s}$.

For non-steady state trajectories it is necessary to use, instead of the actual accumulation rate A, the accumulation rate for balance

$$A^* = A + \frac{\partial H}{\partial t}.$$

In addition, for long-term calculations it is also necessary to vary the ice thickness and velocity profiles according to equations (44) and (38).

8.8. CONCLUDING REMARKS

Although the study of the dynamics of ice masses has still a great number of outstanding problems to be solved, basic equations are available for calculating the velocity distributions in natural ice masses, given the dimensions of the ice mass, the flow law of ice throughout the ice mass, and boundary values of the velocity and strain rate. One approach is to apply numerical and computer techniques directly to the equations of motion in specific cases. On the other hand, ice flow in natural ice masses has certain symmetry which allows simplifications to be made so that more direct equations can be derived for velocity and strain rate in terms of the flow parameters of ice and the boundary dimensions.

Generally, the boundary dimensions of the ice masses can be determined relatively easily and also, in many cases, the boundary velocity. The major difficulty in calculating the velocity distribution is a lack of sufficiently precise information on the flow law of ice. At high stress the strain rate of ice is dependent on a high power of stress; it also varies an order of magnitude for a 20°C change in temperature, and depends on other factors such as the ice crystal sizes and orientation fabrics. This fact calls, on one hand, for an extensive range of accurate long-term steady-state stress—strain rate measurements on ice in the laboratory to establish the flow law and its dependence on these various parameters, with sufficient precision to be able to calculate accurate velocities in ice masses. Alternatively, by making field measurements of velocity, boundary dimensions and the ice properties (temperature, crystal size and orientation) of natural ice masses, the flow law parameters can be deduced.

It has been shown here that for both temperate glaciers and ice caps the longi-

tudnal velocity profile provides a valuable supplement to the transverse and vertical velocity profiles for determining the flow law parameters.

In addition, the analysis of the relative amplitudes of the bedrock and surface undulations provides a new powerful means of determining the ice-flow properties.

For cold ice masses the major factor governing the ice flow is the temperature. Hence detailed field studies are required which make complete measurements of ice mass dimensions, surface velocity distribution, and temperature—depth profiles to establish the flow law precisely. Once this is done it should be possible to calculate the velocity and temperature profiles in other ice masses with the minimum of field measurements.

If the velocity distribution over an ice mass is known, together with the accumulation and ice thickness, then the mass balance can be calculated, not only for the ice mass as a whole but, of more importance, the *distribution* of the net balance over the ice mass. From this, the rate of change of the ice-mass shape may be deduced. This latter results in an elevation change which can be measured most directly by repeated, precise gravimetry surveys. Alternatively, an analysis of the existing shapes and states of balance of ice masses enables further information on the flow properties of the ice to be deduced.

The results of field measurements, in particular those for the Wilkes ice cap project, so far confirm the predictions of the equations for longitudinal velocity and strain rate. As a result, flow parameters are deduced which take account of calculated temperature profiles in the ice mass. The next stage will be the measurement of the temperature distribution through the ice cap to examine the validity of using the calculated temperatures in the present flow analysis, and to give information on the change in climate and the state of balance with time.

The continued combination of extensive field and laboratory measurements with theoretical investigations presents a powerful method for solving the still outstanding problems in the dynamics of ice masses.

9. ACKNOWLEDGEMENTS

This present work has been developed largely during the course of the investigations of two Antarctic ice masses, the Amery Ice Shelf and the Wilkes local ice cap, by the Australian National Antarctic Research Expeditions (ANARE). It forms part of the glaciological programme of the Antarctic Division, Department of Supply, and was undertaken in collaboration with the Department of Meteorology, University of Melbourne.

The author wishes to thank all the members of the ANARE who have taken part in or supported these projects. In particular, special appreciation is accorded the Antarctic Division's expedition glaciologists to whom the valuable field measurements and their evaluation are due. At Wilkes the expedition glaciologists, since the author, whose data have been used here include A. C. Battye (1962), P. J. Morgan (1964), W. A. McLaren (1965), M. L. Pfitzner (1966), D. B. Carter (1967). For the Amery Ice Shelf, the expedition glaciologists supporting the author's own field work include I. H. Landon-Smith (1962) and E. R. Wishart (1963).

The two Antarctic projects have also received valuable support from the Antarctic Branch of the Division of National Mapping, and the Bureau of Mineral Resources, Geology and Geophysics. The work of the expedition field geophysicists, F. Jewell, D. J. Walker, M. Kirton, R. Whitworth and G. A. Allen, has been of particular importance for the Wilkes project.

During the production of the work the author has had the benefit of discussions with the members of the Department of Meteorology of the University of Melbourne. In particular, the valuable guidance of Dr. U. Radok is most appreciated. Dr. M. J. D. Jensscn also provided many useful comments regarding the numerical solution of the heat condition equation in moving ice caps.

Since the first draft of this report the author has had a valuable detailed discussion of the work with Dr. J. F. Nye of the University of Bristol. His many suggestions are much appreciated and have resulted in several important revisions and the addition of the appendices.

Nevertheless, it must be understood that the responsibility for any remaining inadequacies rests entirely with the author.

10. REFERENCES

ABRAMOWITZ, M., *and* STEGUN, I. A. (1964). Handbook of mathematical functions. U.S. Department National Bureau of Standards. Applied Mathematics, Series 55.

ALLEN, C. K., *et al.* (1960). Structure of the lower Blue Glacier, Washington (by C. R. Allen, W. B. Kamb, M. F. Meier and R. P. Sharp). *Journal of Geology* **68**: 601-625.

BADER, H. (1961). The Greenland ice sheet. Cold Regions Science and Engineering, U.S. Army Cold Regions Research and Engineering Laboratory Monographs, Part I, Sect. B.2.

BAKAYEV, U. G. (Ed.) (1966). Soviety Antarctic Expedition Atlas of Antarctica Volume I. Main Administration of Geodesy and Cartography of the Ministry of Geology USSR. Translation by American Geographical Society, New York.

BARDIN, U. I., *and* SUYETOVA, I. A. (1967). Basic morphometric characteristics for Antarctica and budget of the Antarctic ice cover. Proceedings of the Symposium of Pacific Antarctic Sciences, Eleventh Pacific Science Congress, Japanese Antarctic Research Expedition Scientific Reports, Special Issue No. 1.

BATTYE, A. C. (unpublished). Glaciological studies made at Wilkes in 1962. M.Sc. thesis presented to Meteorology Department, University of Melbourne.

BENDER, J. A., *and* GOW, A. J. (1961). Deep drilling in Antarctica. IUGG. IASH Symposium on Antarctic Glaciology. General Assembly of Helsinki. Pub. No. 55: 132-41.

BENFIELD, A. E. (1949). A problem of the temperature distribution in a moving medium. *Quarterly Journal of Applied Mathematics* **6**: 439.

BENFIELD, A. E. (1951). The temperature in an accumulating snowfield. *Monthly Notices of the Royal Astronomical Society, Geophysical Supplement* **6**: 139-147.

BENFIELD, A. E. (1953). The effect of accumulation on temperatures within a snowfield. *Journal of Glaciology* **2**: 250.

BENTLEY, C. K. (1962). Summary of paper and discussion of: Surface slopes and ice thickness in West Antarctica. *Journal of Glaciology* **4**: 315-317.

BLACHUT, T. J., *and* MÜLLER, F. (1966). Some fundamental considerations on glacier mapping. *Canadian Journal of Earth Sciences* **3**: 747-760.

BLACK, H. P., *and* BUDD, W. F. (1964). Accumulation in the region of Wilkes, Wilkes Land Antarctica. *Journal of Glaciology* **5**: 3-16.

BOGOSLOVSKI, U. N. (1958). The temperature conditions (regime) and movement of the Antarctic glacial shield. Physics of the movement of ice. Symposium of Chamonix. IUGG. IASH Pub. No. 47.

BRACE, W. F. (1960). Orientation of anisotropic minerals in a stress field. Geological Society of America, Memoir No. 79: 9-20.

BUDD, W. F. (1966a). The dynamics of the Amery Ice Shelf. *Journal of Glaciology* **6**: 335-358.

BUDD, W. F. (1966b). Glaciological studies in the region of Wilkes, Eastern Antarctica, 1961. *ANARE Scientific Reports* (A) **4**: Pub. No. 88.

BUDD, W. F. (1968). The longitudinal velocity profile of large ice masses. IUGG. IASH XIV General Assembly, Switzerland.

BUDD, W., LANDON-SMITH, J., *and* WISHART, E. (1967). The Amery Ice Shelf. Physics of Snow and Ice. Conference of Low Temperature Science Proceedings, Vol. 1, Part 1: 447-467.

BUTKOVITCH, T. R., *and* LANDAUER, J. K. (1958). The flow law for ice. Symposium of Chamonix, IUGG. IASH. Pub. No. 47: 318-327.

BUTKOVITCH, T. R., *and* LANDAUER, J. K. (1960). Creep of ice at low stresses. U. S. Army Snow Ice and Permafrost Research Establishment Research Report 72.

CARSLAW, H. S., *and* JAEGER, J. C. (1959). Conduction of Heat in Solids. Oxford.

CARTER, D. (unpublished). Wilkes ice cap project, 1967 (to be published in *ANARE Scientific Reports*).

CLAPP, J. L. (1965). Summary and Discussion of survey control of ice flow studies on Roosevelt Island Antarctica. University of Wisconsin, Geophysical and Polar Research Centre, Department of Geology Research Series 65-1.

CRARY, A. P. (1961). Glaciological studies at Little America Station Antarctica 1957 and 1958. IGY Glaciological Report No. 5. World Data Centre A: Glaciology. American Geographical Society.

CRARY, *et al.* (1962). Glaciological studies of the Ross Ice Shelf (by A. P. Crary, E. S. Robinson, H. F. Bennett, W. W. Boyd Jr.). IGY Glaciological Report No. 6, IGY World Data Centre A: Glaciology. American Geographical Society.

DOBRIN, M. B. (1960). Introduetion to geophysical prospecting, 2nd edition. McGraw-Hill, New York, 446 pp.

DORSEY, N. E. (1940). Properties of ordinary water substance in all its phases: water-vapour, water, and all the ices. American Chemical Society Monograph, Series No. 81.

EMILIANI, C. (1961.) Cenozoic climatic changes as indicated by the stratigraphy and chronology of deep sea cores of globigerina-ooze facies. *Annals of the New York Academy of Sciences* **95**: 521.

FAIRBRIDGE, R. W. (Ed.) (1967). The encyelopedia of atmospheric sciences and astrogeology. Rhinhold, New York.

GERRARD, *et al.* (1952). Measurement of the velocity distribution along a vertical line through a glacier (by Gerrard, J. A. F., Perutz, M. F., *and* Roch, A.) *Proceedings of the Royal Society, London* (A) **213**: 546-558.

GIOVINETTO, M. B. (1964). The drainage systems of Antarctica: Accumulation. Antarctic snow and ice studies. *Antarctic Research Series* (American Geopbysieal Union) **2**: 127-155.

GIOVINETTO, *et al.* (1966). The regime of the western part of the Ross Ice Shelf drainage system (by Giovinetto, M., Robinson, E. S., *and* Swithinbank, C. W. M. *Journal of Glaciology* **6**: 55-68.

GLEN, J. W. (1955). The creep of polycrystalline iee. *Proceedings of the Royal Society* (A) **228**: 519-538.

GLEN, J. W. (1958). The flow law of ice. Symposium of Chamonix. IUGG. IASH Pub. No. 47: 171-183.

GLEN, J. W., *and* PERUTZ, M. F. (1954). The growth and deformation of ice crystals. *Journal of Glaciology* **2**: 397-403.

GOW, A. J. (1963a). The inner structure of the Ross Iee Shelf at Little America V, Antaretica, as revealed by deep core drilling. IUGG. IASH Commission of Snow and Ice General Assembly of Berkeley. Pub. No. 61: 272-284.

GOW, A. J. (1963b). Results in the 309m borehole at Byrd Station, Antarctica. *Journal of Glaciology* **4**: 771-784.

GOW, A. J., UEDA, H. T., *and* GARFIELD, D. E. (1968). Antaretic ice sheet: preliminary results of first core hole to bedrock. *Science* **161**: 1011-1013.

HAEFELI, R. (1961) Contribution to the movement and form of iee sheets in the Arctie and Antarctic. *Journal of Glaciology* **3**: 1133-1151.

HAEFELI, R. (1963). A numerical and experimental method of determining ice motion in the central parts of ice sheets. IUGG. IASH Commission of Snow and Ice. General Assembly of Berkeley. Pub. No. 61: 253-260.

HANSEN, B. L. (1967). (Personal communication to Dr. U. Radok coneerning completion of Byrd deep drilling project.)

HANSEN, B. L., *and* LANDAUER, J. K. (1958). Some results of ice cap drill hole measurements. IUGG. IASH Symposium of Chamonix. Pub. 47: 313-317.

HANSEN, B. L., *and* LANGWAY, C. C. (1966). Deep core drilling in ice and core analysis at Camp Century Greenland, 1961-1966. *Antarctic Journal of the United States* **1**: 207-208.

HEUBERGER, J. C. (1954). Borehole studies on the ice eap Greenland. Glaciology Vol. I (Groenland. Glaciologie, Volnme I. Forages sur l'inlandsis.) Paris, Herman & Cie.

JAEGER, J. C. (1964). Elasticity Fracture and Flow. Methuen.

JENSSEN, M. J. D., *and* RADOK, U. (1961). Transient temperature distributions in ice eaps and ice shelves. IUGG. IASH Symposium of Helsinki, p. 112.

JENSSEN, M. J. D., *and* RADOK, U. (1963). Heat conduction in thinning ice sheets. *Journal of Glaciology* **4**: 347.

KAMB, W. B. (1959a). Theory of preferred erystal orientation. *Journal of Geology* **67**: 153-170.

KAMB, W. B. (1959b). Ice petrofabric observations from Blue Glacier Washington in relation to theory and experiment. *Journal of Physical Research* **64**: 1891-1910.

KANASEWICH, E. R. (1963). Gravity measurements on the Athabasca Glacier, Alberta, Canada. *Journal of Glaciology* **4**: 617-632.

KICK, W. (1966). Measuring and mapping glacier variations. *Canadian Journal of Earth Sciences* **6**: 775-781.

KIZAKI, K. (1962). Ice fabric studies on Hamna Ice Fall and Honnörbrygga Glacier, Antarctica. Antarctic Record No. 16: 1392-1412.

KIZAKI, K. (1969). Ice fabric study of Mawson region, East Antarctica. *Journal of Glaciology* **8**: 253-276.

KIZAKI, K. (unpublished). Ice frabric analysis of surface near Casey Range, East Antarctica (to be publisbed).

KONECNY, G. (1966). Applications of photogrammetry to surveys of glaciers in Canada and Alaska. *Canadian Journal of Earth Sciences* **3**: 783-798.

LAGALLY, M. (1932). Zur Thermodynamik der Gletscher. *Zeitschrift Gletscherkunde* **20**: 199-214.

LAGALLY, M. (1934). Mechanik und Thermodynamik des stationären Gletschers. Ergebnisse des kosmoschen Physik (Akad. Verlagsgesellschaft, Leipzig) Bd. 2. 94 pp.

LAGALLY, M. (1939). Die Zähigkeit des Gletschereises und die Tiefe der Gletscher. *Zeitschrift Gletscherkunde* **18**.

LANGWAY, C. C. (1962). Some physical and chemical investigations of a 411m-deep Greenland ice core for climatic changes. IUGG. IASH Commission of Snow and Ice. Symposium of Obergurgl Pub. No. 48: 101-118.

LEE, H. K., *and* UYEDA, S. (1965). Review of heat flow data. Terrestrial heat flow. Geophysical Monograph No. 8 (American Geophysical Union): 87-190.

LLIBOUTRY, L. (1959). Une théorie du frottement du glacier sur son lit. *Annales de Géophysique* **15**: 250-265.

LLIBOUTRY, L. (1963). Le régime thermique de la base des calottes polaires. IUGG. IASH General Assembly of Berkeley Pub. No. 61: 232-244.

LLIBOUTRY, L. (1964). Subglacial "supercavitation" as a cause of the rapid advances of glaciers. *Nature* **202**: 77.

LLIBOUTRY, L. (1964 *and* 1965). Traité de glaciologie. Tome 1 and Tome 2. Paris, Masson et Cie.

LLIBOUTRY (1966). Bottom temperatures and basal low-velocity layer in an ice sheet. *Journal of Geophysical Research* **71**: 2535-2543.

LLIBOUTRY, L. (1968). General theory of subglacial cavitation and sliding of temperate glaciers. *Journal of Glaciology* **7**: 21-58.

LOEWE, F. (1967). The water budget in Antarctica. Proceedings of the Symposium on Pacific Antarctic Sciences, Eleventh Pacific Science Congress. Japanese Antarctic Research Expedition. Scientific Reports, Special Issue, No. 1: 101-110.

MACDONALD, G. J. F. (1960). Orientation of anisotropic minerals in a stress field: rock deformation. Geological Society of America Mem. 79: 1-8.

MCLAREN, W. A. (1966). Ice cap study, Wilkes, Antarctica. *Antarctic* (New Zealand Antarctic Society) **4** (8).

MCLAREN, W. A. (1968). A study of the local ice cap near Wilkes, Antarctica. *ANARE Scientific Reports* (A) **4**. Pub. No. 103.

MATHEWS, W. H. (1959). Vertical distribution of velocity in Salmon Glacier, British Columbia. *Journal of Glaciology* **3** (26).

MEIER, M. F. (1958). Vertical profiles of velocity and the flow law of glacier ice. IUGG. IASH Symposium of Chamonix. Pub. No. 47: 1969-1970.

MEIER, M. F. (1960). Mode of flow of Saskatchewan Glacier, Alberta, Canada. Geological Survey Professional Paper 351.

MEIER, M. F. (1969). Calculations of slip of Nisqually Glacier on its bed: no simple relation of sliding velocity to shear stress. IUGG. IASH General Assembly of Switzerland. Snow and Ice. Pub. No. 79: p. 49-57.

MELLOR, M. (1959). Creep tests on Antarctic glacier ice. *Nature* **184**: 717.

MELLOR, M. (1960). Temperature gradients in the Antarctic ice sheet. *Journal of Glaciology* **3**: 773.

MELLOR, M. (1961). The Antarctic ice sheet. Cold regions science and engineering. USA CRREL Monographs Part I, Sect. B.1.

MELLOR, M. (1964). Snow and ice on the Earth's surface. Cold regions science and engineering, Part II Physical Seience, C. The physics and mechanics of ice. U.S. Army Cold Regions Research and Engineering Laboratory.

MELLOR, M., *and* SMITH, J. H. (1966). Creep of snow and ice. U.S. Army CRREL Research Report 220 (also Sapporo Conference, 1966, Physics of Snow and Ice, Part 2).

MOCK, S. T. (1967). Calcnlated patterns of accumulation on the Greenland ice sheet. *Journal of Glaciology* **6**: 795-804.

MORGAN, P. J. (unpublished). Photogrammetric and geophysieal methods of determining the mass budget of an ice cap. M.Sc. thesis submitted to Meteorology Department, University of Melbourne, 1966.

NYE, J. F. (1951). The flow of glaciers and ice sheets as a problem in plasticity. *Proceedings of the Royal Society* (A) **207**: 554-572.

NYE, J. F. (1952a). The mechanics of a glaeier flow. *Journal of Glaciology* **2**: 82.

NYE, J. F. (1952b). A comparison between the theoretieal and the measured long profile of the Unteraar Glacier. *Journal of Glaciology* **2**: 103.

NYE, J. F. (1953). The flow law of ice from measurements in glacier tunnels, laboratory measurements and the Jungfraufirn borehole experiment. *Proceedings of the Royal Society* (A) **219**: 447-489.

NYE, J. F. (1957). The distribution of stress and velocity in glaciers and ice sheets. *Proceedings of the Royal Society* (A) **239**: 113-133.

NYE, J. F. (1958). A theory of wave formation in glaeiers. IUGG. IASH Symposium of Chamonix. Pub. No. 47: 139-154.

NYE. J. F. (1959a). The deformation of a glacier below an iee fall. *Journal of Glaciology* **3**: 387.

NYE, J. F. (1959b). The motion of ice sheets and glaciers. *Journal of Glaciology* **3**: 493-507.

NYE, J. F. (1960). Thc response of glaciers and ice sheets to seasonal and climatic changes. *Proceedings of the Royal Society* (A) **256**: 559-584.

NYE, J. F. (1965a). The frequency response of glaciers. *Journal of Glaciology* **5**: 589-608.

NYE, J. F. (1965b). The flow of a glacier in a ehannel of rectangular, elliptic or parabolic cross section. *Journal of Glaciology* **5**: 661-690.

NYE, J. F. (to be published). The effect of longitudinal stress on the shear stress at the base of an ice sheet. (Submitted to *Journal of Glaciology*, Jan. 1969.)

ÖPIK, E. J. (1964). *Ice ages, in* "The Planet Earth" (D. R. Bates, Editor) 2nd edition, Pergamon Press.

ORVIG, S. (1953). The glaciological studies of the Baffin Island Expedition, 1950: Part 5—On the variation of the shear stress on the bed of an ice cap. *Journal of Glaciology* **2**: 242-246.

PALMER, A. C. (1967). Creep velocity bounds and glacier flow problems. *Journal of Glaciology* 6: 479-488.

PATERSON, W. S. B. (1964). Variations in velocity of Athabasca Glacier with time. *Journal of Glaciology* **5**: 277-286.

PATERSON, W. S. B. (unpublished). Observations on Athabasca Glacier and their relation to the theory of glacier flow. Doctoral thesis, University of British Columbia. Vancouver, B.C., Canada (1962). 158 pp.

PATERSON, W. S. B., *and* SAVAGE, J. L. (1963a). Geometry and movement of the Athabasca Glacier. *Journal of Geophysical Research* **68**: 4513-4520.

PATERSON, W. S. B., *and* SAVAGE, J. L. (1963b). Borehole measurements in the Athabasca Glacier. *Journal of Geophysical Research* **68**: 4521-4536.

PATERSON, W. S. B., *and* SAVAGE, J. L. (1963c). Measurements on Athabasca Glacier relating to the flow law of ice. *Journal of Geophysical Research* **68**: 4537-4543.

PFITZNER, L. (unpublished). The Wilkes ice cap propect 1966. *ANARE Scientific Reports* (A) **4** (to be publisbed).

PHILBERTH, K. (1966). Ein Sehmelzonde zur Messung des Temperaturprofils in Eiskolotten. Umschau in Wissensehaft und Technik, Franfurt am Main, Heft 11/1966, p. 360.

PHILBERTH, B. (1967). Measurements of the permitivity of ice. *Journal of Glaciology* **6**: 765-766.

POWELL, R. W. (1958a). Thermal conductivities and expansion coefficients of water and ice. *Advances in Physics* **7**: 276-297.

POWELL, R. W. (1958b). Preliminary measurements of the thermal conductivity and expansion of iee. *Proceedings of the Royal Society* (A) **247**: 464.

RADOK, U. (1959). Temperatures in polar ice caps. *Nature* **184**: 1056.

RATCLIFFE, E. H. (1962). The thermal conductivity of ice, new data on the temperature coefficient. *Philosophical Magazine* (8th Series) **7**: 1197-1203.

REID, J. R. (1960). Petrofabric analysis of an icc layer from a névé-ice anticlinc, in deformation of the Ross Jce Shelf ncar the Bay of Whales, Antarctica (by J. H. Zumbergcr, M. Giovinetto, R. Kehle, *and* J. Reid). IGY Glaciological Report Series No. 3 (American Geographical Society): 91-113.

RIGSBY, G. P. (1955). Study of ice fabrics, Thule area, Greenland. U.S. Army SIPRE Report 26.

RIGSBY, G. P. (1958a). Fabrics of glacier and laboratory deformed ice. IUGG. IASH Symposium of Chamonix Pub. No. 47, p. 351-8.

RIGSBY, G. P. (1958b). Effect of hydrostatic pressure on velocity of shear deformation of single ice crystals. *Journal of Glaciology* **3**: 274-275.

RIGSBY, G. P. (1960). Crystal orientation in glacier and experimentally deformed ice. *Journal of Glaciology* **3**: 589-606.

ROBIN, G. DE Q. (1955). Ice movemcnt and temperature distribution in glaciers and ice sheets. *Journal of Glaciology* **2**: 523-532.

ROBIN, G. DE Q. (1967). Surface topography of ice shcets. *Nature* **215**: 1029-1032.

ROBINSON, E. S. (1966). On the relationship of ice-surface topography to bed topography on the South Polar Plateau. *Journal of Glaciology* **6**: 43-54.

SCHYTT, V. (1958). Snow studies at Maudheim, snow studies inland: the inner structure of the iee shelf at Maudheim as shown hy core drilling. Norwegian-British-Swedish Antarctic Expedition 1949-52. Seientific Results Vol. IV—Glaciology II, A to C.

SHARP, R. P. (1953). Deformation of a vertical borehole in a piedmont glacier. *Journal of Glaciology* **2** (13).

SHARP, R. P. (1960). Glaciers. University of Oregon Press.

SHOUMSKY, P. A. (1958). The mechanism of ice straining and its rccrystallization. IUGG. IASH Symposium of Chamonix Pub. No. 47: 244-248.

SHOUMSKY, P. A. (1961a). On the theory of glacier motion. IUGG. IASH Symposium on Antarctic Glaciology. General Assembly of Helsinki Pub. No. 55: 142-149.

SHOUMSKY, P. A. (1961b). The dynamics and morphology of glaciers. IUGG. IASH Symposium on Antarctic Glaciology General Assembly of Helsinki Pub. No. 55: 152-161.

SHOUMSKY, P. A. (1963a) Pressure and density fields of glaciers;

SHOUMSKY, P. A. (1936b). Kinematics of the stationary glacier (translated from Rnssian). Results of the researches on the program of the IGY. Glaciological Researches, Articles IX Section of IGY Program No. 9.

SHOUMSKY, P. A. (1963c). On the theory of glacier variations. IUGG. IASH Bulletin VIII Année No. 1: 45-56.

SHOUMSKY, P. A. (1967). The distribution of stress velocity and temperature in glaciers. Physics of Snow and Ice, International Conferenee on Low Temperature Science. Sapporo, Japan, 1966. The Institute of Low Temperature Science, Hokkaido University. Proceedings, Vol. I, Part 1, p. 371-384.

SHOUMSKY, P. A., *and* ZOTIKOV, I. A. (1963). On the mass and heat exehange in the Antaretic ice shelves. IUGG. IASH General Assembly of Berkeley. Commission of Snow and Ice. Pub. No. 61 225-231.

SHOUMSKY, P. A., KRENKE, A. N. *and* ZOTIKOV, I. A. (1964). Ice and its changes. *From* Rescarch in Geophysics. Vol. 2: 425-4650. Solid earth and interface phenomena. M.I.T. Press.

STEINEMANN, S. (1958). Résultats expérimentaux sur la dynamique de la glace et leur corrélation avec le mouvement et la pétrographie des glaciers. IUGG. IASH Symposium of Chamonix Pub. No. 47: 184-198.

TIEN CHI (1960). Tempcrature distribution of an idealised ice cap. U.S. Army SIPRE Research Report 64.

UEDA, H. T., *and* HANSEN, B. L. (1967). Installation of deep eore drilling equipment at Byrd Station. *Antarctic Journal of the United States* **2**: 120-121.

VIALOV, S. S. (1958a). Regularities of glacial shields movement and the theory of plastic viscous flow;

VIALOV, S. S. (1958b). Regularities of ice deformation. IUGG. IASH Symposium of Chamonix Pub. No. 47: respectively 266-275 and 383-391.

VIALOV, S. S. (1967). On the tbeory of the flow of glaciers. Physies of snow and ice. Inter-

national Conference of Low Temperature Science. Proceedings Vol. I, Part 1: 350-356. Institute of Low Temperature Science, Hokkaido.

VOITKOVSKII, K. F. (1960). The mechanical properties of ice. (Moscow Izd. Akademii. Navk, SSSR.) Translated from the Russian by the American Meteorological Society, Boston. 100 pp.

WALKER, D. J. (1964). Wilkes geopbysical surveys, Antarctica 1962-3. Geophysical Progress Report No. 1964/25. Bureau of Mineral Resources, Geology and Geophysics, Department National Development, Canberra (unpublished).

WALKER, D. J. (1966). Wilkes Geophysical Surveys, Antaretica 1962. Records No. 1966/129, Bureau of Mineral Resources, Geology and Geophysics, Department National Development, Canberra (unpublished).

WEERTMAN, J. (1957a). On the sliding of glaciers. *Journal of Glaciology* **3**: 33-38.

WEERTMAN, J. (1957b). Deformation of floating ice shelves. *Journal of Glaciology* **3**: 38-42.

WEERTMAN, J. (1958). Travelling waves on glaciers. IUGG. IASH Symposium of Chamonix Pub. No. 47: 162-168.

WEERTMAN, J. (1961a). Equilibrium profile of ice caps. *Journal of Glaciology* **3**: 953-964.

WEERTMAN, J. (1961b). Stability of ice age ice sheets. *Journal of Geophysical Research* **66**: 3783-3792.

WEERTMAN, J. (1962). Catastrophic glacier advances. IUGG. IASH Symposium of Obergurgl: 31-39.

WEERTMAN, J. (1964a). The theory of glacier sliding. *Journal of Glaciology* **5**: 287-304.

WEERTMAN, J. (1964b). Rate of growth or shrinkage of nonequilibrium ice sheets. U.S. Army CRREL Research Report 145.

WEERTMAN, J. (1967). An examination of the Lliboutry theory of glacier sliding. *Journal of Glaciology* **6**: 489-494.

WEXLER, H. (1959). Geothermal heat and glacial growth. *Journal of Glaciology* **3**: 420-425.

WEXLER, H. (1960). Heating and melting of floating ice shelves. *Journal of Glaciology* **3**: 626-645.

WEXLER, H. (1961). Growth and thermal structure of the deep ice in Byrd Land, Antarctica. *Journal of Glaciology* **3**: 1075-1087.

WILSON, S. D. (1959). Report on the 1958 Tuto ramp slope indicator measurements, by Shannon & Wilson, for U.S. Army Corps of Engineers.

ZOTIKOV, I. A. (1961). Thermal regime of a glacier of central Antarctica. "Antarctica" (Moscow). Translated by the Israel Program for Scientific Translations, Jerusalem.

ZOTIKOV,, I. A. (1963). On temperatures at depths in glaciers. "Antarctica" (Moscow). Translated by the Israel Program for Scientific Translations, Jerusalem.

APPENDIX I

DERIVATION OF LONGITUDINAL STRESS DEVIATOR GRADIENT WITH RESPECT TO A LONGITUDINAL AXIS OF ARBITRARY INCLINATION

Two-dimensional motion or "plane-strain rate" only is considered.

We adopt a right-hand orthogonal axes system x, z, such that the horizontal is inclined at an arbitrary angle χ to the positive x direction. All angles will be taken positive for an anticlockwise rotation from the χ axis.

Let $-\alpha$ be the surface slope of the ice mass at position x,

$-\beta$ be the basal slope of the ice mass at position x,

z_1 be the ordinate of the surface at position x,

z_2 be the ordinate of the base at position x.

Write $Z = z_1 - z_2$ for the ice thickness at x, and $-\theta = -\alpha + \chi$, $-\phi = -\beta + \chi$.

The stress components at (x, z) are denoted by $(\sigma_x, \tau_{xz}, \sigma_z)$. We consider an ice mass of constant density ρ.

Let g be the gravitational acceleration, and write $g_x = +\ g \sin \chi$, $g_z = -\ g \cos \chi$ for its components in the axes' directions.

The equations of equilibrium for slow steady motion may then be written as

$$\frac{\partial \sigma_x}{\partial x} + \frac{\partial \tau_{xz}}{\partial z} + \rho g_x = 0 \tag{1}$$

$$\frac{\partial \sigma_z}{\partial z} + \frac{\partial \tau_{xz}}{\partial x} + \rho g_z = 0 \tag{2}$$

These equations are true everywhere in the ice mass for any such axes system so defined.

We require an expression for the longitudinal stress deviator $\sigma_x' = \frac{1}{2}(\sigma_x - \sigma_z)$. Hence, differentiate (1) with respect to z and (2) with respect to x and substract to yield

$$\frac{\partial^2(\sigma_x - \sigma_z)}{\partial x \partial z} = \frac{\partial^2 \tau_{xz}}{\partial x^2} - \frac{\partial^2 \tau_{xz}}{\partial z^2} \tag{3}$$

This equation also does not depend on the choice of the axis orientation. It is only when this equation is integrated that it becomes necessary to specify the boundary conditions in terms of the axis direction.

We integrate (3) with respect to z from z_1 to z

$$\frac{\partial(\sigma_x - \sigma_z)}{\partial x} = -\left(\frac{\partial \sigma_z}{dx}\right)_{z_1} + \left(\frac{\partial \sigma_x}{\partial x}\right)_{z_1} + \left(\frac{\partial \tau_{xz}}{\partial z}\right)_{z_1} - \frac{\partial \tau_{xz}}{\partial z} + \int_{z_1}^{z} \frac{\partial^2 \tau_{xz}}{\partial x^2}\, dz \tag{4}$$

From equation (1) we note at the surface

$$\frac{\partial \sigma_x}{\partial x}\Big)_{z_1} + \frac{\partial \tau_{xz}}{\partial z}\Big)_{z_1} = -\rho g_x \tag{5}$$

Hence (4) may be written

$$\frac{\partial(\sigma_x - \sigma_z)}{\partial x} = -\rho g_x - \frac{\partial \sigma_z}{\partial x}\Big)_{z_1} - \frac{\partial \tau_{xz}}{\partial z} + \int_{z_1}^{z} \frac{\partial^2 \tau_{xz}}{\partial x^2}\, dz \tag{6}$$

Now, integrating again with respect to z, this time from z_1 to z_2, noting the first two terms on the right are constant with z and also $Z = z_2 - z_1$, gives

$$\int_{z_1}^{z_2} \frac{\partial(\sigma_x - \sigma_z)}{\partial x}\, dz = -\rho g_x Z - Z \frac{\partial \sigma_z}{\partial x}\Big)_{z_1} - \tau_{xz_2} + \tau_{xz_1} + \int_{z_1}^{z_2}\int_{z_1}^{z} \frac{\partial^2 \tau_{xz}}{\partial x^2}\, dz dz \tag{7}$$

This equation is exact and expresses the mean longitudinal stress deviator gradient in terms of the boundary conditions at the surface and base of a column of ice. We shall shortly examine the surface and base boundary conditions in detail. But, firstly, it is often required to integrate this equation with respect to x. To do this we note that the left-hand side may be written

$$\int_{z_1}^{z_2} \frac{\partial(\sigma_x - \sigma_z)}{\partial x}\, dz = \frac{\partial \int_{z_1}^{z_2} (\sigma_x - \sigma_z) dz}{\partial x} - (\sigma_x - \sigma_z)_{z_2} \frac{\partial z_2}{\partial x} + (\sigma_x - \sigma_z)_{z_1} \frac{\partial z_1}{\partial x} \tag{8}$$

BOUNDARY CONDITIONS

At the surface we make the assumption that the shear stress parallel to the surface is zero, and that the normal stress is the atmospheric pressure p.

If $-\theta$ is the angle between the x axis and the surface, then the normal and shear stresses are related to the components in the x, z directions at the surface by

$$-p = \sigma_x \sin^2\theta - 2\tau_{xz} \sin\theta \cos\theta + \sigma_z \cos^2\theta \tag{9}$$

$$0 = (\sigma_x - \sigma_z) \sin\theta \cos\theta - \tau_{xz}(\sin^2\theta - \cos^2\theta) \tag{10}$$

For (8) we require only (10) in the form (dividing by $\cos^2\theta$)

$$(\sigma_x - \sigma_z)_{z_1} \tan\theta = -\tau_{xz_1}(1 - \tan^2\theta) \tag{11}$$

Similarly, at the base, if $-\tau_b$ is the basal shear stress parallel to the bed, where $-\phi$ is the angle between the base and the x axis, then

$$-\tau_b = (\sigma_x - \sigma_z) \sin\phi \cos\phi + \tau_{xz}(\cos^2\phi - \sin^2\phi)$$

and therefore

$$(\sigma_x - \sigma_z)_{z_2} \tan\phi = -\tau_{xz_2}(1 - \tan^2\phi) - \frac{\tau_b}{\cos^2\phi} \tag{12}$$

Since $\frac{\partial z_2}{\partial x} = -\tan\phi$ and $\frac{\partial z_1}{\partial x} = -\tan\theta$, using (11), (12) and (8) in (7) gives, writing

$$Z(\bar{\sigma}_x - \bar{\sigma}_z) \qquad \text{for} \qquad \int_{z_1}^{z_2} (\sigma_x - \sigma_z) dz,$$

$$\frac{\partial Z(\bar{\sigma}_x - \bar{\sigma}_z)}{\partial x} = -\rho g_x Z - Z\frac{\partial \sigma_z}{\partial x}\Big)_{z_1} + \tau_{xz_2}\tan^2\phi - \tau_{xz_1}\tan^2\theta + \frac{\tau_b}{\cos^2\phi} + \int_{z_1}^{z_2}\int_{z_1}^{z}\frac{\partial^2\tau_{xz}}{\partial x^2}\,dz\,dz \tag{13}$$

The term $\frac{\partial \sigma_z}{\partial x}\Big)_{z_1}$ is zero for points where the surface is parallel to the x axis. For other slopes, however, this term depends on the longitudinal stress and stress-gradients and the curvature of the surface. We now evaluate this term in full to show under what conditions it may be approximated by $\rho g_z \tan\theta$.

If s denotes the distance along the curved surface,

$$\frac{\partial \sigma_z}{\partial x} = -\frac{\partial \sigma_z}{\partial z}\tan\theta + \frac{\partial \sigma_z}{\partial s}\frac{1}{\cos\theta} \tag{14}$$

Using equation (2) this may be written

$$\frac{\partial \sigma_z}{\partial x} = +\rho g_z \tan\theta + \frac{\partial \tau_{xz}}{\partial x}\tan\theta + \frac{\partial \sigma_z}{\partial s}\frac{1}{\cos\theta}.$$

Similarly expanding $\frac{\partial \tau_{xz}}{\partial x}$ and using (1) gives

$$\frac{\partial \sigma_z}{\partial x} = +\rho g_z \tan\theta + \frac{\partial \tau_{xz}}{\partial z}\tan^2\theta + \frac{\partial \tau_{xz}}{\partial s}\frac{\sin\theta}{\cos^2\theta} + \frac{\partial \sigma_z}{\partial s}\frac{1}{\cos\theta}$$

$$= \rho g_z \tan\theta - \frac{\partial \sigma_x}{\partial x}\tan^2\theta - \rho g_x \tan^2\theta + \frac{\partial \tau_{xz}}{\partial s}\frac{\sin\theta}{\cos^2\theta} + \frac{\partial \sigma_z}{\partial s}\frac{1}{\cos\theta} \tag{15}$$

Now, at the surface, if σ_n, σ_1 are the normal and longitudinal stresses and $\sigma_1' = \frac{1}{2}(\sigma_1 - \sigma_n)$

$$\tau_{xz} = \sigma_1' \sin 2\theta \qquad \text{and} \qquad \sigma_z = \sigma_n \cos^2\theta + \sigma_1 \sin^2\theta.$$

Hence

$$\frac{\partial \tau_{xz}}{\partial s} = \frac{\partial \sigma_1'}{\partial s}\sin 2\theta + \sigma_1' 2\cos 2\theta \frac{\partial \theta}{\partial s}$$

and

$$\frac{\partial \sigma_z}{\partial s} = -\sigma_n 2\cos\theta\sin\theta\frac{\partial \theta}{\partial s} + \frac{\partial \sigma_1}{\partial s}\sin^2\theta + \sigma_1 2\sin\theta\cos\theta\frac{\partial \theta}{\partial s}.$$

Substituting in (15) and taking surface values,

$$\frac{\partial \sigma_z}{\partial x}\Big)_{z_1} = \rho g_z \tan\theta - \frac{\partial \sigma_x}{\partial x}\Big)_{z_1}\tan^2\theta - \rho g_x \tan^2\theta + \frac{\partial \sigma_1}{\partial s}2\sin\theta\tan\theta$$

$$+ \sigma_1' 2\cos 2\theta\tan\theta\frac{\partial \theta}{\partial x} - \sigma_n \sin 2\theta\frac{\partial \theta}{\partial x} + \frac{\partial \sigma_1}{\partial s}\sin\theta\tan\theta + \sigma_1 \sin 2\theta\frac{\partial \theta}{\partial x} \tag{16}$$

Hence, to take as the first approximation

$$\left.\frac{\partial \sigma_z}{\partial x}\right)_{z_1} \approx \rho g_z \tan\theta,$$

it is necessary (and sufficient) that not only the slope θ be small but also the slope gradient, i.e., $\frac{1}{\theta}\frac{\partial\theta}{\partial s} \sim \frac{1}{\sigma_1}\frac{\partial \sigma_1}{\partial s}$ or less. Since the longitudinal stresses vary with the surface slope this is usually the case. However, abrupt changes of surface slope or stress (e.g., surface crevasses) will not be covered by the approximate formula.

Finally, substituting (16) in (13) and writing the components of g in full gives

$$\begin{aligned}\frac{\partial Z(\bar{\sigma}_x - \bar{\sigma}_z)}{\partial x} = &-\rho g Z \sin\chi - \rho g Z \cos\chi \tan\theta - Z\left.\frac{\partial \sigma_x}{\partial x}\right)_{z_1} \tan^2\theta \\ &- \rho g Z \sin\chi \tan^2\theta + Z\frac{\partial \sigma_1'}{\partial s} 2\sin\theta\tan\theta \\ &+ \sigma_1' Z\, 2\cos 2\theta \tan\theta \frac{\partial\theta}{\partial x} - Z\sigma_n \sin 2\theta \frac{\partial\theta}{\partial x} \\ &+ Z\frac{\partial \sigma_1}{\partial s}\sin\theta\tan\theta + \sigma_1 Z \sin 2\theta \frac{\partial\theta}{\partial x} + \tau_{xz_2}\tan^2\phi \\ &- \tau_{xz_1}\tan^2\theta + \frac{\tau_b}{\cos^2\phi} + \int_{z_1}^{z_2}\int_{z_1}^{z} \frac{\partial^2 \tau_{xz}}{\partial x^2}\, dz\, dz \end{aligned} \tag{17}$$

This equation is exact; it has arbitrary orientation χ for the x axis, and applies everywhere along the ice mass with the same rectilinear co-ordinates, and hence it may be directly integrated with respect to x, without resorting to curvalinear co-ordinates. From this equation the conditions required for various simplified forms may be determined.

SPECIAL CASE OF SMALL SLOPES

For small slopes χ, θ, ϕ, and slope gradients (i.e., neglecting second and higher orders), all except the first two and last two terms of equation (17) are negligible, so that it reduces to the form given by Budd (1968),

$$\frac{\partial Z\bar{\sigma}_x'}{\partial x} = -\tfrac{1}{2}\left[\rho g Z(\alpha - f) - \int\int \frac{\partial^2 \tau_{xz}}{\partial x^2}\, dz\, dz\right] \tag{18}$$

where $\bar{\sigma}_x' = \tfrac{1}{2}(\bar{\sigma}_x - \bar{\sigma}_z)$, $f = \dfrac{\tau_b}{\rho g Z}$, $\alpha = \chi + \theta$. In this case only the surface slope is relevant and it is therefore immaterial whether the axes are taken horizontal, parallel to the surface or parallel to the base.

Other simplified forms of (17) may be readily obtained by choosing the longitudinal axis in directions such as: horizontal ($\chi = 0$), or parallel to the surface ($\theta = 0$, $\chi = \alpha$), or parallel to the base ($\phi = 0$, $\chi = \beta$), at some particular position.

APPENDIX II

THE FLOW LAW OF ICE FROM THE LONGITUDINAL STRESS GRADIENT

To convert the equation for longitudinal stress gradient to an equation in strain rate gradient we re-examine the flow law of ice.

It is only satisfactory to replace $\bar{\sigma}'_x$ by $B\bar{\dot{\varepsilon}}_x^{1/n}$ if $\tau_{xz} \ll \frac{(\sigma_x - \sigma_z)}{2}$ or if $n \approx 1$. The major problem then is to consider the relation between $\bar{\sigma}'_x$ and $\bar{\dot{\varepsilon}}_x$ when τ_{xz} is not necessarily small.

We abandon the power law formulation of the stress-strain relation for ice

$$\dot{\varepsilon}_{ij} = \frac{(\tau)^{n-1}}{B^n} \sigma'_{ij} \tag{1}$$

since n and B are not constant with stress. Instead, we adopt a "generalized viscosity" relationship of the form

$$\dot{\varepsilon}_{ij} = \frac{1}{\eta} \sigma'_{ij} \tag{2}$$

where $\eta(\tau, \theta)$ is a function of both stress and temperature.

For the octahedral shear stress τ, the strain rate $\dot{\varepsilon}$, (2), gives

$$\dot{\varepsilon} = \frac{1}{\eta} \tau \tag{3}$$

Hence

$$\eta = \frac{\tau}{\dot{\varepsilon}} \tag{4}$$

This may be regarded as an alternative definition of η. Equation (3) may be regarded as the flow law of ice and for each constant temperature represents a single curve on $\dot{\varepsilon}$ versus τ diagram. It is these curves we wish to determine.

So, substituting for the average longitudinal stress deviator through the ice column $\bar{\sigma}'_x = \overline{\eta\dot{\varepsilon}_x}$ in the equation for stress gradient

$$\frac{\partial \bar{\sigma}'_x}{\partial x} = \frac{1}{2} \rho g(\alpha - f) - \frac{1}{2} \frac{\partial^2 \iint \tau_{xz}\, dz\, dz}{\partial x^2} \tag{5}$$

we obtain

$$\frac{\partial \overline{\eta \dot{\varepsilon}_x}}{\partial x} = \frac{1}{2}\rho g(\alpha - f) - \frac{1}{2}\frac{\partial^2 \iint \tau_{xz}\, dz\, dz}{\partial x^2} \tag{6}$$

$$= \frac{1}{2}\rho g \delta\alpha^* \quad \text{(as a definition of } \delta\alpha^*\text{)} \tag{7}$$

or

$$\overline{\eta \dot{\varepsilon}_x}\Big|_{x_1}^{x} = \frac{1}{2}\rho g \int_{x_1}^{x} \delta\alpha^* dx \tag{8}$$

We now define a weighted mean flow parameter η^* through a vertical column by

$$\eta^* = \frac{\overline{\eta \dot{\varepsilon}}}{\bar{\dot{\varepsilon}}}.$$

We now obtain (for fluctuations around a mean value, i.e., taking $\bar{\dot{\varepsilon}}_{x_1} = 0$ for $\delta\alpha^* = 0$)

$$\bar{\dot{\varepsilon}}_x = \frac{\rho g}{2\eta^*} \int \delta\alpha^* dx \tag{9}$$

or

$$\bar{\dot{\varepsilon}}_x = \frac{1}{\eta^*}\bar{\sigma}'_x \tag{10}$$

where

$$\bar{\sigma}'_x = \frac{1}{2}\rho g \int \delta\alpha^* dx \tag{11}$$

Hence, from the ratio of the longitudinal stress to longitudinal strain-rate $\bar{\sigma}_x'$ and $\dot{\varepsilon}_x$ we obtain η^* for each τ and θ. We now use these to determine the flow law in terms of octahedral values.

Since, in terms of the octahedral values, $\eta^* = \frac{\bar{\tau}}{\bar{\dot{\varepsilon}}}$, we can now obtain the flow law of ice calculating $\dot{\varepsilon}$ from η^* and τ for each value and illustrate this by then plotting $\dot{\varepsilon}$ against τ.

For two-dimensional flow the octahedral shear stress $\bar{\tau}$ is calculated from

$$\bar{\tau} = \sqrt{\overline{\tau_{xz}^2 + \sigma_x'^2}} \simeq \sqrt{\bar{\tau}_{xz}^2 + \bar{\sigma}_x'^2} \tag{12}$$

taking

$$\bar{\tau}_{xz} = \tfrac{1}{2}\rho g \bar{\alpha} Z \quad \text{and} \quad \bar{\sigma}'_x = \tfrac{1}{2}\rho g \int \delta\alpha^* dx \tag{13}$$

Here $\bar{\alpha}$ is taken as the mean surface slope over a distance x about 10 to 20 times the ice thickness.

These values of stress are derived directly from the measured elevation and ice-thickness profiles. The surface strain rate ε_s can be measured but, to obtain the average strain rate through the column, something must be known about the ratio $\dot{\varepsilon}_s/\dot{\varepsilon}_x = \lambda$, say.

This normally requires information on the velocity—depth profile. However,

if the ice is not slipping at the base, then we may expect the strain rates to vary with depth in a similar way to the velocity V, i.e.,

$$\frac{\dot{\varepsilon}_s}{\bar{\dot{\varepsilon}}_x} = \frac{V_s}{\bar{V}_x} = \lambda \tag{14}$$

For cold ice caps the velocity profile depends on the temperature profile and estimates can be calculated (cf. Section 4).

In the absence of a velocity profile, the value of λ can be assumed to lie between 2/3 and 1, being near 90% for typical ice-cap temperature profiles. In terms of the measured surface strain-rates, then, we may write

$$\dot{\varepsilon}_s = \frac{\rho g}{2\eta^* \lambda} \int \delta\alpha^* dx \quad \text{or} \quad \eta^* = \frac{\bar{\sigma}'_x}{\lambda \dot{\varepsilon}_s} \tag{15}$$

From the measured variations in surface strain rates $\dot{\epsilon}_s$ and surface slope α the generalized viscosity $\eta^*(\tau, \theta)$ can be determined from (15) and then, using the values of mean octahedral shear stress from (12) and (13) and mean temperature for the column at that position, a point on the stress—strain rate relationship $\dot{\varepsilon}(\tau, \theta)$ can be established by plotting

$$\dot{\varepsilon} = \lambda \dot{\varepsilon}_s \frac{\sqrt{\bar{\tau}_{xz}^2 + \bar{\sigma}_x'^2}}{\bar{\sigma}'_x} \quad \text{versus} \quad \bar{\tau} = \sqrt{\bar{\tau}_{xz}^2 + \bar{\sigma}_x'^2}.$$

To obtain the complete set of curves for $\dot{\varepsilon}(\tau, \theta)$ many values of $\dot{\varepsilon}_s$, covering a wide range of shear stress τ and temperature θ, are required. For a temperate ice-mass we may expect the ratio of the longitudinal strain-rate to longitudinal stress to depend just on the magnitude of the octahedral shear stress.